University of Manchester

The role of PMCA1 in the development of heart failure.

A thesis submitted to the University of Manchester for the degree of Doctor of Philosophy in the Faculty of Biology, Medicine and Health

2022

Tahir Nazir

School of Medical Sciences
Division of Cardiovascular Sciences
Faculty of Biology, Medicine and Health

Table of contents

List of figures

List of tables

List of abbreviations

ANOVA	Analysis of variance
ANP	Atrial natriuretic peptide
ATP	Adenosine triphosphate
Bax	Bcl-2-associated-X protein
Bcl-2	B-cell lymphoma 2
BNP	Brain natriuretic peptide
BSA	Bovine serum albumin
BW	Body weight
CaM	Calmodulin
CASK	Calcium-calmodulin dependent serine protein kinase
cDNA	Complementary DNA
Cn	Calcineurin
dIVS	Diastolic interventricular septum thickness
dLVD	Diastolic left ventricular diameter
dLVPW	Diastolic left ventricular posterior wall thickness
DNase	Deoxyribonuclease
dP/dtmax	Maximum derivative of change in pressure rise over time
dP/dtmin	Maximum derivative of change in pressure fall over time
DPX	Distyrene, plasticizer and xylene
ECG	Electrocardiography
EF	Ejection fraction
eNOS	Endothelial nitric oxide synthase
ERK	Extracellular signal-regulated kinase
FS	Fractional shortening
GAPDH	Glyceraldehyde-3-phosphate dehydrogenase
GWAS	Genome wide association studies
HW	Heart weight
I.P.	Intraperitoneal
IVS	Interventricular septal
LV	Left ventricle
MAPK	Mitogen activated protein kinase

mRNA	Messenger RNA
NCX	Na^+ / K^+ exchanger
NFAT	Nuclear factor of activated T-cells
nNOS	Neuronal nitric oxide synthase
NO	Nitric oxide
PBS	Phosphate buffered saline
PCR	Polymerase chain reaction
PDZ-BD	PDZ protein-binding domain
PMCA1-4	Plasma membrane calcium ATPase 1-4
PW	Posterior wall
qPCR	Quantitative real time polymerase chain reaction
RAAS	Renin-angiotensin-aldosterone system
RASSF1	Ras-associated factor 1
RT	Reverse transcription
RWT	Relative wall thickness
SEM	Standard error of the mean
SERCA	Sarco(endo)plasmic reticulum calcium ATPase
sFRP2	Secreted frizzled related protein 2
sIVS	Systolic interventricular septum thickness
sLVD	Systolic left ventricular diameter
sLVPW	Systolic left ventricular posterior wall thickness
SNP	Single nucleotide polymorphism
Tau	Time constant of relaxation
TL	Tibia length

Abstract

A thesis submitted to the University of Manchester in July 2022 by Tahir Nazir for the degree of Doctor of Philosophy entitled

'The role of PMCA1 in the development of heart failure'

Heart Failure remains a major cause of morbidity and mortality worldwide. Whilst a number of pharmacological treatments are used in heart failure management, there is no targeted therapy available to tackle the cardiac remodelling that often precedes decompensated heart failure. Plasma membrane calcium ATPase 1 (PMCA1) is the most prevalent isoform of PMCA in the heart, and human genome wide association studies have shown a link between PMCA1 and hypertension and other cardiovascular diseases. Previous work from our group has provided functional evidence of the association between reduced PMCA1 expression and hypertension and cardiac arrhythmias in murine models. Our group have previously generated two novel PMCA1 mutant mouse lines using Cre/loxP technology including a cardiomyocyte specific deletion ($PMCA1^{cko}$) and a global heterozygous deletion ($PMCA1^{HT}$), both of which show reduced expression of PMCA1.

This study was designed to explore the role played by PMCA1 in heart failure and to evaluate cardiac remodelling in mice with reduced expression of PMCA1. For this study, eight week old $PMCA1^{cko}$ mice were subjected to transverse aortic constriction (TAC) or sham operation for a period of two weeks along with their age and gender-matched controls. In a separate experiment, eight week old male $PMCA1^{HT}$ mice and their controls were subjected to transverse aortic constriction (TAC) and sham operation for a period of five weeks. In TAC procedure, the transverse aorta was ligated (over a curved blunt 27G needle) between the brachiocephalic trunk and the left common carotid artery using a surgical suture that produces approximately 25% narrowing of the aortic lumen, whilst in mice undergoing the sham operation the aorta was exposed and a surgical suture passed around it but not ligated. Echocardiogram and haemodynamic analysis were performed at the end of the experiment and animals were sacrificed. Cardiac tissue samples were collected for histology, qPCR and proteomic analysis.

Under basal physiological conditions, no significant difference was found in the cardiac structure and function of the transgenic ($PMCA1^{cko}$ and $PMCA1^{HT}$) and control mice. Two

weeks after TAC, PMCA1^{cko} mice developed decompensated heart failure with evidence of left ventricular dilatation, systolic dysfunction and pulmonary oedema, whereas the control group developed compensated myocardial hypertrophy with no heart failure. PMCA1^{cko} mice were also found to have a significantly higher degree of myocardial fibrosis on histology examination. Expression of other calcium handling genes such as PMCA4, NCX, SERCA2 and RyR remained unchanged. On the other hand, PMCA1^{HT} mice demonstrated development of concentric myocardial hypertrophy after five weeks TAC whilst the wildtype controls developed eccentric myocardial hypertrophy.

These data show that PMCA1 plays a major role in enabling heart to adapt with pressure overload and pathological hypertrophy. That is why following its deletion, the myocardium is unable to effectively respond to the pressure overload and as a result, decompensated heart failure develops. However, the loss of single allele of PMCA1 (PMCA1^{HT}) does not appear to affect TAC induced cardiac hypertrophy. PMCA1's protective role during the development of pathological cardiac hypertrophy may help to explore novel treatment options for patients with heart failure.

A mechanistic explanation for the development of dilated cardiomyopathy after PMCA1 deletion in cardiomyocytes would require further probing of the cellular pathways involved in hypertrophy and fibrosis. Future work to explore PMCA1's role should involve generation of a cardiac fibroblast specific PMCA1 knock out model to evaluate some of these pathways. Using a selective PMCA1 inhibitor such as caloxin 1b3, future TAC experiments would help to determine PMCA1's potential to be an effective therapeutic target for the treatment of heart failure.

Declaration

I declare that no portion of the work referred to in this thesis has been submitted in support of an application for another degree or qualification at this or any other university or other institute of learning.

Tahir Nazir

School of Medical Sciences

Faculty of Biology, Medicine and Health

Copyright statement

i. The author of this thesis (including any appendices and/or schedules to this thesis) owns certain copyright or related rights in it (the "Copyright") and s/he has given The University of Manchester certain rights to use such Copyright, including for administrative purposes.

ii. Copies of this thesis, either in full or in extracts and whether in hard or electronic copy, may be made only in accordance with the copyright, Designs and Patents Act 1988 (as amended) and regulations issued under it or, where appropriate, in accordance with licensing agreements which the University has from time to time. This page must form part of any such copies made.

iii. The ownership of certain Copyright, patents, designs, trademarks and other intellectual property (the "Intellectual Property") and any reproductions of copyright works in the thesis, for example graphs and tables "Reproductions"), which may be described in this thesis, may not be owned by the author and may be owned by third parties. Such Intellectual Property and Reproductions cannot and must not be made available for use without the prior written permission of the owner(s) of the relevant Intellectual Property and/or Reproductions.

iv. Further information on the conditions under which disclosure, publication and commercialisation of this thesis, the Copyright and any Intellectual property and/or Reproductions described in it may take place is available in the University IP Policy (see http://documents.manchester.ac.uk/DocuInfo.aspx?DocID=24420), in any relevant Thesis restriction declarations deposited in the University Library, The University Library's regulations (see htttp://www.library.manchester.ac.uk/about/regulations/) and in The University's policy on Presentation of Theses

Acknowledgements

Firstly, I would like to take this opportunity to thank my supervisor Prof. Cartwright whose help and guidance throughout this project has been pivotal to help me persevere with my research. She has always been there to offer scientific advice, encouragement, and support. I am also grateful to Dr Ashraf Kitmitto (my co-supervisor) for giving useful advice with experimental aspects of this work. Additionally, many thanks to the members of the Cartwright lab group: Mr Sukhpal Prehar; Dr Min Zi; Flo Baudoin; Dr Alex Njegic, Dr Ardiansah Nugroho (Bayu) and Dr Nicholas Stafford, who were there to help me whenever needed.

I found the courage to start my PhD rather late in my NHS career (i.e after having been a consultant physician for several years). This big step was only made possible by the unconditional love and support from my wife Dr Nisa Shah who has been my rock and has always encouraged me to make my dreams come true. I would be an absolutely lost soul without her. My lovely children Hassan and Ayesha always bring joy to lit up the most difficult periods and are great source of happiness in my life. I am grateful to my parents who taught me to work hard and never give up!

I would also like to offer my gratitude to colleagues in the lab, especially Eftah, Farah, Yulia, Hatim and Alex Chelu for always being helpful.

Lastly, I am grateful to my colleagues at Lancashire Teaching Hospitals NHS foundation trust for being flexible to allow the changes in my job plan to undertake this PhD.

Chapter 1 - Introduction

1.1 Heart Failure

1.1.1 Introduction

According to the World Health Organisation, over 17 million people die from the diseases of cardiovascular system every year, making them the leading cause of death worldwide (Mensah et al., 2019). Heart failure (HF) is a clinical syndrome in which the heart is unable to pump sufficient amounts of blood to meet metabolic demands of the body and is a major and escalating health issue globally (Roger, 2013). Improved clinical outcomes from acute cardiovascular events and an increase in the ageing population have led to a significant rise in the prevalence of HF (Savarese & Lund, 2017). Population-based studies report incidence of HF to be higher in men compared to women. HF is uncommon in people below 55 years of age (incidence 0.2%), with a rise in incidence to 1.8-3 % in patients aged 55-74 years and a staggering five-fold increase in incidence to 15% in those aged 85 and above (Roger, 2021). This epidemic is estimated to affect approximately 26 million people worldwide, with over half a million patients living in the United Kingdom alone, where it is predicted that 5% of all deaths are due to HF (Cowie, 2017). The financial burden of managing this condition is huge; globally it costs over $108 billion per year with nearly $65 billion as direct and $3 billion as indirect cost of managing heart failure (Cook et al., 2014).. HF is a condition with significant mortality; 40% patients die in the first year after diagnosis with a further 10% annual mortality (Pocock et al., 2013). Five year survival rate post diagnosis is as low as 58% in HF patients, which is worse than many cancers (Taylor et al., 2019a). It also has a significant effect on patients' quality of life. Dyspnoea at minimal exertion, compounded by lack of energy severely limits patients' physical activity leading to loss of independence with daily life tasks. HF patients report a poorer quality of life on Short Form 36 (SF-36) quality of life questionnaire compared to many other chronic illnesses (Chatzinikolaou et al., 2021).

1.1.2 Risk factors for heart failure

Coronary artery disease is by far the most common risk factor for heart failure in the developed countries, accounting for nearly half of the cases in patients aged 75 and above; followed by hypertensive heart disease, cardiomyopathy, valvular heart disease, congenital heart diseases, infiltrative diseases, arrhythmias and viral myocarditis (Lüscher, 2015). Valve disease which was responsible for only 10% cases of heart failure a couple of decades ago is

now rising due to an increase in elderly population with age-related aortic stenosis (Cowie, 2017). Diabetes Mellitus, smoking and dyslipidaemia also increase the risk of developing heart failure (Bui et al., 2011).

1.1.3 Pathophysiology of heart failure

Increased myocardial stress resulting from the factors mentioned above leads to a number of adaptive mechanisms within the heart. These include an increase in pre-load to improve myocardial performance in keeping with Frank-Starling's law, alteration in myocyte apoptosis and myocardial hypertrophy to augment cardiac pump function and activation of neurohormonal mechanisms (Cohn, 1995; Haddad et al., 2008). The cardiac adrenergic nerves release nor-adrenaline, which not only increases cardiac contractility but also leads to activation of renin-angiotensin-aldosterone system (RAAS) and sympathetic nervous system in an attempt to maintain tissue perfusion. Whilst these adaptations are intended to help the heart maintain its function in the acute phase, they eventually perpetuate a deleterious cycle of worsening cardiac output and tissue perfusion.

The initial myocardial response of myocyte hypertrophy and apoptosis subsequently leads to cardiac remodelling that worsens the loading condition of remaining myocytes resulting in inefficient contractility. Stimulation of the sympathetic nervous system causes tachycardia and arrhythmias (Chaggar et al., 2009). Renal hypo-perfusion due to a reduction in the mean arterial pressure, and sympathetic stimulation leads to secretion of renin from kidneys (Kemp & Conte, 2012). Renin is a peptide released from juxtaglomerular apparatus and converts angiotensinogen to angiotensin I in the liver which is subsequently changed to angiotensin II in the lungs, facilitated by the action of angiotensin converting enzyme (ACE). Angiotensin II is a potent vasoconstrictor that leads to an increase in systemic vascular resistance; additionally, it also stimulates the release of a mineralocorticoid hormone, aldosterone. Aldosterone acts on renal collecting tubules resulting in sodium (and water) absorption leading to an increase in circulating volume (Rea & Dunlap, 2008). Other neurohormonal systems also become activated in HF including vasopressin, natriuretic peptides, endothelium derived vasoactive substances and cytokines. A simplified account of these adaptive changes is shown in figure 1.1. These mechanisms are counterproductive in the long-term leading to a pressure and volume overload that results in the progression of heart failure.

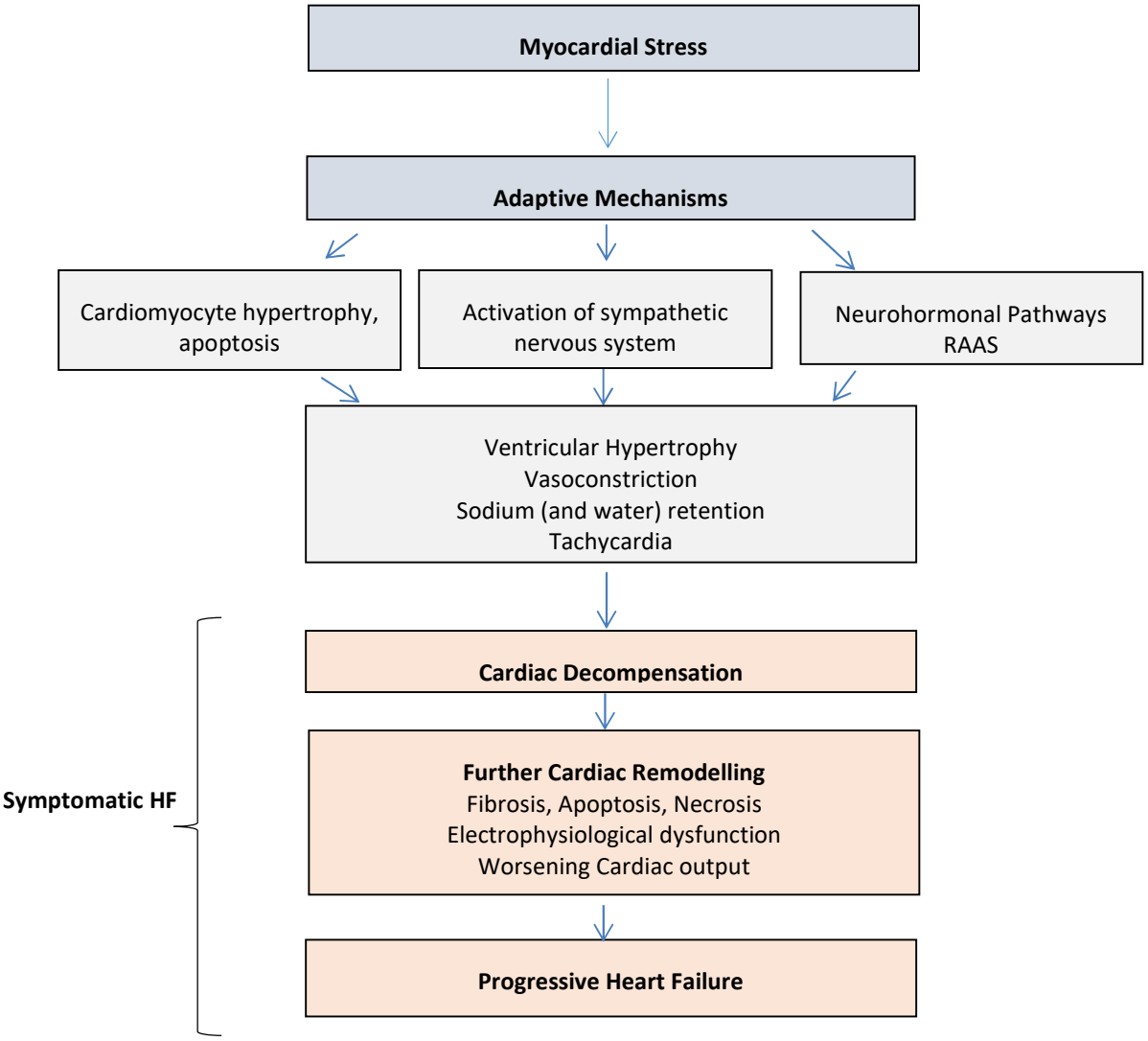

Figure 9.1: A schematic diagram of pathophysiology of heart failure. Myocardial stress triggers an adaptive response at various levels including cellular adaptation, activation of sympathetic nervous system and neurohormonal pathways. This results in ventricular hypertrophy, vasoconstriction, tachycardia and fluid retention; however, this fails to maintain cardiac output and tissue perfusion, leading to symptomatic heart failure. Further cardiac remodelling results in progressive disease and death (adapted from Kemp and Conte, 2012).

1.1.4 Current treatment strategies for heart failure

Most of the pharmacological treatments are aimed at modifying some of the aforementioned adaptive responses with a view to slowing the progression of HF (Feldman

et al., 2017). Beta blockers inhibit the sympathetic nervous system hence preventing tachycardia, arrhythmias and myocardial ischemia. ACE-inhibitors and angiotensin receptor blockers (ARB) counteract mediators of RAAS pathway to reduce cardiac remodelling and vasoconstriction. Mineralocorticoid receptor antagonists (MRA) e.g Spironolactone and Eplerenone block aldosterone action and prevent sodium reabsorption (Zannad et al., 2011). Diuretics produce a symptomatic decongestion of the lungs by eliminating excessive fluid, in turn reducing the cardiac preload and improved cardiac stroke volume. Sodium Glucose co-transporter 2 (SGLT2) inhibitors are a relatively new class of oral hypoglycaemics drugs which reduce the risk of cardiovascular death and hospitalisation in heart failure patients in patients with or without diabetes mellitus (Vaduganathan et al., 2022). SGLT2 inhibitors promote glucose and water excretion from kidneys hence exerting a diuretic effect in heart failure but may have a role in improving myocardial energetics and reducing in cardiac oxidative stress (Das et al., 2021). Patients with cardiac conduction abnormalities e.g left bundle branch block can benefit from cardiac resynchronisation therapy (CRT) which is a form of cardiac pacemaker with or without a defibrillator device (Cleland et al., 2005) . Sadly, patients with advanced heart failure do not respond to most of the above treatments and require left ventricular assist device and eventually, cadaveric cardiac transplantation, which has a very limited availability. None of the treatments explained above target cellular mechanisms and signalling pathways responsible for cardiomyocyte hypertrophy, which play a pivotal role in development of heart failure.

It is clear that despite advancements in pharmacological and non- pharmacological treatments for heart failure, patients remain at a higher risk of death (Cowie, 2017). Currently available treatments do not offer a cure and only provide a moderate benefit in symptom control and a relatively small reduction in mortality. There is an acute and pressing need for the development of novel therapeutics to improve the quality of life and survival rates of patients with heart failure.

1.2 Myocardial Hypertrophy

1.2.1 Myocardial Hypertrophy and its consequences

The heart has an ability to adapt to an increased haemodynamic workload. Compensatory changes such as faster heart rate and increased myocardial contractility are triggered when the heart cannot fulfil the metabolic demands of the body; these adjustments are considered

to reduce systolic stress on ventricular walls (Fagard, 1997). These adaptive mechanisms are only capable of maintaining cardiac output in the initial phases of increased myocardial stress and are followed by an increase in myocardial size. Myocardial hyperplasia leads to cardiac growth during foetal development; however, this ceases in neonatal life and any subsequent increase in cardiac size takes place by cellular hypertrophy (Schwinger, 2021). Cardiac hypertrophy is characterised by increased synthesis of contractile proteins, increased extracellular matrix, changes in sarcomere organisation and altered gene expression (Conrad et al., 1991). Progressive changes in ventricular size, shape and function in response to physiological and pathological stimuli are called 'cardiac remodelling'. Cardiac remodelling and hypertrophy aim to improve the cardiac pump function in order to improve tissue perfusion and relieve congestion.

Although, initially an adaptive response, these compensatory mechanisms often fail to manage the effects of increased myocardial stress in the long term and eventually, lead to dilatation of heart, thinning of ventricular walls, cell death, loss of contractile proteins and reduced ejection fraction resulting in the clinical syndrome of heart failure (Pitoulis & Terracciano, 2020). This is further complicated by a higher risk of acute coronary events, arrhythmias and sudden death. It is generally agreed that patients with left ventricular hypertrophy (LVH) are at greater risk of cardiovascular morbidity and death; there seems to be a direct relationship between left ventricular mass and future cardiac complications (Giamouzis et al., 2021) The Framingham Heart Study also confirms left ventricular hypertrophy to be an independent risk factor for cardiovascular mortality (Levy et al., 1990).

1.2.2 Types of myocardial hypertrophy

Myocardial hypertrophy takes place in a number of physiological and pathological conditions. Maturational or developmental cardiac hypertrophy is a form of physiological hypertrophy occurring in early adulthood regulated by growth hormone and insulin like growth factor-1 (IGF-1). It is characterised by protein synthesis resulting in a proportionate growth in myocyte width and length; this leads to a uniform rise in ventricle and septal wall thickness (Maillet et al., 2013). Whilst the ventricular size and function increase as a result of developmental hypertrophy, its geometry and overall morphology remains unaltered.

Elevated oxygen demand from the musculoskeletal system during sustained physical exercise and increased circulating blood volume in pregnancy, both result in physiological hypertrophy of heart

(figure 1.2). Physiological hypertrophy in these conditions yields up to 20% increase in cardiac size (Powers et al., 2014) and is reversible once the initial stimulus is removed. The changes resolve within a few weeks after child birth or cessation of physical training (Xiao et al., 2014).

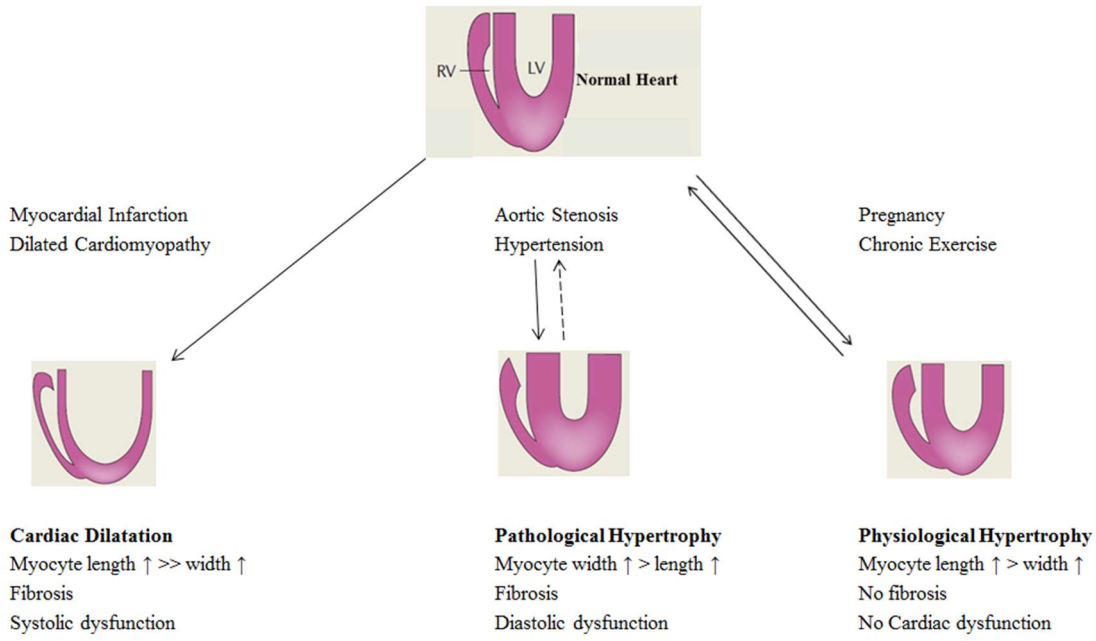

Figure 1.2 : Types of myocardial hypertrophy. In response some stimuli such as myocardial infarction, there is an elongation of cardiomyocytes resulting in cardiac dilatation. Pressure overload results in an increase in cardiomyocyte width resulting in pathological hypertrophy. Exercise and pregnancy can lead to physiological cardiac hypertrophy which does not manifest any cardiac dysfunction or fibrosis. (Adapted from Heineke and Molkentin, 2006). (RV – right ventricle, LV- left ventricle)

The heart adapts to a variety of stimuli, for example, an elevated cardiac afterload (e.g pressure overload due to aortic stenosis or hypertension) produces concentric hypertrophy due to a disproportionate increase in myocyte width, whereas myocardial infarction and dilated cardiomyopathy result in elongation of myocytes and cardiac dilatation also called eccentric hypertrophy. Chronic exercise and pregnancy cause physiological hypertrophy with

no fibrosis and no cardiac dysfunction. Disease processes such as hypertension, valvular disease (aortic stenosis, aortic regurgitation, mitral regurgitation), cardiomyopathies and ischaemic heart disease produce pathological cardiac hypertrophy, which can be further classified based upon initial stimulus and eventual cardiac morphology. Haemodynamic stress on the heart can be of two types: volume overload and pressure overload. Pressure overload as a consequence of aortic stenosis or hypertension results in thickening of left ventricular walls and septum with a net reduction in its internal diameter, termed as concentric left ventricular hypertrophy. This is due to a disproportionate growth of cardiac myocytes in their width than in their length (Heineke & Molkentin, 2006). Concentric LVH results in poor ventricular relaxation, impaired end diastolic filling, increased stiffness and diastolic dysfunction, and seems to be associated with a poor prognosis (Conrad et al., 1991; Verdecchia et al., 1995). The volume overload caused by incompetent heart valves e.g aortic or mitral regurgitation and leads to dilatation of left ventricle and a proportionate rise in its wall thickness; this compensatory change is called eccentric left ventricular hypertrophy. This is underpinned by cardiomyocyte growth more pronounced in their length compared to the width (Müller & Dhalla, 2013). Relative wall thickness (RWT) is a useful echocardiographic parameter that can help to distinguish between concentric and eccentric hypertrophy. It is calculated by adding posterior wall thickness (PW) and inter-ventricular septal thickness (IVS) and dividing it by the LV end diastolic diameter (LVEDD) (ie. RWT= PW+IVS/ LVEDD) (Gardin, 2016). Hearts with eccentric LVH have a lower RWT and those with concentric LVH have a higher RWT value(Wang et al., 2014). It is important to note that with the persistence of pressure overload stimulus, the concentric cardiac hypertrophy eventually decompensates into eccentric cardiac hypertrophy resulting in dilatation of the left ventricle (Nauta et al., 2020).

1.2.3 Molecular basis of myocardial hypertrophy

At a cellular level, the initial stimuli promoting myocyte hypertrophy can be divided into biomechanical and neurohormonal groups. Biomechanical stimuli that produce stretch or deformation of cells, are considered to be mediated via stretch-sensitive receptors. The transmembrane receptors integrins link extracellular matrix with the cytoskeleton and interact with molecules, such as melusin, to form a cellular sensory apparatus that detects cell stretch (Brancaccio et al., 2003; Ross & Borg, 2001). Additionally, within each sarcomere, zinc containing muscle LIM proteins are attached to specific proteins at the Z-disc and may

serve as another stretch sensing cellular mechanism (Knöll et al., 2002). When stimulated by biomechanical stress, these apparatus activate signalling molecules; integrins transduce signals via focal adhesion kinase (FAK), melusin and GTPases, and muscle LIM protein activate calcineurin-nuclear factor of activated T cell (NFAT) signalling pathway (Heineke et al., 2005).

Neurohormonal stimuli trigger a cascade of cellular signalling pathways through cell-membrane bound G-protein-coupled receptors (GPCR) with intracellular tyrosine kinase or serine/ threonine kinase domains (Heineke & Molkentin, 2006). These signalling pathways include MAPK signalling, P13K-AKT pathway, calcineurin-NFAT, MEK1-ERK1/2 and Ras, and often comprise a sequence of kinases resulting in phosphorylation and ultimately play their role in regulation of myocardial hypertrophy. This is shown in figure 1.3. With the current level of understanding, it appears that some of these pathways have a dichotomous effect, and are involved in pathological as well as physiological myocardial hypertrophy, making it difficult to use them as therapeutic targets (Heineke & Molkentin, 2006).

Re-expression of the foetal gene programme is the hallmark of early myocardial response to mechanical and neurohormonal stress. Transduction of factors like Nkx 2.5, GATA4, MEF2 (myocyte enhancer factor 2) and NFAT (nuclear factor of activated T cell) result in activation of a number of cardiac foetal genes such as myosin heavy chain isoform α (αMHC), alpha-skeletal actin (αSKA), atrial natriuretic peptide (ANP) and brain natriuretic peptide (BNP) (Dirkx et al., 2013).

In mice, embryonic heart mainly expresses β MHC while adult heart contains higher levels of αMHC; the latter has an elevated ATPase activity resulting in faster energy release and sarcomere shortening (Holubarsch et al., 1985). However, during pathological hypertrophy in adult murine heart, myosin isozyme shift takes place resulting in proportionately higher expression of β MHC, which has a lesser ATPase activity, subsequently lowering the energy used for contraction; this is considered to be a compensatory mechanism during early phases of myocardial stress (Taegtmeyer et al., 2010). In human heart, β MHC is the major isoform throughout the life (Razeghi et al., 2001). In failing human heart, a decrease in αMHC expression and a relative increase in β MHC expression have been reported (Kurabayashi et al., 1988). Although β MHC expression is reduced in the failing human heart compared to the healthy heart; it is the greater reduction in α MHC in heart failure that leads to an overall increase in β MHC / α MHC ratio (van der Pol et al., 2020).

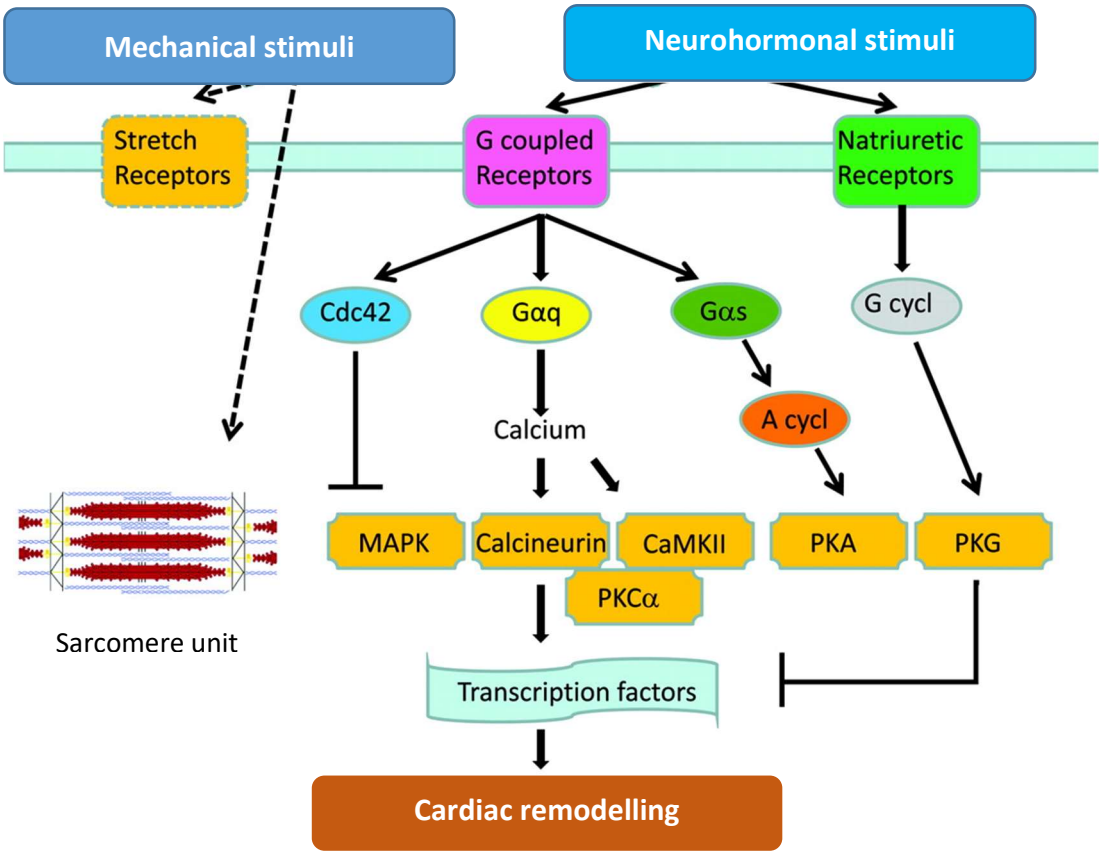

Figure 1.3: Key molecular pathways involved in cardiac remodelling. Membrane bounded receptors sense neurohormonal stresses and both membrane bound receptors and sarcomere. This results in modulation of phospholipase C and adenylyl (A cycl) and guanylyl cyclases (G cycl). Subsequently, this leads to transcription of genes involved in foetal gene program and new cellular growth (adapted from Kehat & Molkentin, 2010).

Pathological hypertrophy is also associated with elevated circulating levels of ANP and BNP. These peptides are released secondary to mechanical stretch of atria and ventricles and stimulate natriuresis (sodium excretion) and vasodilatation hence reducing circulating volume and blood pressure. Natriuretic peptides also down-regulate the pro-hypertrophic calcineurin-NFAT signalling pathway. Circulating BNP is neutralised by an endothelial peptidase called Neprilysin which has recently been used as a therapeutic target in heart failure treatment. Sacubitril, a Neprilysin inhibitors increased bioavailability of BNP and has been shown to improve clinical outcomes in patients with heart failure (McMurray et al., 2014).

The afore-mentioned adaptations in cardiomyocytes are accompanied by changes in cardiac fibroblasts. These cells, unlike myocytes, are not post mitotic and can proliferate and in fact, replace myocytes after injury or infarction, leading to cardiac fibrosis (Boluyt et al., 1994; Weber et al., 1995). Cardiac fibrosis results in systolic and diastolic dysfunction as well as arrhythmias. Electromechanical function of the heart critically relies on an effective cross talk between cardiomyocytes and cardiac fibroblasts (Rother et al., 2015). Cardiac fibroblasts affect cardiomyocytes' viability, volume and calcium handling via soluble mediators (Cartledge et al., 2015). This two-way communication between cardiac myocytes and fibroblasts in health and disease takes into consideration age and stimulus dependant signals to develop a coordinated response to stress in order to minimise its impact on cardiac structure and function (Nicin et al., 2021). There is also emerging evidence that cardiac fibroblasts may also play a role to regulate myocyte hypertrophy by secreting IGF-1 secreted frizzled related protein 2 (sFRP-2) and micro-RNAs that act by paracrine pathways and direct cell-cell interaction to regulate myocyte hypertrophy (Mohamed et al., 2016).

No doubt, it is very important to prevent and control pathological cardiac hypertrophy in order to reduce the risk of development of heart failure, cardiac morbidity and death. However, interestingly, most of the strategies employed to achieve this, target either extra cardiac factors (e.g controlling hypertension) or involve surgical correction of elevated cardiac afterload (e.g aortic valve replacement); there is no satisfactory therapeutic modality available to address cellular pathways within the heart responsible for myocardial hypertrophy.

Myocardial hypertrophy and failure are associated with a number of alterations in cellular mechanisms in myocytes leading to a poor pump function of the heart (Harvey & Leinwand, 2011). Ion and receptor mediated signalling pathways play a major role in controlling cardiac contractility (Lehnart et al., 2009). The delicate regulation of calcium movement into and out of the cell and sarcoplasmic reticulum is finely tuned by numerous regulatory processes during health and undergoes significant derangement in heart failure (Davlouros et al., 2016).

1.3 Calcium Homeostasis

1.3.1 Calcium homeostasis in normal heart

Being a ubiquitous second messenger, calcium plays an important role in cell signalling during a wide range of physiological processes (Hofer & Lefkimmiatis, 2007). The function of the heart as an effective pump is the result of synchronous contraction and relaxation of cardiac myocytes, which in turn depend upon dynamic changes in intracellular calcium levels. A number of calcium transport mechanisms work in harmony to move calcium across the plasma membrane i.e between cytoplasm and extracellular fluids, and also between cytosol and cellular organelles (Luo & Anderson., 2013). Coordinated efforts of these transport systems lead to a sharp rise and fall in cytosolic calcium levels with every contraction of the cardiac myocyte, known as calcium transient (Bers., 2002).

1.3.2 Excitation-contraction coupling (ECC)

The process of electrical excitation of cardiac myocytes and the resultant contraction is termed cardiac excitation-contraction coupling (Bers, 2001). Calcium plays a pivotal role in electrical activity of the heart and directly activates cardiac myofilaments leading to their contraction (Pogwizd et al., 2001). Mishandling of calcium by myocytes results in cardiac arrhythmias and impaired systolic and diastolic function of heart.

It is well established that as the sarcolemma depolarises during cardiac action potential, voltage-dependant L-type Ca^{2+} channels (LCC, dihydropyridine receptors) are activated allowing a small amount of calcium to enter the resting cells. This inward calcium current (I_{Ca}) facilitates the release of larger quantities of Ca^{2+} from sarcoplasmic reticulum by activating ryanodine receptors (RYR2). The process of Ca^{2+} induced Ca^{2+} release (CICR) ultimately results in an increase in the free intracellular Ca^{2+} concentration. Marked changes in the levels of free intracellular Ca^{2+} in cardiac myocytes during various stages of cardiac contraction- relaxation cycle have been observed; in diastole Ca^{2+} concentration is as low as 100 nM which significantly rises to 1 µM in systole. Intracellular Ca^{2+} binds to troponin-C, neutralising its inhibitory effect which allows cross-bridges to form between actin and myosin filaments resulting in initiation of contraction (Phrommintikul & Chattipakorn., 2006).

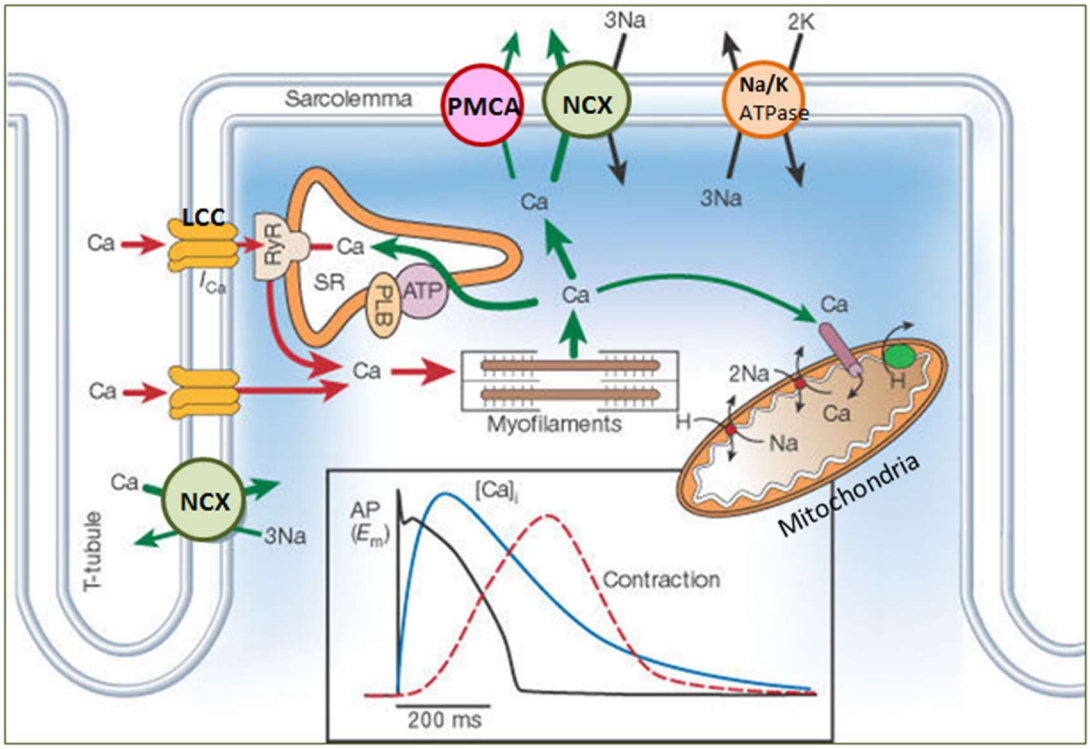

Figure 1.4: Excitation contraction coupling. As a result of action potential depolarisation of the sarcolemma, Ca^{2+} enters the cells through voltage gated L-type calcium channels (LCC) . This leads to the release of Ca^{2+} from the sarcoplasmic reticulum (SR) via ryanodine receptors (RYR2). The resulting increased intracellular Ca^{2+} activates the myofilaments and contraction of myocyte during systole. Subsequently, Ca^{2+} is removed from the cytosol by sarcoplasmic reticulum Ca^{2+} ATPase (SERCA), sodium Ca^{2+} exchanger (NCX), plasma membrane Ca^{2+} ATPase (PMCA) and mitochondrial Ca^{2+} uniporter during diastole. Na^+ /K^{2+} ATPase removes Na^+ from the cytosol to maintain membrane gradient of Na^+, (adapted from Bers., 2002).

Figure 1.4 shows the process of Ca influx and exodus from cardiomyocytes in detail. A number of mechanisms lead to termination of CICR, these include local depletion of Ca^{2+} in sarcoplasmic reticulum, RyR switch off and simultaneous closure of LCC (Stern, 1992). To avoid any further un-intended calcium leak into the cytosol, calcium within the sarcoplasmic reticulum is bound to calsequestrin, which is a high-capacity calcium binding protein. Although, the primary function of calsequestrin appears to be safely storing Ca^{2+} in sarcoplasmic reticulum as local intra-SR Ca^{2+} buffer ; in addition, it also plays a role in the regulation of RyR (Beard et al., 2005). Calsequestrin form a regulatory complex along with Triadin (TRD) and Junctin (JN) which is closely associated with RyR exerting an inhibitory effect on RyR. However, rising intra-SR Ca^{2+} levels lead to conformational change leading to a dissociation of CASQ2-TRD-JN complex from RyR thus removing the inhibitory effect (Chen et al., 2013).

Mutations in calsequestrin gene (CASQ2) lead to disturbances in calcium transients in myocytes and are associated with arrhythmias and sudden cardiac death (Murphy et al., 2011). Catecholaminergic polymorphic ventricular tachycardia (CPVT) is a potentially fatal inherited cardiac dysrhythmia characterised by episodes of ventricular tachycardia during adrenergic stimulation and is associated with mutations of RyR and CASQ2 gene (Faggioni et al., 2012). Although CASQ2 linked CPVT is rarer than RyR associated CPVT but it presents with a more severe form of ventricular tachycardia (Roston et al., 2018).

In order for cardiac myocyte relaxation to occur, calcium must be removed from the cytosol leading to a significant reduction in intracellular Ca^{2+} concentration. This sharp fall in Ca^{2+} levels facilitates its detachment from troponin C (Sun & Irving, 2010). Calcium efflux from the cytosol occurs by four main routes; sarcoplasmic reticulum Ca^{2+} ATPase (SERCA), sodium Ca^{2+} exchanger (NCX), plasma membrane Ca^{2+} ATPase (PMCA), and mitochondrial Ca^{2+} uniporter (Fearnley et al., 2011). These mechanisms vary in their calcium handling capacity in different species. In human, SERCA is the main calcium removal route responsible for over two thirds of calcium efflux from cytosol, followed by NCX that removes approximately one quarter calcium and removal of the remaining 2% is equally shared between PMCA and mitochondrial uniporter (Bassani et al., 1994). However, in murine ventricular myocytes, SERCA has a much higher activity compared to NCX ; its removes a major bulk of intracellular calcium (92%) whereas NCX only transports 7% of calcium. This leaves 1% intracellular calcium to be removed by PMCA and mitochondrial Ca^{2+} uniporter (Hove-Madsen & Bers, 1993). Quantitative analysis of calcium efflux in rabbit cardiac myocytes is similar to those of human (Bers, 1997).

Force of contraction of cardiac myocytes depends upon intracellular concentration of Ca^{2+}, which produces both isometric contraction and rapid fibre shortening (Solaro & Rarick, 1998). Myofilaments are highly sensitive to Ca^{2+} under physiological conditions (Chung et al., 2016); however, during disease processes e.g myocardial ischemia this sensitivity is reduced due to local acidosis, increased magnesium and phosphate levels resulting in impaired contraction (Siddiqui et al., 2016). Conversely, their sensitivity to Ca^{2+} is increased by inotropic drugs and caffeine that leads to an improved systolic function (Bers, 2002).

In addition, sarcomere mutations associated with hypertrophic cardiomyopathy also increase

myofilament Ca^{2+} sensitivity (Akhtar & Elliott, 2018). Conversely, gene mutations linked with dilated cardiomyopathy often lead to a reduced myofilament Ca^{2+} sensitivity (Harris & de Tombe, 2019).

1.3.3 Mechanisms of calcium efflux from cytosol in cardiomyocytes

As described above Ca^{2+} enters the myocytes through depolarisation activated Ca^{2+} channels triggering Ca^{2+} release from sarcoplasmic reticulum. This raises the free intracellular Ca^{2+} $[Ca^{2+}]i$ concentration leading to contraction of myocyte. For relaxation to occur, $[Ca^{2+}]i$ must fall by transporting Ca^{2+} out of cytosol. Calcium efflux from the cytosol takes place by four mechanisms involving sarco(endoplasmic) calcium ATPase (SERCA), Na^{+} / Ca^{2+} exchanger (NCX), Plasma membrane calcium ATPase (PMCA) and mitochondrial uniporter (MCU) (Bers, 2002).

1.3.4 Sarco(endoplasmic) calcium ATPase (SERCA)

SERCA removes Ca^{2+} from the cytoplasm into the (sarco)endoplasmic reticulum lumen, against its concentration gradient (Strehler & Treiman, 2004). It transports two Ca^{2+} ions by utilising energy acquired by hydrolysing 1 ATP molecule (Guerrero-Hernandez et al., 2010). SERCA is coded on three distinct genes and by alternative splicing a total of 10 isoforms of SERCA have been described (Periasamy & Kalyanasundaram, 2007). SERCA3 is the most ubiquitous isoform and is found in non-muscle tissues, whereas SERCA1 is expressed in skeletal muscles and SERCA2 is expressed in cardiac and skeletal muscles (Brini & Carafoli, 2009). The most prevalent isoform in cardiac myocytes is SERCA2a; its deletion has been found to be embryonic lethal in murine models (Periasamy et al., 1999).

Sarcolipin (SLN) and phospholamban (PLB) both lower SERCA's affinity to bind Ca^{2+} hence leading to an inhibition of Ca^{2+} re-uptake. Overexpression of SLN has been shown to reduce SR calcium stores and is associated with increased muscle fatigability after repeated electrical stimulation (MacLennan et al., 2003). PLB is a muscle phosphoprotein that in its dephosphorylated form acts as a more specific inhibitor to SERCA 2a isoform and leads to an impairment in Ca^{2+} re-uptake in SR resulting in poor myocyte relaxation (Tada et al., 1983). However, when phosphorylated by either cyclic adenosine monophosphate-dependent protein kinase A (PKA) or Ca^{2+}/calmodulin-dependant protein kinase II, PLB loses its inhibitory effect on SERCA2a. This subsequently increases Ca^{2+} reuptake leading to elevated

SR calcium stores and myocyte relaxation (Kiriazis & Kranias, 2000). Researchers have demonstrated that cardiac specific knock out of PLB in murine models leads to an improved Ca^{2+} handling, increased SR Ca^{2+}content and faster sarcomere relaxation. Conversely, overexpression of PLB results in a significant decline in SERCA activity, diminished SR Ca^{2+} reserve, impaired diastolic Ca^{2+} clearing, poor ventricular relaxation and eventually, cardiomyopathy (Andino et al., 2008; Bluhm et al., 2000; Dash et al., 2001) .

A reduction in SERCA activity in cardiomyocyte can lead to cardiac dysfunction. Li and colleagues (2012) reported development of end stage heart failure in mice with cardiomyocyte specific excision of SERCA 2 gene (Li et al., 2012). In this study, there was evidence of a compensatory upregulation of NCX with resultant accumulation of sodium in cardiomyocytes and intracellular acidosis, both of which seemed to have played a role in the progression of heart failure. Edwards and colleagues (2021) also found that mice with cardiomyocyte specific SERCA2 knockout rapidly progressed to end stage heart failure in 7 – 10 weeks (Edwards et al., 2021). SERCA2a gene therapy has been shown to improve cardiac contractility with reduced risk of fatal ventricular arrhythmias (Sikkel et al., 2014). This preclinical work paved the way for a small phase 2 trial on adult patients with advanced heart failure that combined SERCA gene therapy (using an adenovirus vector) along with left ventricular assist device (LVAD). An absolute level of transgene DNA was low in this study and no functional benefit was observed in the treatment group (Lyon et al., 2020). This study highlighted some challenges in delivering gene therapy in humans.

1.3.5 Na^+ / Ca^{2+} exchanger (NCX)

Sarcolemmal sodium-calcium exchanger comprises ten dimeric trans-membrane protein helices and plays an important role in removing Ca^{2+} from cells (Liao et al., 2012). This is a low affinity but high capacity pump that can move thousands of Ca^{2+} ions per second; at least ten times more than PMCA (Patterson et al., 2007). The function of NCX heavily relies on both intra and extracellular concentrations of Na^+ and Ca^{2+} because it utilises electrochemical gradient of Na^+ across the plasma membrane, leading to the influx of three Na^+ ions into the myocyte in exchange of one Ca^{2+} (Weber et al., 2003). Although normally NCX works in Ca^{2+} exodus position in some pathological conditions the exchanger works in the reverse direction i.e allowing Ca^{2+} influx. These include elevated intracellular Na^+ concentration (e.g treatment with Digoxin that inhibits Na^+ / K^+ ATPase), and abnormally

prolonged action potential and inhibition of other Ca^{2+} influx channels (Bers, 2002). A reduction in L-type Ca^{2+} current is noted in cardiomyocyte specific NCX knockout mouse model as an adaptive response to avoid Ca^{2+} overload in cardiomyocytes in the absence of NCX (Pott et al., 2007). An atrial specific NCX knockout mouse model has been reported to demonstrate disorganised and arrhythmic electric potentials with lack of P wave and burst of abnormal pacemaker activity (Torrente et al., 2015).

1.3.6 Plasma membrane calcium ATPase (PMCA)

Plasma membrane calcium ATPase belongs to the P-type transport ATPases family and constitutes one of the slow systems for removal of Ca^{2+} from cells. As opposed to NCX, PMCA is a high affinity, low capacity Ca^{2+} transport mechanism - removing 1 Ca^{2+}ion per 1 ATP molecule hydrolysed (Guerini et al., 2000). The overall amount of Ca^{2+} removed by PMCA in humans is small and is considered to be in the range 1 -1.5% (Bassani et al., 1994). Similarly, in rat ventricle myocytes PMCA is estimated to remove 1% to 2.6 % Ca^{2+}, in contrast to SERCA (87-92%) and NCX (7- 8.7%) (Bers, 2002; Negretti et al., 1993). In murine cardiomyocytes, PMCA1 is considered to remove <1% of Ca^{2+} (Hove-Madsen & Bers, 1993). Although, quantitatively PMCA1 seems to have a modest role in Ca^{2+} exodus under the basal conditions, it plays a vital role in maintaining intracellular calcium homeostasis, and studies have shown that inhibiting PMCA leads to impaired myocyte relaxation (Bers et al., 1993). PMCAs will be reviewed in detail later in this chapter.

1.3.7 Mitochondrial Uniporter (MCU)

The mitochondrial uniporter is a protein channel that facilitates the transport of Ca^{2+} into mitochondria from the cytosol. MCU has a very low affinity for Ca^{2+}; however, in the presence of microdomains of elevated Ca^{2+} concentration in the vicinity of mitochondria and SR, it is able to transport Ca^{2+} into mitochondria (Marchi & Pinton, 2014). Although, one of the key roles of MCU is to make Ca^{2+} available to the mitochondrial matrix where it is utilised in energy generation processes; it also helps in maintaining calcium homeostasis in myocytes (Contreras et al., 2010). Whilst the amount of calcium uptake by MCU is very small compared to other membrane pumps (Negretti et al., 1993); none the less, MCU deletion in cardiomyocytes has been shown to increase cytosolic $Ca^{2+}$and improved contractility under basal conditions (Drago et al., 2012). In another study, adult mice with cardiomyocyte

specific deletion of MCU were found to be protected from ischaemia-reperfusion injury and demonstrated normal basal mitochondrial Ca^{2+} levels (Kwong et al., 2015). However, MCU deleted mice were unable to immediately sprint unless warmed up for half an hour, suggesting that MCU is a critical regulator of short term mitochondrial Ca^{2+} loading which is essential for an acute stress response. Luongo and colleagues (2015) also demonstrated that cardiomyocyte specific deletion of MCU led to a reduction in the infarct size and preserved cardiac function, most likely due to a reduced oxidative stress (Luongo et al., 2015). However, the hearts of the mice lacking in MCU did not show a contractile response to β-adrenergic stimulation which suggests that MCU is required to modulate Ca^{2+} dependant stress induced cardiac response. It is likely that these responses are mediated by Ca^{2+}–calmodulin-dependent protein kinase II (CaMKII) interaction with MCU during myocardial ischaemia, reperfusion and infarction (Joiner et al., 2012) .

1.4 Calcium homeostasis in the failing heart

As outlined above, excitation-contraction coupling essential for effective function of the heart, depends upon meticulously orchestrated influx and exodus of Ca^{2+} in cardiomyocytes. In this context, is not surprising that Ca^{2+} mishandling by myocytes results in cardiac arrhythmias, systolic and diastolic ventricular dysfunction (Røe et al., 2015). It is also worth noting that voltage gated L-type Ca^{2+} channels that are responsible for Ca^{2+} influx have been targeted for pharmacological therapy in the management of hypertension, angina and cardiac dysrhythmias for decades (Godfraind, 2017). Calcium channel blocking drugs including dihydropyridines and non-dihydropyridines such as amlodipine and diltiazem selectively inhibit L-type Ca^{2+} channels thus reducing Ca^{2+} entry into vascular smooth muscle cells and cardiomyocytes, resulting in vasodilatation and reduced chronotropy respectively and are frequently used in everyday clinical practice (Gad, 2014). On the similar grounds, ion channels involved in Ca^{2+} exodus are also likely to harbour a great potential to serve as new targets in the future management of cardiovascular disease.

Failing hearts demonstrate multiple abnormalities in Ca^{2+} handling including an elevated diastolic Ca^{2+} concentration, a lower Ca^{2+} transient amplitude and prolongation of Ca^{2+} transient (Gorski et al., 2015). A number of underlying mechanisms have been identified to account for these abnormalities; including impaired inactivation of L-type Ca^{2+} channels

(LCC), down regulation of SERCA2a, increased SERCA inhibition by phospholamban, increased NCX expression, altered Na^+ regulation and defective β-adrenergic pathways are some of the possible explanations (Karwi et al., 2018; Li et al., 2016; Luo & Anderson, 2013). Some of these changes have been shown in figure 1.5.

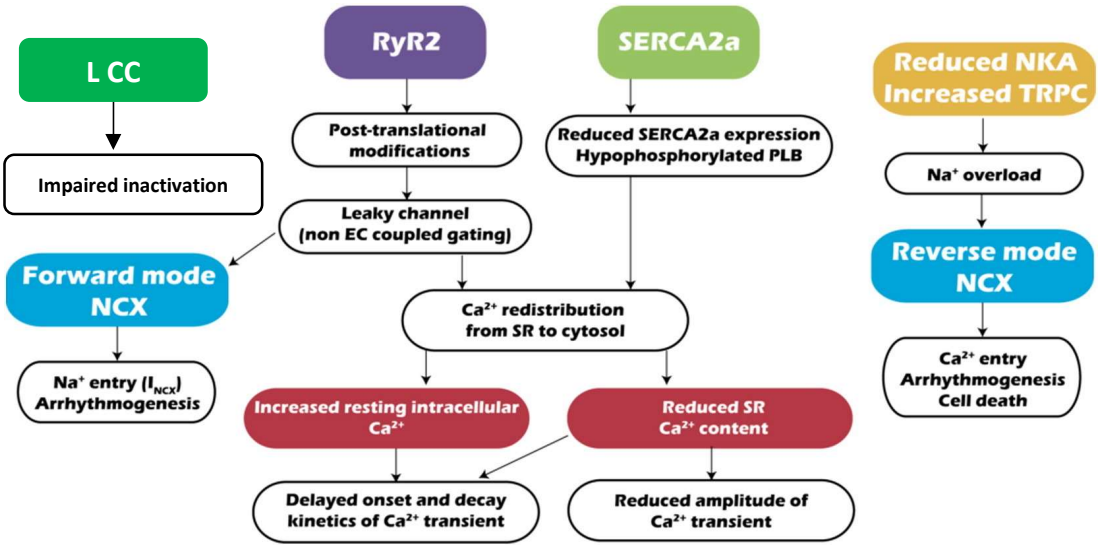

Figure 1.5: Changes in Ca^{2+} handling in the failing heart.
Ca^{2+} mishandling in heart failure : alterations in L -type Ca^{2+} channels (LCC), RyR2, SERCA, NCX and Na^+/K^+ ATPase (NKA) channels results in an impairment of Ca^{2+} and Na^+ that leads to reduced systolic function and arrhythmogenesis. (adapted from (Cho et al., 2016).

Although L-type Ca^{2+}channel (LCC) density is not increased in heart failure, since there is a blunted Ca^{2+} transient amplitude, there is a loss of Ca^{2+}dependent inactivation of LCC resulting in greater Ca^{2+}influx (Bers, 2006). Studies of animal models reveal a dysfunction of Ca^{2+} release from SR in heart failure (Durham et al., 2007; Kranias & Bers, 2007; Yano et al., 2005). There is a reduction in physical coupling between LCC and RyR2 channels due to changes in their structural relationship in heart failure, leading to Ca^{2+}leakage from sarcoplasmic reticulum (Neef & Maier, 2007). RyR2 hyperphosphorylation by protein kinase A (PKA) has been witnessed in both human and experimental heart failure models (Marx et al., 2000). In heart failure, chronically hyperphosphorylated RyR2 becomes leaky resulting in a reduction of SR Ca^{2+} load which can further reduce the contractility of the failing heart (Yano et al., 2005). HF is also associated with significant alterations in calsequestrin and SR which may be responsible for increased cytosolic Ca^{2+}in diastole (Kranias & Bers, 2007). Conversely,

over-expression of SERCA in both animal and human models has been shown to improve myocardial contractility (Eisner et al., 2013; Shanks et al., 2017). Ablation of phospholamban, hence removing SERCA inhibition also results in improved myocardial centrality and reduced LV hypertrophy (Kaneko et al., 2016).

Moreover, there are also alterations in the function of NCX in heart failure. As NCX can work in both directions, reduced Ca^{2+} transient, prolonged action potential and elevated intracellular Na^{+} lead to a reversal of NCX activity hence allowing Ca^{2+} influx into myocytes during systole (Wehrens et al., 2005). Increased Ca^{2+} influx helps minimise contractile dysfunction in heart failure; however, this also increases workload for NCX to remove this additional Ca^{2+}. Some researchers believe this to be the key factor leading to overexpression of NCX in heart failure models (Bers, 2006). Cardiac specific NCX1 knockout in mice is associated with a mild reduction in cardiac contractility despite a normal Ca^{2+} transient (Henderson et al., 2004). This may be partly due to a substantial reduction in the measurements of voltage dependant L-type Ca^{2+} currents and a difference in the morphology of action potential between wild type and NCX1 knockout myocytes; the latter lacked a plateau after initial upstroke and depolarisation.

Cardiac arrhythmias are common in patients with advanced and end stage heart failure (Lip et al., 2016). Abnormal Ca^{2+} handling is one of the root causes of cardiac rhythm abnormalities; higher Ca^{2+} leak from SR in HF can lead to spontaneous Ca^{2+}release; a well-known trigger to increase likelihood of abnormal automaticity leading to serious ventricular arrhythmias (Dridi et al., 2020). Spontaneous Ca^{2+} from Ca^{2+} overloaded sarcoplasmic reticulum leads to delayed after depolarisation (DAD) occurring after repolarisation. Three unique Ca^{2+} activated membrane currents have been implicated in the generation of DADs as a result of spontaneous Ca^{2+} release ; a Ca^{2+} -activated non-selective transient inward current, Ca^{2+} -activated Cl^{-} conductance and an electrogenic forward-mode Na^{+} /Ca^{2+} exchange current (Houser, 2000). When DADs are of sufficient amplitude, they result in action potential leading to ectopic beats. In case of conduction abnormalities, this may also cause arrythmias and fibrillation (Fozzard, 1992).

NCX overexpression in transgenic mice has been shown to cause significant impairment of excitation contraction coupling with an increased risk of heart failure (Reuter et al., 2004). Additionally, there is also evidence to suggest that myofilaments become less sensitive to

Ca^{2+} in the failing heart (Kobayashi et al., 2008). There is also an alteration in potassium (K^+) current in HF which can influence cellular Ca^{2+} regulation. Abnormalities of Ca^{2+} handling in heart failure make a research into Ca^{2+} transport and Ca^{2+} handling genes a plausible avenue to identify treatment targets for cardiac hypertrophy and failure (Siri-angkul et al., 2021).

A reduction in PMCA activity can also coexist with down regulation of SERCA and has been previously reported in cardiomyopathic hamster model (Kuo et al., 1992). More recent work on human tissue suggest closer working and cross talk between PMCA and SERCA in human health and disease contributing towards Ca^{2+} homeostasis (Boczek et al., 2021; Philippe et al., 2015).Interestingly, PMCA4 inhibition can reverse ventricular hypertrophy produced by trans-aortic constriction in murine heart (Mohamed et al., 2016). However, the despite these advancements, the role of PMCA in the failing heart remains unclear and is currently under investigation by our group. The next section is dedicated to provide a detailed review of the structure, function and regulation of PMCA along with its various roles in health and disease in human and mice.

1.5 Plasma Membrane Calcium ATPase (PMCA)

As highlighted above, PMCA is a high affinity, low-capacity calcium exodus pump that is ubiquitously expressed. It is a member of the P-type adenosine tri-phosphatase family which also includes a number of important protein channels e.g. SERCA, Na^+/K^+ ATPase and H^+ ATPase responsible for regulation of ion concentrations (Pedersen & Carafoli, 1987). PMCA was first identified over fifty years ago in red blood cells, where it assumes a central role in Ca^{2+} homeostasis (Schatzmann, 1966). However, under basal conditions, in cardiac myocytes PMCA appears to have a relatively small contribution in maintenance of cytosolic Ca^{2+} compared to SERCA and NCX (Guerini, 1998). PMCA has four isoforms which play important roles in human health and disease as described below.

1.5.1 PMCA and their relevance to human disease

Genome-wide association studies (GWAS) provide an important tool to investigate the association between genetic variants and the risk of disease (Witte, 2010). Recent advances in technology have made it possible to identify millions of single nucleotide polymorphism

(SNPs) located at specific loci across the human genome with an objective to decipher genetic basis of disease (Gibbs et al., 2003). GWAS have provided useful data regarding significance of PMCA in human health and disease by identification of mutations in genes encoding PMCA isoforms and their associations with diseases (Stafford et al., 2017), this is further elaborated in the following paragraphs.

1.5.1.1 PMCA1

As outlined in the previous sections, cardiovascular diseases lead to a significant mortality and morbidity in humans. Hypertension is a major risk factor for cardiovascular disease and is considered to be caused by genetic, environmental and life style factors (Lawes et al., 2008). Large scale human GWAS have shown mutations around Atp2b1 locus to be associated with altered blood pressure control; this is the gene that encodes PMCA1(Cho et al., 2009; Levy et al., 2009). The association between PMCA1 and hypertension seems to affect adults from Asian and European ethnicities, and can increase the life time risk of developing hypertension by 17-37% (Levy et al., 2009). Moreover, there is also emerging evidence that SNP rs12817819 at Atp2b1 is also associated with resistant hypertension in a cohort of hypertensive patients with co-existing coronary artery disease (Fontana, McDonough, Gong, El Rouby, Sa, et al., 2014). Studies on Chinese population shows that this association seems to affect children as well, and in fact, pregnant women with single nucleotide mutation rs2681472 at Atp2b1 locus are at higher risk of developing early onset pre-eclampsia – a serious condition during pregnancy presenting with hypertension, proteinuria and can lead to seizures (Wan et al., 2014; Xi et al., 2014).

In addition to this, some NSPs in the Atp2b1 also appear to increase the risk of coronary artery disease and myocardial infraction in Asian and European population (Ferguson et al., 2013; Takeuchi et al., 2015; Weng et al., 2016).

1.5.1.2 PMCA2

Studies show that PMCA2 is essential normal function of central nervous system and hearing. In mice, a spontaneous single point mutation in PMCA2 is linked with deafness and unsteadiness due to an alteration in sensory transduction in the inner ear and neurotransmitter release (Street et al., 1998). Similarly, Atp2b2 (the gene that encodes

PMCA2) mutants with mutations in PMCA's 10th transmembrane domain results in progressive hearing loss in heterozygous and severe deafness in homozygous mice (Carpinelli et al., 2013). In a case control study, gene expression profiling of lymphoblasts from individuals with autism (a neurodevelopmental disorder with a strong genetic underpinning and a wide phenotype spectrum) and their healthy siblings demonstrated Atp2b2 to be differentially expressed in these two cohorts (Hu et al., 2009). GWAS on families with autism have identified single nucleotide polymorphism in PMCA2 gene (Atp2b2) with some of them limited to male gender and other affecting females too (Carayol et al., 2011; Prandini et al., 2012). It is therefore concluded that Atp2b2 has a role in nervous system development and function, most likely through regulation of intracellular Ca^{2+} homeostasis and its influence on Ca^{2+} mediated signalling in neurons (Krey & Dolmetsch, 2007).

1.5.1.3 PMCA3

As described above, PMCA3 is encoded by Atp2b3 gene and its expression restricted to central nervous system. Mutations in this gene have been linked with X-linked cerebellar ataxia – a hereditary condition resulting in unsteadiness and poor coordination (Zanni et al., 2012). The sequencing of protein-coding genes in a patient with cerebellar ataxia demonstrated a mutation in the calmodulin binding domain of PMCA3 with subsequent evidence of impaired Ca^{2+} clearance in human cultured cells (Calì et al., 2015). Additionally, Atp2b3 mutation has also been detected in tissues from aldosterone producing adenoma, a condition that can lead to the development of secondary hypertension, suggesting that this isoform may have a role in non-neuronal endocrine tissue, too (Beuschlein et al., 2013).

1.5.1.4 PMCA4

GWAS have shown that single nucleotide polymorphisms (SNP) in Atp2b4 result in development of resistance to malaria in West African children. Because, PMCA4 is the main Ca^{2+}extrusion pump in erythrocytes, it is considered that an alteration in its structure and expression may result in an impaired intra-cellular Ca^{2+} homeostasis, thus having a detrimental effect on the parasite reproduction within the red blood cells (Timmann et al., 2012). Another SNP (rs10900585) in Atp2b4 has been found to reduce infection by a severe form of malaria (Plasmodium Falciparum) by nearly two third (Bedu-Addo et al., 2013). An

SNP in Atp2b4 has also been linked with spastic paraplegia, most likely due to an abnormal Ca^{2+} homeostasis in neuronal cells resulting from impaired PMCA4 function (Ho et al., 2015)

1.5.2 PMCA in the cardiovascular system

PMCA1 and 4 have largely a ubiquitous expression in human and mice issues. While in most tissues PMCA1 is found in relative abundance compared to PMCA4, these isoforms are found in equal ratios in the heart and play significant role in functioning of cardiovascular system (Stauffer et al., 1993). The early and ubiquitous expression of PMCA1 suggests that it has an important role in Ca^{2+} clearance from cytosol and it assumes a housekeeping role. Global knockout of PMCA1 is embryonic lethal (Prasad et al., 2004). Although it seems to have a minor role in Ca^{2+} extrusion at basal conditions in heart; however cardiac specific NCX knockout in mice showed that cardiac Ca^{2+}homeostasis and cardiac function was preserved into adulthood due to an upregulation of PMCA expression (Hurtado et al., 2005). Similar results were seen in SERCA2 knockout mice (Louch et al., 2010). This evidence suggests that although cardiac PMCA plays a minor role in Ca^{2+}export at basal levels, it has a great ability to adapt and upregulate itself at the time of stress when other Ca^{2+} clearing mechanisms fail, hence serving as a backup system in the Ca^{2+} homeostasis in heart, in addition to its important contribution in signal transduction.

While PMCAs have a minor role in Ca^{2+} extrusion from cardiac cells compared to NCX and SERCA; in vascular smooth muscle cells, PMCA is responsible for transporting significantly more amounts of Ca^{2+} contributing to vessel relaxation in conjunction with SERCA (Pritchard et al., 2010). It would not come as a surprise that vascular smooth muscle cell specific PMCA1 knockout mice showed significantly higher systolic blood pressure. These mice were also found to have increased phenylephrine induced centrality in their femoral rings and cultured vascular smooth muscle cells from these animals showed an increased Ca^{2+}concentrations (Kobayashi et al., 2012) . A number of GWAS (as highlighted above) have reported PMCA1's role in hypertension in humans, as well. Additionally, it has been reported that myometrial vessels in pre-eclamptic women showed a significant impairment of Ca^{2+}clearance resulting in poor vessel relaxation; inhibition of PMCA with carboxyeosin normal myometrial vessels mimicked the changes seen in pre-eclampsia. Authors suggested that increased peripheral resistance and hypertension in pre-eclapmsia may be mediated through reduced expression of PMCA in the vessels (Wimalasundera et al., 2010). Interestingly, PMCA's role in peripheral

vasculature is not limited to PMCA1; PMCA4 overexpression in mice results in hypertension, which is mediated by a reduced production neuronal nitric oxide (nNOS) – a potent vasodilator. Previous work from our group has demonstrated that mice with reduced expression of PMCA1 in a heterozygous global PMCA1 deletion model develop significantly elevated blood pressure at 12 months age compared to the age matched wild type controls (Little et al., 2017). In this study, heterozygous global deletion of PMCA1 led to an increased vessel wall and narrowing vessel lumen with ageing. Hypertension is a frequent and well established risk factor for heart failure (Oh & Cho, 2020), which makes this finding of a particular significance to the current peace of research.

In addition to the impact on peripheral vasculature, reduction in the expression of PMCA is also known have an effect on cardiac structure and function. Hearts of mice with cardiomyocyte specific deletion of PMCA1 were found to be at a higher risk of cardiac rhythm abnormalities and were more susceptible to atrial arrhythmias under programmed electrical stimulation which confirms that PMCA1 is required for electrical stability of atria (Wang et al., 2017; Wilson, 2017). PMCA4 has also been found to be involved in regulating the sodium channel ($Na_v1.5$) activity mediated by nNOS pathway resulting in Long QT syndrome – an arrhythmogenic condition associated with syncope and sudden cardiac death (Cheng et al., 2009). The authors demonstrated that α-1 syntrophin connects the cardiac sodium channel ($Na_v1.5$) α subunit to the PMCA4-nNOS complex where the later has an inhibitory role on the sodium channels. Mutations in α-1 syntrophin led to a release in the inhibition of neuronal nitric oxide synthase by PMCA4b resulting in an accentuation of peak and late sodium current via nitrosylation of the cardiac sodium channel.

In a separate research project aimed to explore the differences in murine heart after myocardial infarction created by the ligation of left anterior descending artery, colleagues from our group have previously shown that global heterozygous deletion of PMCA1 offers a protective role in the immediate post MI period. Hearts from PMCA1 mice showed a smaller infarct size and reduced frequency of cardiac arrhythmias one week after MI compared to their wild type counterparts (Stankovikj, 2017).

Of particular relevance here is the PMCA's role in regulation of myocardial hypertrophy. PMCA4 is known to attenuate calcineurin-NFAT signalling and its overexpression reduces pathological remodelling in heart (Wu et al., 2009a). Interestingly, our group have recently found that PMCA4 is involved in regulation of cardiac hypertrophy by pathways other than

the one described above; PMCA4 deletion in cardiac fibroblasts results in an increased secreted frizzled related protein-2 (sFRP2) which inhibits Wnt signal transduction pathway (Mohamed et al., 2016). This study shows that as a result, PMCA4 deletion in cardiac fibroblasts not only protects against myocardial hypertrophy after long term pressure overload generated by trans-aortic constriction but it also reverses an established hypertrophy in mouse models. Furthermore, the argument for PMCA4's role in regulation of hypertrophy is strengthened by the report that PMCA4 ablation was shown to prevent development of spontaneous hypertrophy in a mutant mouse model of hypertrophic cardiomyopathy (Prasad et al., 2014). Moreover, PMCA4 also interacts with dystrophin family of proteins (Williams et al., 2006), which are found to be reduced in dilated cardiomyopathy and myocarditis. In addition, overexpression of PMCA4b in vivo shows a reduced β adrenergic contractile response (Mohamed et al., 2009).

Whilst, reduced expression of PMCA1 is associated with elevated blood pressure with ageing, as described above (Little et al., 2017); little is known about its role in cardiac hypertrophy and failure making it an interesting research subject as a therapeutic target. Caloxin1b3 is a novel selective inhibitor of PMCA1 which has a great affinity to bind PMCA1 and is shown to increase cytosolic Ca^{2+} in vascular endothelium (Szewczyk et al., 2010). The discovery of selective inhibitor makes PMCA1 a prime candidate for heart failure research which can be successfully targeted by pharmacological therapy, as well.

1.5.3 The structure of PMCA

The PMCA comprises 10 hydrophobic trans-membrane domains and two cytosolic loops spanning between domains 2-3 and 4-5, with a cytosolic NH2 tail on one end and a COOH tail on the other (Monteith et al., 1998; Strehler et al. 2001). The COOH terminal is considered to be the functionally most important component of the PMCA; it contains the auto-inhibitory calmodulin (CaM) binding motif that interacts with auto-inhibitory regions on the cytosolic loops in the absence of Ca^{2+}/ CaM during low intracellular Ca^{2+} concentrations rendering the pump in a close state, as shown in figure 1.6 (Bruce, 2018). However, when intracellular Ca^{2+} is elevated, Ca^{2+}/ CaM bind to the CaM binding motif on COOH terminus releasing its auto-inhibitory effect and changing the pump to an 'open' conformation which increase its affinity for Ca^{2+}hence initiating Ca^{2+}exodus from the cell

(James et al., 2015). This terminal also contains sites that are involved in regulating protein kinase C (PKC) and protein kinase A (PKA). A PDZ binding motif is also located on the COOH terminal that increases PMCA activity by its dimerization and also plays a role in recruitment of scaffolding proteins, actin cytoskeleton and signalling complexes (DeMarco et al., 2002; DeMarco & Strehler, 2001). Structural studies have shown that PMCA is located in caveolae which are invaginations in the plasma membrane, along with Na^{+} /Ca^{2+} exchanger (Zhang et al., 2009).

The amino acid sequence on the NH2 terminus of PMCA exhibits the most diversity amongst its various isoforms. The cytosolic loop between 4^{th} and 5^{th} transmembrane domains contains conserved aspartate and lysine residues responsible for catalytic phosphorylation and ATP binding respectively (Falchetto et al., 1992). As discussed in the later paragraphs, PMCA isoforms display some variations in the NH2 and COOH terminals; however, approximately 90% of primary sequence of the enzyme is conserved (Strehler et al., 2007). While there is structural diversity in PMCA amongst different species; rodent and human PMCA isoforms exhibit nearly 99% sequence homology. As mentioned about PMCA has 4 isoforms and the structural diversity of PMCA isoforms underpins their ability to perform a versatile range of functions in different tissues (Strehler et al., 2007).

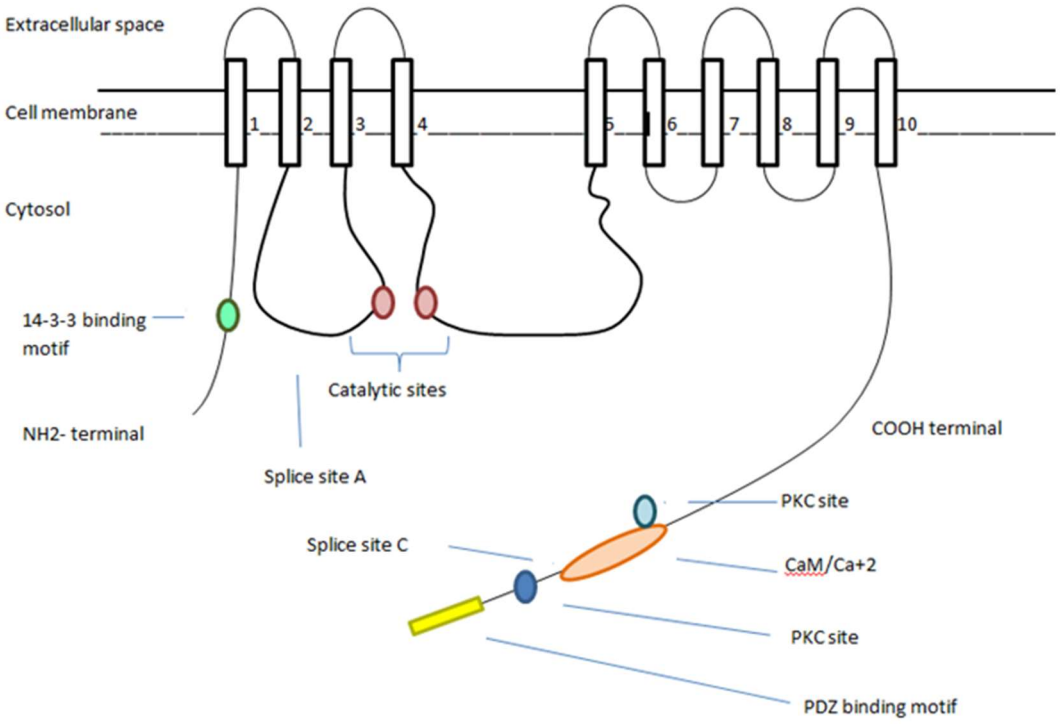

Figure 1.6: A schematic diagram representing the structure of PMCA and its binding sites. Calcium-calmodulin complex is formed upon an increase in cytosolic Ca^{2+} which then binds to Ca^{2+} /CaM-binding site leading to activation of PMCA. COOH terminal also contains binding sites for PKA, PKC and PDZ. Catalytic sites are present on two cytosolic loops while the N-terminal contains 14-3-3 binding motif. Splice site A is present between the 2nd and 3rd cytosolic loop and spice site C is located at the COOH terminal (adapted from Bruce, 2018).

1.5.4 Regulation of PMCA

Thus far, a number of regulators of PMCA function have been identified; these include the major regulator calmodulin (CaM) and a number of mediators with a relatively minor role in its regulation including acid phospholipids, unsaturated fatty acids and trypsin (Niggli et al., 1981). As highlighted above, CaM binds to PMCA's cytosolic domain conforming it to the open or activated form by releasing its auto inhibition. This results in approximately six-fold increase in its affinity for Ca^{2+} (Enyedi et al., 1987). PMCA affinity for CaM varies in its different isoforms, PMCA2 and 3 have approximately five to ten fold higher affinity for CaM compared to other isoforms (Brini & Carafoli, 2009). In addition, CaM may also indirectly modulate PMCA activity by activation of CaMKII (Hoshijima, 2005).To date, erythrocyte PMCA is the only form that is known to be activated by variations in the cytosolic Ca^{2+} levels

even in the absence of CaM (Elwess et al., 1997). Phosphoinositide4, 5-biphosphate(PIP_2) is another activator of PMCA and responsible for nearly half of its basal activity (Lopreiato et al., 2014). It has also been reported that PMCA phosphorylation by protein kinase C (PKC) and PMCA1 isoform phosphorylation by protein kinase A (PKA) also increases pump activity, albeit to modest levels (Elwess et al., 1997; Guerini et al., 2003).

1.5.5 PMCA isoforms and their expression in embryonic and adult life

There are four isoforms of PMCA , PMCA1 - 4 which are encoded by specific genes Atp2b1-4 located at human chromosomal loci 12q21-q23, 3p25-p26, Xq28 and 1q25-q32; whereas, in mice these genes are found on chromosomes loci 10C3, 6E3, XA7.3 and 1E4 (Strehler & Zacharias, 2001). In both humans and mice adults, PMCA 1 and 4 are expressed ubiquitously and PMCA2 and 3 have a tissue specific expression (Hammes et al., 1998; Stafford et al., 2017). PMCA2 is restricted to cerebellum, cochlear hair cells, liver, kidney, uterus and mammary glands (Furuta et al., 1998; Reinhardt & Horst, 1999; Stahl et al., 1992). PMCA3 is only found in brain. In addition to these isoforms, alternative splicing at a site between 2^{nd} and 3^{rd} cytosolic loop (site A) and at calmodulin binding region on the C terminal end (site C) results in over 25 splice variants of PMCA (Stauffer et al., 1993). These splice variants possess changes in their amino acid sequence at the C terminal end and are further subdivided into 'splice form *a*' and 'splice form *b*' based upon presence or absence of exons (Di Leva et al., 2008). Of these variants, 'splice form *a'* follows a tissue specific distribution while 'spice form *b'* is ubiquitously expressed and seems to have housekeeping functions (Stafford et al., 2017). Tissue specific PMCA splice variants are considered to have unique membrane localisation, functional characteristics and signalling properties (Domi et al., 2007). These splice variants undertake a range of functions in these tissue such as supporting wound healing in corneal epithelium by altering the Ca^{2+} homeostasis (Talarico & Mangini, 2007) and rapid extrusion of Ca^{2+} from the hair cells of inner ear to maintain their responsiveness to sound stimulation (Yamoah et al., 1998). Adult brain is probably the only tissue that expresses all isoforms and splice variants of PMCA (Boczek et al., 2019). PMCA1b and PMCA4b are the most prevalent splice variants found in tissues (Keeton et al., 1993; Stahl et al., 1992).

Over the last couple of decades little attention is paid to better understand the PMCA's expression during development of the embryo. Animal studies using in-situ hybridisation technique demonstrate that expression of PMCA isoforms in the embryonic life takes place in a stepwise fashion. The ubiquitous PMCA1 is the first isoform expressed as early as 9.5 days post conception (dpc) in mice with the highest concentration in brain by 18.5 dpc. The remaining isoforms start their expression at around 12.5 dpc. The expression of PMCA 2 is confined to the nervous system by 16.5 dpc. PMCA3 is first detected at 12.5dpc and initially has a widespread expression but by 16.5 dpc, it is restricted to the brain. PMCA 4's ubiquitous expression starts at 12.5 dpc and continues to increase all the way to birth and even in the post-natal period (Zacharias & Kappen, 1999). The work carried out by our group suggests that PMCA1 is most probably expressed earlier in the embryonic life than described above; this is supported by the fact that global deletion of PMCA is embryonic lethal and leads to intrauterine death embryos earlier than 9.5 days post conception.

1.5.6 PMCA and the intracellular Ca^{2+} dynamics

In addition to PMCA's contributions to maintenance of global intracellular Ca^{2+} concentration; it also plays an important part in the regulation of local intracellular Ca^{2+} dynamics by producing sub-sarcolemmal micro-domains of lower Ca^{2+} levels. This is how PMCA is able to influence the downstream signalling pathways and can negatively regulate Ca^{2+} dependent signalling molecules (Stafford et al., 2017). By using a novel fluorescent indicator fusion protein PMCA4-GCaMP2 in cardiomyocytes, our group have previously demonstrated the evidence of sub-plasmalemmal Ca^{2+} levels changes in the vicinity of PMCA4 location in rat cardiomyocytes (T. M. A. Mohamed et al., 2013). In addition to this, it has also been suggested that PMCA may also influence the pH and ATP concentration of the sub-plasmalemmal compartment leading to a further impact on the major signalling pathways in heart (Daugirdas et al., 1995; Tiffert & Lew, 2011).

1.5.7 PMCA interaction with signalling proteins

PMCA plays a major role in regulation of Ca^{2+} dependant signalling molecules by creating low Ca^{2+} sub-sarcolemmal microdomains and protein- protein interactions (Oceandy et al., 2011a). As seen in the figure 1.4, some of these interactions take place at the PDZ Motif at the COOH terminal while the others occur at the NH2 terminal. Membrane associated

guanylate kinase (MAGUK), calcium-calmodulin dependant serine protein kinase (CASK), LIM family protein CLP36, PMCA-interacting single PDZ protein (PISP), Na/H exchanger regulator factor 2 (NH-ERF2) and neuronal nitric oxide (nNOS) interact on the COOH terminal of PMCA whereas trafficking protein 14-3-3 interacts with NH2 terminal (DeMarco & Strehler, 2001; Goellner et al., 2003; Rimessi et al., 2005; Kai Schuh et al., 2001). Some of these interactions are common to all PMCA isoforms whilst the others are restricted to specific isoforms.

As the focus of this piece of work is heart failure, it is of relevance that PMCA is also known to interact with mediators of hypertrophy; an overexpression of PMCA4 in human embryonic kidney cells (HEK293) has been shown to attenuate Ras-mediated signalling (Armesilla et al., 2004). PMCA4 overexpression has also been found to have an inhibitory effect on nuclear factor of activated T-cells (NFAT) signalling eventually resulting in a reduction of pathological myocardial remodelling (Wu et al., 2009). It may be the structural and biochemical diversity of PMCA isoforms that dictates the nature of its interactions and subsequently determines its interacting partners.

In view of the evidence presented above, it is obvious that PMCA isoforms play a spectrum of diverse roles in the cardiovascular system ranging from their involvement in regulation of myocardial hypertrophy, heart failure, hypertension, cardiac arrhythmias and Ca^{2+} homeostasis. This project will build on the work previously carried out by our group on characterisation of PMCA1's role in heart failure and will further explore the cellular and molecular pathways involved in the development of decompensated systolic dysfunction in $PMCA1^{cko}$ mice.

1.6 Conclusion

Undoubtedly, cardiovascular disease remains a major cause of morbidity and mortality worldwide. Heart failure is a common condition with an increasing prevalence and involves approximately half a million people living in UK. Current treatment modalities offer modest improvements in mortality and quality of life for this patient cohort. Cardiac hypertrophy often precedes the development of decompensated heart failure. PMCA isoforms have emerged as major players in cardiovascular physiology with an array of diverse roles. In order to explore new therapeutic targets for heart failure, it is absolutely essential to investigate the role of PMCA1 in heart failure.

1.7 Hypothesis

As outlined in the previous sections, genome wide association studies have shown a link between hypertension and PMCA1 (Fontana et al., 2014; Levy et al., 2009). Additionally, previous published work from our lab provides functional evidence of this link by demonstrating the development of hypertension in mice with reduced levels of PMCA1 at the age of twelve months (Little et al., 2017). Moreover, work from our group has also shown that reduced expression of PMCA1 increases the risk of cardiac arrhythmias (Wang et al., 2017; Wilson, 2017). Chronically elevated blood pressure and cardiac arrhythmias are both associated with a higher risk of developing heart failure. Hence, based on our current understanding of the role of PMCA1, it is hypothesised that reduced levels of PMCA1 will increase the risk of the development of heart failure in mice.

1.8 Objectives of this research project

1. Determine whether reduced expression of PMCA1 predisposes mice to heart failure
2. Characterise cardiovascular remodelling in PMCA1 mutant mice as a result of pathophysiological stress.
3. Investigate the mechanism by which deletion of PMCA1 may lead to heart failure.

Chapter 2 - Materials and methods

2.1 Animals

Mice used in this project were housed in University of the Manchester's secure and pathogen free facility incorporating a 12 hours dark/ light cycle with *ad libitum* access to food and water. Animal studies were performed in accordance with the United Kingdom Animals (Scientific Procedures) Act and following local guidelines set by University of the Manchester Ethics Committee.

The Cre/LoxP system gene targeting system was previously used in our laboratory to generate PMCA$^{F/F}$ mice in which LoxP sites were used to flank exon 2 of PMCA1 (Ryan et al 2015). Generation of PMCA1$^{F/F}$ mouse line is explained schematically in figure 2.1. Only male mice were used for this research project, previous work from our group shows no difference in the cardiac structure and function between male and female sex in these mouse lines (Wilson, 2017).

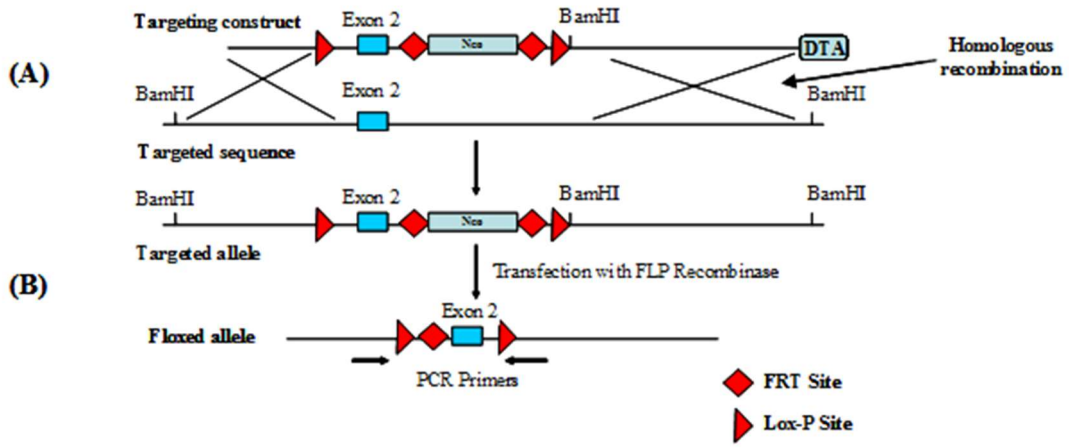

Figure 2.1 : The schematic illustration of the Cre/LoxP system.

The targeting construct comprises two LoxP sites flanking exon 2 of PMCA1, a short 5` arm homology of 1.7 kb, a neomycin resistance gene (neo) flanked by FRT sites, a long (5.7 kb) 3`homology arm, a diphtheria toxin A (DTA) expression cassette and an exogenous *BamHI* restriction site. This construct undergoes homologous recombination in the embryonic stem cells to produce the targeted allele (A) which is then transfected with FLP recombinase to remove neo cassette and give the PMCA1$^{F/F}$ allele (B). Figure taken from Ryan *et al.*, 2015.

From the PMCA1$^{F/F}$ line two further lines were generated and used in this thesis, (1) Global heterozygous deletion of PMCA1 (PMCA1^{HT}) and (2) cardiomyocyte specific PMCA1 knock out mice (PMCA1^{cko}).

Global heterozygous deletion of PMCA1 ($PMCA1^{HT}$) was achieved by crossing $PMCA1^{F/F}$ mice with CMV-Cre mice as detailed in Little *et al.*, 2017. It should be noted that total deletion of PMCA1 is embryonic lethal. Generation of this mouse line is shown in figure 2.2.

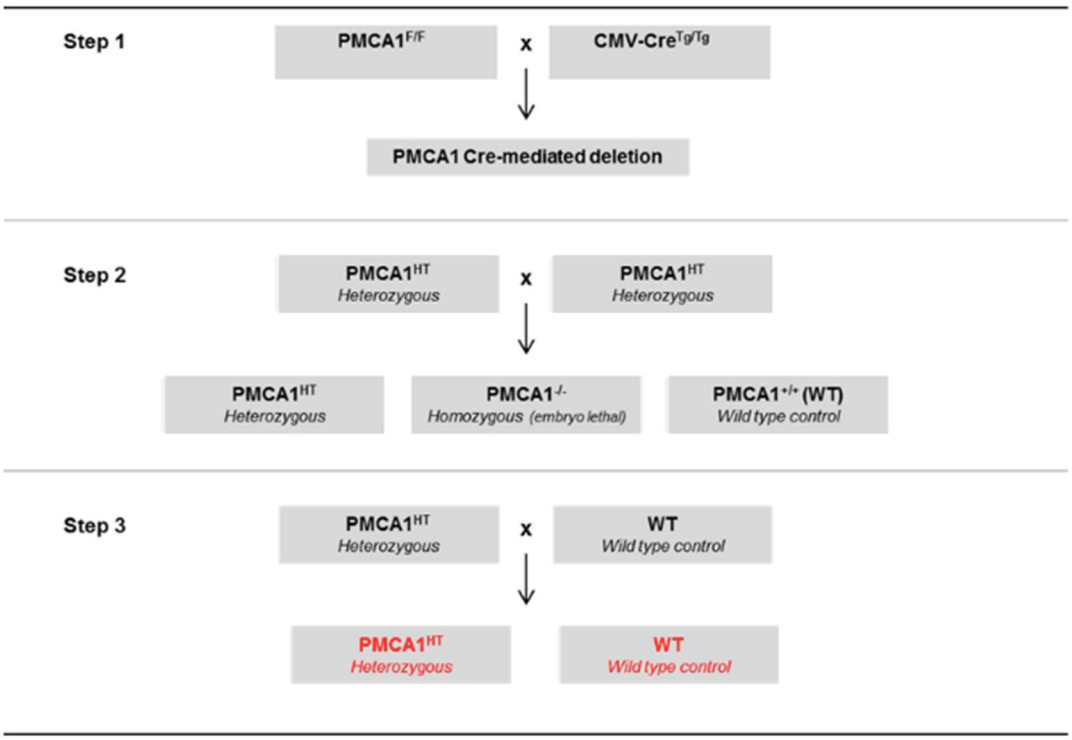

Figure 2.2: The breeding strategy for heterozygous and homozygous global deletion models of PMCA1.

In step1, homozygous mice carrying *LoxP* sites ($PMCA1^{F/F}$) were crossed with CMV-$Cre^{Tg/Tg}$ to derive heterozygous mice carrying one wild type and single floxed allele of PMCA1 (CMV-Cre/$PMCA1^{F/+}$). In step 2, CMV-Cre/$PMCA1^{F/+}$ mice were bred to generate CMV-Cre^{Tg}/$PMCA1^{F/+}$ (heterozygous), CMV-Cre^{Tg}/$PMCA1^{F/F}$ (homozygous) and CMV-Cre^{Tg}/$PMCA1^{+/+}$ (wild type/controls). Homozygous PMCA1 knockout mice (CMV-Cre^{Tg}/$PMCA1^{F/F}$) were found to be embryonic lethal. In step 3, heterozygous mice were crossed with wild type (WT) mice resulting in litters containing only heterozygous and wild type mice which would be used as littermate controls.

Cardiomyocyte-specific PMCA1 knock out mice ($PMCA1^{cko}$) were generated by crossing $PMCA1^{F/F}$ mice with mice expressing Cre-recombinase driven by the αMHC promoter (Agah et al., 1997; Wang et al., 2017). This is shown in figure 2.3.

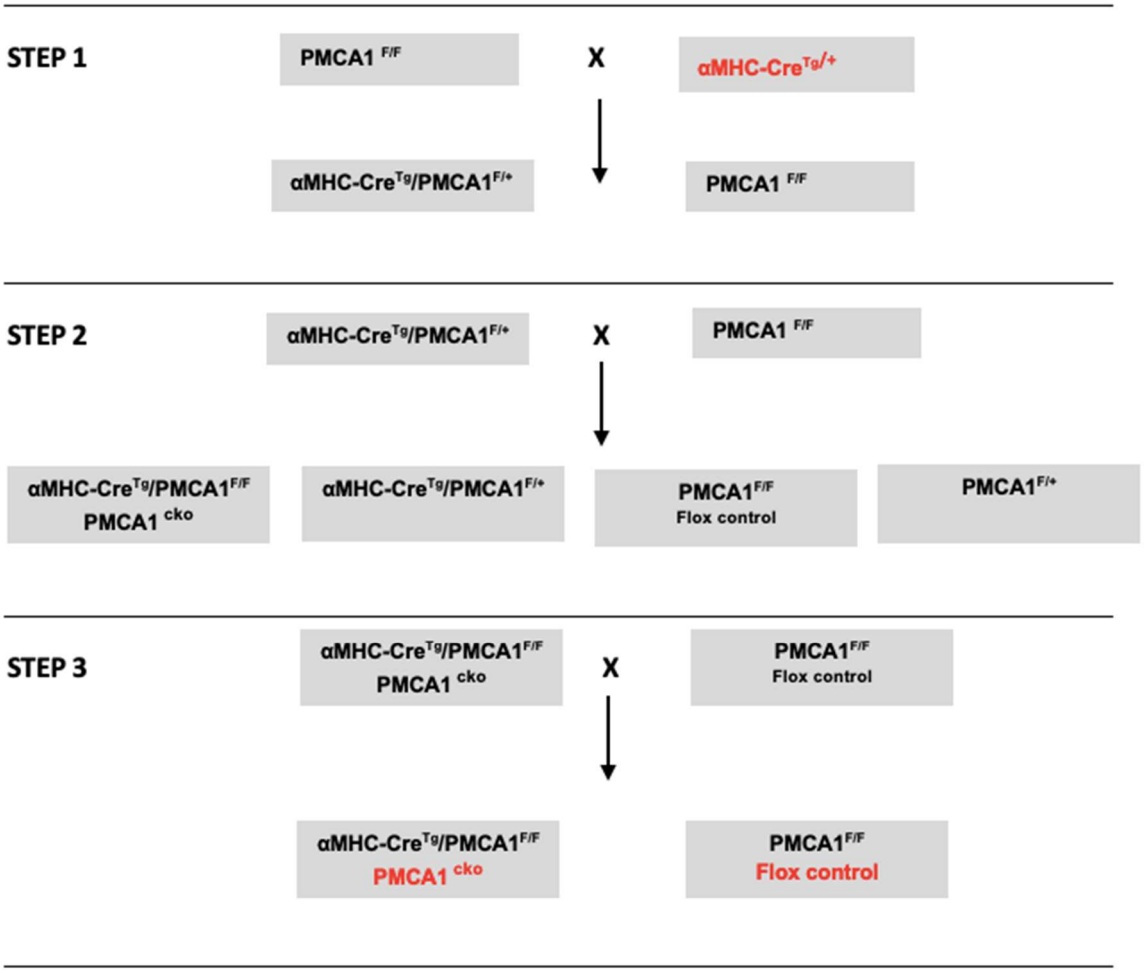

Figure2.3 : Breeding strategy for the generation of PMCA1^{cko} animals and controls.

Step 1: PMCA1$^{F/F}$ mice were crossed with mice expressing the αMHC-Cre only (αMHC-Cre$^{Tg/+}$). The resulting mice were heterozygous in relation to PMCA1 and either carried the αMHC-Cre transgene (αMHC-Cre^{Tg}/PMCA1$^{F/+}$) or did not (PMCA1$^{F/+}$). Step 2: αMHC-Cre^{Tg}/PMCA1$^{F/+}$ mice from step 1 were crossed with PMCA1$^{F/F}$ mice resulting in 4 different types ; αMHC-Cre^{Tg}/PMCA1$^{F/F}$, αMHC-Cre^{Tg}/PMCA1$^{F/+}$, PMCA1$^{F/F}$, PMCA1$^{F/+}$. Step 3: αMHC-Cre^{Tg}/PMCA1$^{F/F}$ mice generated in step 2 were crossed with PMCA1$^{F/F}$ to result in the final offspring: mice carrying a cardiomyocyte-specific PMCA1 deletion (PMCA1^{cko}, αMHC-Cre^{Tg}/PMCA1$^{F/F}$) and littermate controls (PMCA1$^{F/F}$).

2.1.1 Confirmation of successful deletion of PMCA1 in PMCA1^{HT} and PMCA1^{cko} models

PMCA1 is known to be a house keeping gene and its homozygous global deletion is embryonic lethal, very early in the foetal development (Okunade et al., 2004). Little and colleagues have previously demonstrated that global heterozygous deletion of PMCA1 leads to approximately 45- 55% lower expression of PMCA1 mRNA in heart, brain, kidney and aorta (Little et al., 2017). The authors also found significantly lower expression of PMCA1

protein in these organs of PMCA1^{HT} mice. The present study also found a significantly lower expression of PMCA1 mRNA in these mice and this is described in detail in chapter 3.

Wang and colleagues (2017) demonstrated a significantly lower expression of PMCA1 protein in the cardiac tissue of PMCA1^{cko} mice compared to the PMCA1$^{F/F}$ mice by western blot assay (Wang et al., 2017). The authors confirmed this finding by immunohistochemical straining of cardiac tissue, as well.

Previous unpublished work from our group (Dr Nick Stafford- personal communication) also shows significantly lower expression of PMCA1 protein in the cardiomyocytes of PMCA1^{cko} mice. The following data has kindly been provided by Dr Nick Stafford (Post-doctoral research associate) from Prof Cartwright's group (University of Manchester). Protein extracts from the lysates from cardiomyocytes from PMCA1^{cko} and PMCA1$^{F/F}$ animals were assessed by western blot analysis. The membranes were probed with rabbit anti-PMCA1 antibody (140kDa) and mouse anti- α-tubulin was used as loading control; 55 kDa.

The data presented in the figure 2.4 shows an intense band of PMCA1 in PMCA1$^{F/F}$ animals at 140kDa and a very faint band in PMCA1^{cko}. The quantification (B) confirms that PMCA1^{cko} cardiomyocytes had significantly (62.9 % ± 14) lower levels of PMCA1 protein compared to the PMCA1$^{F/F}$ animals ($p<0.05$). These data confirm that cardiomyocyte specific deletion of PMCA1 leads to approximately a two third lower levels of PMCA1 in PMCA1^{cko} animals and forms a strong basis for this experimental model.

A

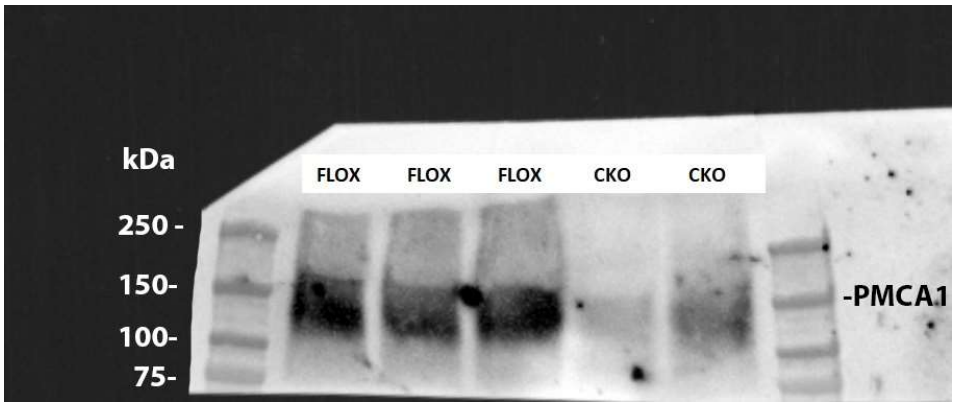

B

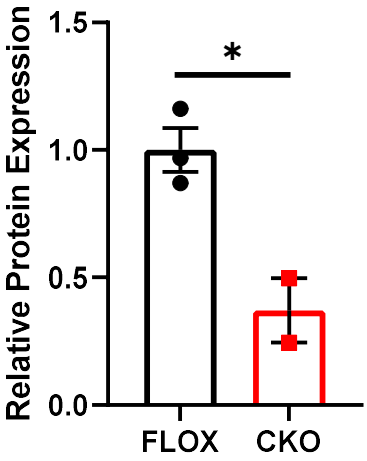

Figure 2.4 : PMCA1 protein levels in PMCA1^{cko} cardiomyocytes.

(A) Western blot analysis of lysate from neonatal rate cardiomyocytes. PMCA1 band seen at 140kDa in PMCA1$^{F/F}$ cohort. (B) Quantitative analysis of band density of western blot from PMCA1^{cko} and PMCA1$^{F/F}$ cardiomyocytes. (n= 3 in PMCA1$^{F/F}$ and n=2 in PMCA1^{cko})

Data presented as mean ± SEM with unpaired t-test used for analysis. (*$p < 0.05$) FLOX = PMCA1$^{F/F}$ CKO = PMCA1^{cko}

Data provided by Dr Nick Stafford.

2.2 Genotyping of animals

Genotyping of the mice was performed as per the following steps.

2.2.1 DNA extraction from ear tissue biopsies

Ear tissue biopsies were taken from mice and stored at -20^{0}C. On the day of DNA extraction, tissue biopsies were thawed and incubated in 200 µl lysis buffer (50 mM Tris-HCl pH 8, 100 mM EDTA, 0.5% SDS) and 10 µl proteinase K (20mg/ml) at 56^{0}C for 6 – 8 hours. The digested products were centrifuged at 13000 rpm at room temperature for 10 minutes. The supernatant was transferred to a new labelled microfuge tube and 300 µl of isopropanol was added (an amount equivalent to the supernatant). Samples were centrifuged for 5 minutes at 13000 rpm at room temperature to precipitate the DNA. The supernatant was discarded, and the remaining DNA pellet was washed in 100 µl of 70% ethanol and centrifuged for 5 minutes at 13000 rpm at room temperature. The supernatant was discarded, and the pellet was left to air dry at room temperature. After drying, the pellet was re-suspended in 50-200 µl of DNAse / RNAse free H_2O (based upon the pellet size). The DNA samples were stored at 4°C until required for further analysis.

2.2.2 Polymerase Chain Reaction (PCR) genotyping

For PMCA1 heterozygous mice (PMCA1^{HT}) PCR, the DNA (1 µl; 1:10 diluted) was added to 29 µl of previously prepared reaction mixture consisting of 0.9 µl of 10 µM forward primer, 0.9 µl of 10 µM reverse primer, 0.3 µl of 25 mM magnesium acetate, 12.2 µl of sterile water and 15 µl of Phusion Green High-Fidelity master mix (Thermofisher). A negative control sample was used with 1 µl of sterile water instead of DNA. A Venti^{TM} 96-well thermal cycler (Applied Biosystems) was used following the programme detailed in figure 2.5 C. The expected amplicon size for WT allele is 6662 bp and for the mutant allele 4703bp. This has been illustrated in figure 2.5 A and B. The primer pair sequences and the product sizes used for the PCR genotyping PMCA1^{HT} mice have been described in table 2.1.

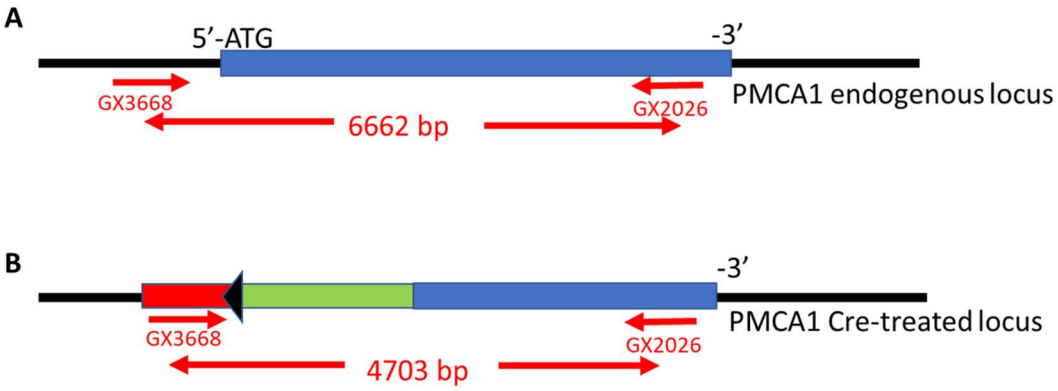

C

Step	Temp.	Duration	Cycle(s)
Denaturing	98^{0}C	3 min	X 1
Denaturing	98^{0}C	0.3 min	X 35
Annealing	72^{0}C	0.3 min	
Extension	72^{0}C	6 min	
Completion	72^{0}C	7 min	X 1
Hold	4^{0}C	∞	

Figure 1.5: The illustration of PCR amplification during genotyping of PMCA1^{HT} mice.

(A) In WT mice, PCR reaction using GX2026 (forward) and GX3668 (reverse) primers produced amplicon size of 6662 bp whilst in PMCA1^{HT} mice (B) the expected size of the amplicon is 4703 bp (C) Thermal cycling conditions for PMCA1^{HT} PCR.

Primer	Primer Sequence 5' - 3'	Expected PCR product size (bp)	
		Wild Type allele	Excised Allele
PMCA1^{HT} Forward	AGGTGGCTTTAAGACCAGAAACAGGACAGG	6662	4703
PMCA1^{HT} Reverse	CTGTGGAGTACATGCTTCGTTCTGC		

Table 1.1: Primer pair sequences and product sizes used for genotyping reactions in PMCA1^{HT} mice.

For cardiomyocyte-specific PMCA1 knock out mice (PMCA1^{cko}) PCR, genotype analysis was undertaken to amplify the targeted DNA regions, in order to identify the insertion of lox-P sites and any Cre-mediated excision.

The mouse prepared DNA (1 µl) was added to 24 µl of reaction mixture consisting of 1 µl of forward primer, 1 µl of reverse primer, 0.3 µl of 25 mM magnesium acetate, 12 µl of sterile water and 15 µl of Q-Load 2X master mix (New England Bio Lab). A negative control sample was used with 1 µl of sterile water instead of DNA. A Venti^{TM} 96-well thermal cycler (Applied Biosystems) was used following the programme detailed in table 2.2.

Step	Temp.	Duration	Cycle(s)
Denaturing	95^{0}C	0.3 min	X 1
Denaturing	95^{0}C	0.3 min	X 35
Annealing	57^{0}C	1 min	
Extension	68^{0}C	0.5 min	
Completion	68^{0}C	5 min	X 1
Hold	4^{0}C	∞	

Table 1.2: Thermal cycling conditions for PMCA1^{cko} PCR.

The primer pair sequences and the product sizes used for the PCR genotyping PMCA1^{cko} mice have been described in table 2.3.

Primer	Primer Sequence 5' - 3'	Expected PCR product size (bp)	
		Floxed allele	Excised Allele
PMCA1^{cko} Forward	CCAGAGACCATTCATGGCTTCTACC	3449	1300
PMCA1^{cko} Reverse	AATGCTCTCTGAGCGTATGGTCTGG		
αMHC Cre^{Tg} Forward	ATGACAGACAGATCCCTATCTCC	Absent	Cre - 250
αMHC Cre^{Tg} Reverse	CTCATCACTCGTTGCATCGAC		

Table 1.3: Primer pair sequences and product sizes used for genotyping reactions in PMCA1^{cko} mice.

2.2.3 Gel electrophoresis of PCR products

Amplified PCR products and HyperLadder™ (Bioline) DNA ladder were run on 0.6-1.5% agarose gel based upon the expected size of amplicon. The agarose gel consisted of agarose dissolved in TAE buffer (40 mM Tris base, 20 mM acetic acid, 1 mM EDTA), containing 0.06 µl/ml Midori Green (Geneflow Limited). It was run at 100V for 30 minutes. Subsequently, DNA products were imaged using ChemiDoc™ XRS+ imaging system (BioRad).

2.3 Animal studies

During all *in vivo assess*ments and biochemical analysis, the researcher was blinded to the mouse genotype. This is to remove any bias and ensure validity of the research.

2.3.1 Transverse Aortic Constriction

To evaluate the effect of PMCA1 in heart failure development, transverse aortic constriction (TAC) was performed. In this model permanent constriction was imposed around the aorta thereby limiting left ventricular outflow and creating a pressure overload condition in the LV. TAC can result in cardiac hypertrophy and fibrosis and progression to heart failure in the long-term (Oceandy et al., 2009b). In this experiment, mice were subjected to either a TAC or sham operation. All surgery was performed by Dr Min Zi with the assistance of Mr Sukhpal Prehar and the author. Before the surgery, mice were injected subcutaneously with 0.1 mg/kg body weight of Buprenorphine as pre-operative analgesia. Anaesthesia was induced with 5% isoflurane in 100% O_2 and maintained at 3% isoflurane in 100% O_2 throughout the procedure. Following induction of anaesthesia, the mice were intubated orally and mechanically ventilated with a Minivent 845 (Harvard Apparatus), set at 200 breaths per minute and tidal volume of 0.1 ml. Mini thoracotomy was performed to open the chest cavity and visualise the aortic arch. In mice subjected to TAC, the aorta was ligated (over a curved blunt 27G needle which was removed before chest cavity was closed) between the brachiocephalic trunk and the left common carotid artery using a surgical suture that produces approximately 25% narrowing of the aortic lumen. This is shown in the figure 2.6.

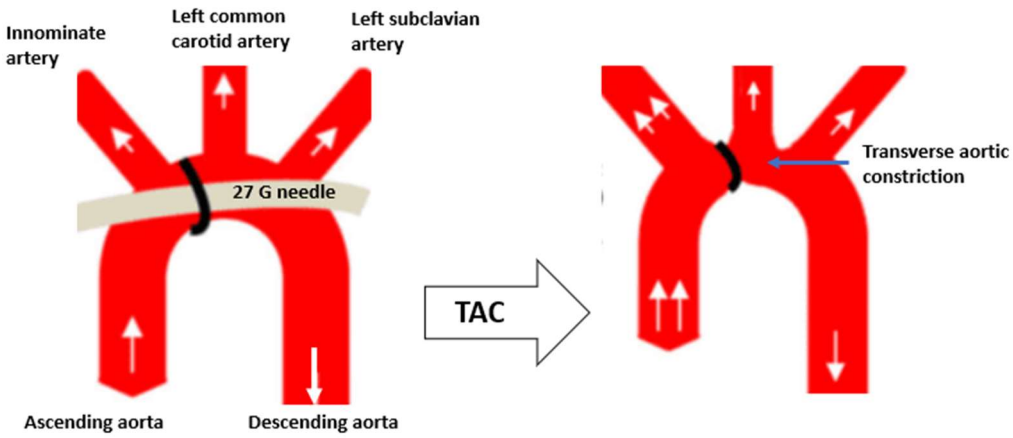

Figure 1.6: The illustration of creating Transverse Aortic Constriction (TAC).

Transverse aorta is ligated with a surgical suture over a curved blunt 27G needle between the innominate artery and the left common carotid artery. The needle is then removed which leaves approximately 25% stenosis in the aortic lumen. (adapted from Luo et al., 2015)

This precise location and surgical technique produces an observable increase in pressure gradient between the left and right carotid artery of ~25-30 mmHg (Zi et al., 2014). In mice undergoing the sham operation the aorta was exposed and a surgical suture passed around it but not ligated. For both sham and TAC animals, the chest was closed, and 0.1 ml/30 g body weight of saline was administered via intraperitoneal injection. Initially, mice were recovered in a chamber filled with 100% O_2 and then placed in a 30^{o}C incubation before transfer to normal housing. In addition to normal chow diet, mice were provided with mashed chow for the first 3-4 days. Animals were monitored regularly for signs of distress until experimental endpoint at which animals were sacrificed and heart tissues collected. Peri-operative mortality from the TAC (or sham) procedure in the experiments described in this thesis was very low (<10%) which is in keeping with acceptable mortality rate described in the literature (deAlmeida et al., 2010).

As described in the later chapters, murine studies have shown that cardiac hypertrophy starts to develop as early as day 3 after the TAC procedure and continues for 2 -3 weeks after TAC. Cardiac hypertrophy remains compensated in wild type mice until four to six weeks after TAC and then decompensated heart failure develops (Chen et al., 2012; Zi et al. 2019).

This was the reason that the heterozygous global deletion of PMCA1 mouse line ($PMCA1^{HT}$) TAC was continued for five weeks. However, cardiomyocyte specific PMCA1 knockout mice ($PMCA1^{cko}$) are known to be susceptible to cardiac arrhythmias (Wilson, 2017; Wang et al. 2017) and previous small pilot project undertaken in our lab showed a trend towards early decompensation of heart failure in this mouse cohort. For this reason, $PMCA1^{cko}$ mice were subject TCA for duration of two weeks only.

2.3.2 Echocardiography

Two-dimensional trans-thoracic echocardiography was used to assess the structure and function of the mouse heart. The precordium was shaved, and animals were given a light anaesthesia by 2-4% isoflurane and were put on a heat pad at 37^0C. Ultrasound transmission gel was applied to the thorax to optimise the quality of images. The heart was imaged in parasternal long axis and short axis views using a Vevo 7700 (Visual Sonics) high resolution imaging system machine. M-mode images were generated by appropriately positioning the M-mode cursor on these views. Echocardiography was performed by Dr Min Zi and was the acquired data was analysed by the author.

On the two-dimensionally directed M-mode, left ventricle diameter in systole and diastole (dLVD and sLVD), interventricular septum (dIVS and sIVS) and posterior wall thickness (dPW and sPW) were measured using the leading-edge method. Measures of systolic function of the left ventricle including LV fractional shortening (%FS) and LV ejection fraction (%EF) were calculated as follows:

$$\% FS = [(dLVD - sLVD)/dLVD] \times 100$$

$$\% EF = [(dVol - sVol)/dVol] \times 100$$

where dVol is the end diastolic volume [$dVol = 1.047 \times (dLVD)^3$]

and sVol is the end systolic volume [$sVol = 1.047 \times (sLVD)^3$]

2.3.3 Haemodynamic measurements

Haemodynamic assessments were carried out by Dr Min Zi and were analysed by the author. Mice were anaesthetised using intra-peritoneal tribromoethanol (Avertin; 480 mg/kg) and were placed in a supine position on a warming pad at 37°C. An anterior cervical midline incision was made and both sternohyoid muscles were retracted. The right common carotid artery was exposed under the operating microscope and ligated at the distal end to avoid

the regurgitation of blood from the head. The proximal end was clamped to occlude blood flow from the heart. A 1.4-Fr high-fidelity catheter (Millar Instruments) was advanced into the right carotid artery and down the aorta. The catheter was then further advanced into the left ventricle. A drop in diastolic pressure when the catheter was passed across the aortic valve and into the LV chamber confirmed its position in the LV. After stabilization, the pressure signals were continuously recorded. The measurements included, heart rate, left ventricular end-systolic and end-diastolic pressures, maximal change of left ventricular systolic pressure (dP/dt_{max}) and diastolic pressure (dP/dt_{min}). Using the Power Lab System (Millar Instruments), these data were analysed to calculate the indices of LV contractility and relaxation. Mice were sacrificed after haemodynamic measurements were made.

2.4 Heart weight, body weight, lung weight and tibial length measurements

Body weight (gm) was recorded prior to termination. Following sacrifice by cervical dislocation, heart and lungs were dissected away from fat and surrounding tissue, blood was drained on blotting paper and the organs were weighed (mg). Tibia were dissected away and measured (mm). Heart tissue was subsequently washed with phosphate buffered saline (PBS), snap frozen in liquid nitrogen and transferred to -80^0C freezer for storage until required.

2.5 Histological analysis

After the animals were sacrificed, hearts were dissected from the surrounding tissues and excess blood cleaned by flushing with phosphate buffered saline. Transverse sections were cut through the ventricles and fixed in 4% paraformaldehyde (PFA) for 72 hours at 4^0C. The fixed sections were transferred to individually labelled histology cartridges and immersed in 70% ethanol. Following this, tissues were processed overnight using a Leica ASP300 tissue processor, which involved placing tissue samples in an increasingly higher concentration of alcohol before being immersed in xylene and finally molten paraffin wax (table 2.4).

Reagent	Time (min)	Reagent	Time (min)
1. 70% alcohol	20	8. Xylene	20
2. 70% alcohol	30	9. Xylene	30
3. 90% alcohol	45	10. Xylene	40
4. 90% alcohol	60	11. Wax	70
5. 100% alcohol	30	12. Wax	70
6. 100% alcohol	45	13. Wax	70
7. 100% alcohol	60		

Table 1.4: Tissue processor protocol

The sections were embedded in molten paraffin wax and allowed to cool down at 4^0C for 24 hours. Next day, these sections were sliced in 5μm thickness using a Leica RM2255 paraffin microtome and mounted on poly-1-lysine coated glass slides and oven dried at 37^0C.

Before staining, the slides were put on the heat block to remove the wax, then placed in xylene for 3 minutes. The tissue sections were subsequently rehydrated in industrial methylated spirit (IMS) in reducing concentrations (100%, 90% and 75%), leaving them in the solution for 2 minutes, each time. Finally, slides were rinsed with running tap water for 5 minutes while taking care that water did not directly fall on the tissue sections.

2.5.1 Haematoxylin and Eosin (H&E) staining for cell size analysis

Slides were left immersed in Haematoxylin solution (Sigma Aldrich) for 5 minutes to stain the nuclei and rinsed under running tap water for 5 minutes. The sections were differentiated by immersing in acidic alcohol solution (1% HCl in 70% alcohol) for 5 minutes and washed with running tap water for several minutes. The slide rack was then placed in the filtered Eosin solution and thoroughly rinsed with running tap water. The tissue sections were dehydrated by placing in increasing concentrations of IMS (90%, 95% and 100%) for 2 minutes each. The slide racks were later immersed in xylene thrice (5 minutes each) to remove alcohol from the tissue sections. After drying the excess xylene from the slides, cover slips were mounted with

DPX (Distyrene, Plasticiser and Xylene – Merck). Slides were left in the fume hood to dry overnight.

Slides were scanned on the Pannoramic P250 Flash III slide scanner (3DHistech). Image J software was utilised to measure the cross-sectional cell area. This is done by tracing the individual cell perimeter which is then turned into the area by software and a minimum of 100 cells per section were measured to calculate the average value.

2.5.2 Masson's Trichrome staining and cell fibrosis analysis

Once the slides were rehydrated by immersing them in reducing concentrations of IMS, they were placed in Bouin's solution (at 56^0C) for 2 hours. Following this, the slides were rinsed under running tap water for 10 minutes and stained in filtered haematoxylin for 5 minutes. The slides were rinsed for 5 minutes and then differentiated in acid-alcohol followed by another rinse for 5 minutes. The slides were then immersed in the red solution (GCC diagnostics) for 5 minutes followed by a rinse under tap water for 5 minutes. The slides were then stained with aniline blue (GCC diagnostics) for 10 minutes and thoroughly rinsed under tap water, thereafter. Subsequently, the slides were differentiated in 1% acetic acid for 1 minute. At the end, slides were dehydrated again by immersing them in IMS in increasing concentration, excess alcohol removed with xylene and cover slips mounted with DPX, as described above.

The slides were imaged with Pannoramic P250 Flash III slide scanner (3DHistech) and degree of fibrosis quantified using Image J software, after blinding the researcher of genotypes and treatment groups of mice.

2.6 Biochemical analysis

2.6.1 Real time PCR

Real time PCR is a multi-step process involving RNA isolation, conversion of RNA to cDNA (by reverse transcription) and the quantification of cDNA.

2.6.1.1 RNA isolation from cardiac tissue

In order to prevent RNA degradation, the glass homogeniser tubes were cleaned with RNAs Zap (Sigma Aldrich); 500 µl Trizol was added to the heart tissue, and it was homogenised, while holding on ice, until all tissue was of uniform consistency. The homogenate was

incubated at room temperature for 15 minutes, following which 200 µl chloroform was added. The mixture was vigorously shaken for 15 seconds and left at room temperature for 2 minutes. Samples were then centrifuged at 10,000 rpm at 4^0C for 15 minutes. The upper, aqueous phase of the solution was transferred to a new microfuge tube and 250 µl propan-2-ol was added to precipitate RNA and left at the room temperature for 10 minutes. Following centrifugation at 4^0C at 13000 rpm for 10 minutes, the supernatant was discarded, and the RNA pellet was washed with 70% ethanol and centrifuged at 13000rpm at 4^0C for 10 minutes. Following this, the ethanol was discarded, and the pellet air-dried. The pellet was re-suspended in 50-70 µl (depending on the pellet size) of DNAse/ RNAse free water. The concentration and integrity of RNA was determined by measuring the absorbance at 260 nm using a NanoDrop spectrophotometer ND-1000 (Thermo Scientific). One absorption unit is approximately equivalent to RNA concentration of 40 µg/ml and A_{260}/A_{280} ratio greater than 1.8 is indicative of high-quality RNA.

All RNA samples were treated with amplification grade DNAse (Sigma Aldrich) following the manufacturer's instructions and were stored at -80^0C.

2.6.1.1.1 Reverse transcription polymerase chain reaction

DNAse treated samples were converted to cDNA by using High-capacity RNA-to-cDNA kit (Applied Biosystems) following the manufacturer's recommended protocol. This included preparation of reverse transcriptase (RT) master mix; total volume depending upon the number of RNA samples to be converted. Reverse-transcriptase negative (RT-ve) samples were prepared as negative controls. The mixture was gently mixed and placed on ice. This assay used 1µg of RNA mixed with reaction reagents listed in table 2.5. After mixing 1µg of RNA with the reaction mixture, the contents were briefly spun down to remove air bubbles. Following which the samples were loaded into Venti^{TM} 96-well thermal cycler (Applied Biosystems). Thermal cycling conditions are described in table 2.6.

Component	Volume (µl)
10X RT buffer	2.0
25X dNTP mix	0.8
1-X ST random primers	2.0
Multiscribe reverse transcriptase	1.0
Nuclease free H_2O	4.2
Total per reaction	10.0

Table 1.5: High-capacity RNA-to-cDNA kit (Applied Biosystems) components per single reaction

	Temp (^{0}C)	Time (min)
Step 1	25	10
Step 2	37	120
Step 3	85	5
Step 4	4	∞

Table 1.6: Thermal cycling conditions for RNA to cDNA conversion

2.6.1.1.2 SYBR Green quantitative PCR (qPCR)

The qPCR was performed using the Brilliant II SYBR Green qPCR kit (Agilent Technologies) as per the manufacturer's recommended protocol. The components of this kit are outlined in table 2.7.

Component	Volume (µl)
SYBR Green	5.0
Quantitect primer essay	1.0
Reference dye	0.15
cDNA	1.0
Nuclease free H_2O	2.85
Total per reaction	10.0

Table 1.7: Brilliant II SYBR green qPCR Master Mix (Agilent Technologies) components per reaction

Stage	Temp(^{0}C)	Time (sec)	Cycles
Holding	95	180	X 1
Cycling	95	5	X 40
	60	25	
Melt Curve	95	15	X 1
	60	60	
	95	15	
	60	15	
Holding	4	∞	

Table 1.8 Thermal cycling conditions for SYBR Green qPCR

All qPCR reactions were prepared as triplicate in a 96 well plate, on ice along with 4 negative controls. Pre-made specific primers (Quantitect Primer Assay, Qiagen) for calcium transport

channels, markers of hypertrophy and fibrosis including PMCA1 (Atp2b1), PMCA4 (Atp2b4), SERCA2 (Atp2a2), NCX (Scl8a1), RyR (Ryr1), ANP (Nppa) , BNP (Nppb), Collagen 1 (COL 1α 1), Collagen 3 (COL 1α 3) and house-keeping gene Gapdh (Glyceraldehyde 3-Phosphate Dehydrogenase) were used. For gene amplification, 7500 H Fast Real-Time PCR system (Applied Biosystems) was used and programmed as detailed in table 2.7.

To standardise all values, the CT values of genes of interest were normalised against the endogenous control (Gapdh) and the experimental controls (WT or WT sham). The miRNA fold change was calculated using the delta-delta CT method ($2^{-\Delta\Delta CT}$).

2.7 Statistical Analysis

All data are presented as mean ± standard error of mean (SEM) and analysed using GraphPad Prism software. Statistical tests were applied depending on the data set. Student's unpaired t-test was used when comparing one variable between two groups whilst two-way ANOVA was used when comparing two variables (i.e., genotype and treatment) between groups. In all experiments carried out as part of this research, a p value less than 0.05 ($p<0.05$) indicates statistical significance (Hsu & Lee, 2010; Shen & He, 2014). For post hoc analysis, Tukey's test was used which is one of the most commonly employed test while analysing paired data (Kim, 2015).

Chapter 3 -

Heterozygous global deletion of PMCA1 and its impact on cardiac structure and function

3.1 Introduction

Hypertension is an established risk for cardiovascular disease in general, and heart failure, in particular (Lawes et al., 2008). Out of the four known isoforms of plasma membrane calcium ATPases (PMCA); isoform 1 and 4 are highly expressed in the cardiovascular system (Stauffer et al., 1993). Genome wide association studies (GWAS) have demonstrated an association between blood pressure, hypertension and ATP2B1 – the gene encoding for plasma membrane calcium ATPase 1 (PMCA1) (Levy et al., 2009). This observation appears to be consistent amongst people from different ethnic origins (Wan et al., 2014; Xi et al., 2014). These observational studies have generated further interest into possible roles played by PMCAs in the cardiovascular system, during health and disease.

3.1.1 Reduced expression of PMCA1 and hypertension

At a functional level, previous published work from our group has shown that global heterozygous PMCA1 null ($PMCA1^{HT}$) mice develop significantly elevated blood pressure at 12 months age compared to the age matched wild type control (Little et al., 2017). In this mouse model, heterozygous global deletion of PMCA1 leads to an exacerbated narrowing of vascular lumen with increased vessel wall thickening with ageing. The reduction in the vessel lumen precedes the development of hypertension in $PMCA1^{HT}$ mice. Mice lacking PMCA1 specifically in the vascular smooth muscle have also been shown to develop hypertension (Kobayashi et al., 2012). Alteration in calcium homeostasis and resultant increased vasoconstriction was considered to be the root cause for elevated BP in PMCA1 vascular smooth muscle knock out mice. The consistent finding of hypertension in mice with reduced PMCA1 expression from the above studies confirm the link between PMCA1 and hypertension discovered in human GWAS. This, in turn, opens avenues for further work to look into PMCA1's role in cardiac function and the development of heart failure.

Previous work by our group demonstrated that reduced levels of PMCA1 are associated with prolongation of QT interval in mice, suggesting a key role for PMCA1 in the regulation of cardiac rhythm (Wilson, 2017). Being one of the most abundant form of PMCA in the heart (Strehler, 2013), together with PMCA4 (Stauffer 1993); it is plausible that PMCA1 may also

contribute to the regulation of cardiac growth and hypertrophy. However, no published studies, thus far have examined the role of PMCA1 in a pressure overload model.

3.2 Hypothesis

The ultimate aim of this project is to identify whether the deletion of PMCA1 has any impact on the structure and the function of the heart under pathological stress. Previously work from our group has shown that a heterozygous deletion of PMCA1 ($PMCA1^{HT}$) leads to the development of hypertension in mice with increasing age. Hypertension is a well-established risk factor for the development of cardiovascular disease such as ischaemic heart disease and heart failure (Tomek & Bub, 2017). Our hypothesis is that a heterozygous deletion of PMCA1 will have a detrimental effect on the heart and lead to exacerbates cardiomyopathy after pressure overload produced by transverse aortic constriction.

3.2.1 Aims

1. Characterise $PMCA1^{HT}$ and wild type mice at the basal level to explore if there is a difference in cardiac structure and function, and whether deletion of PMCA1 leads to alterations in the expression of calcium transporting channels.
2. Characterise cardiovascular modelling in $PMCA1^{HT}$ and wild type mice after pathological stress caused by pressure overload induced by 5 weeks TAC.

3.3 Materials and methods

The materials and methods used to carry out these experiments have been described in detail in chapter 2. However, a brief description of the mouse line used in these experiments is outlined in the lines below.

3.3.1 Animals used in these experiments

PMCA1 is a housekeeping gene, and it is well established that homozygous global deletion of PMCA1 is embryonic lethal. Our group have generated two novel moues lines using Cre/Lox P system. For the experiments described in this chapter, the global heterozygous deletion of PMCA1($PMCA1^{HT}$) in a murine model is used and only male mice were included in the experiments. As explained in the previous chapter, $PMCA1^{HT}$ mice were generated by

crossing PMCA1$^{F/F}$ mice with CMV-Cre mice. These mice have reduced levels of PMCA1 in multiple organs including kidney, brain, aorta and heart (Little et al., 2017).

TAC procedure was performed according to the method described in section 2.3.1.

3.4 Results

In order to determine whether reduced expression of PMCA1 predisposes mice to heart failure, the initial step is to address the first aim for this project i.e to characterise PMCA1^{HT} and wild type mice at the basal level to explore if there is a difference in cardiac structure and function, and whether deletion of PMCA1 leads to alterations in the expression of calcium transporting channels.

3.4.1 Determination of genotype of PMCA1 heterozygous (PMCA1^{HT}) mice

For this study, the mice were bred by crossing PMCA1^{HT} mice with wild type (WT) mice, therefore the genotype of the resulting pups was determined by performing PCR on DNA prepared from the ear biopsies. DNA was extracted from ear tissue biopsies to identify PMCA1^{HT}and wild type (WT) controls. Primers were designed to amplify a 6.6kb PCR fragment of the WT allele or 4.7kb of the targeted allele (this has been described in detail in section 2.2.2). Following gel electrophoresis, a single 6.6 kb band represented a WT pup, whilst PMCA1^{HT} pups had both 6.6kb WT and 4.4kb mutant amplicons (Figure 3.1A). WT and PMCA1^{HT} have been born in the expected 1:1 ratio: from 53 mice genotyped in this project to date 26 have been WT and 27 PMCA1^{HT} (Figure 3.1B).

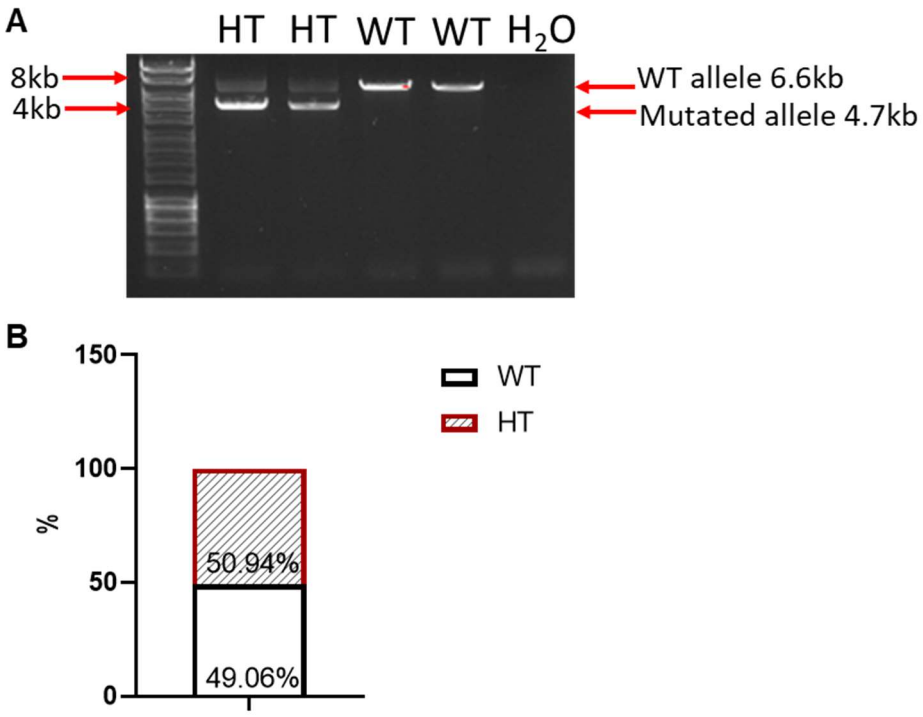

Figure 3.1: PCR analysis using DNA extracted from ear snips.

(A) DNA PCR results demonstrating genotypes used in this research. PMCA1 heterozygous mice carry both wild type and mutated alleles and wild type mice only contain wild type allele. (B) Percentage of WT and HT mice genotyped in this study (WT= Wild type, HT= PMCA1^{HT}, H_2O=water control)

3.4.2 Characterisation of PMCA1 heterozygous (PMCA1^{HT}) mice at basal level

PMCA1^{HT} mice developed to adulthood as normal and were visually indistinguishable from the wild type control littermates in terms of their weight (Figure 3.2). At 12 weeks of age, these male mice were subject to a number of assessments to characterise cardiac structure and function. For the basal assessments, experiments were carried out on 8 wild type and 9 PMCA1^{HT} mice.

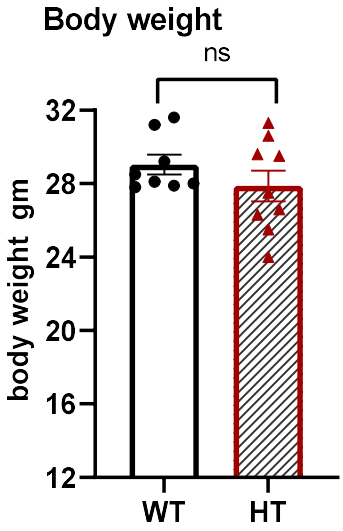

Figure 3.2: Body weight of representative WT and PMCA1^{HT} mice at 12 weeks of age. Data presented as mean ± SEM. Unpaired Student's t-test was used for analysis. (ns non-significant). WT= wild type, HT = PMCA1^{HT}

3.4.2.1 Effect of global heterozygous deletion of PMCA1 on structure and function of the heart

To assess the consequences of heterozygous deletion of PMCA1 on cardiac structure and function 12 weeks old PMCA1^{HT} male mice and their WT control littermates underwent echocardiography and haemodynamic analysis.

3.4.2.2 Echocardiography in 12 weeks old in wild type andPMCA1^{HT} mice.

To establish whether heterozygous deletion of PMCA1 led to any structural changes under basal conditions, transthoracic two-dimensional and M-mode echocardiography with parasternal short-axis views was performed on 12-week-old PMCA1^{HT} male mice and their age and sex-matched WT controls under light general anaesthesia. The left ventricular diameter, the interventricular septum and the posterior wall thickness were measured both in systole and diastole from the M-mode recordings and heart rate was recorded. Echocardiographic analysis revealed no significant difference in the left ventricular structure and function of 12 weeks old PMCA1^{HT} male mice compared to the controls (figure 3.2 and table 3.1). In particular, no significant difference was observed in LV chamber diameter, wall thickness and function.

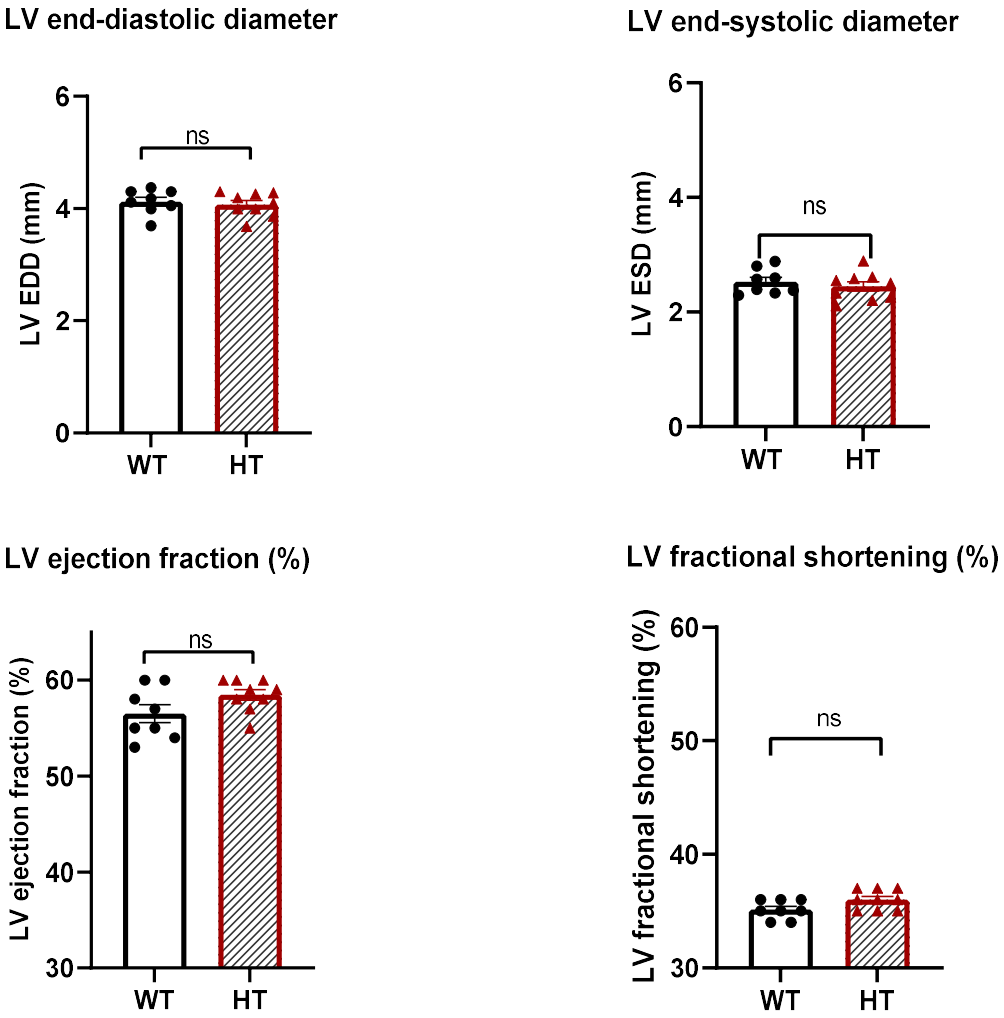

Figure 3.3: Echocardiography analysis in 12 weeks old WT and PMCA1^{HT} mice. Data presented as mean ± SEM. Unpaired Student's t-test was used for analysis. (ns non-significant). WT= wild type, HT = PMCA1^{HT}

Parameter	WT (n=8)	HT (n=9)	*p*
dIVS (mm)	0.93±0.09	0.92±0.06	0.86 ns
sIVS (mm)	1.34±0.08	1.38±0.05	0.91 ns
dPW (mm)	0.73±0.09	0.77±0.11	0.35 ns
sPW (mm)	1.07±0.07	1.02±0.09	0.48 ns
HR (b/min)	455±21	441±17	0.34 ns

Table 3.1: Echocardiography parameters of 12 weeks old PMCA1^{HT} mice. Data presented as mean ± SEM. Unpaired Student's t-test was used for analysis. (ns non-significant). WT= wild type, HT = PMCA1^{HT}

dIVS: diastolic inter ventricular septum, sIVS: systolic inter ventricular septum, dPW: diastolic posterior wall, sPW: systolic posterior wall, HR: heart rate. WT= wild type HT = PMCA1^{HT}

3.4.2.3 Haemodynamic measurements in 12 weeks old in wild type and PMCA1^{HT} mice.

Pressure-volume loop analysis was used to assess whether heterozygous deletion of PMCA1 had an impact on cardiac contractility. The pressure-volume catheter was inserted into the left ventricle via the right common carotid artery to record maximum dP/dt (dP/dt_{max}) and minimum dP/dt (dP/dt_{min}) as indicators of contraction and relaxation, respectively. PMCA1^{HT} mice had normal cardiac contractile function compared to their age-matched controls, at 12 weeks of age (table 3.2).

PMCA1^{HT} and their age-matched WT littermate controls underwent haemodynamic assessment. Systolic and diastolic functions of the heart were assessed by measuring dP/dt_{max} and dP/dt_{min} respectively; no significant difference was found between the two genotypes.

Parameter	WT (n=8)	HT (n=9)	*p*
dP/dt_{max} (mmHg/s)	5189±258	5966±638	0.41 ns
dP/dt_{min} (mmHg/s)	-4572±388	-4617±478	0.79 ns

Table 3.2: Haemodynamic assessment of 12 weeks old WT and PMCA1^{HT} mice. Data presented as mean ± SEM**.** Unpaired Student's t-test was used for analysis. (ns non-significant). WT= wild type, HT = PMCA1^{HT}

3.4.2.4 Normalised heart weight and lung weight

To determine whether heterozygous deletion of PMCA1 led to cardiac hypertrophy or signs of heart failure heart and lungs were dissected from 12 weeks old PMCA1^{HT} and their age-matched WT controls. No significant difference was found between the heart weight/body weight (HW/BW) and heart weight/tibial length (HW/TL) of 12 weeks old PMCA1^{HT} and controls (figure 3.4).

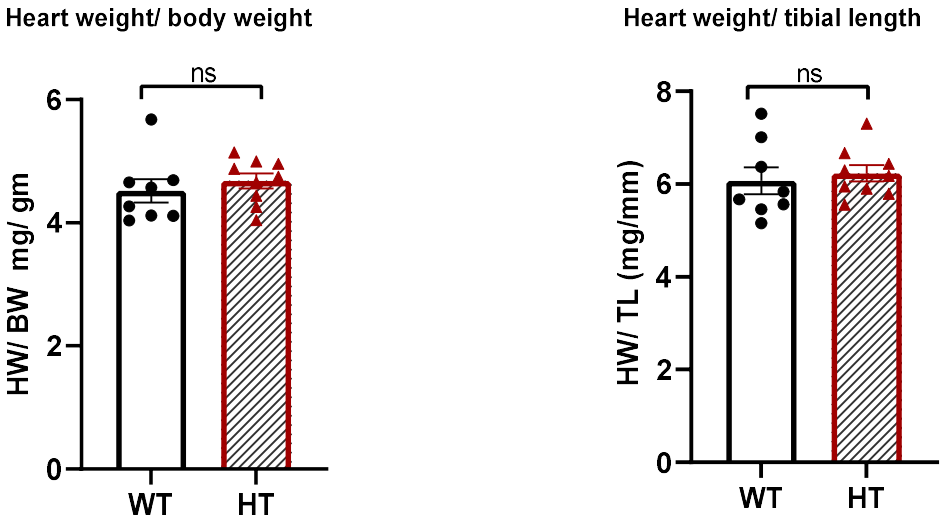

Figure 3.4: Heart weight/bodyweight and heart weight/tibial length ratio in 12 weeks old WT and PMCA1^{HT} mice. Data presented as mean ± SEM**.** Unpaired Student's t-test was used for analysis. (ns non-significant). WT= wild type HT = PMCA1^{HT}

Lungs isolated from 12 weeks old PMCA1^{HT} and their age-matched WT control littermates were weighed and were compared. There was no significant difference in the observed lung congestion and lung weight of these two cohorts either (figure 3.5).

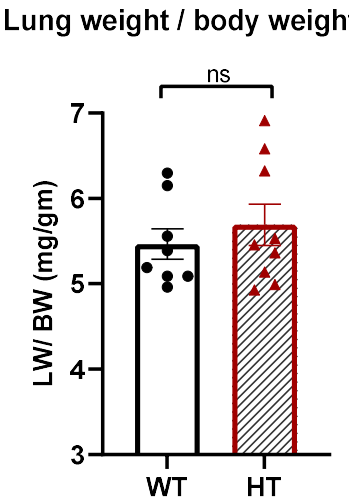

Figure 3.5: Lung weight/body weight ratio in 12 weeks old WT and PMCA1^{HT} mice. Data presented as mean ± SEM**.** Unpaired Student's t-test was used for analysis. (ns non-significant). WT= wild type HT = PMCA1^{HT}

3.4.2.5 Does global heterozygous deletion of PMCA1 lead to altered expression of genes involved in calcium transport?

Reverse transcription polymerase chain reaction (RT-PCR) was performed to determine whether global heterozygous deletion of PMCA1 leads to compensatory changes in the relative expression (to gapdh) of other calcium handling genes including PMCA4, sarco/endo plasmic reticulum calcium ATPase-2 (SERCA2), sodium calcium exchanger (NCX), and ryanodine receptor (RyR). The results confirmed that PMCA1^{HT} mice had approximately 50% lower expression of PMCA1 RNA compared to their WT littermates as previously showed by Little et al 2017. However, the relative expression of PMCA4 (Atp2b4), SERCA2 (Atp2a2), NCX (Scl8a1) and RyR (Ryr1) RNA was similar in both cohorts (figure 3.6).

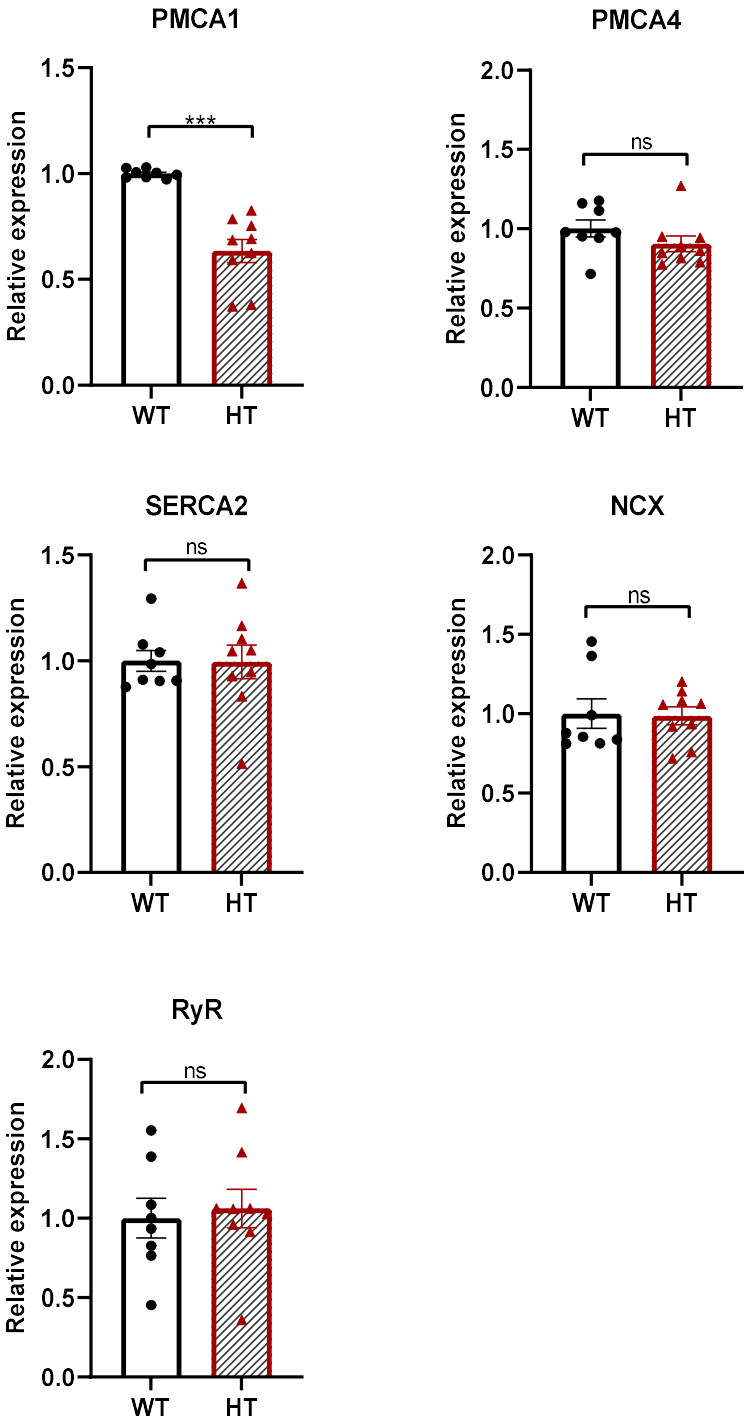

Figure 3.6: RT-PCR analysis of several calcium handling genes in 12 weeks old WT and PMCA1^{HT} mice. Data presented as mean ± SEM**.** Gapdh was used as housekeeping gene and y-axis represents relative expression. Unpaired Student's t-test was used for analysis. (ns non-significant, ***p<0.001) WT= wild type HT = PMCA1^{HT}

3.4.2.6 Does global heterozygous deletion of PMCA1 cause basal changes in gene markers of cardiac remodelling?

To investigate whether global reduction of PMCA1 lead to altered cardiac remodelling or fibrosis, quantitative PCR was performed on the RNA samples isolated from 12 weeks old PMCA1^{HT} and their age-matched controls to examine the expression of brain natriuretic peptide (BNP - nppb) and Collagen 1 (Col1α1). The result showed that BNP and Col1α1 expression in PMCA1^{HT} mice was not significantly different from WT controls (figure 3.7).

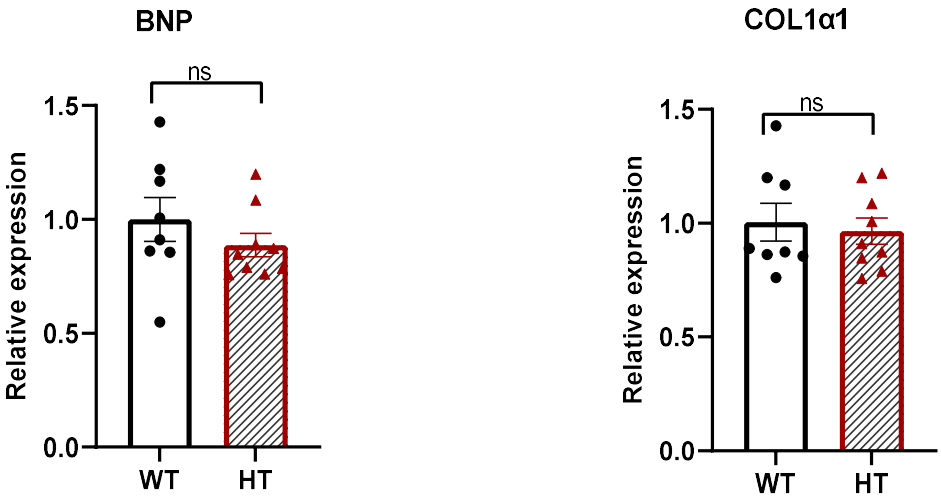

Figure 3.7: The expression of cardiac remodelling marker BNP and COL1α1 in 12 weeks old WT and PMCA1^{HT} mice. Data presented as mean ± SEM**.** Gapdh was used as housekeeping gene and y-axis represents relative expression. Unpaired Student's t-test was used for analysis. (ns non-significant). WT= wild type HT = PMCA1^{HT}

3.4.2.6 Summary

To summarise, the basal analysis confirms that 12 week old PMCA1^{HT} male mice and their wild type littermates have no difference in their cardiac structure and function as assessed by transthoracic echocardiography and haemodynamic analysis. On a molecular level, PMCA1^{HT} mice have approximately 50% lower expression of PMCA1 but the level of expression of other calcium handling genes shows no significant difference. Expression of

BNP and COL1α1 showed no significant difference in the two cohorts suggesting that there is no difference in the left ventricular hypertrophy and fibrosis at the basal level, which corroborated the normalised heart weight data.

3.4.3 How does heterozygous global deletion of PMCA1 impact the heart under pathological stress?

To address the next aim to characterise cardiovascular modelling in PMCA1^{HT} and WT mice after pathological stress caused by transverse aortic constriction, PMCA1^{HT} mice and their wild type littermates were subjected to transverse aortic constriction (section 2.3.1) that creates a pressure overload model of cardiac stress.

3.4.3.1 Transverse aortic constriction (TAC) to induce pressure overload

TAC procedure was performed for 5 weeks on 8-week old male PMCA1^{HT} mice and WT mice. The number of mice per experimental group is shown in table 3.3 (the same n numbers were used in all subsequent analysis unless specified otherwise). Echocardiogram, haemodynamic and molecular analysis were performed.

Genotype: surgical procedure	WT: sham	WT: TAC	PMCA1^{HT}: sham	PMCA1^{HT}: TAC
n	8	8	12	13

Table 3.3: The number of animals in the sham and TAC groups, and their genotypes.

3.4.3.2 The effect of heterozygous deletion of PMCA1 on cardiac structure and function 5 weeks post TAC

To assess the consequences of 5 weeks TAC for on the structure and function of the heart PMCA1^{HT} mice and their wild type control littermates underwent transthoracic two-dimensional and M-mode echocardiography with parasternal short-axis views, and haemodynamic measurements 5 weeks after the application of TAC. The results are as follows.

3.4.3.2.1 Transverse aortic constriction for PMCA1^{HT} and WT mice

To generate pressure overload, transverse aortic constriction (TAC) experimental model was used. The maximal pressure within the left ventricle (P_{max}) serves as a marker of pressure overload created by TAC. It was recorded before sacrificing the animals by using the invasive cardiac catheterisation. The data shows no significant difference in the P_{max} between the WT: sham (92.0±12.8 mmHg) and PMCA1^{HT}: sham (94.6±8.2 mmHg) groups. Following the TAC procedure, WT mice as well as PMCA1^{HT} mice demonstrated a significant increase in the P_{max} ($p<0.001$). However, there was no significant difference between the two cohorts (151.12±14.9 mmHg vs 146.4±13.6 mmHg). Compared to their sham counterparts, both genotypes showed a similar degree of increase in the P_{max} following TAC procedure (56.2± 6.7 vs 54.9±7.2 p= 0.76). This data shows that TAC procedure exerted a similar pressure overload on WT and PMCA1^{HT} mice (figure 3.8).

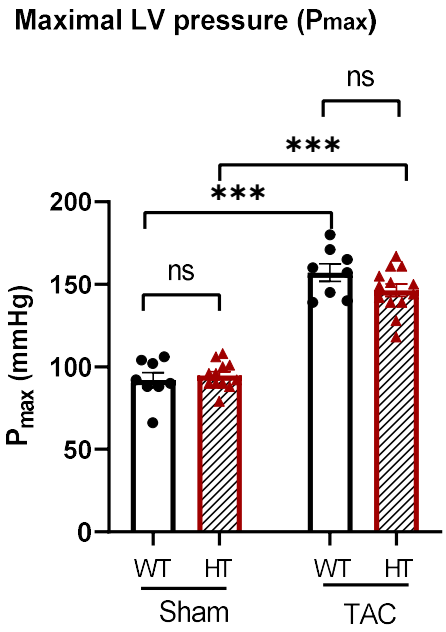

Figure 3.8: Maximal left ventricular pressure (P_{max}) in WT and PMCA1^{HT} mice following five weeks TAC. Data presented as mean ± SEM with two-way ANOVA used for analysis. Tukey's test was used for post-hoc analysis (ns non-significant, ***p<0.001). WT= wild type, HT = PMCA1^{HT}

3.4.1 The effect of TAC induced cardiac stress on cardiac structure and function in PMCA1^{HT} mice

Echocardiography was performed, under light anaesthesia, to confirm if the pressure overload created by TAC had led to the development of left ventricular hypertrophy and to establish if there was any difference in the cardiac structure and function between the two experimental groups (PMCA1^{HT} and WT mice). The left ventricular diameter, the interventricular septum and the posterior wall thickness were measured both in systole and diastole. Heart rate was documented.

3.4.1.1 Echocardiography analysis to determine structural changes to the heart in PMCA1^{HT} mice after five weeks TAC

To assess the consequences of TAC induced pressure overload on cardiac structure and function PMCA1^{HT} mice and their littermate controls underwent transthoracic two-dimensional and M-mode echocardiography with parasternal short-axis views.

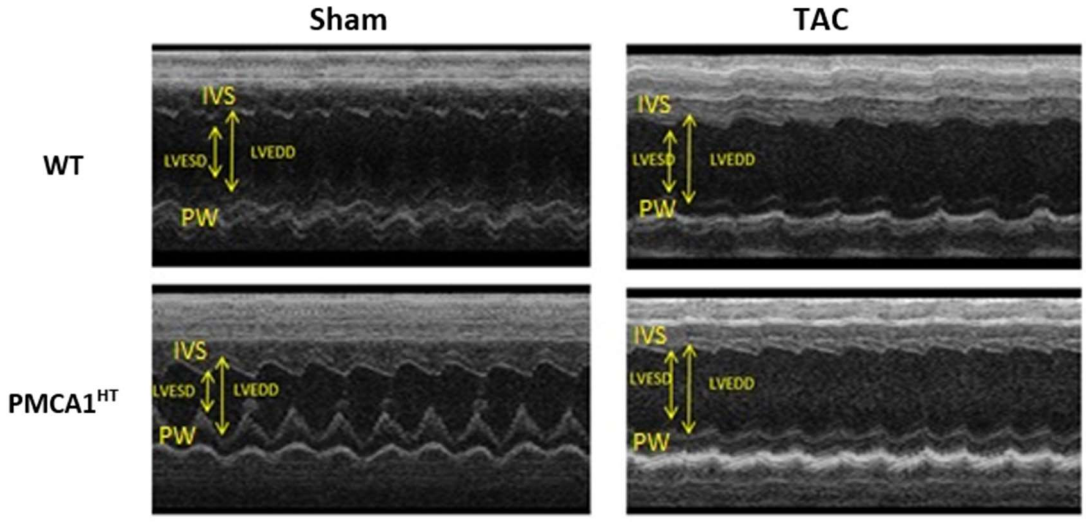

Figure 3.9: M-mode images of WT and PMCA1^{HT} mice having undergone sham or TAC surgery captured on the Visual Sonics Vevo 770. Images indicate left ventricular end systolic diameter (LVESD) and end diastolic diameter (LVEDD), interventricular septum IVS) and posterior wall (PW).

Under light anaesthesia, transthoracic echocardiography was performed in order to assess whether the pressure overload created by TAC had led to the development of left ventricular hypertrophy and to explore if there was any difference in the cardiac structure and function between the two experimental groups (WT and PMCA1^{HT} mice). The left ventricular diameter, the interventricular septum and the posterior wall thickness were measured in systole and diastole. A representative image is shown in figure 3.9. These results are shown in figure 3.10.

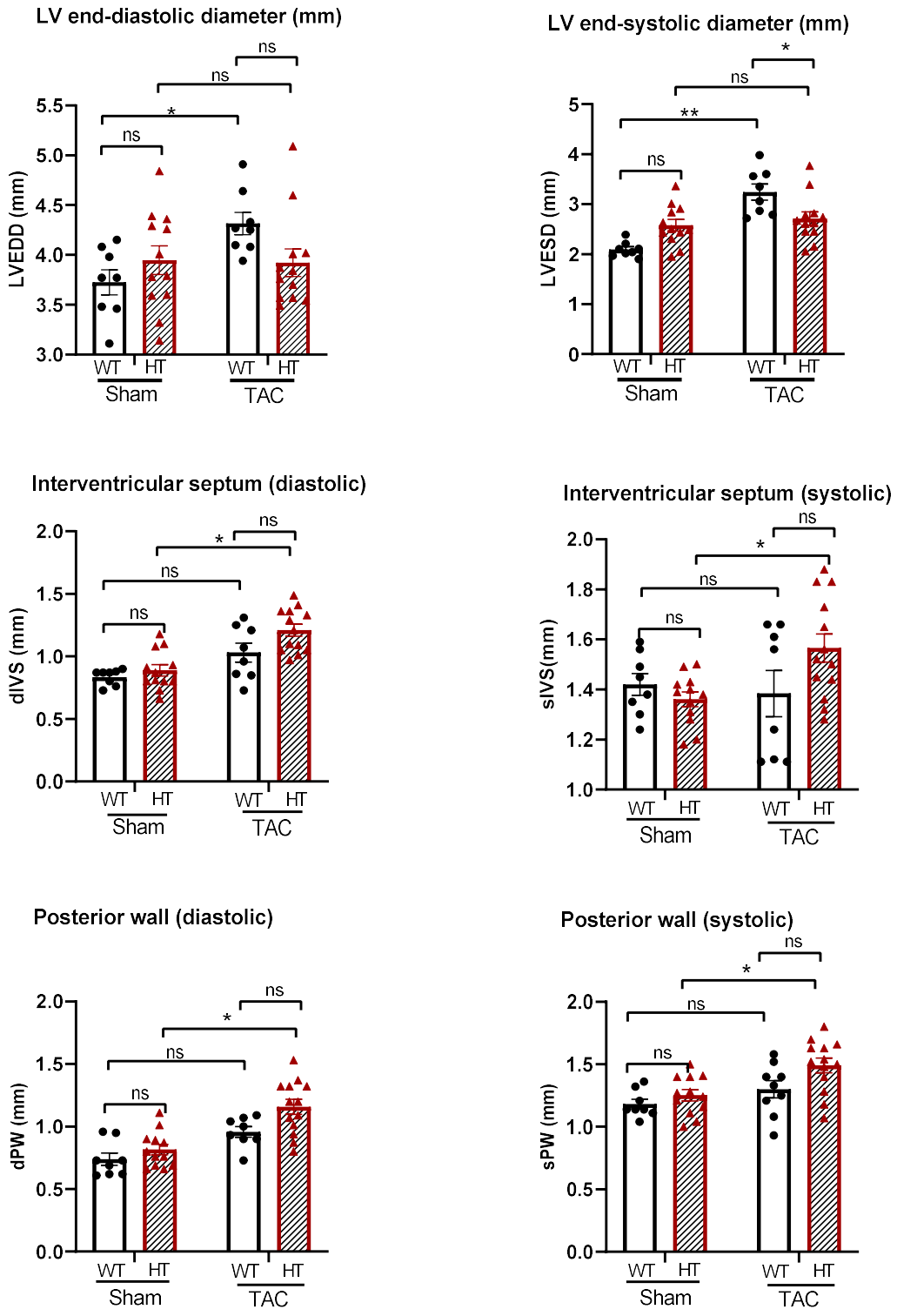

Figure 3.10: Echocardiographic structural analysis of WT and PMCA1^{HT} mice after five weeks TAC.

Data presented as mean ± SEM with two-way ANOVA used for analysis. Tukey's test was used for post-hoc analysis (ns non-significant, * $p<0.05$, ** $p<0.01$). WT= wild type, HT= PMCA1^{HT}

Data from echocardiography shows no significant difference in the cardiac structural parameters between WT and PMCA1^{HT} mice after five weeks of undergoing sham surgery. Following five weeks TAC, WT mice showed a significant increase in the LV end-diastolic diameter (LVEDD) compared to the sham mice of the same genotype (4.31mm±0.32 vs 3.71mm±0.35, $p<0.05$). However, whilst PMCA1^{HT}:TAC cohort also showed a trend towards an increased LVEDD compared to the PMCA1^{HT}:sham group , it did not reach statistical significance (3.94mm±0.49 vs 3.74mm±0.41, $p=0.08$). No significant difference was found between the LVEDD measured from PMCA1^{HT}:TAC and WT:TAC cohorts.

Similarly, mice from both genotypes did not show a significant difference in their LV end-systolic diameter after five weeks of sham surgery. There was a significant increase in LVESD measured in WT:TAC and PMCA1^{HT}:TAC mice compared to the sham mice of the same genotype (3.24mm±0.45 vs 2.10mm±0.15, $p<0.001$ and 2.71mm±0.47 vs 2.56mm±0.40, $p<0.05$, respectively). On a direct comparison between WT:TAC and PMCA1^{HT}:TAC groups, the former had a significantly higher LVESD (3.24mm±0.45 vs 2.71mm±0.47, $p<0.05$).

Other echocardiographic parameters including the thickness of inter-ventricular septum and posterior wall were also measured. Whilst both genotypes showed an increase in the diastolic interventricular septum (dIVS) thickness in response to TAC (compared to the mice that underwent sham surgery), the increase was statistically significant in PMCA1^{HT} :TAC group ($p<0.05$). However, this resulted in a similar dIVS thickness in both PMCA1^{HT} and WT mice five weeks after TAC (1.20mm±0.17 vs 1.03mm±0.21, $p= 0.08$).

The thickness of systolic interventricular septum (sIVS) was also similar in both genotypes after sham surgery and after five weeks of TAC PMCA1^{HT} mice showed a significant increase in in sIVS compared to the mice that underwent sham surgery (1.57mm±0.20 vs 1.36mm±0.10, $p <0.05$). No significant difference was found in the thickness of sIVS between in the mice from both genotypes after five weeks of TAC procedure.

Five weeks of TAC led to a significant increase in the thickness of diastolic and systolic posterior wall (dPW and sPW) in PMCA1^{HT} mice compared to their sham controls (1.16mm±0.26 vs 0.82mm ±0.14, $p<0.05$ and vs1.49 mm±0.21 vs 1.25mm ±0.15, $p<0.05$ respectively). No significant difference was found in the dPW and sPW thickness in the mice from both genotypes after the TAC or sham surgery.

Relative wall thickness (RWT) is an important echocardiographic parameter that can help to distinguish between concentric and eccentric hypertrophy. The data showed that both PMCA1^{HT} and WT controls had no significant difference in the RWT after the sham surgery (0.45 ±0.08 vs 0.44±0.11, p= 0.30). Following five week TAC, PMCA1^{HT}:TAC mice showed a significant rise in the RWT compared to the WT:TAC cohort (0.61 ±0.11 vs 0.47±0.07, p 0.02). The finding of a lower relative wall thickness in WT:TAC mice suggests the development of eccentric left ventricle hypertrophy.

In summary, following five weeks TAC, PMCA1^{HT} mice developed an increased thickness of ventricular walls (IVS, PW and RWT) without an increase in the chamber size in keeping with concentric hypertrophy. Whereas WT mice show significant dilatation of the left ventricular chamber in systole and diastole as evidenced by an elevated LVESD and LVEDD compared to their genotype controls. In addition, WT mice showed significantly more dilated LV in systole compared to PMCA1^{HT}:TAC mice. WT mice also showed a relatively lower degree of increase in the thickness of interventricular septum, posterior wall and RWT, suggestive of thinning of ventricular walls accompanying the dilation of left ventricle. These echocardiographic findings in WT:TAC mice are in keeping with eccentric cardiac hypertrophy.

3.4.1.2 Echocardiography analysis to determine functional changes to the heart in PMCA1^{HT} mice after five weeks TAC

As shown above, echocardiography revealed PMCA1^{HT} mice developed concentric cardiac hypertrophy without any accompanying left ventricular dilatation. Further analysis of this data was performed to assess left ventricular systolic function (figure 3.11).

Ejection fraction and fractional shortening are well recognised parameters to assess the left ventricular systolic function. These are calculated by using the left ventricular volume and diameter in systole and diastole in the following formulae (Chengode, 2016).

$$\text{LV ejection fraction} = \frac{(\text{LV end diastolic volume} - \text{LV end systolic volume})}{(\text{LV end diastolic volume})} \times 100$$

$$\text{LV fractional shortening} = \frac{(\text{LV end diastolic diameter} - \text{LV end systolic diameter})}{(\text{LV end diastolic diameter})} \times 100$$

As expected, WT and PMCA1^{HT} mice subjected to sham surgery showed no difference in either ejection fraction or fractional shortening. Following five weeks of TAC, mice from both genotypes developed a significant worsening of their LV systolic function as evidenced by a

relatively lower LV FS and LV EF (compared to their genotype controls). However, WT:TAC mice showed a marked deterioration in their LV FS and LV EF compared to their genotype sham controls (25 ±4.9% vs 42.7±4.7%, $p<0.0001$ and 60.3 ±7.9% vs 81.6 ±4.7%, $p<0.0001$, respectively). PMCA1^{HT} mice did have a lower LV EF and FS compared to sham controls (31 ±4.9% vs 38.2±4.4%, $p<0.05$ and 67.0 ±6.5% vs 73.6±3.6%, $p<0.0001$, respectively). Comparison of both groups subject to TAC revealed that WT mice had significantly lower LV FS% than PMCA1^{HT} ($p <0.05$). The data also showed a trend towards a lower LV EF in WT:TAC mice compared to PMCA1^{HT}: TAC; however, it was not statistically significant ($p=0.06$). Heart rate was measured during echocardiography whilst mice were under light isoflurane anaesthesia. Heart rate was similar in all four experimental groups. In summary, the above data reveal that following five weeks TAC, both genotypes developed worsening in their LV contractile function; however, PMCA1^{HT} mice developed lesser deterioration in their LV systolic function compared to the WT cohort.

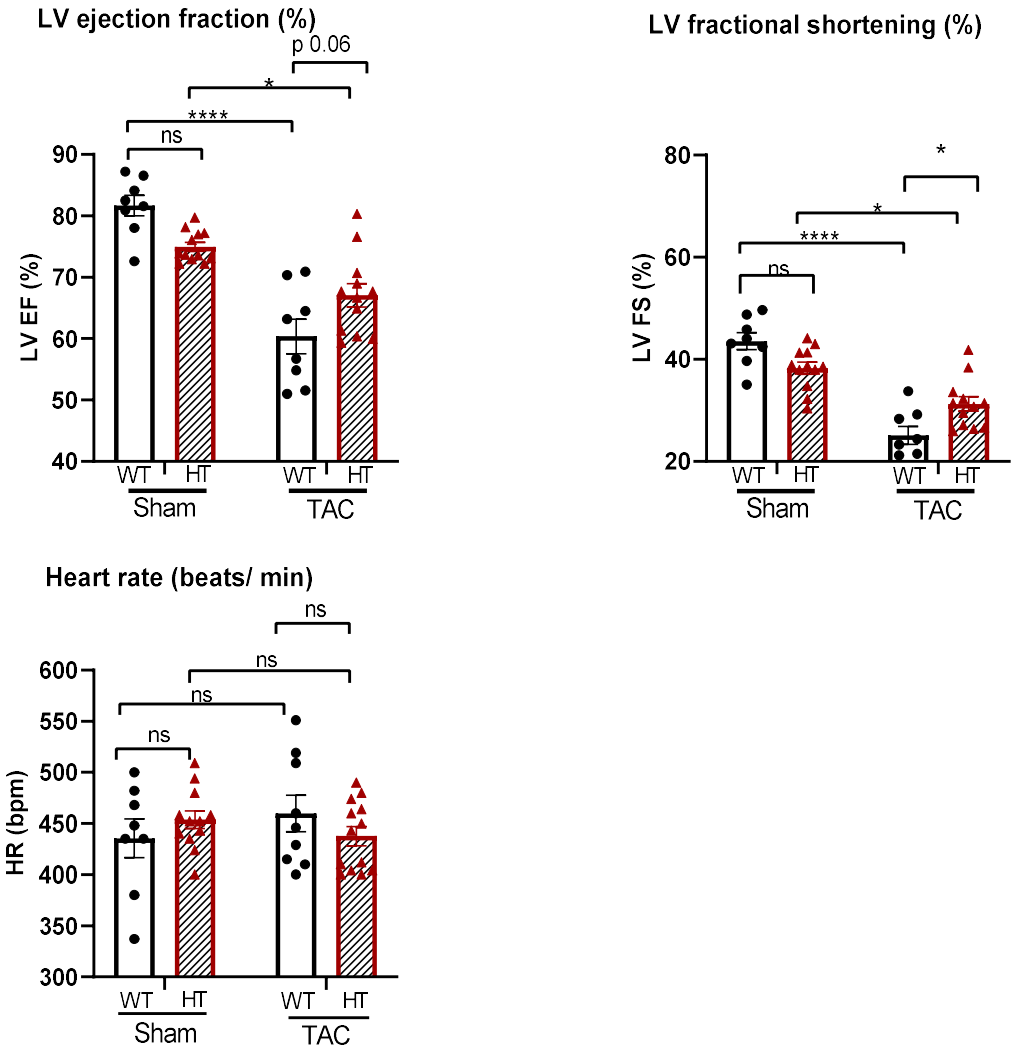

Figure 3.11: Echocardiography analysis of functional changes in PMCA1^{HT} mice after five weeks TAC.

Data presented as mean ± SEM with two-way ANOVA used for analysis. Tukey's test was used for post-hoc analysis (ns non-significant, * p <0.05, **** p<0.0001). WT= wild type, HT= PMCA1^{HT}

3.4.1.3 Haemodynamic analysis to determine changes in cardiac function in PMCA1^{HT} mice after five weeks TAC

Pressure-volume loop analysis was used to examine the effect of global heterozygous deletion of PMCA1 on cardiac function following pathological stress exerted by transverse aortic constriction for a period of five weeks. The pressure-volume (PV) catheter was inserted into the left ventricle via the right common carotid artery to record the diastolic and systolic

blood pressure. The catheter was subsequently advanced to the left ventricle to record the haemodynamic measurements. Due to technical issues, the PV catheter could not be inserted in two mice (one from PMCA1^{HT} TAC and the other from PMCA1^{HT} sham group), hence those mice were excluded from the data analysis. The results are presented in figure 3.12.

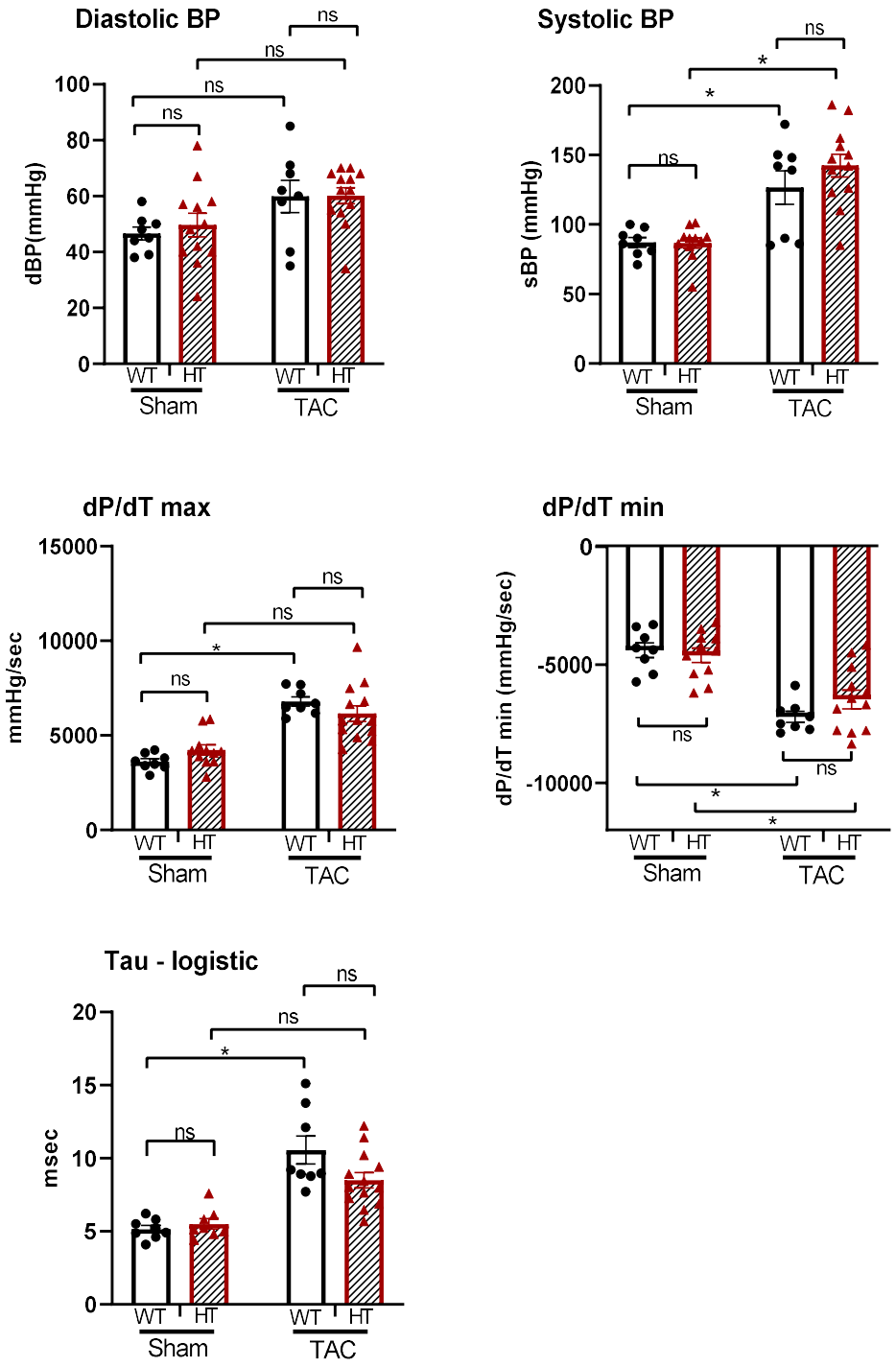

Figure 3.12: Haemodynamic measurements in PMCA1^{HT} mice after five weeks TAC.
Systolic and diastolic blood pressure as measured in the right common carotid artery. Left ventricle force of contraction and relaxation (dP/dt_{max} and dP/dt_{min}) and Time constant for isovolumetric relaxation of left ventricle (logistic Tau - f). Data presented as mean ± SEM with two-way ANOVA used for analysis. Tukey's test was used for post-hoc analysis (ns non-significant, * $p < 0.05$). WT = wild type, HT = PMCA1^{HT}

The diastolic and systolic BP as measured in the carotid artery were not significantly different between WT and PMCA1^{HT} mice five weeks after the sham procedure (diastolic BP 46.6 ±6.5 mmHg vs 49.6 ± 14.1 mmHg, p=0.32; systolic BP = 87.1 ±9.8mmHg vs 86.1 ±12.3 mmHg, p=0.60). A significant rise was noted in the systolic BP in both genotypes after five weeks of TAC compared to the sham controls (WT 126.5 ±34.1mmHg vs 87.1 ±9.8 mmHg, p<0.05; PMCA1^{HT} 142.3 ±28.7mmHg vs 86.1 ±12.3 mmHg, p<0.05). There was no significant difference in the diastolic BP between WT and PMCA1^{HT} mice after TAC procedure (58 mmHg ±9.3 vs 60 mmHg ± 4.0, p=0.90). However, PMCA1^{HT} mice showed a trend towards relatively higher systolic BP five weeks after TAC compared to the WT:TAC cohort; however, this was not statistically significant (142.5 ±28.mmHg vs 126.3 ± 34.1 mmHg, p=0.48).

The difference between the systolic and diastolic blood pressure is called pulse pressure. There was no significant difference in the pulse pressure between WT and PMCA1^{HT} mice after five week of sham surgery (38.5 ±7.3 mmHg vs 36.9 ± 9.9 mmHg, p=0.38). Mice from both genotypes developed a rise in the pulse pressure five weeks after TAC surgery, however there was no significant difference in the pulse pressure between WT: TAC and PMCA1^{HT} :TAC cohorts (63.8 ±11.1 mmHg vs 66.1 ± 13.8 mmHg, p=0.09).

The maximum rate of pressure change in the left ventricle (per unit change in time) (dP/dt_{max}) is a measure of the force of contraction, whereas the minimum rate of pressure change in the left ventricle (per unit change in time acts as measure of the force of relaxation (dP/dt_{min}). In essence, dP/dt_{max} and dP/dt_{min} serve as indicators of cardiac contraction and relaxation, respectively. The dP/dt_{max} measurement showed no significant difference between WT and PMCA1^{HT} mice after sham procedure (3611 mmHg/ sec ±232 vs 4590 mmHg/ sec ± 993, p= 0.14). The dP/dt_{min} data also did not show any significant difference between WT and PMCA1^{HT} mice after sham procedure (-4385 mmHg/ sec ±881 vs -4191 mmHg/ sec ± 469, p =0.97).

Five weeks TAC, as expected, led to a significant increase in dP/dt_{max} in both WT and PMCA1^{HT} mice (compared to genotype match sham cohorts), however this increase was not statistically significant in PMCA1^{HT} mice . In addition, there was no significant difference in dP/dt_{max} between WT and PMCA1^{HT} mice after TAC procedure (6788 mmHg/sec ±676 vs 6160 mmHg/sec ± 635, p=0.51). Similarly, after five weeks TAC, mice from both genotypes exhibited a significant fall in their dP/dt_{min} compared to their genotype matched sham

controls (WT -7202 mmHg/ sec ±648 vs 4385 mmHg/ sec ±881, p <0.05; PMCA1^{HT} -6469 mmHg/ sec ±1373, p <0.05). However, there was no significant difference in the dP/dt_{min} between WT:TAC and PMCA1^{HT} :TAC groups (-7202 mmHg/ sec ±648 vs -6469 mmHg/ sec ±1373, p=0.43).

Logistic Tau (ƭ) is the time constant of isovolumetric relaxation of the left ventricle. Logistic Tau measurement showed no significant difference between WT and PMCA1^{HT} mice after sham procedure (4.91 sec ±0.30 vs 5.9 sec ± 0.82, p 0.25). However, after TAC procedure WT mice showed a trend towards prolonged logistic tau values (10.8 sec ±1.49 vs -7.7 sec ± 0.70, p 0.057). This suggests development of higher levels of diastolic dysfunction in WT mice after TAC procedure compared their PMCA1^{HT} counterparts.

3.4.3.2.3 Heart weight and lung weight measurements 5 weeks after TAC

Hearts and lungs were dissected from PMCA1^{HT} and WT mice five weeks after TAC or sham procedure, in order to determine whether heterozygous deletion of PMCA1 led to cardiac hypertrophy or signs of heart failure. The results are presented in figure 3.13.

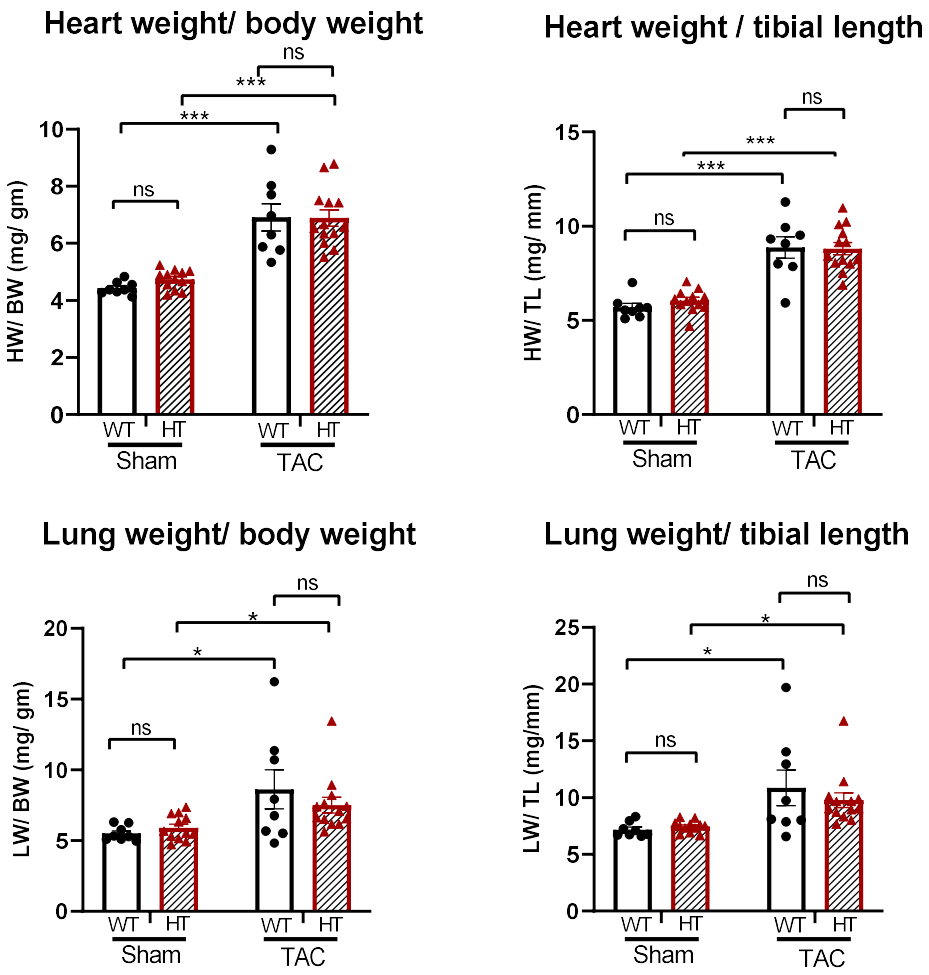

Figure 3.13: Heart weights and lung weights from PMCA1^{HT} mice 5 weeks after TAC. Data presented as mean ± SEM with two-way ANOVA used for analysis. Tukey's test was used for post-hoc analysis (ns non-significant, * p <0.05, *** p 0.0001). WT = wild type, HT = PMCA1^{HT}).

The heart weight and lung weight data from wild type and PMCA1^{HT} mice after 5 weeks of TAC (or sham) procedure presented in the bar chart above (figure 3.9). There is no significant difference in heart weight (HW/ BW and HW/ TL) of wild type and PMCA1^{HT} mice from sham or the TAC group. As expected, TAC induced a robust hypertrophic response with WT:TAC mice having a significantly higher heart weight compared to WT shams (8.86 mg/mm±0.56 vs 5.69 mg/mm ±0.20 p 0.0001). Similarly, PMCA1^{HT} mice after TAC have significantly higher heart weight compared to PMCA1^{HT} mice sham group (8.80mg/ mm ±0.32 vs 6.04 mg/mm ±0.17, p 0.0001). These findings suggest development of left ventricular hypertrophy in the

mice following pressure overload caused by TAC procedure in both genotypes. On the similar lines, there is no significant difference in lung weight (LW/ BW and LW/ TL) of wild type and PMCA1^{HT} mice from sham or the TAC group. WT mice from the TAC group develop significantly higher lung weight compared to WT sham group (10.86 mg/mm±0.96 vs 7.17mg/mm ±0.22 p 0.017) and similarly PMCA1^{HT} mice after TAC also have significantly higher lung weight compared to PMCA1^{HT} mice sham group (9.77mg/mm±0.64 vs 7.45mg/mm±0.15, $p<0.04$). Higher lung weights in TAC mice demonstrate presence of pulmonary congestion secondary to pressure overload exerted by narrowing of the aortic lumen.

3.4.3.2.4 Histological analysis of hypertrophic response in PMCA1^{HT} mice 5 weeks after TAC.

The data presented above demonstrates that following the TAC procedure, mice of both genotypes (WT and PMCA1^{HT}) develop left ventricular hypertrophy. However, cardiac hypertrophy can also be observed from the enlargement of individual cardiomyocytes. In order to assess and compare the hypertrophic response, the mean cross- sectional area or the average cell size of cardiomyocytes was measured after staining the sections with Haematoxylin and Eosin (H&E), as shown in figure 3.14A. Measurements of the cardiomyocyte cross sectional area are presented in figure 3.14B.

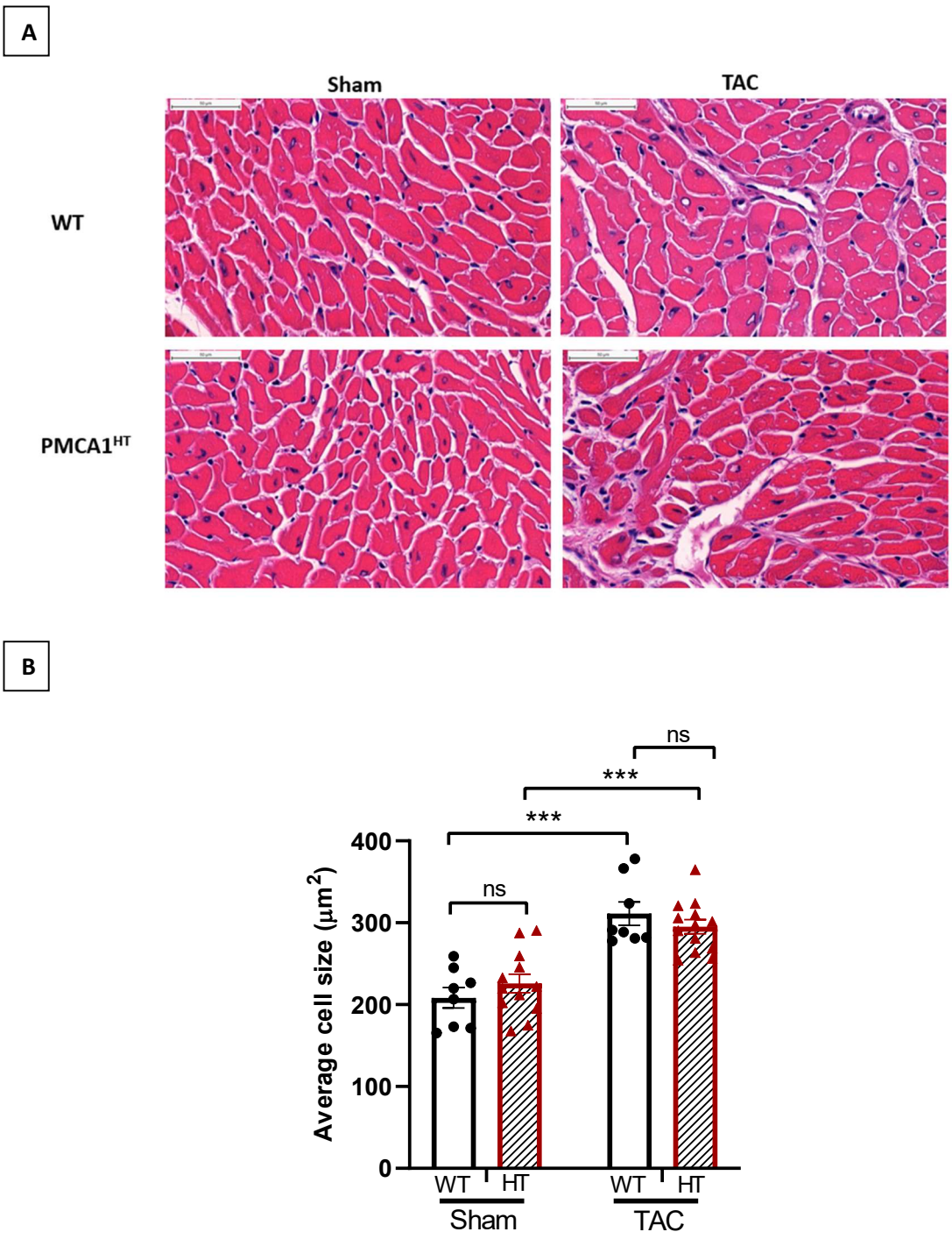

Figure 3.14: Cardiomyocyte cross-sectional area in PMCA1^{HT} mice after five weeks TAC.
(A) Representative H&E-stained histological cross sections from WT and PMCA1^{HT} mice. Scale bar represents 50 µm. (B) Average cardiomyocyte cross section area. One hundred cells were counted from two sections per animal and the average presented above.
Data presented as mean ± SEM with two-way ANOVA used for analysis. Tukey's test was used for post-hoc analysis (ns non-significant, ***p 0.0001). WT= wild type, HT= PMCA1^{HT}

The results show that there is no significant difference in the average cell size of WT:sham and PMCA1^{HT}:sham mice (206.6 µm^2±14.3 vs 232.7 µm^2 ±16.7, p=0.27). TAC led to an increase in average cell size compared to the genotype matched sham controls in both WT (306.6 µm^2±12.0 vs 206.6 µm^2 ±14.3, p<0.001) and PMCA1^{HT} mice (295.2 µm^2±13.1 vs 232.7 µm^2 ±16.7, p<0.0001). However, there was no significant effect of genotype, with both genotypes developing a similar degree of cardiomyocyte hypertrophy after TAC, resulting in no significant difference in the average cell size of WT:TAC and PMCA1^{HT}:TAC mice (306.6 µm^2±12.0 vs 295.2 µm^2 ±13.1, p0.55). These findings confirm that TAC procedure was successful in producing a significant hypertrophic response of similar extent in mice from both genotypes.

As natriuretic peptides are established markers of cardiomyocyte hypertrophy, quantitative real time-polymerase chain reaction (qRT-PCR) was used to assess ANP (nppa) and BNP (nppb) RNA expression in WT and PMCA1^{HT} mice after five weeks of TAC or the sham procedure. The results are shown in figure 3.15.

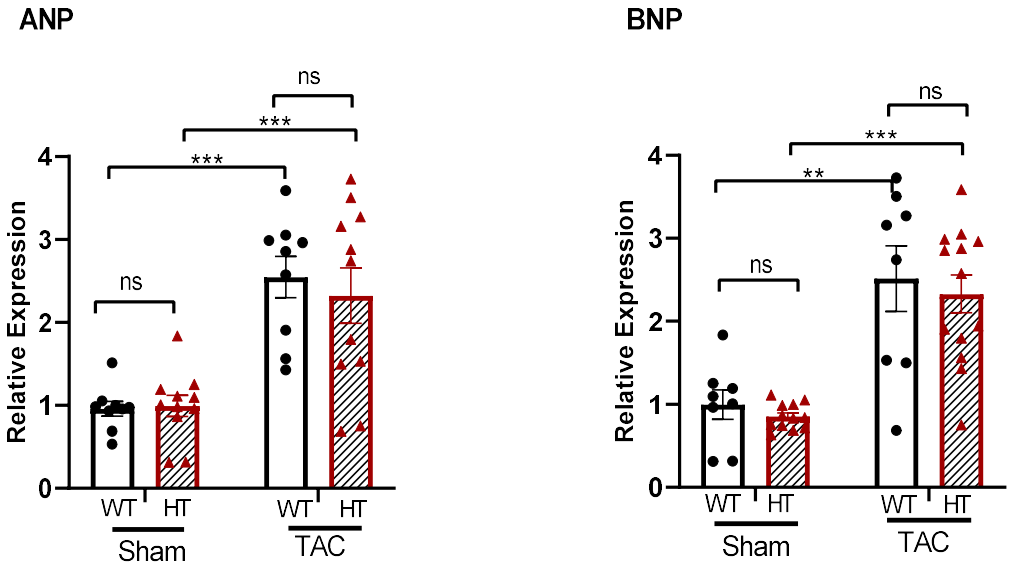

Figure 3.15: RT-PCR analysis of ANP (nppa) and BNP (nppb) RNA expression in PMCA1^{HT} mice after five weeks TAC. Gapdh was used as housekeeping gene and y-axis represents relative expression. Data presented as mean ± SEM with two-way ANOVA used for analysis. Tukey's test was used for post-hoc analysis (ns non-significant, ** p 0.001, *** p 0.0001). WT = wild type, HT = PMCA1^{HT}

For the RT-PCR analysis, gapdh was used as housekeeping gene and the data was normalised to Gapdh expression. The RT-PCR analysis shows that the expression of ANP (nppa) and BNP (nppb) is similar in WT and PMCA1^{HT} mice after sham procedure (p=0.99). After five weeks TAC, mice from both genotypes demonstrated a significantly higher expression of ANP (nppa) and BNP (nppb) compared to the sham cohorts (p<0.001). However, following five weeks TAC, ANP (nppa) RNA expression was similar between both genotypes (p=0.93). Similarly, no significant difference was found in the BNP (nppb) RNA expression between WT:TAC and PMCA1^{HT}:TAC groups (p 0.90).

3.4.3.2.5 Histological analysis of fibrosis PMCA1^{HT} mice 5 weeks after TAC.

Pressure overload exerted by transverse aortic constriction induces pathological stress on the myocardium that may also lead to myocardial fibrosis. Histological sections obtained from the left ventricle were stained with Masson's Trichrome to assess and compared the degree of fibrosis (figure 3.16A). The area of myocardial fibrosis through the whole section of left ventricle was quantified by using Image J (NIH Image) and expressed as a percentage of the total stained area. The results show that there is no significant difference in the fibrosis levels in the hearts from WT and PMCA1^{HT} mice after the sham procedure (1.33 %± 0.26 vs 1.10% ±0.11, p0.36). TAC resulted in a similar increase in myocardial fibrosis in both genotypes (6.1% ±0.35 vs 5.85% ±0.34, p=0.64). These findings highlight that in addition to stimulating myocyte hypertrophy, the TAC procedure and the resultant pressure overload led to a significant myocardial fibrosis that was equivalent in mice from both genotypes (figure 3.16 B).

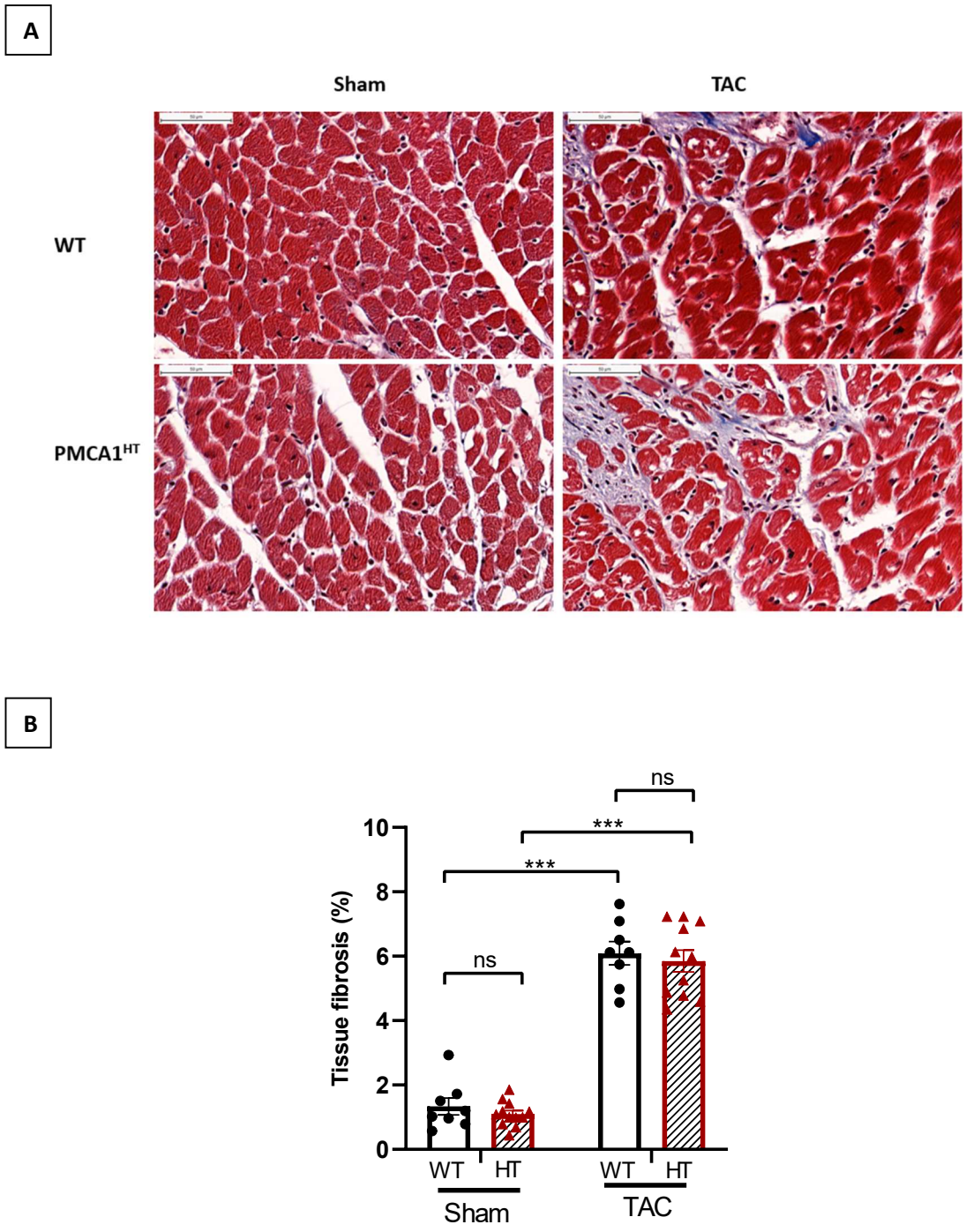

Figure 3.16: The level of myocardial fibrosis in PMCA1^{HT} mice after two weeks TAC.
(A) Representative Masson's Trichrome stained transverse histological cross sections. Scale bar represents 50 µm. (B) Percentage fibrosis calculated from the analysis of Masson's Trichrome stained histological cross sections. This was calculated as the % of fibrosis in the whole section through the left ventricle. Data presented as mean ± SEM with two-way ANOVA used for analysis. Tukey's test was used for post-hoc analysis (ns non-significant, *** p 0.0001). WT = wild type, HT = PMCA1^{HT}

Collagen types 1 and 3 (COL1α1 and COL1α3) are well established markers of tissue fibrosis (Ely et al., 2010). In this study, qRT-PCR was used to assess the relative expression of COL1α1 and COL1α3 in WT and PMCA1^{HT} mice after five weeks of TAC or sham surgery (figure 3.17).

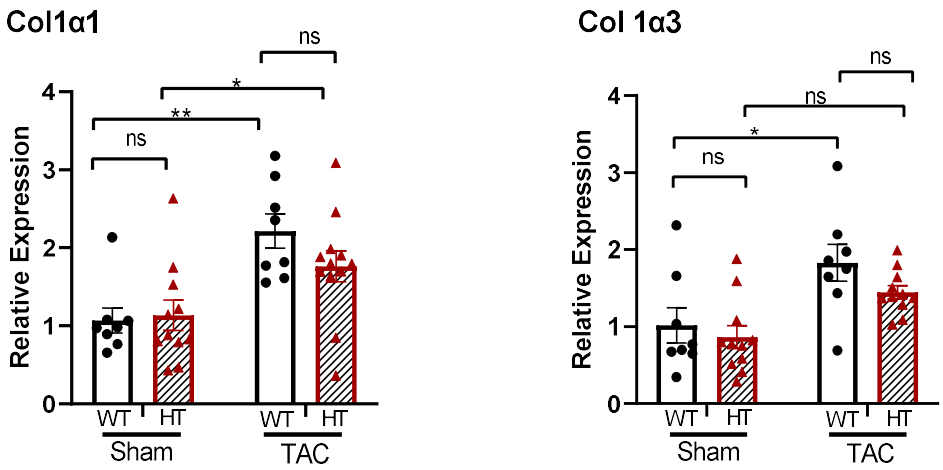

Figure 3.17: RT-PCR analysis of COL1α1 and COL1α3 RNA relative expression in WT and PMCA1^{HT} mice after five weeks TAC. Gapdh was used as housekeeping gene and y-axis represents relative expression. Data presented as mean ± SEM with two-way ANOVA used for analysis. Tukey's test was used for post-hoc analysis (ns non-significant, * p <0.05, ** p<0.01). WT = wild type, HT = PMCA1^{HT}

The RT-PCR analysis shows no significant difference in the relative expression of COL1α1 and COL1α3 in WT and PMCA1^{HT} mice five weeks after sham procedure. Following five weeks TAC, the expression of COL1α1 was significantly increased in both WT and PMCA1^{HT} mice compared to their genotype matched shams (p <0.01 and <0.05 respectively). The mice from both genotypes also showed a trend towards an increase in expression of COL1α3, although this increase in expression was only statistically significant in WT type mice (p<0.05). No significant difference in the expression of either COL1α1 or COL1α3 was found by comparing the TAC groups from the two genotypes (p=0.39 and 0.99 respectively).

3.4.3.2.6 Analysis of markers of apoptosis in PMCA1^{HT} mice after five weeks TAC

Apoptosis play a critical role in the initiation and progression of tissue fibrosis during the development of heart failure (Piek et al., 2016). The process of apoptosis is regulated by a number of proteins including BAX (Bcl2 -associated X protein) and Bcl2 (Gürtl et al., 2009). qRT-PCR was used to assess BAX and Bcl2 RNA expression in WT and PMCA1^{HT} mice after two weeks of TAC or sham surgery (figure 3.18).

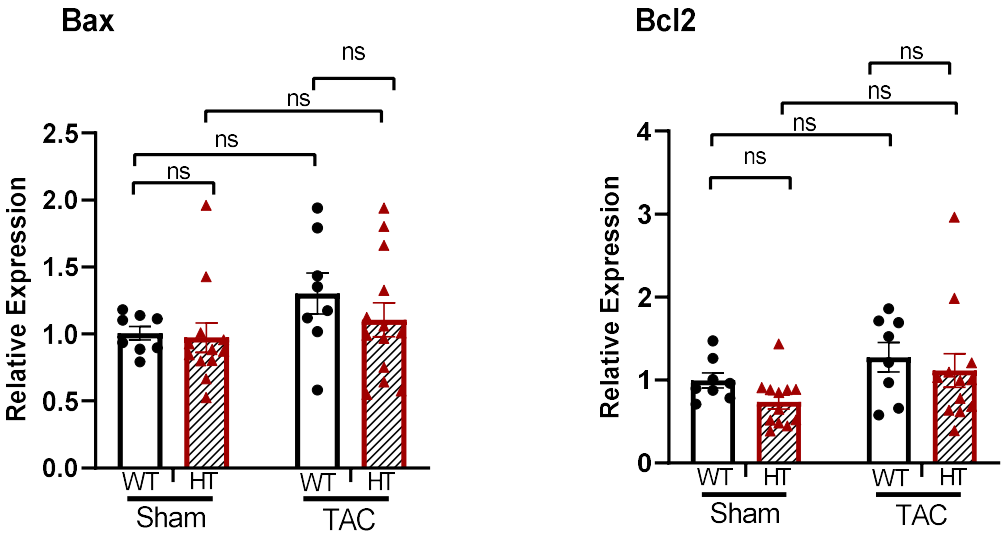

Figure 3.18: RT-PCR analysis of Bax and Bcl2 relative expression in WT and PMCA1^{HT} mice after five weeks TAC. Gapdh was used as housekeeping gene, y-axis represents relative expression. Data presented as mean ± SEM with two-way ANOVA used for analysis. Tukey's test was used for post-hoc analysis (ns non-significant). WT = wild type, HT = PMCA1^{HT}

The qRT-PCR analysis shows no significant difference in the expression of BAX and Bcl2 in WT and PMCA1^{HT} mice subjected to the sham procedure. After five weeks TAC, a trend towards higher relative expression of BAX and Bcl2 was noted in the mice from both genotypes compared to their genotyped matched shams; however, it was not statistically significant. In the two groups of mice subjected to TAC; on direct comparison, no difference in expression of either gene was found.

3.4.3.2.7 Analysis of the expression of calcium handling genes in PMCA1^{HT} mice after five weeks TAC

In order to assess the effects of pressure overload on the gene expression in WT and PMCA1^{HT} mice five weeks after TAC, qRT-PCR was conducted. The expression of PMCA1, PMCA4 and other calcium handling genes including SERCA2, NCX and RyR were assessed. The results are shown in figure 3.19.

These results confirm that PMCA1^{HT}: sham mice have lower expression of PMCA1 compared to WT: sham ($p<0.05$) and although both genotypes show a trend towards an elevated expression of PMCA1 after TAC procedure; none the less, PMCA1^{HT}: TAC mice also show significantly lower expression of PMCA1 compared to WT: TAC. The expression of PMCA4 is similar in both genotypes after sham and TAC procedure.

The impact of global deletion of PMCA1 under the conditions of pressure overload on the expression of other key genes involved in calcium handling in the cardiomyocyte was also examined by qRT-PCR. The RNA expression levels of PMCA4, SERCA2, NCX and RyR were assessed.

Expression of other Ca^{+2} handling channels [SERCA2 (Atp2a2), NCX (Scl8a1) and RyR (Ryr1)] is similar in both genotypes after sham procedure (figure 3.19). SERCA2 expression increases in both genotypes after TAC procedure ($p<0.05$); however, the expression of NCX and RyR1 shows no statistically significant changes after TAC procedure, in mice from either genotype.

In summary, RT PCR data shows that the main difference between the PMCA1^{HT} and WT mice is a lower expression of PMCA1 in the former. Whilst the expression of a number of genes increases in response to the pressure overload caused by transverse aortic constriction (TAC), there is no significant difference between the two genotypes.

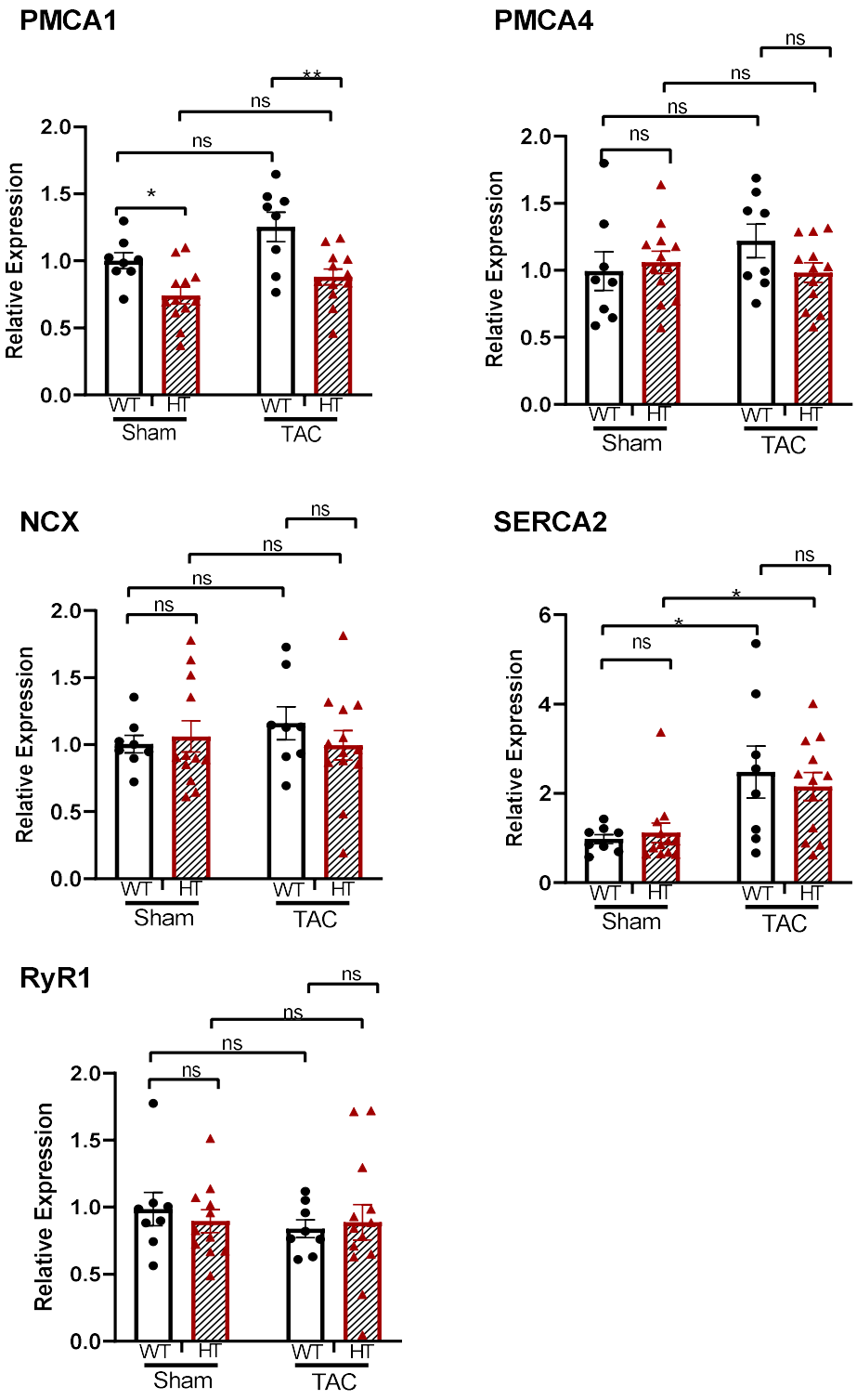

Figure 3.19: RT-PCR analysis of the expression of calcium handling genes in PMCA1^{HT} mice after five weeks TAC. Gapdh was used as housekeeping gene and y-axis represents relative expression. Data presented as mean ± SEM with two-way ANOVA used for analysis. Tukey's test was used for post-hoc analysis (ns non-significant, * $p < 0.05$, ** $p < 0.01$). WT = wild type, HT = PMCA1^{HT}

3.5 Discussion

As outlined in the beginning of this chapter, the main aim of this project was to identify whether the deletion of PMCA1 has any impact on the structure and the function of the heart under pathological stress caused by pressure overload. The author hypothesised that a heterozygous deletion of PMCA1 would have a detrimental effect on the heart leading to exacerbation of cardiomyopathy after pressure overload exerted by transverse aortic constriction. This study was started with a hypothesis that due to their susceptibility to develop hypertension PMCA1^{HT} mice would have a worse outcome after five weeks of TAC. However, the results did not prove this and in fact PMCA1^{HT} mice developed compensated hypertrophy after TAC and their phenotype was not any worse from the heart failure perspective compared to the wild type mice.

3.5.1 Global heterozygous PMCA1 deletion does not affect cardiac structure and function at the basal level

Since PMCA1 is ubiquitously expressed and is established as a house keeping gene, this is the reason that a homozygous global PMCA1 deletion leads to embryonic lethality, very early in the foetal development (Okunade et al., 2004). However, Little and colleagues have shown in their study that global heterozygous deletion of PMCA1 results in approximately 50% less expression of PMCA1 mRNA in heart, brain and aorta (Little et al., 2017). The authors further supported the lower mRNA expression results with protein analysis confirming a significantly lower expression of PMCA1 protein in the organs described above. However, these findings have not been consistent; Liu et al. used a traditional gene deletion model and found no difference in PMCA1 protein levels in urinary bladder of PMCA1^{HT} mice compared to the aged matched wild type cohort (Liu et al., 2007). The discrepancy in the above studies may be due to using different gene deletion technologies and using different tissue to examine PMCA1 expression. In keeping with the previous published work, in the present study, PMCA1 mRNA expression was approximately halved in PMCA1^{HT} mice compared to the wild type control. There was no stunting of growth in PMCA1^{HT} mice who achieved similar weights to WT mice. It was also found that approximately 50% lower expression of PMCA1 was sufficient for the normal development and maturation of heart in PMCA1^{HT} mice, because on 2D echocardiography the there was no significant difference in the structure and function of heart (cardiac contractility and the left ventricle dimensions) of PMCA1^{HT} and WT mice at 12

weeks of age. This data is further supported by haemodynamic measurements, pressure-volume loop analysis and measurement of heart and lung weight in both genotypes. It indicates that under basal conditions global heterozygous deletion of PMCA1 does not affect the structure or the function of heart. This is in line with previous observation by Little and colleagues on 18months old PMCA1^{HT} mice (Little et al., 2017).

Heterozygous global deletion of genes involved in Ca^{2+} extrusion is not known to have a deleterious effect on the heart under basal conditions. Similar results have been reported by researchers who found no difference the structure and performance of heart in humans with Darier's disease which is characterised by heterozygous disruption of SERCA2 (Mayosi et al., 2006). The authors reported that myocardium could compensate for the loss of one copy of SERCA2 (i.e heterozygous deletion) by a reduced expression and increased phosphorylation of inhibitory protein phospholamban and increased expression of NCX, hence cellular Ca^{2+} metabolism and cardiac structure and function remained preserved. Upregulation of the remaining normal SERCA2 allele might also play a role. A mouse model with heterozygous deletion of NCX has been reported to exhibit electrical changing involving depolarisation potentials; however, no abnormalities in cardiac structure or function were noted (Bögeholz et al., 2015). Bögeholz and colleagues also did not find any significant changes in the expression of key Ca^{2+} handling and structural proteins following the heterozygous deletion of NCX in mice. These data confirm that lower levels of Ca^{2+} exodus proteins resulting from their heterozygous deletion are sufficient for a normal development and maturation of heart.

The present study also shows that mRNA expression of other Ca^{2+} handling channels remains un-altered in PMCA1^{HT} mice under basal conditions. A group found similar results after cardiomyocyte specific knock out of NCX1, who found no compensatory increase in the other Ca^{2+} handling proteins (Henderson et al., 2004). Previous published research work also did not report any compensatory increase in PMCA4, NCX or SERCA in six months old PMCA1^{HT} mice (Little et al., 2017). In addition, we found no difference in the levels of BNP expression in 12 weeks old PMCA1^{HT} mice compared to the wild type littermates suggesting no difference in the levels of hypertrophy, under basal conditions.

Pressure overload exerted by TAC is known to induce several changes in the gene expression in the heart that undergoes re-modelling. These changes represent, in part, compensatory

mechanisms initiated in heart to deal with the stress caused by pressure overload but may also be due to wider systemic consequences of cardiac re-modelling (van den Bosch et al., 2006) . Firstly, after subjecting 8 week old PMCA1^{HT} and wild type mice to transverse aortic constriction (TAC) for five weeks, RT PCR shows that the former had a lower expression of PMCA1 in the sham group and whilst there is some increase in the PMCA1 expression following TAC, PMCA1^{HT} mice consistently had lower PMCA1 expression. Although, the expression of mRNA does not always translate into equivalent protein levels (Liu et al., 2016), none the less, a lower PMCA1 expression in this cohort validates the experimental model.

3.5.2 Global heterozygous deletion of PMCA1 does not affect the development of myocardial hypertrophy after pressure overload exerted by TAC

Cardiac myocytes undergo hypertrophy in response to a variety of stimuli such as pressure overload, muscle injury and intrinsic defects in the contractile apparatus. The process is mediated by a wide range of endocrine, paracrine and autocrine pathways (Heineke & Molkentin, 2006). Some of the interaction partners of PMCA4, including calcineurin and Ras effector Ras-association domain family 1 isoform A (RASSF1A) contribute to the modulation of hypertrophy. In the calcineurin-NFAT signalling pathway, activated calcineurin promotes dephosphorylation of NFAT which subsequently translocates into the nucleus and participates in calcium inducible gene transcription (Molkentin, 2004). RASSF1A on the other hand downregulate extracellular regulated kinases (ERK) 1&2 leading to an inhibition of hypertrophy (Oceandy et al., 2009).

The above evidence has formed the basis for researchers to investigate the role of PMCA in the regulation of cardiac hypertrophy. PMCA4 inhibition has been demonstrated to result in attenuated hypertrophic response to transverse aortic constriction and may even reverse pre-existing myocardial hypertrophy (Mohamed et al., 2013). However, deletion of PMCA4 does not appear to prevent exercise induced physiological hypertrophy (Wu et al., 2009). Recent work from our group have shown that PMCA4's modulation of cardiac hypertrophy is not limited to the signal transduction pathways described above. Deletion of PMCA4 in cardiac fibroblasts promotes increased secreted frizzled related protein-2 (sFRP2) levels which attenuates Wnt signal pathway resulting in inhibition of hypertrophy in cardiac myocytes (Mohamed et al., 2016).

PMCA1, the most abundant PMCA isoform in the heart, is also known interact with calcineurin (Holton et al., 2010), which raise the possibility of its involvement in the regulation of cardiac hypertrophy. Lower concentrations of PMCA have been found in human heart tissue in cardiac failure patients compared to those with normal cardiac function. Cardiac arrhythmias are common in heart failure patients and account for nearly 50% of the mortality in those with an advanced disease (Santangeli et al., 2017). The possibility of genetic susceptibility to cardiac rhythm abnormalities in this patient cohort is becoming a major area of heart failure research (Oceandy et al., 2011). The present study shows that WT and PMCA1^{HT} mice that underwent sham procedure did not develop myocardial hypertrophy; however, mice from both genotypes developed significant hypertrophy following TAC procedure. It is important to note that haemodynamic study confirmed no difference in P_{max} value (maximal left ventricular pressure during systole) suggesting a similar increase in the workload was exerted by TAC in both WT and PMCA1^{HT} mice. This ensures consistency in experimental parameters and practices for both treatment groups, hence removing any bias.

Following TAC procedure, although PMCA1^{HT} mice have significantly thicker interventricular septum and posterior wall, compared to the wild type mice. This indicates development of concentric hypertrophy in PMCA1^{HT} mice and eccentric hypertrophy in the WT mice. Moreover, hearts from both genotypes have similar normalised weights confirming the development of similar degree of hypertrophy. These findings are further supported by histological analysis of average cell size that shows a relative increase in the average cardiomyocyte size (cross sectional area) following TAC, but with no additional difference due to genotype. In addition, five weeks after TAC, mice from both genotypes exhibited a decline in cardiac contractility as manifested by a significant drop in ejection fraction and fractional shortening (compared to the sham cohorts). However, WT:TAC mice had a significantly lower LV fractional shortening and a trend towards a lower ejection fraction compared to the PMCA1^{HT} :TAC mice.

A decline in cardiac systolic function in the TAC groups was accompanied by a relative increase in their normalised lung weights in keeping with a degree of pulmonary congestion and oedema, with both genotypes effected similarly. In the TAC experiment, researchers have reported that after an initial period of compensated hypertrophy; the heart goes into decompensation with a decline in contractility and the development of features of heart

failure usually 4-6 weeks post TAC surgery (Chen et al., 2012; Toischer et al., 2010). This is in keeping with our observation in the present five weeks long study. Previously, colleagues from our group found no difference in the degree of the degree of left ventricular hypertrophy in mice undergoing TAC for two weeks or five weeks; however, the deterioration of LV function was found to higher with longer duration of TAC and increasing animal age (Zi et al., 2019). Interesting previous work by colleagues from our lab has shown that wild type mice developed exaggerated eccentric cardiac hypertrophy and higher endocardial circumference and LV lumens compared PMCA1^{HT} mice 1 week following experimental myocardial infarction (MI) suggesting some protective role of PMCA1 in early phases after suffering an MI (Stankovikj, 2017).

In addition, haemodynamic analysis demonstrated a higher systolic blood pressure (BP) in the mice after TAC without any impact of the genotype. A rise in the BP readings recorded from carotid catheterisation has been noted in TAC experiments by other teams, too (De Montgolfier et al., 2019). Although PMCA1^{HT} mice are known to have a susceptibility to the development of hypertension (Little et al., 2017) , in the present study mice from both genotypes developed higher systolic BP after TAC compared to the genotyped matched shams; there is no significant difference in the BP of WT and PMCA1^{HT} after the TAC procedure. This is most likely due to the fact the mice in this study were relatively younger i.e 13 weeks old at the time of invasive haemodynamic assessments whereas Little and colleagues (2017) found a higher blood pressure in PMCA1^{HT} mice at 12 months of age. Moreover, the prolongation of logistic tau (ƭ) which is a time constant of ventricular relaxation is prolonged, more so in the wild type mice, suggestive of some diastolic impairment in these mice after TAC procedure.

Natriuretic peptides (ANP and BNP) are widely recognized as markers of myocardial hypertrophy and rise following pressure overload due to TAC (Sergeeva & Christoffels, 2013). Increased expression of ANP and BNP has been consistently seen in murine TAC model (Nishikimi et al., 2006). Our results also show a significant increase in the expression of natriuretic factors following TAC in both genotypes. As mentioned earlier the histology data shows increased cardiomyocyte cross sectional area suggestive of hypertrophy which is further supported by the echocardiography. An elevated expression of natriuretic peptides after TAC also confirms the echocardiography and histology data. However, it appears that global heterozygous deletion of PMCA1 does not affect the expression of ANP and BNP

following pressure overload.

Cardiac hypertrophy secondary to chronic pressure overload is also accompanied by increased levels of myocardial fibrosis, as a part of the cardiac re-modelling process (Matsushita et al., 2018). This is observed in our study as well; expression collagen 1 and 3 were significantly elevated in both genotypes five weeks following TAC. Histological data following examination of transverse heart sections stained with Masson's Trichrome also demonstrated a significant rise in myocardial fibrosis in WT and PMCA1^{HT} mice following TAC. However, it appears that global heterozygous deletion of PMCA1 has no impact on the extent of myocardial fibrosis following pressure overload. Myocardial fibrosis is associated with the loss of contractile function and the development of heart failure (Segura et al., 2014). Comparable levels of fibrosis and expression of collagen genes in mice from both genotypes after TAC supports the findings from echocardiography whereby on most parameters WT and PMCA1^{HT} mice had no significant difference after TAC.

The present study showed that some echocardiography parameters showed development of eccentric cardiac hypertrophy in wild type mice with LV systolic dysfunction; however, these findings were not supported on the assessment of heart weight and haemodynamic analysis. Performing a TAC experiment in older PMCA1^{HT} mice and possibly for a longer duration may lead to the development of more definite phenotype changes which can help us to explore the impact of reduced PMCA1 expression on the cardiac structure and function. However, such an approach involving TAC for longer duration may be complicated by the development of more severe phenotype and poorer outcomes with the possibility of some animals being lost to heart failure before the completion of study (Bosch et al., 2021).

3.5.2.1 Global heterozygous deletion of PMCA1 does not affect the expression of other Ca^{2+} handling genes after 5 weeks of TAC

Pressure overload exerted by TAC is known to induce several changes in the gene expression in heart that undergoes re-modelling. These changes represent, in part, compensatory mechanisms initiated in heart to deal with the stress caused by pressure overload but may also be due to wider systemic consequences of cardiac re-modelling (van den Bosch et al., 2006) . This study shows that mice from both genotypes demonstrate a trend towards higher expression of PMCA1 five weeks after TAC; however, it was not statistically significant. The

expression of PMCA4 was not significantly increased after TAC in mice from both genotypes, as well. This shows that there is no significant increase in the expression of PMCAs after TAC and it is also important to note that global heterozygous deletion of PMCA1 does not affect the expression of other important PMCA form expressed in the heart i.e PMCA4.

Effect of pressure overload on the expression other important Ca^{+2} handling channels has been described in the literature (Toischer et al., 2010; Wang et al., 2003). Our results show an increase in the SERCA2 expression following TAC in mice from genotypes. Toischer et al. has also shown an increase in the expression of SERCA 2 in the initial few days of TAC (Toischer et al., 2010), other researchers have demonstrated a fall in the SERCA2 expression 8 weeks after TAC (Lu et al., 2011). The difference in the expression of SERCA2 at various time points following TAC may be due to the fact that heart manifests compensated left ventricular hypertrophy in the early phases after TAC whereas at the later stages the heart develops decompensated heart failure. Heart failure is known to be associated with lower expression of SERCA2 due to a negative feedback loop (Park & Oh, 2013).

NCX is an important calcium extrusion protein which has been shown to have altered expression in many cardiac hypertrophy and heart failure models including after transverse aortic constriction (Sipido et al., 2002). Lu and colleagues demonstrated an increased expression of NCX following pressure overload (Lu et al., 2011). There is also a report of increased NCX expression in catecholamine cardiac hypertrophy, as well (Chorvatova et al., 2004). However, the present study did not find any significant difference in the expression of NCX in either genotype following TAC. It is worth considering that Lu et al. reported a significant increase in the NCX expression eight weeks following TAC, in comparison to our study where TAC was only continued for five weeks. It is possible, if we had allowed our experiment to continue for a similar duration, NCX expression might have increased. This is because of the fact that a longer duration of TAC may result in decompensated heart failure. A higher expression of NCX has been repeatedly observed in decompensated heart failure scenario (Moon et al., 2008; Pott et al., 2011). NCX overexpression being an adaptive response to pressure overload, it is plausible that this response is dependent upon the duration of TAC. In the present study, a higher expression of SECA2 was noted after TAC and it is possible that it compensated for a lack of increased expression of NCX. With a higher

expression of SERCA2 in the present study, probably more calcium got pumped back into the sarcoplasmic reticulum rather than in the cytosol. To investigate this further, it would have been useful to assess the expression of L-type calcium channels which are reported to be downregulated in cardiac hypertrophy and failure (Hu et al., 2016).

In summary, our study shows that the heterozygous deletion of PMCA1 does not affect the development of LV hypertrophy in mice after TAC. Some interesting trends in the gene expression following five weeks of TAC on WT and PMCA1^{HT} mice were observed. Whilst there is a lower mRNA expression of PMCA1 cardiac tissue following global heterozygous deletion of PMCA1 (an observation that is consistent in sham and TAC groups), there is no compensatory increase in the expression of PMCA4 after TAC. It also demonstrates that global heterozygous deletion of PMCA1 does not alter the expression of other Ca^{2+} exodus channels in the heart.

This study has a number of limitations. Firstly, the duration of TAC was five weeks and probably this duration was not enough to develop a definite heart failure phenotype in mice from either genotype. Secondly, PMCA1 is a Ca^{2+} exodus channel and it is plausible that its heterozygous deletion may lead to some alterations intracellular Ca^{2+} concentration and calcium transient however in the present study, no assays were performed to assess changes in intracellular Ca^{2+} levels. Lastly, to assess the changes in the expression of Ca^{2+} exodus channels, this study relied on the RT-PCR analysis to quantify mRNA expression. However, it is well established that changes in mRNA expression may not always correlate with the alteration of corresponding protein expression, future work would look at the protein expression as well. In addition, this study focused on the mouse model with heterozygous global deletion of PMCA1 whereby the levels of PMCA1 are generally halved not only in cardiomyocytes but potentially all cell types that express PMCA1, including cardiac fibroblasts. The latter play an important role by producing growth factors, cytokines and other signaling molecules. Mohamed and colleagues have previously shown that deletion of another cardiac PMCA (PMCA4) in cardiac fibroblasts reduces cardiac hypertrophy whereas this effect is not produced by deleting PMCA4 in cardiomyocytes (Mohamed et al., 2016). PMCA1 may also undertake different roles in cardiomyocytes and fibroblasts, hence its heterozygous deletion in one cell cohort should be considered to understand the impact on cardiac structure and function.

Future work on the heterozygous deletion of PMCA1 should consider a longer duration of TAC. In this study, we used 8 weeks old male mice for the TAC and the sham procedure, and the study was completed when mice were 13 weeks old. Ageing is a well-established risk factor cardiovascular disease including hypertension and heart failure (Buford, 2016). Previous work from colleagues in our lab has shown that $PMCA1^{HT}$ mice develop hypertension with from the age of 9-12 months (Little et al., 2017). This was mediated by inward eutrophic remodeling of resistance arteries resulting in increased vessel wall thickness and reduced lumen diameter; however, there was no significant difference in the cardiac structure and function of WT and $PMCA1^{HT}$ mice despite the later having hypertension at that age (Little et al., 2017). Due to the susceptibility of $PMCA1^{HT}$ mice to develop hypertension with ageing, an experiment using older mice (> 9 months old) for TAC study should be considered. Moreover, due to PMCA1 expression in both cardiomyocytes and cardiac fibroblasts, future work should consider using tissue specific PMCA1 knockout models such as cardiomyocyte specific PMCA1 knockout and cardiac fibroblast specific PMCA1 knockout to examine the effects of reduced PMCA1 expression in specific cardiac tissue on cardiac phenotype under basal conditions and haemodynamic stress. Cardiomyocyte specific PMCA1 knockout model is discussed in the next chapter. Additionally, it will be interesting to examine the impact of heterozygous deletion of PMCA1 on the intracellular Ca^{2+} dynamics under the basal conditions and after TAC to help further our understanding of its impact on cellular pathways.

3.6 Conclusion

This study shows that global heterozygous deletion of PMCA1 results in a lower expression of PMCA1 in murine heart but does not affect cardiac structure or function under basal conditions. When subjected to pressure overload by transverse aortic constriction for five weeks, $PMCA1^{HT}$ mice develop radial hypertrophy and a decline in the cardiac contractility. Whilst both groups exhibit a higher systolic BP following TAC, there is no difference between the two genotypes. Global heterozygous PMCA1 deletion does not appear to adversely affect the cardiac structure or function following TAC for 5 weeks. In conclusion, the loss of single allele of PMCA1 does not appear to play a role in TAC induced cardiac hypertrophy. This may mean that the reduced levels of PMCA1 as a result of heterozygous global deletion of PMCA1 are sufficient for normal cardiac structure and function under the basal conditions.

In addition, it also implies that younger adult mice (13 weeks old in this study) can also cope with haemodynamic stress caused by TAC despite having lower levels of PMCA1. These results further pave the way to consider the impact of a cardiomyocyte specific homozygous deletion of PMCA1 on cardiac structure and function which is described in the next chapter.

Chapter 4 - Cardiomyocyte specific deletion of PMCA1 and its impact on cardiac structure and function under pathological stress

4.1 Introduction

It is well established that ventricular muscle undergoes hypertrophy in response to an increased workload in an attempt to maintain adequate cardiac output to ensure organ perfusion. Left ventricular hypertrophy is often accompanied by further cardiac remodelling including fibrosis and is an independent risk factor for ischaemic heart disease, cardiac dysrhythmias, and heart failure. Therefore, understanding and targeting the pathways that underpin the progression from compensatory cardiac hypertrophy to clinical heart failure is critical to prevent adverse cardiovascular events.

As described in chapter 3, global heterozygous deletion of PMCA1 does not result in any changes in cardiac structure and function, under basal conditions. Similarly, previous work by colleagues from our group has demonstrated that cardiomyocyte specific deletion of PMCA1 does not produce any overt spontaneous structural change *in-vivo* (Wilson, 2017), hence for this study we planned and performed experiments to explore whether PMCA1 undertook an enhanced role during cardiac stress. PMCA4 is known to modulate transverse aortic constriction (TAC) induced cardiac hypertrophy via the calcineurin-NFAT pathway, and also via altered expression of secreted frizzled related protein 2 (sFRP2) (Mohamed et al., 2016; Wu et al., 2009). Therefore, pressure overload by TAC was chosen as a left ventricular hypertrophy model to explore the role of cardiomyocyte specific deletion of PMCA1 in pathological hypertrophy.

4.1.1 The role of PMCA in cardiac hypertrophy

The association between hypertension and heart failure is already well established. As discussed in the previous chapter, genome wide association studies (GWAS) have demonstrated a link between blood pressure, hypertension and ATP2B1 – the gene encoding for plasma membrane calcium ATPase 1 (PMCA1) (Ehret et al., 2011). Previous work by our group demonstrated that cardiomyocyte specific deletion of PMCA1 ($PMCA1^{cko}$) in mice is associated with heart rhythm abnormalities, particularly due to an impaired ventricular depolarisation (Wilson, 2017). In a separate set of experiments, after the deletion of PMCA1 hearts were found to be more susceptible to atrial arrythmias under stress conditions (Wang et al., 2017). An increased susceptibility to ventricular and atrial arrhythmia was noted in $PMCA1^{cko}$ mice in the absence of any cardiac structural abnormality, suggesting a key role for PMCA 1 in the regulation of cardiac rhythm. Cardiac arrhythmias are common in heart

failure and are associated with significantly higher risk of mortality and morbidity in this patient cohort (Ellison et al., 2003). Being the most abundant form of PMCA in the heart (Stauffer et al., 1993), it is plausible that PMCA1 may also contribute to the regulation of cardiac growth and hypertrophy. These associations make PMCA1, a prime target for further research to explore its role in cardiac hypertrophy and ultimately in the development of heart failure. However, no published studies, thus far have examined the role of PMCA1 in a pressure overload model.

4.1.2 Animal models of cardiac hypertrophy

In-vivo experimental models of cardiac hypertrophy have enabled researchers to enhance their understanding of the way the heart responds to various physiological and pathological stimuli (Breckenridge, 2010). When compared to the isolated organ or cellular models, whole animal models offer the opportunity to study the cardiac function and heart failure phenotype (Camacho et al., 2016). The choice of animal model depends upon the cardiovascular process being studied and how the results can be extrapolated to human health and disease. Cost and convenience are other important considerations. With these in view, over the last few decades, the mouse has emerged as the small animal model of choice for cardiovascular research. Great homology with the human genome, ease of creating genetic manipulation and short lifespan make the mouse an ideal model for high throughput studies (Amgalan & Kitsis, 2019).

Exercise models, involving swimming or running, both are widely used to induce physiological left ventricular hypertrophy in mice. Although labour intensive, both models are generally easy to set up and cheap to run (Schaible & Scheuer, 1984). On the contrary, pressure overload created by transverse aortic constriction (TAC) is a useful model to produce pathological left ventricular hypertrophy and ultimately, multisystem effects of heart failure. The use of TAC in a murine model was first described by Rockman and colleagues, nearly thirty years ago (Rockman et al., 1991). This technique typically produces a difference in the peak flow velocity between the right and left carotid artery resulting in 25-30 mmHg pressure gradient (Zi et al., 2014a). This pressure overload, in turn, induces significant and predictable left ventricular hypertrophy with likelihood of its progression to left ventricular failure.

4.1.3 Hypothesis and aims

Previously, work from our group has shown that a cardiomyocyte specific deletion of PMCA1 ($PMCA1^{cko}$) leads to cardiac rhythm abnormalities. Cardiac arrhythmias are prevalent in patients with heart failure and confer a substantially high risk of mortality and morbidity in this cohort. The aim of this research project is to identify whether the cardiomyocyte specific deletion of PMCA1 has any impact on the structure and the function of the heart under pathological stress. Our hypothesis is that a cardiomyocyte specific deletion of PMCA1 will have a detrimental effect on the heart and lead to exacerbated cardiomyopathy after pressure overload produced by transverse aortic constriction (TAC).

The aims of the project were to

Characterise cardiovascular remodelling in $PMCA1^{cko}$ and $PMCA1^{FLOX/FLOX}$ ($PMCA1^{F/F}$) mice after pathological stress caused by pressure overload induced by 2 weeks TAC.

a. Assess the structural changes in heart as a result of reduced expression of PMCA1 in a TAC model of cardiac stress.
b. To determine the functional changes in heart in the context of reduced expression PMCA1 in the TAC model.
c. To characterise the level of cardiac apoptosis and fibrosis.
d. Assess if the reduced expression of PMCA1 in a TAC model has any impact of the expression of other calcium handling genes.

4.2 Results

In order to determine whether reduced expression of PMCA1 predisposes mice to heart failure under pathological stress exerted by transverse aortic constriction (TAC); $PMCA1^{cko}$ and $PMCA1^{F/F}$ were both subject to TAC for two weeks. Echocardiographic, haemodynamic, histological and biochemical analysis was undertaken to assess if there is a difference in cardiac structure and function, and whether deletion of PMCA1 leads to alterations in the expression of calcium transporting channels.

4.2.1 DNA genotyping to identify PMCA1 cardiomyocyte specific knockout (PMCA1^{cko}) mice and PMCA1$^{F/F}$ controls

To determine the genotype of the pups born as a result of a breeding αMHC-Cre:PMCA1$^{F/F}$ mice with PMCA1$^{F/F}$ PCR was performed on DNA extracted from the ear tissue biopsies. The expected amplicon size for floxed allele is 3449 bp and for the excised allele 1300 bp (see section 2.2.2 for detailed methods). Mice carrying the cre transgene would exhibit a 250bp amplicon. In the first PCR reaction, the floxed allele (3449bp) was amplified, as shown in figure 4.1 A. Following this, a second PCR reaction was performed to amplify αMHC_Cre (250bp), shown in figure 4.1 B. The final results are shown in figure 4.1C.

Both PMCA1^{cko} and PMCA1$^{F/F}$ mice carry floxed allele (3449bp) and only PMCA1^{cko} mice carry αMHC-Cre (250bp). Following gel electrophoresis, a single 250bp band represented a PMCA1^{cko} pup, whilst PMCA1$^{F/F}$ pups did not exhibit any bands.

A

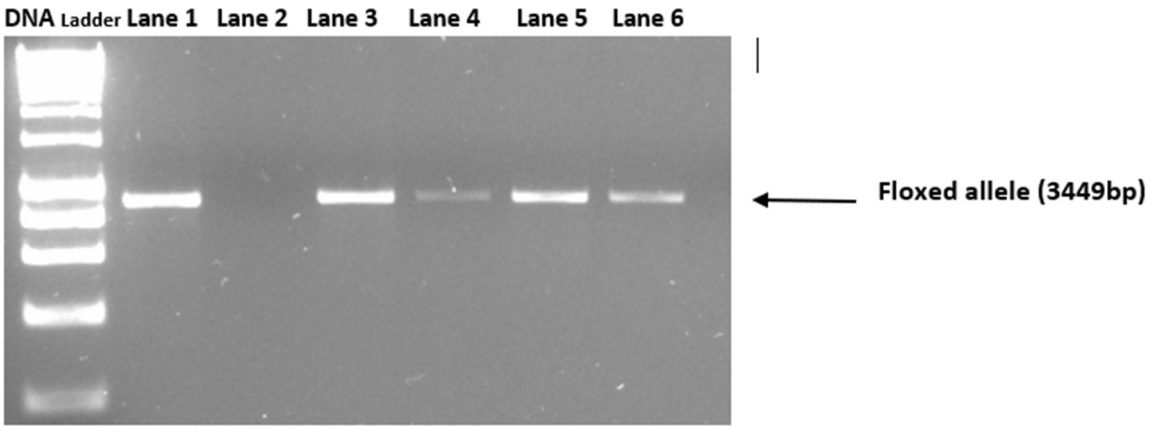

B

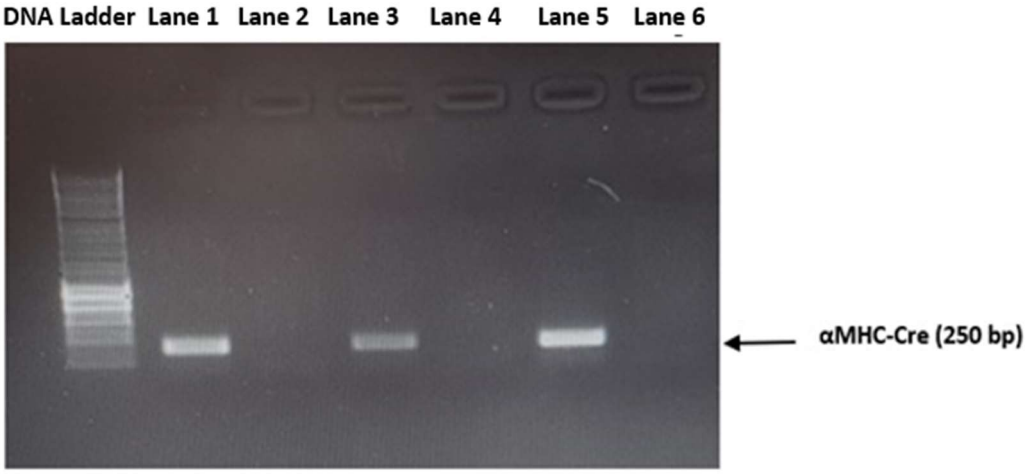

C

Lane	Genotype	Lane	Genotype
1	PMCA1^{cko}	4	PMCA1$^{F/F}$
2	H_20 control (negative control)	5	PMCA1^{cko}
3	PMCA1^{cko}	6	PMCA1$^{F/F}$

Figure 4.1: PCR analysis of DNA extracted from ear tissue biopsies. (A) Both PMCA1^{cko} and PMCA1$^{F/F}$ mice carry a floxed allele 4.49kb. Lane 2 contain H_20 control. (B) Only, PMCA1^{cko} mice carry the αMHC-Cre at 250bp. (C) A table showing the results of genotyping.

Both PMCA1^{cko} and PMCA1$^{F/F}$ mice carry floxed allele (3449bp) and only PMCA1^{cko} mice carry αMHC-Cre (250bp). Following gel electrophoresis, a single 250bp band represented a PMCA1^{cko} pup, whilst PMCA1$^{F/F}$ pups did not exhibit any bands.

Genotype results, throughout the whole study, showed that as expected 50% of the resulting pups were PMCA1^{cko} and 50% of pups were PMCA1$^{F/F}$

4.2.2 Animal used in this experiment

At 8 weeks of age, PMCA1^{cko} and PMCA1$^{F/F}$ control mice underwent surgical transverse aortic constriction or a sham operation. After two weeks, cardiac structure and function was assessed by echocardiogram and cardiac catheterization. Following the sacrifice of animals, histological examination and molecular analysis was performed. The number of animals in each group is shown in table 4.1.

Genotype: surgical procedure	**PMCA1$^{F/F}$: sham**	**PMCA1$^{F/F}$: TAC**	**PMCA1^{cko}: sham**	**PMCA1^{cko}: TAC**
N	8	11	11	13

Table 3.4: The number of animals in the sham and TAC groups, and their genotypes.

The above-mentioned n numbers of animals were used in the subsequent experiments described in this chapter except where specifically mentioned otherwise. In this project, the intraoperative mortality during the TAC or the sham procedure was low (<10%). All animals except one, who survived the surgical operation reached the designated end point of the experiment.

4.2.2.1 Transverse aortic constriction for PMCA1$^{F/F}$ and PMCA1^{cko} mice.

Transverse aortic constriction is a widely used experimental model to generate pressure overload in mice. The degree of aortic narrowing coincides closely with the degree of left ventricular hypertrophy. The maximal pressure within the left ventricle (P_{max}) recorded via

cardiac catheterisation before sacrificing the animals is a marker of cardiac afterload and was used to assess pressure overload following TAC.

The data shows no significant difference in the P_{max} between the WT: sham (90.4±4.3 mmHg) and PMCA1^{cko}: sham (97.0±2.7 mmHg) groups. Following the TAC procedure, WT mice as well as PMCA1cko mice showed an increase in the P_{max}; however, there was no significant difference between the two cohorts (143.4±5.4 mmHg vs 150.2±5.1 mmHg). Compared to their sham counterparts, both genotypes showed a similar degree of increase in the P_{max} following TAC procedure (53.1± 3.9 vs 52.3±2.7 p= 0.89). This clearly goes on to establish that TAC procedure exerted a similar pressure overload on WT and PMCA1^{cko} mice following TAC (figure 4.2).

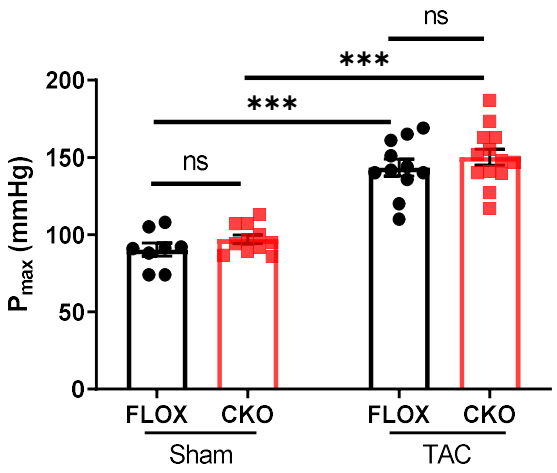

Figure 4.2: Maximal left ventricular pressure (P_{max}) in PMCA1$^{F/F}$ and PMCA1^{cko} mice following two weeks TAC. Data presented as mean ± SEM with two-way ANOVA used for analysis. Tukey's test was used for post-hoc analysis (ns non-significant, ***p<0.001. FLOX = PMCA1$^{F/F}$ CKO = PMCA1^{cko}

4.2.3 The effect of TAC induced cardiac stress on cardiac structure and function in PMCA1^{cko} mice

The effects of TAC induced cardiac stress on the cardiac structure and function PMCA1^{cko} mice were assessed by using echocardiography, invasive haemodynamic assessment, measurement of heart and lung weights and histology. The results are presented in the sections below.

4.2.3.1 Echocardiography analysis to determine structural changes to the heart in PMCA1^{cko} mice after two weeks TAC

To assess the consequences of TAC induced pressure overload on cardiac structure and function PMCA1^{cko} mice and their littermate controls underwent transthoracic two-dimensional and M-mode echocardiography with parasternal short-axis views.

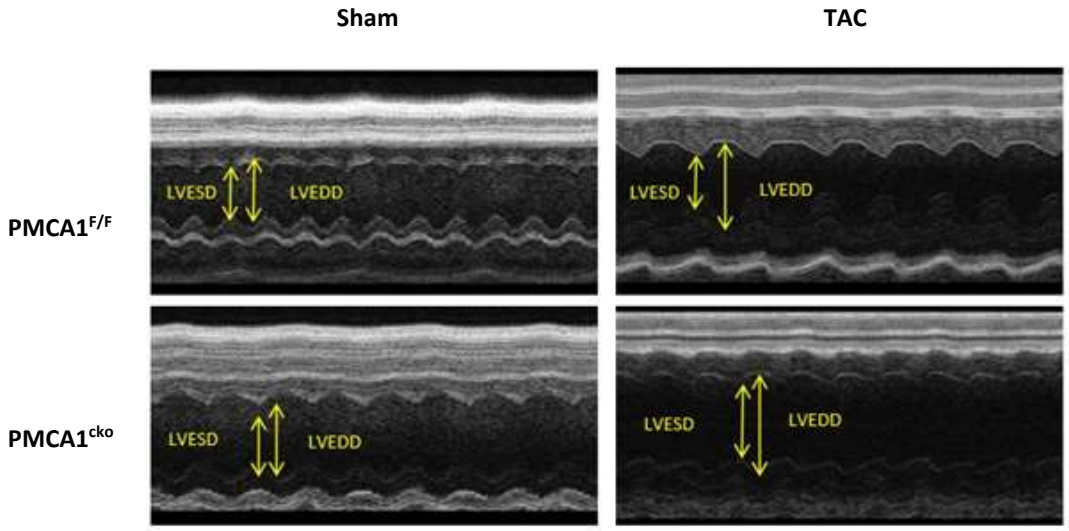

Figure 4.3: M-mode images of PMCA1^{cko} and PMCA1$^{F/F}$ mice having undergone sham or TAC surgery. Images indicate left ventricular end systolic diameter (LVESD) and end diastolic diameter (LVEDD) from M-mode echocardiography.

Echocardiography was performed, under light anaesthesia, to determine whether the pressure overload created by TAC had led to the development of left ventricular hypertrophy and to explore if there was any difference in the cardiac structure and function between the two experimental groups (PMCA1^{cko} and PMCA1$^{F/F}$ mice). The left ventricular diameter, the interventricular septum and the posterior wall thickness were measured in systole and diastole. A representative image is shown in figure 4.3 and the results are quantified in figure 4.4.

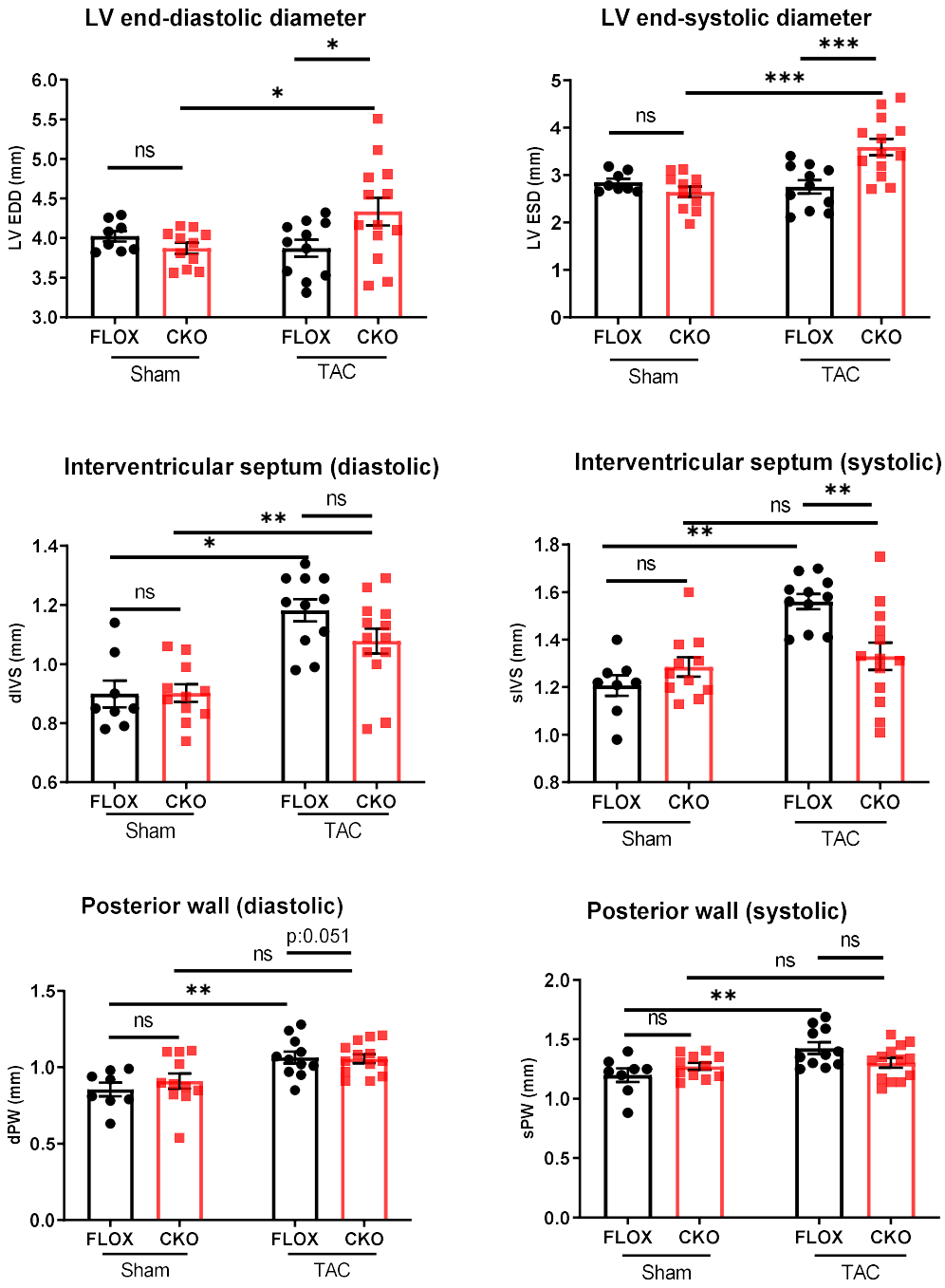

Figure 4.4: Echocardiographic structural analysis of PMCA1$^{F/F}$ and PMCA1^{cko} mice after two weeks TAC.

Left ventricular end-diastolic, end-systolic diameter, Interventricular septum thickness in diastole and systole, Posterior wall thickness in diastole and systole.

Data presented as mean ± SEM with two-way ANOVA used for analysis. Tukey's test was used for post-hoc analysis (ns non-significant, * p<0.05, ** p<0.01, ***p<0.001). FLOX = PMCA1$^{F/F}$ CKO = PMCA1^{cko}

When comparing PMCA1^{cko} and PMCA1$^{F/F}$ animals that had undergone sham surgery no significant difference was found in any of the parameters measured by echocardiography. Following 2 weeks TAC the PMCA1^{cko} mice showed a significant increase in the LVEDD compared to the sham mice of the same genotype (4.33mm±0.17 vs 3.87mm±0.068, p<0.05) and compared to the PMCA1$^{F/F}$:TAC cohort (4.33mm±0.17 vs 3.87mm±0.10, p<0.05). Whilst no significant increase in LVEDD was observed in PMCA1$^{F/F}$ mice as a result of TAC. A similar pattern was observed when LV diameter was measured in systole (LVESD) with a significant increase in LVESD measured in PMCA1^{cko}:TAC mice compared to the sham mice of the same genotype (3.58mm±0.17 vs 2.66mm±0.10, p<0.001) and the PMCA1$^{F/F}$:TAC cohort (3.58mm±0.17 vs 2.85mm±0.17, p<0.001).

Other echocardiographic parameters including the thickness of inter-ventricular septum and posterior wall were measured. Whilst both genotypes showed an increase in the dIVS thickness in response to TAC (p<0.01) this resulted in a similar dIVS thickness in both PMCA1^{cko} and PMCA1$^{F/F}$ controls (1.08 mm±0.04 vs 1.18mm±0.03, p= 0.21). PMCA1$^{F/F}$:TAC mice showed a significant rise in the thickness of sIVS compared to PMCA1$^{F/F}$:sham mice; however, there was had no difference in the thickness of sIVS in PMCA1^{cko}:TAC mice when compared to PMCA1^{cko}:sham mice (p0.89). On direct comparison between both TAC cohorts, PMCA1$^{F/F}$ mice had a significantly thicker sIVS compared to PMCA1^{cko} (1.56mm±0.03 vs 1.33mm±0.05, p<0.01). Two weeks TAC led to a significant increase in the thickness of dPW of PMCA1$^{F/F}$ mice compared to their sham controls (1.06mm ±0.04 vs0.85mm±0.04, p<0.01). PMCA1^{cko}:TAC cohort also showed a strong trend towards a thicker dPW compared to the PMCA1^{cko}:Sham group; however it was not statistically significant (p0.051). Analysis of sPW showed that whilst TAC led to a significant increase in sPW in PMCA1$^{F/F}$ mice (1.43mm± 0.05 vs 1.20mm± 0.05 p<0.001) there was no increase in the thickness of sPW in PMCA1^{cko} when compared to sham controls (p+0.91).

As highlighted in the previous chapters, relative wall thickness (RWT) is a useful echocardiographic parameter that can help to distinguish between concentric and eccentric hypertrophy. The data from this experiment showed that both PMCA1^{cko} and PMCA1$^{F/F}$ controls had no significant difference in the RWT after the sham surgery (0.47 ±0.05 vs 0.48±0.04, p= 0.09). Following two week TAC, PMCA1$^{F/F}$:TAC mice showed a significant rise in the RWT compared to PMCA1^{cko} :TAC mice (0.67 ±0.07 vs 0.46±0.05, p 0.008). The finding of a lower relative wall thickness in PMCA1^{cko}:TAC cohort is in keeping with eccentric left

ventricle hypertrophy.

In summary, following two weeks TAC, PMCA1$^{F/F}$ mice developed an increased thickness of ventricular walls without an increase in the chamber size in keeping with concentric hypertrophy. Whereas PMCA1^{cko} mice show significant dilatation of the left ventricular chamber in both systole and diastole as evidenced by an elevated LVESD and LVEDD compared to their genotype controls. PMCA1^{cko}:TAC mice also showed a lower degree of thickness of interventricular septum. posterior wall and lower RWT, suggestive of thinning of ventricular walls accompanying the dilation. These echocardiographic findings in PMCA1^{cko} :TAC mice are suggestive of eccentric cardiac hypertrophy.

4.2.3.2 Echocardiography analysis to determine functional changes to the heart in PMCA1^{cko} mice after two weeks TAC

As shown above, echocardiography revealed PMCA1^{cko} mice developed eccentric cardiac hypertrophy accompanied by left ventricular dilatation. Further analysis of this data was performed to assess left ventricular systolic function (figure 4.5).

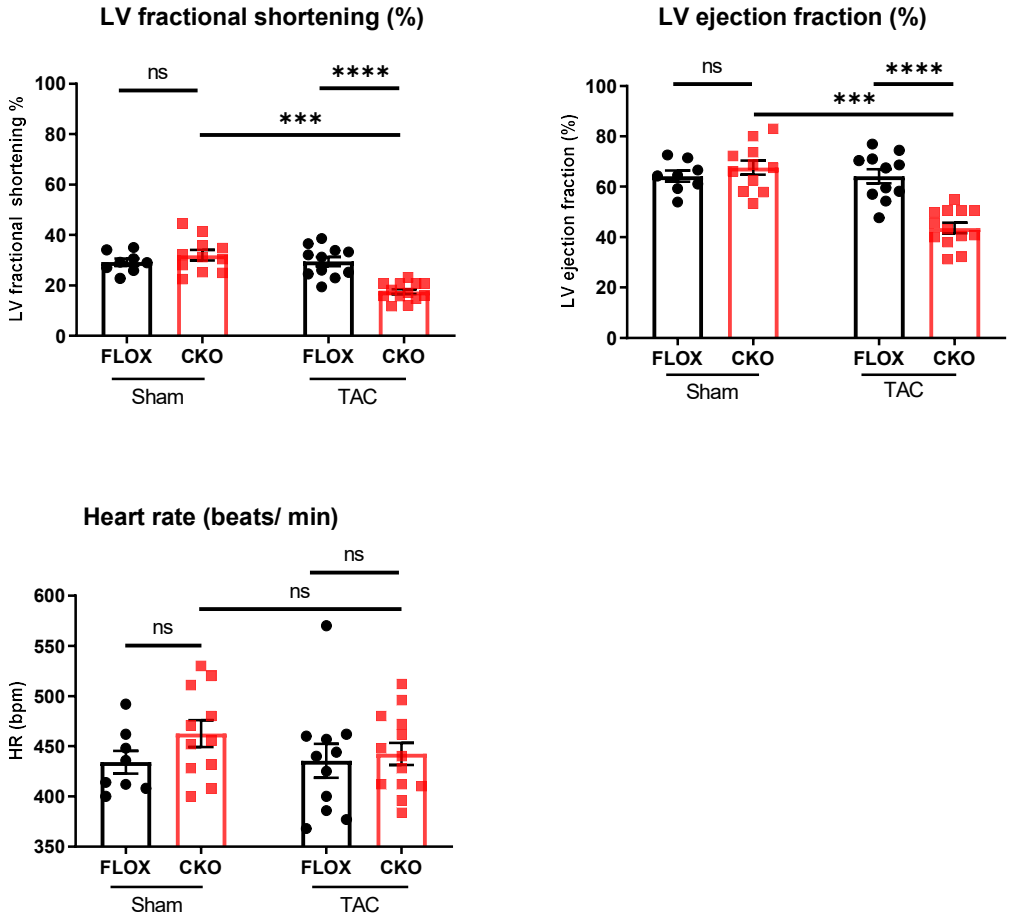

Figure 4.5: Echocardiography analysis of functional changes in PMCA1^{cko} mice after two weeks TAC.

Left ventricular fractional shortening (FS), left ventricular ejection fraction (EF), and heart rate (HR) were measured in PMCA1^{cko} and PMCA1$^{F/F}$ mice after two weeks TAC or sham surgery. Data presented as mean ± SEM with two-way ANOVA used for analysis. Tukey's test was used for post-hoc analysis (ns non-significant, ***p 0.0001, **** p<0.0001). FLOX = PMCA1$^{F/F}$ CKO = PMCA1^{cko}

PMCA1^{cko} and PMCA1$^{F/F}$ mice subjected to sham surgery showed no difference in either fractional shortening or ejection fraction. Following two weeks of TAC, PMCA1$^{F/F}$ mice maintained contractile function as indicated by both FS% and EF% when compared to sham controls. However, a significant reduction in both FS% and EF% was observed in the PMCA1^{cko}:TAC group compared to shams. Comparison of both groups subject to TAC revealed that PMCA1^{cko} mice had significantly lower LV FS% and LV EF% than PMCA1$^{F/F}$. Heart

rate was measured by echocardiography whilst mice were under isoflurane anaesthesia. Heart rate was similar in all four experimental groups.

In summary, the above data reveal that following two weeks TAC, PMCA1^{cko} mice develop significant left ventricular systolic dysfunction as evidenced by lower LV fractional shortening and ejection fraction, whilst contractile function is unaffected in PMCA1$^{F/F}$.

4.2.3.3 Haemodynamic analysis to determine changes in cardiac function in PMCA1^{cko} mice after two weeks TAC

Pressure-volume loop analysis was used to assess the impact of cardiomyocyte specific deletion of PMCA1 on cardiac contractility following pathological stress exerted by transverse aortic constriction for a period of two weeks. The pressure-volume (PV) catheter was inserted into the right common carotid artery to record the diastolic and systolic blood pressure. Subsequently, it was advanced further into the left ventricle where haemodynamic data was acquired. In one animal from the PMCA1$^{F/F}$:TAC group, carotid catheterisation was unsuccessful hence no haemodynamic data could be gathered . The results are presented in the figure 4.6.

Both systolic and diastolic BP were similar in PMCA1$^{F/F}$ and PMCA1^{cko} mice after sham surgery. Following TAC, systolic BP rose significantly in both groups, although there was no difference in BP between the two TAC groups. However, diastolic BP did not rise in either group of mice as a result of the TAC procedure.

Pulse pressure represents the difference between the systolic and diastolic blood pressure. There was no significant difference in the pulse pressure between PMCA1$^{F/F}$ and PMCA1^{cko} mice two weeks after sham surgery (41.1 ±11.8 mmHg vs 36.7 ± 8.3 mmHg, p=0.77). Mice from both genotypes demonstrated a widening of the pulse pressure two weeks after TAC surgery, however there was no significant difference in the pulse pressure between PMCA1$^{F/F}$:TAC and PMCA1^{cko}:TAC mice (81.7 ±18.4 mmHg vs 72.6 ± 14.9 mmHg, p=0.96).

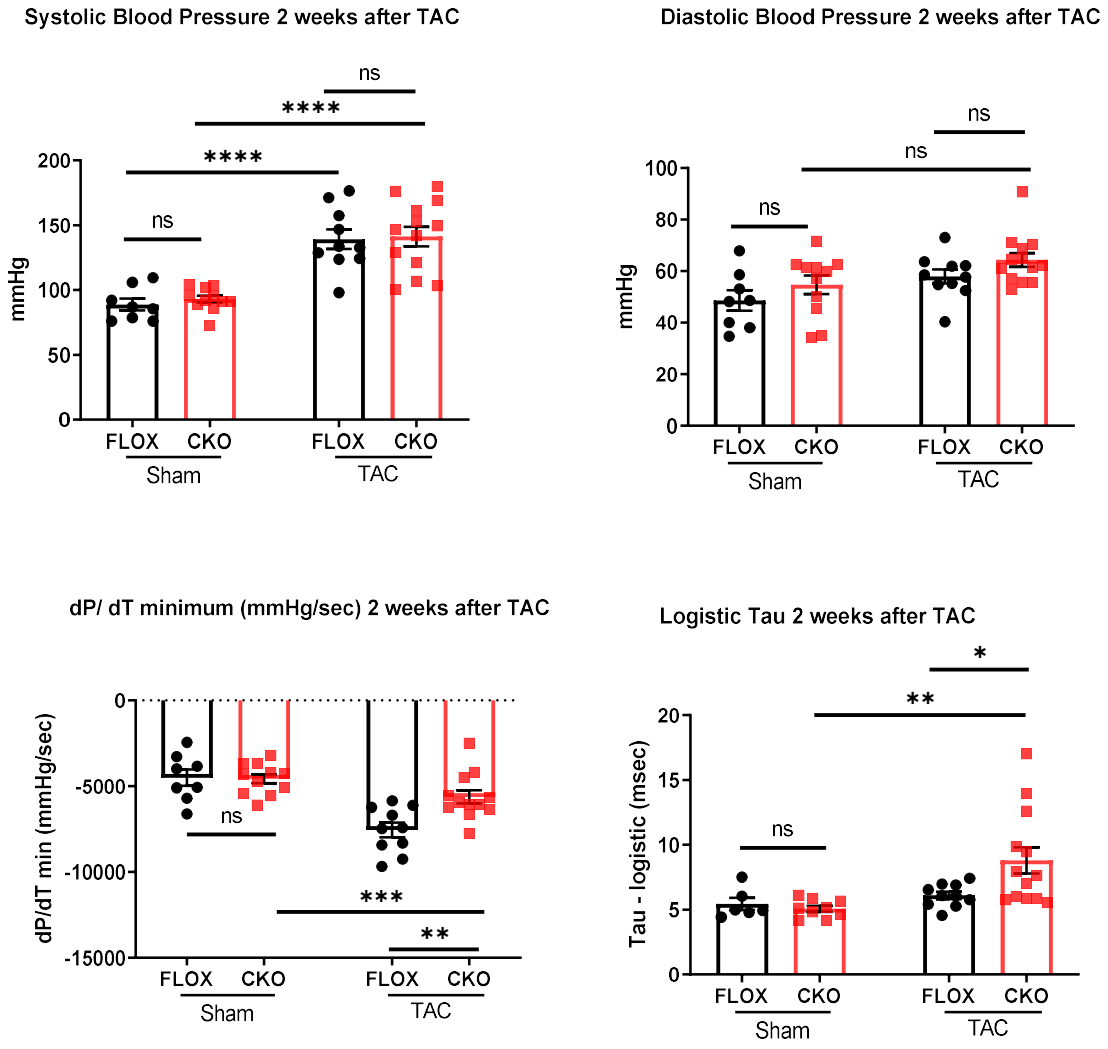

Figure 4.6: Haemodynamic measurements in PMCA1^{cko} mice after two weeks TAC.
Systolic and diastolic blood pressure as measured in the right common carotid artery. Left ventricle force of relaxation (dP/dt$_{min}$) and time constant for isovolumetric relaxation of left ventricle (logistic Tau - f).
Data presented as mean ± SEM with two-way ANOVA used for analysis. Tukey's test was used for post-hoc analysis (ns non-significant, * p <0.05,** p <0.01, ***p 0.0001, **** p<0.0001).
FLOX = PMCA1$^{F/F}$ CKO = PMCA1^{cko}

The minimum rate of pressure change in the left ventricle (per unit change in time) acts as measure of the force of relaxation (dP/dt$_{min}$). Therefore, dP/dt$_{min}$ serves as an indicator of cardiac relaxation. There was no difference in dP/dt$_{min}$ in PMCA1$^{F/F}$ and PMCA1^{cko} mice after sham procedure (-4502 mmHg/ sec ±482 vs -4650 mmHg/ sec ± 272, p 0.52). The dP/dt$_{min}$ falls significantly in both genotypes following the TAC procedure suggestive of improved relaxation of the left ventricle. However, there was a significant difference in dP/dt$_{min}$

between PMCA1$^{F/F}$ and PMCA1^{cko} mice after TAC procedure (-7544 mmHg ±423 vs -5616 mmHg ± 391, p 0.004), suggestive of poor relaxation of left ventricle in the latter group. Poor relaxation of the left ventricle is a marker of diastolic dysfunction.

The maximum rate of pressure change in the left ventricle (per unit change in time) acts as measure of the force of contraction (dP/dt_{max}) and is used a parameter of cardiac contractility. There was no significant difference in dP/dt_{max} between PMCA1$^{F/F}$ and PMCA1^{cko} mice two after sham procedure (4288 mmHg/sec ±390 vs 4608 mmHg/sec ± 536, p=0.35). There was an increase in the dP/dt_{max} in mice from both genotypes after two weeks of TAC however there was no significant difference in dP/dt_{max} between PMCA1$^{F/F}$:TAC and PMCA1^{cko} :TAC mice (6294 mmHg/sec ±423 vs 6082 mmHg/sec ± 780, p=0.08).

Logistic Tau (ƭ) is the time constant of isovolumetric relaxation of the left ventricle. Logistic Tau measurement showed no significant difference between PMCA1$^{F/F}$ and PMCA1^{cko} mice that had undergone sham surgery. However, after TAC procedure PMCA1^{cko} mice showed higher logistic tau values (8.8 sec ±1.0 vs 6.1 sec ± 0.27, p 0.03). This suggests development of higher levels of diastolic dysfunction in PMCA1^{cko} mice after TAC when compared to the PMCA1$^{F/F}$ controls.

4.2.3.4 Heart and lung weight in PMCA1^{cko} mice after two weeks TAC

Two weeks after TAC or sham procedure the animals were sacrificed and key measurements including heart weight, lung weight, body weight and tibial length were recorded, as described in section 2.4. The results are shown in figure 4.7. No significant difference was found in the body weights of PMCA1$^{F/F}$ and PMCA1^{cko} mice after the sham procedure (30.5 ± 3.0 gm vs 30.2 ±2.2 gm, p 0.98) or after the TAC procedure (29.3 ± 1.6 gm vs 28.8 ±2.1 gm, p 0.93). The TAC procedure was not associated with significant weight changes in mice from either genotype.

PMCA1$^{F/F}$ and PMCA1^{cko} mice that underwent the sham procedure had no significant difference in their heart weight (HW) normalised to either body weight (BW) or tibial length (TL). Two weeks after TAC mice from both genotypes exhibited an increased heart weight normalised to body weight and to tibial length, compared to their sham counterparts. PMCA1^{cko}:TAC mice did show an increase in HW:TL ratio when compared to PMCA1$^{F/F}$:TAC.

However, normalisation of HW to BW did not show a statistically significant difference between these two groups (p=0.09).

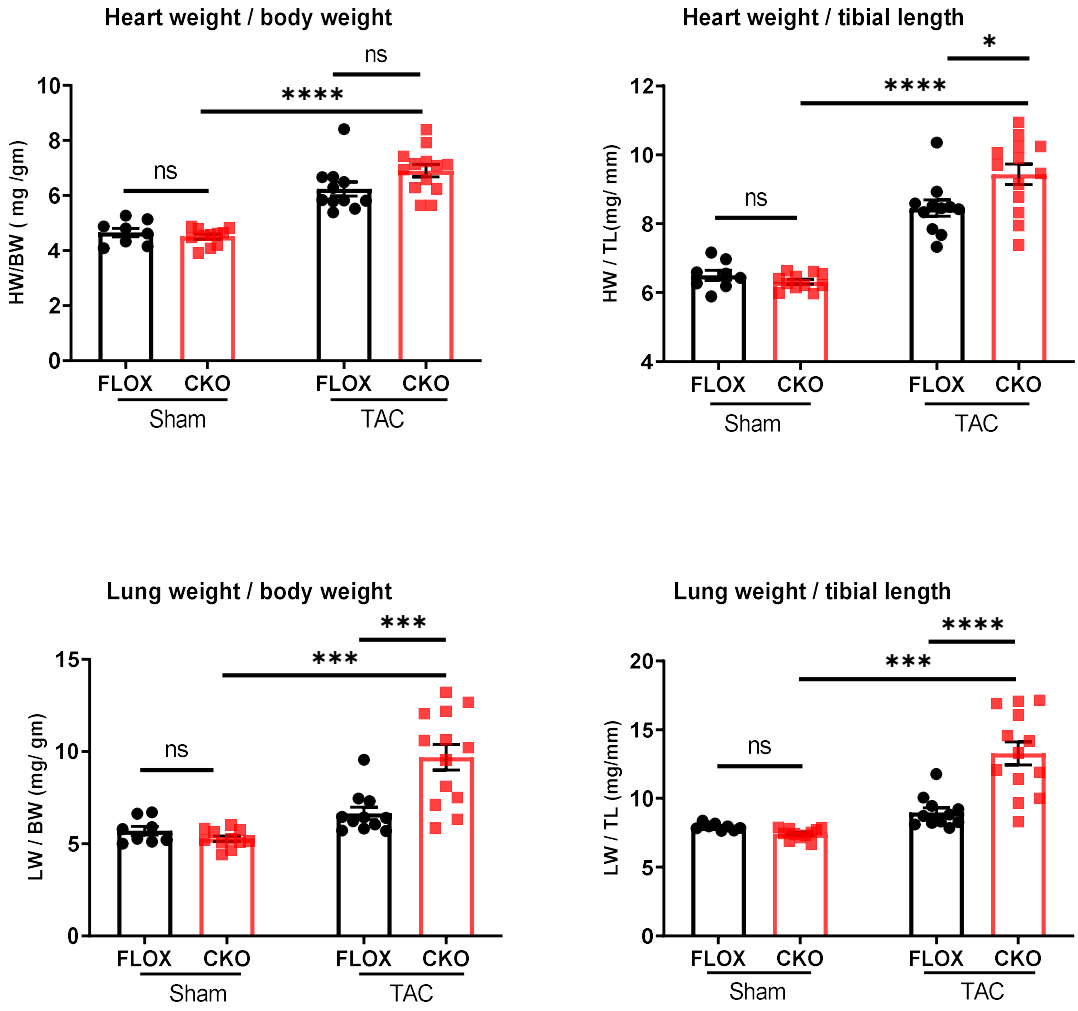

Figure 4.7: Normalised heart weight and lung weight of wild type and PMCA1^{cko} mice after two weeks TAC.
Heart weight (HW) normalised to body weight (BW) and heart weight normalised to tibial length (TL), respectively. Lung weight (LW) normalised to the body weight and to tibial length, respectively.
Data presented as mean ± SEM with two-way ANOVA used for analysis. Tukey's test was used for post-hoc analysis (ns non-significant, * p<0.05, ***p 0.0001, ****p<0.0001). FLOX = PMCA1$^{F/F}$ CKO = PMCA1^{cko}

No difference in lung weight (LW) normalised to either body weight or tibial length was observed between genotypes when mice underwent the sham procedure (p=0.93), and

LW:TL / LW:BW were unchanged in PMCA1$^{F/F}$ subjected to TAC. However, there was a significant elevation in the normalised lung weight of PMCA1^{cko}:TAC mice when compared to the PMCA1^{cko}: sham groups. Direct comparison, after two weeks TAC, showed that PMCA1^{cko} mice had a significantly higher lung weight (when normalised to either body weight or tibial length) than PMCA1$^{F/F}$ controls.

The above data clearly show that whilst the normalised heart weight increased in mice from both genotypes, two weeks after TAC procedure, the PMCA1^{cko} :TAC group exhibited a greater increase in the HW:TL compared to the floxed controls counterparts. In addition, two weeks TAC in PMCA1^{cko} mice led to an increase in normalised lung weight indicative of heart failure.

4.2.3.5 Analysis of the hypertrophic response in PMCA1^{cko} mice after two weeks TAC

The echocardiography and the heart weight data presented above reveals the development of left ventricular hypertrophy in both PMCA1^{cko} and PMCA1$^{F/F}$ mice subjected to TAC for two weeks. As the cardiac hypertrophy observed in-vivo is a cumulative effect of the enlargement of individual cardiomyocytes, the mean cross-sectional area or the average cell size was used to determine and compare the hypertrophic response.

Cardiac tissue sections were stained with haematoxylin and eosin (H&E) and the mean cardiomyocyte cross- sectional area measured and calculated (figure 4.8). No significant difference was found in the average cardiomyocyte cell size of PMCA1$^{F/F}$ and PMCA1^{cko} sham mice. The TAC procedure led to the development of significant cardiomyocyte hypertrophy in mice from both genotypes when compared to their respective sham controls (PMCA1$^{F/F}$: 266.9 μm^2±8.1 vs 201.0 μm^2±8.4, $p<0.001$; PMCA1^{cko}: 264.5 μm^2 ±14.3 vs 199.6 μm^2 ±4.6, $p<0.001$). However, both genotypes developed a similar degree of cardiomyocyte hypertrophy after TAC, hence there was no difference in the average cardiomyocyte cell size in PMCA1$^{F/F}$ and PMCA1^{cko} mice undergoing TAC. These data confirm that at the individual cardiomyocyte level, TAC induced a significant myocyte hypertrophic response of similar extent in mice from both genotypes.

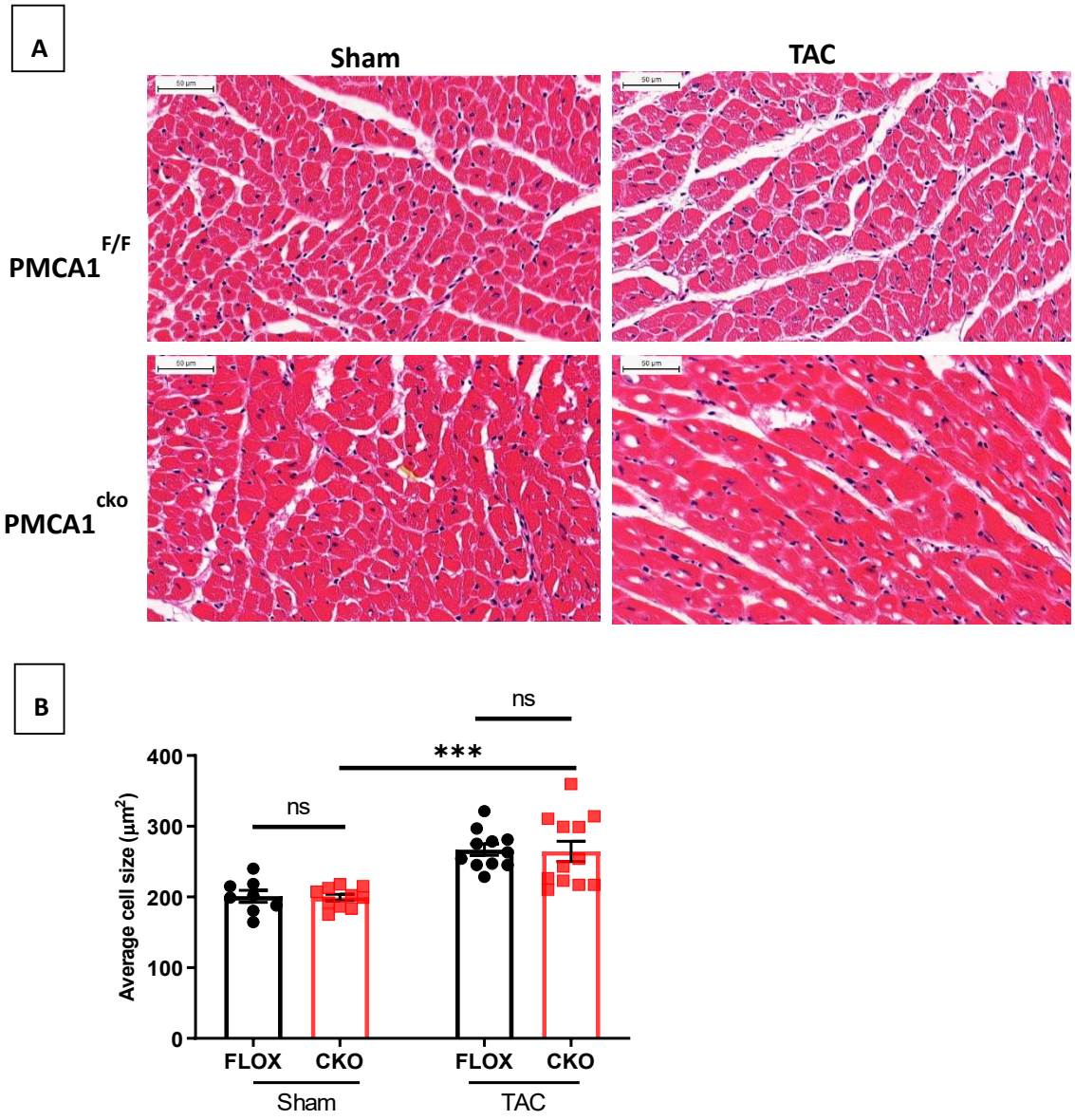

Figure 4.8: Cardiomyocyte cross-sectional area following 2 weeks TAC.

(A) Representative H&E stained histological cross sections from PMCA1$^{F/F}$ and PMCA1^{cko} mice. Scale bar represents 50 µm. (B) Average cardiomyocyte cross section area. One hundred cells were counted from two sections per animal and the average presented above.

Data presented as mean ± SEM with two-way ANOVA used for analysis. Tukey's test was used for post-hoc analysis (ns non-significant, ***p 0.0001). FLOX = PMCA1$^{F/F}$ CKO = PMCA1^{cko}

Natriuretic peptides, atrial (ANP) and B-type natriuretic peptide (BNP) are established markers of cardiomyocyte hypertrophy and growth (Kuhn et al., 2002). Quantitative real time-polymerase chain reaction (qRT-PCR) was used to assess ANP (NPPA) and BNP (NPPB)

RNA expression in PMCA1$^{F/F}$ and PMCA1^{cko} mice after two weeks of TAC or the sham procedure. The results are shown in figure 4.9.

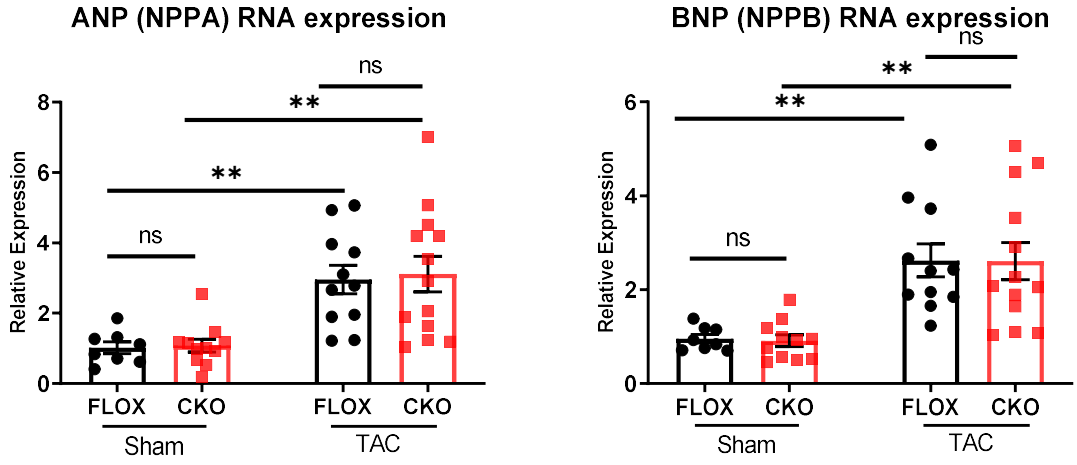

Figure 4.9: RT-PCR analysis of ANP (NPPA) and BNP (NPPB) RNA expression in PMCA1^{cko} mice after two weeks TAC. Gapdh was used as housekeeping gene and the data was normalised to gapdh expression. Data presented as mean ± SEM with two-way ANOVA used for analysis. Tukey's test was used for post-hoc analysis (ns non-significant, ** p <0.01).
FLOX = PMCA1$^{F/F}$ CKO = PMCA1^{cko}

The RT-PCR analysis shows that the expression of ANP (NPPA) and BNP (NPPB) is similar in PMCA1$^{F/F}$ and PMCA1^{cko} mice after sham procedure (p=0.99). After two weeks TAC, mice from both genotypes demonstrated a significantly higher expression of ANP (NPPA) and BNP (NPPB) compared to the sham cohorts (p <0.01). Following two weeks TAC, ANP (NPPA) RNA expression was similar between both genotypes (p=0.91). Similarly, no significant difference was found in the BNP (NPPB) RNA expression between PMCA1$^{F/F}$:TAC and PMCA1^{cko}:TAC groups (p:0.90).

4.2.3.6 Analysis of myocardial fibrosis in PMCA1^{cko} mice after two weeks TAC

In addition to stimulating left ventricular hypertrophy, pathological stress caused by the pressure overload can also lead to myocardial fibrosis. Histological sections of mouse hearts were stained with Masson's Trichrome to assess and compare the degree of fibrosis (shown in figure 4.10).

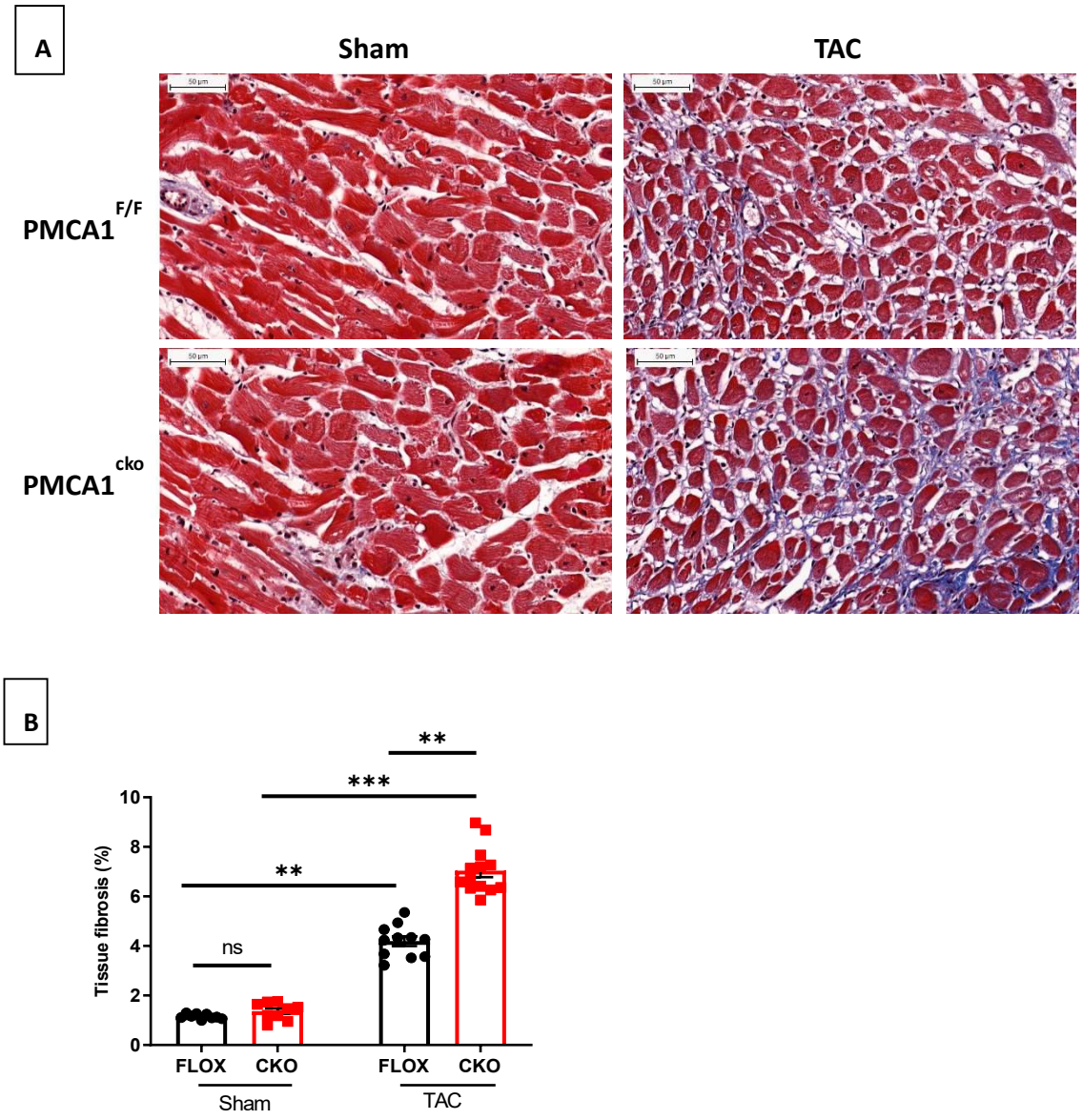

Figure 4.10: The level of myocardial fibrosis in PMCA1^{cko} mice after two weeks TAC.

(A) Representative Masson's Trichrome stained transverse histological cross sections. Scale bar represents 50 µm. (B) Percentage fibrosis calculated from the analysis of Masson's Trichrome stained histological cross sections. This was calculated as the % of fibrosis in the whole section through the left ventricle. Data presented as mean ± SEM with two-way ANOVA used for analysis. Tukey's test was used for post-hoc analysis (ns non-significant, ** p<0.01, ***p 0.0001). FLOX = PMCA1$^{F/F}$ CKO = PMCA1^{cko}

Quantification of the myocardial fibrosis area was performed using Image J software (NIH Image) and was presented as a percentage of the total stained area. The results show there is little fibrosis in the hearts from PMCA1$^{F/F}$ and PMCA1^{cko} mice after the sham procedure. Whilst two weeks TAC leads to a significant increase in the level of fibrosis in both PMCA1^{cko}

and PMCA1$^{F/F}$ this increase is significantly higher in PMCA1^{cko} mice (7.0 % ± 0.26 vs 4.2% ± 0.19, p <0.01).

Collagen types 1 and 3 (COL1α1 and COL1α3) are recognised markers of tissue fibrosis, including myocardial fibrosis (Ely et al., 2010). In this study, qRT-PCR was used to assess COL1α1 and COL1α3 RNA expression in PMCA1$^{F/F}$ and PMCA1^{cko} mice after two weeks of TAC or sham surgery (figure 4.11).

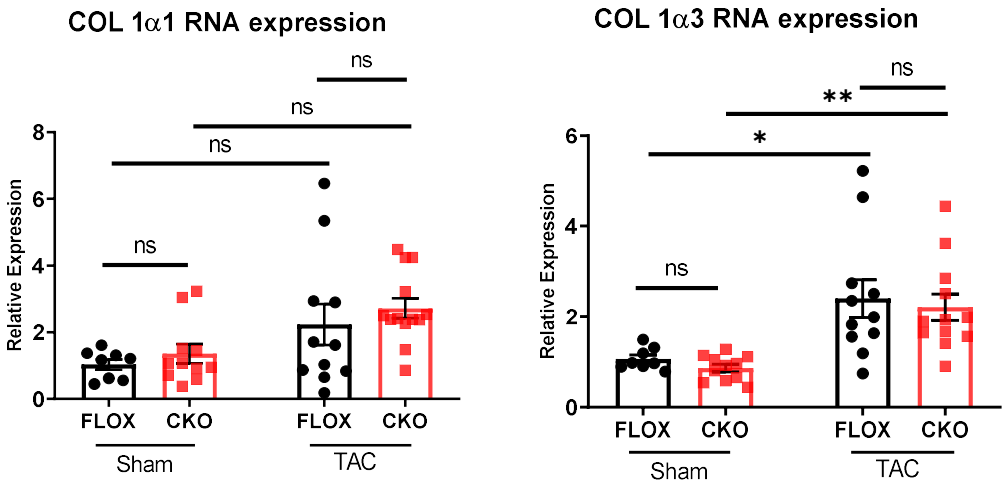

Figure 4.11: RT-PCR analysis of COL1α1 and COL 1α3 RNA expression in PMCA1^{cko} mice after two weeks TAC. Gapdh was used as housekeeping gene and the data was normalised to gapdh expression. Data presented as mean ± SEM with two-way ANOVA used for analysis. Tukey's test was used for post-hoc analysis (ns non-significant, * p <0.05, ** p<0.01). FLOX = PMCA1$^{F/F}$ CKO = PMCA1^{cko}

The RT-PCR analysis shows no significant difference in the expression of COL1α1 and COL1α3 in PMCA1$^{F/F}$ and PMCA1^{cko} mice after sham procedure. Following two weeks TAC, mice from both genotypes showed a trend towards an increase in expression of COL1α1, although this increase in expression was not statistically significant. However, the expression of COL1α3 was significantly increased in both PMCA1$^{F/F}$ and PMCA1^{cko} mice after two weeks TAC vs sham cohorts from the respective genotypes. No significant difference in the expression of either COL1α1 or COL1α3 was found by comparing the TAC groups from the two genotypes (p=0.90).

4.2.3.7 Analysis of markers of apoptosis in PMCA1^{cko} mice after two weeks TAC

Apoptosis often accompanies tissue fibrosis during the development of heart failure; BAX (Bcl2 -associated X protein) and Bcl2 are known to regulate the process of apoptosis (Gürtl et al., 2009). qRT-PCR was used to assess BAX and Bcl2 RNA expression in PMCA1$^{F/F}$ and PMCA1^{cko} mice after two weeks of TAC or sham surgery (figure 4.12).

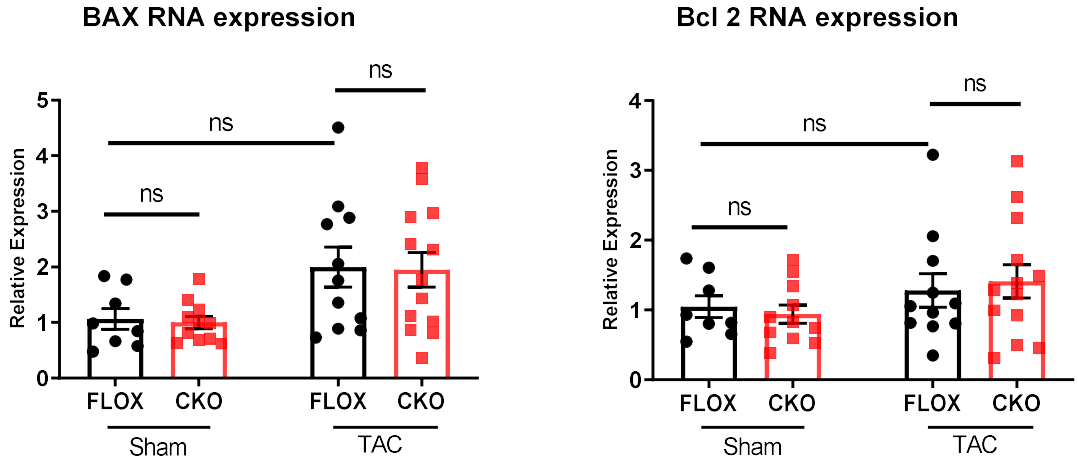

Figure 4.12: RT-PCR analysis of BAX and Bcl2 RNA expression in PMCA1^{cko} mice after two weeks TAC. Gapdh was used as housekeeping gene and the data was normalised to gapdh expression. Data presented as mean ± SEM with two-way ANOVA used for analysis. Tukey's test was used for post-hoc analysis (ns non-significant). FLOX = PMCA1$^{F/F}$ CKO = PMCA1^{cko}

The qRT-PCR analysis shows no significant difference in the expression of BAX and Bcl2 in PMCA1$^{F/F}$ and PMCA1^{cko} mice subjected to the sham procedure. Two weeks post TAC, mice from both genotypes demonstrated a trend towards higher expression of BAX and Bcl2 compared to the sham cohorts (p values 0.14 and 0.07 for BAX and 0.80 and 0.3 for Bcl2, respectively); however, the rise was not statistically significant. In addition, there was no difference in expression of either gene when comparing the two groups of mice subjected to TAC.

4.2.3.8 Analysis of the expression of calcium handling genes in PMCA1^{cko} mice after two weeks TAC

In order to determine whether deletion of PMCA1 under the conditions of pressure overload has led to a change in the expression of genes involved in calcium handling in the

cardiomyocyte, qRT-PCR was conducted. The RNA expression levels of PMCA4, SERCA2, NCX and RyR were examined. The results are presented in the figure 4.13.

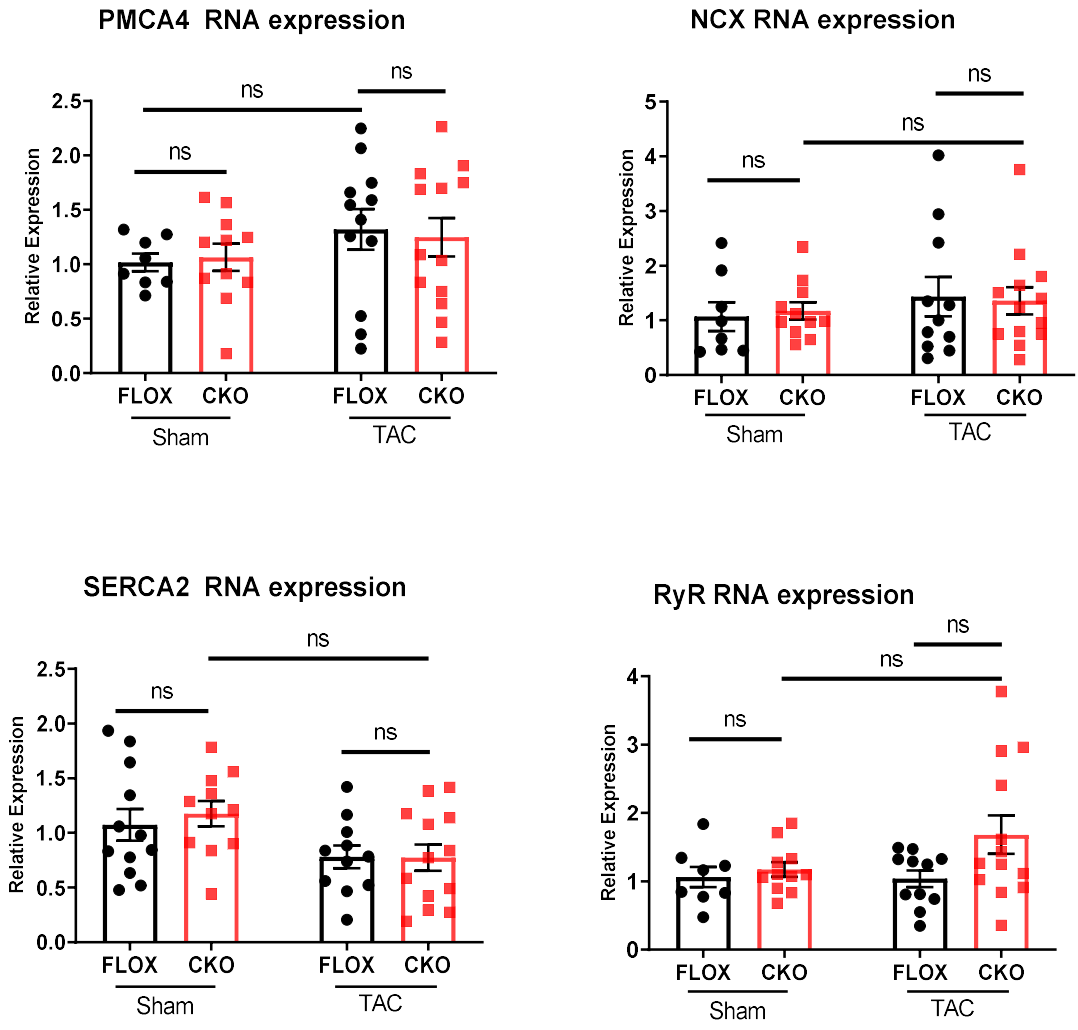

Figure 4.13: RT-PCR analysis of the expression of calcium handling genes in PMCA1^{cko} mice after two weeks TAC. Gapdh was used as housekeeping gene and the data was normalised to gapdh expression. Data presented as mean ± SEM with two-way ANOVA used for analysis. Tukey's test was used for post-hoc analysis (ns non-significant). FLOX = PMCA1$^{F/F}$ CKO = PMCA1^{cko}

To determine whether there was an increase in the expression of PMCA4 as a result of deletion of PMCA1 under 2 weeks TAC conditions qRT-PCR was performed. Under sham conditions there was no difference in the level of PMCA4 in PMCA1^{cko} compared to PMCA1$^{F/F}$ controls. Mice of both genotypes had a trend towards higher expression of PMCA4 after TAC; however, this did not reach the level of statistical significance (p=0.6 and 0.5 respectively).

PMCA4 expression was not significantly different between the two genotypes after the TAC procedure.

Key calcium handing genes involved in cardiac excitation-contraction coupling were examined to determine if either deletion of PMCA1 or pressure overload induced by TAC for two weeks led to altered expression. Both NCX and RyR expression levels remained constant under TAC conditions and were not impacted as a result of reduced expression of PMCA1. Similarly, under sham conditions the expression of SERCA2 showed no significant difference between genotypes and there was no significant difference in SERCA2 expression between the two genotypes after the TAC.

4.3 Discussion

In the light of previous work from our group which demonstrated that cardiomyocyte specific deletion of PMCA1 ($PMCA1^{cko}$) led to cardiac rhythm abnormalities; this research project started with a hypothesis that a cardiomyocyte specific deletion of PMCA1 will also have a detrimental effect on the structure of the heart and it will lead to exacerbation of cardiomyopathy after pressure overload produced by transverse aortic constriction. This hypothesis was based upon the fact that cardiac arrhythmias are common in patients with heart failure and confer a substantially high risk of mortality and morbidity in this group (Lip et al., 2016). Therefore, the main aim of this project was to identify whether the cardiomyocyte specific deletion of PMCA1 exerts any impact on the structure and the function of the heart under pathological stress in a pressure overload model.

The results confirm that transverse aortic constriction exerted a similar pressure overload in $PMCA1^{F/F}$ and $PMCA1^{cko}$ mice. Structurally, $PMCA1^{cko}$ mice showed a significant dilatation of the left ventricle both in diastole and systole after two weeks TAC compared to the $PMCA1^{F/F}$ cohort. This was accompanied by a relatively higher normalised heart weight and lung weight in $PMCA1^{cko}$ mice after TAC. $PMCA1^{cko}$ mice also had worse left ventricular systolic function after TAC. On histological analysis, average myocardial cell size increased in both genotypes after TAC; however, there was no significant difference between genotypes. $PMCA1^{cko}$ mice had evidence of worse myocardial fibrosis after TAC procedure and pressure volume analysis showed exaggerated diastolic dysfunction in this group of mice. Molecular analysis showed a trend towards increased expression of genes encoding cardiac hypertrophy and fibrosis after TAC; however, there was no significant difference between the two genotypes. As this

experimental model consisted of deletion of PMCA1 – a calcium extrusion pump, the expression of other calcium handling genes was also analysed to determine if there was a compensatory change in their expression. The expression of calcium handling genes showed no significant difference between the two genotypes after TAC or sham procedure.

For this study PMCA1$^{F/F}$ mice were used as experimental controls, their generation is described in chapter 2. Although, prolonged expression of α-MHC Cre has been described to be cardiotoxic, particularly in older mice (8 – 12 months old) and is associated with left ventricular dysfunction and myocardial fibrosis (Pugach et al., 2015). However, previous work performed in our lab has shown no difference in the cardiac structure and function of 8 weeks old both αMHC-Cre^{neg} and αMHC-Cre^{tg} mice after undergoing TAC or sham procedure (N. P. Stafford, 2013). Additionally, α-MHC Cre mice did not exhibit any ECG changes or susceptibility to cardiac rhythm abnormalities (Wilson et al., 2022). This evidence goes on to support that the use of α-MHC Cre mice and floxed mice is appropriate as controls in this study and the phenotype changes seen in PMCA1^{cko} mice after TAC are not an artefact caused by Cre expression.

It is well established that in response to a number of stimuli such as pressure overload and muscle injury, cardiomyocyte undergo hypertrophy. A broad spectrum of endocrine, paracrine and autocrine pathways are involved in initiation and regulation of this hypertrophic response (Heineke & Molkentin, 2006). Plasma membrane calcium ATPase 4 acts in collaboration with including calcineurin and Ras effector Ras-association domain family 1 isoform A (RASSF1A) and regulates myocardial hypertrophy. These two pathways work differently; in calcineurin-NFAT signalling pathway, activated calcineurin promotes dephosphorylation of NFAT which subsequently translocates into the nucleus and participates in calcium inducible gene transcription (Molkentin, 2004). Whereas, RASSF1A on the other hand downregulate extracellular regulated kinases (ERK) 1&2 leading to an inhibition of hypertrophy (Oceandy et al., 2009).

The above evidence has formed the basis for researchers to investigate the role of PMCA in the regulation of cardiac hypertrophy. PMCA4 inhibition has been demonstrated to result in attenuated hypertrophic response to transverse aortic constriction and may even reverse pre-existing myocardial hypertrophy (Mohamed et al., 2013). However, deletion of PMCA4 does not appear to prevent exercise induced physiological hypertrophy (Wu et al., 2009b). Recent work from our group have shown that modulation of cardiac hypertrophy by PMCA4

is not limited to the signal transduction pathways described above. Deletion of PMCA4 in cardiac fibroblasts promotes increased secreted frizzled related protein-2 (sFRP2) levels which attenuates Wnt signal pathway resulting in inhibition of hypertrophy in cardiac myocytes (Mohamed et al., 2016).

PMCA1, the most abundant PMCA isoform in the heart, is also known interact with calcineurin (Boczek et al., 2017). This raises the possibility of PMCA1's involvement in the regulation of cardiac hypertrophy. Human cardiac tissue from patients with end stage heart failure has lower concentrations of PMCA1 and PMCA4 compared to those with a normal functioning heart (Borlak & Thum, 2003). Cardiac arrhythmias are common in heart failure patients and account for nearly 50% of the mortality in those with an advanced disease (Santangeli et al., 2017). The possibility of genetic susceptibility to cardiac rhythm abnormalities in this patient cohort is becoming a major area of heart failure research (Campuzano et al., 2009; Duygu et al., 2013). PMCA4 is known to form a complex with neuronal nitric oxide (nNOS); the complex also binds with α1-syntrophin (Williams et al., 2006b). Interestingly, α1-syntrophin gene mutation (A390V) is associated with long QT syndrome, possibly mediated through altered calcium metabolism due to inability of the mutated for to bind PMCA4 (Cheng et al., 2009). Long QT syndrome is an established cause of sudden cardiac death (O'Neal et al., 2017). More recently, our group has shown that reduced levels of PMCA1 can also lead to a down regulation of ion channels (kcnd2) ultimately resulting in the prolongation of QT interval in mice (Wilson, 2017). These data offer a unique insight into the roles played by PMCA1 in the regulation of cardiac rhythm. Being the most abundant form of PMCA in the heart; it is plausible that it may also contribute to the regulation of cardiac growth and hypertrophy. However, no published studies, thus far have examined PMCA1's role in a pressure overload model. The key data emerging with genome wide association studies linking PMCA1 and hypertension, and the functional evidence emerging from the work carried out by Little and colleagues (Little et al., 2017) leads us to think that PMCA1 may have a role in pressure overload . From these data, we would predict that cardiomyocyte specific deletion of PMCA1 would exacerbate the response to pressure overload.

4.3.1 Cardiomyocyte specific deletion of PMCA1 led to left ventricular dilatation and worse left ventricular systolic function 2 weeks after TAC

Previous work undertaken by our group demonstrates that under the basal conditions, cardiomyocyte specific deletion of PMCA1 has no impact on cardiac structure and function (Wilson, 2017). The data from this research project shows that PMCA1^{cko} mice developed dilated cardiomyopathy with systolic dysfunction whilst PMCA1$^{F/F}$:TAC mice did not develop heart failure despite having a comparable degree of left ventricular hypertrophy.

Firstly, it is important that TAC produces a comparable degree of narrowing of the aortic lumen and in turn, exerts a similar pressure overload in both control and the experimental cohorts. The maximum left ventricular systolic pressure (P_{max}) is a reliable indicator of the cardiac afterload which is increased in the TAC model. P_{max} was measured by cardiac catheterisation and found to have no significant difference between PMCA1$^{F/F}$:TAC and PMCA1^{cko}:TAC mice. This observation rules out influence of experimental bias in the post TAC phenotype differences between PMCA1$^{F/F}$ and PMCA1^{cko} mice.

Left ventricular hypertrophy is often a consequence of pressure overload conditions such as systemic hypertension and aortic stenosis, and acts as an independent marker of poor clinical outcomes (Levy et al., 2009). The murine transverse aortic constriction (TAC) model offers an excellent platform to explore and study the scientific basis of myocardial hypertrophy. Research has shown that following TAC there an abrupt increase in the left ventricular systolic pressure with an initial fall in contractility, which is soon followed by the development of myocardial hypertrophy starting as early as day 3 and eventually reaching its peak by day 10 post TAC with no further increase in the left ventricular mass index by day 20 (Nakamura et al., 2001). However, despite the application of a similar degree of transverse aortic constriction, considerable inconsistencies in the degree and type of left ventricular hypertrophy have been reported by different groups (Barrick et al., 2007; Zi et al., 2019b). In general, the degree of aortic narrowing coincides closely with the degree of left ventricular hypertrophy. In our lab this technique typically produces a 25-30 mmHg pressure gradient between the right and left carotid artery (Zi et al., 2014a). In this research project, PMCA1$^{F/F}$ and PMCA1^{cko} mice did not develop myocardial hypertrophy after going through the sham procedure. This finding is similar to the recent work by Zi and colleagues, who did not find any significant LV hypertrophy in mice after sham procedure (Zi et al., 2019). However, significant myocardial hypertrophy was witnessed in mice from both genotypes two weeks

after TAC procedure. PMCA1^{cko} mice had significantly higher heart weight (normalised to their tibial length). Moreover, hearts from both genotypes have similar normalised weights confirming the development of similar degree of hypertrophy. This was accompanied by a higher normalised lung weight in PMCA1^{cko} :TAC cohort, as well. These findings suggest an exaggerated myocardial hypertrophy response in PMCA1^{cko} mice along with the development of pulmonary oedema, two weeks after TAC. These findings were further supported by echocardiography data, which showed evidence of the left ventricular dilatation and systolic dysfunction.

Usually, during the TAC experiments, myocardial hypertrophy does not show any signs of decompensation until 4 weeks after TAC and a decline in cardiac contractility often develops 4-6 weeks post TAC leading to a decompensated heart failure (Chen et al., 2012). Although, some investigators have reported the presence of compensated left ventricular hypertrophy with preserved systolic function for up-to 8 weeks after TAC (Garcia-Menendez et al., 2013; Zi et al., 2019). In fact, Zi et al. (2019) also interestingly showed that 8 weeks old mice usually develop compensated hypertrophy after two week TAC whereas older mice (10-12 weeks old) develop cardiac dysfunction after two week TAC. In line with these published reports, one would expect PMCA1^{cko} mice to also demonstrate concentric compensated left ventricular hypertrophy two weeks after TAC. However, the PMCA1^{cko}:TAC showed poor left ventricular systolic function with dilatation of the left ventricle and thinning of the ventricular wall, highly suggestive of decompensated heart failure. The absence of decompensation in PMCA1$^{F/F}$:TAC controls indicates that cardiomyocyte specific deletion of PMCA1 results in poor tolerance of pressure overload with a resultant dilated cardiomyopathy and heart failure.

Diastolic dysfunction may herald the development of dilated cardiomyopathy and decompensated heart failure. In addition to resulting in systolic impairment, TAC can also lead to poor left ventricle relaxation and filling i.e diastolic dysfunction. During the initial period following TAC, enhanced left ventricular relaxation has been observed in published reports (Moens et al., 2009). This appears to be a compensatory response in dealing with pressure overload. Development of diastolic dysfunction has been reported in the literature to typically start developing from 4 weeks after TAC (Platt et al., 2018). Haemodynamic analysis in this study shows that PMCA1^{cko}:TAC also showed poor diastolic function compared to the PMCA1$^{F/F}$ controls. This means that a cardiomyocyte specific knockout of

PMCA1 adversely impacts on heart's ability to compensate for pressure overload resulting in the development of both diastolic and systolic dysfunction within two weeks of TAC. It also further enhances the argument that PMCA1 may be a key player in the regulation of cardiac adaptations to stressful stimuli and may act as a therapeutic target in prevention of heart failure.

4.3.2 Hearts from PMCA1^{cko} mice exhibit exaggerated myocardial fibrosis after TAC

Myocardial fibrosis is commonly seen in decompensated heart failure resulting from a variety of cardiovascular diseases including ischemic heart disease, hypertensive heart disease and primary cardiomyopathies (Hinderer & Schenke-Layland, 2019). Due to a limited regenerative capacity of cardiomyocytes, the response to an injury is primarily mediated by the residing fibroblasts leading to pathological changes in the composition extra cellular matrix ending up in loss of cardiac muscle contractility and pathological cardiac remodeling. Cardiac fibrosis has been well described in murine TAC models and is broadly categorized into an early 'reactive interstitial fibrosis' which serves as an adaptive response to maintain cardiac structure and function, and a late 'replacement fibrosis' where necrosed cardiomyocytes are replaced by collagen deposition (Travers et al., 2016). In general, the degree of myocardial fibrosis correlates with the severity of cardiac dysfunction (D. Xiao et al., 2019). In this research, although mice from both genotypes developed higher degree myocardial fibrosis following TAC; the PMCA1^{cko}:TAC cohort displayed significantly worse levels of myocardial fibrosis compared to the PMCA1$^{F/F}$:TAC group. This can be translated as the enhanced pathological cardiac remodeling after pressure overload in the animals with cardiomyocyte specific deletion of PMCA1. Myocardial fibrosis is known to be associated with reduced nitric oxide signaling via down regulation of cyclic GMP and diminished protein kinase G activity (Sweeney et al. , 2020). Several other profibrotic factors such as TGFβ, IL11 and angiotensin II may also play their role in tandem with nitric oxide signaling (Wu et al., 2019). Unlocking any possible direct or indirect cross talk between PMCA1 and the mediators of myocardial fibrosis will be an interesting research avenue to be explored in the future.

4.3.3 Cardiomyocyte specific deletion of PMCA1 has no effect on the expression of other calcium handling genes

It is well established that cardiomyocyte specific deletion of PMCA1 leads to a significant reduction of PMCA1 protein levels in murine myocardium (Wang et al., 2017a). Hence, it is plausible that any subsequent phenotype changes, such as decompensated heart failure in this research project, could be attributed to the ablation of PMCA1 in the cardiac tissues. However, it is important to explore whether cardiomyocyte specific deletion of PMCA1 also has any impact on the expression of other calcium handling genes, in order to remove any confounding factors and bias. As outlined in the results section, this research project did not find any significant difference in the expression of important calcium handling genes including NCX, SERCA2, RyR and PMCA4 between $PMCA1^{cko}$ and $PMCA1^{F/F}$ mice. This finding favours the relative lack of PMCA1 in myocardium as causative factor leading to the phenotype changes. Interestingly, a trend towards reduced SERCA2 expression following TAC in both genotypes was noted in our study. Borlak and colleagues have described reduced expression of SERCA2 in the human cardiac tissue belonging to patients with advanced heart failure (Borlak & Thum, 2003). A reduction in SERCA2 expression has also been reported in TAC-induced failing murine heart models (Lu et al., 2011).

4.3.4 How does PMCA1 play a role in cardiac decompensation?

Whilst, under basal conditions, PMCA1 has no recognizable effect on cardiac structure and function, and its contribution to the global calcium homeostasis in the heart is also modest. It is interesting to imagine how it may regulate the cardiac response under stress and how cardiomyocyte specific deletion of PMCA1 leads to decompensated heart failure in pressure overload circumstances. Published literature shows that calcium handling remains preserved in wild type mice one week after TAC in keeping with compensated myocardial hypertrophy (Toischer et al., 2010). Previous work from our group has shown that $PMCA1^{cko}$ cardiomyocytes shows lower calcium transient peak during systole (Stafford, 2013). However, there were no other significant changes in the cellular calcium extrusion after cardiomyocyte specific deletion of PMCA1.

There is evidence to suggest that PMCA1 and NCX may be located in a close proximity in T-tubules (Despa et al., 2003). There is a prolongation of NCX current decay in $PMCA1^{cko}$ cardiomyocytes which suggests NCX has to work harder and for longer to compensate for

the loss of PMCA1 in PMCA1^{cko} cardiomyocytes. However, whilst NCX can compensate for the loss of PMCA1 under physiological conditions; under stressful condition such as repetitive electric stimulation or Ca^{2+} overload, NCX compensation in PMCA1^{cko} atrial cardiomyocytes was not adequate. Hence, there was evidence of cardiac arrythmias in PMCA1^{cko} cardiomyocyte (Wang et al., 2017).

The results from this research project clearly show that cardiomyocyte specific ablation of PMCA1 in mice increases their likelihood of development of heart failure after pressure overload. Although mechanistically, it is unclear how this decompensation is mediated and what are the key cellular signaling pathways leading to this phenotype change. Due to PMCA1's association with hypertension, both in genome wide association studies and murine models, it seems that the link between PMCA1 and heart failure is also of utmost clinical significance.

In the next chapter, the association between cardiomyocyte specific PMCA1 deletion and heart failure is explored further by undertaking mass spectrometry proteomic assays of PMCA1$^{F/F}$ and PMCA1^{cko} mice, both after the TAC and the sham procedure.

4.4 Conclusion

PMCA1 has no identifiable impact on the structure and function of heart under physiological conditions, this study shows that cardiomyocyte specific deletion of PMCA1 results in the development of dilated cardiomyopathy with left ventricular systolic dysfunction and pulmonary oedema two weeks after TAC. Cardiomyocyte specific deletion of PMCA1 did not appear to adversely affect the expression of other calcium handling genes. This indicates that PMCA1 may be a key player in enabling heart to adapt with pressure overload and pathological hypertrophy. Hence, following its deletion, the myocardium is unable to effectively respond to the pressure overload and as a result, heart failure develops. PMCA1's protective role during the development of pathological cardiac hypertrophy may help to explore novel treatment options for patients with heart failure.

Chapter 5 - Proteomic analysis of PMCA1^{cko} and PMCA1$^{F/F}$ mice after TAC and sham procedures

5.1 Introduction

As demonstrated in the previous chapter, mice with cardiomyocyte specific deletion of PMCA1 (PMCA1^{cko}) develop dilated cardiomyopathy with systolic dysfunction and pulmonary oedema, two weeks after the TAC procedure. However, the mechanistic pathways involved in the development of heart failure in this mouse cohort are not clear. Proteomic analysis using mass spectrometry and liquid chromatography are well established techniques that can be used for protein identification to elucidate molecular mechanisms. In order to explore the molecular pathways important to our project, left ventricle tissue from WT TAC, WT sham, PMCA1^{cko} TAC, PMCA1^{cko}sham (5 mice per group) was subjected to proteomic analysis.

5.2 Aims

The main aims of the proteomic study are to

i) Analyse the significantly regulated proteins in the proteomic analysis of LV samples
ii) Explore the large protein databases STRING and Reactome to determine the associations of significantly regulated proteins and gain insights into their role in physiological and pathological processes.
iii) Identify associations with relevance to cellular pathways involved in myocardial hypertrophy and heart failure

5.3 Materials and methods

Proteomics experimental design and work were carried out by the Bio-MS research facility at the University of Manchester, following the predefined researcher-led sample preparation protocol. This involved taking samples from the frozen LV tissue from mice, preparing these for LC-MS/MS analysis in order to separate and identify various proteins. Sample preparation was carried out by the author at the Core MS facility University of Manchester under direct guidance from Dr David Knight and Mr Ronan O'Cualain.

5.3.1 Sample lysis and protein extraction

The Covaris LE220+ system was used for sample lysis and protein extraction. The protein samples were kept on ice whilst waiting to be processed in order to avoid denaturation. On the Covaris LE220+, the system temperature was set at 10°C. The S-Trap lysis buffer was diluted to xxx from the stock solution to a working concentration (5% SDS with 50 mM TEAM, pH 7.5). The working S-Trap buffer was then added to the protein samples in the Covaris glass tubes. Sonolab 8.2 software was used for sample processing on the Covaris LE220+ system. The lysed sample extracts were transferred to individually labelled tubes for next steps in the process, including reduction and alkylation.

5.3.2 Reduction and alkylation using dithiothreitol and iodoacetamide

Cysteine bonds are important components of a protein's secondary structure. Breaking these bonds offers better access for trypsin and other digestive enzymes to convert proteins into peptides. The process of reduction and alkylation helps to break these cysteine bonds within the protein structure and modify the free cysteine. 5mM dithiothreitol (DTT, Fisher) was used to break cysteine bonds to facilitate better digestion and conversion of protein to peptide. After a incubation for 5 minutes , iodoacetamide (184.96 gm/mol, 99% purity, IAM, Sigma Aldrich) was added for the modification of the free cysteines. Following another incubation for 5 minutes, 5mM DTT was added to quench the alkylation reaction. Finally, the samples were centrifuged at 14,000 relative centrifugal force (RCF) for 10 minutes using the Eppendorf 5430R centrifuge. The supernatant protein lysate was removed into a labelled tube using a clean pipette to proceed to the next step of quantifying the protein.

5.3.3 Measuring protein concentration using Millipore Direct Detect

Millipore Direct Detect Biomolecular Quantification System was used to quantify the protein concentration in the lysate. Samples were loaded on to the Millipore Direct detect sample cards (DDAC00010-GR) and placed into the Millipore instrument card holder. The Millipore Direct detect is reliable for the measurement of protein lysates between 0.3 and 5 mg.mL-1. In case of readings higher than 5 mg.mL-1, samples were diluted in SDS S-Trap lysis buffer containing 10 mM DTT with 15 mM IAM and were measured again in triplicate.

5.3.4 S-Trap™ 96-well plate digestion

To the SDS lysate from the previous step, 5ul of 12% aqueous phosphoric acid at 1:10 for a final concentration of 1.2% phosphoric acid was added and thoroughly mixed with vortex. This was followed by the addition of S-Trap binding buffer to the acidified lysis buffer and mixed again. After mixing thoroughly, the colloidal protein particulate was formed and the solution appeared translucent. After this, the S-Trap plate was put on top of a clean 96 well plate and the acidified SDS lysate was added to the plate. The plate was then centrifuged at 1,500 g for 2 minutes on the Megafuge 16 centrifuge. This step was repeated until there was no visible sample remained in the S-Trap plate. The protein was drained and trapped within the protein-trapping matrix of the plate. The resultant captured protein was washed three times with 200µl of S-Trap binding buffer and centrifuged at 1500 RCF for 2 minutes.

The S-Trap digestion plate was moved on the top of a clean receiver plate and digestion buffer containing trypsin was added into the top of the wells and incubated in the Thermomixer for 1 hour at 47°C .

Subsequently, 80 µL digestion buffer was added to all the wells of the S-Trap digestion plate to elute the peptides. The plate was centrifuged at 1,500 g for 2 minutes and 80 µL 0.1% aqueous formic acid was added to all wells of the S-Trap digestion plate and centrifuged again. The peptides were further eluted by adding 40 µL of 30% aqueous acetonitrile containing 0.1% formic acid to assist in the recovery of hydrophobic peptides. The final acetonitrile concentration was approximately 5% v/v.

5.3.5 96-well plate R3 desalt and clean up for mass spec analysis

At this stage, 10 µL of prepared POROS R3 (Thermo Fisher Scientific) was added to the wells on the filter plate. The filter plate and beads were washed with 200 µL of 0.1% formic acid in acetonitrile and centrifuged at 1,500 g for 2 minutes. This step was repeated twice and plate was washed again with 0.1% formic acid in water. The samples (200 µL) were then loaded on to the plate and beads and incubated on the plate mixer for 5 minutes at 500 rpm. The liquid flow through was removed and transferred to the original sample tubes. The beads were washed twice with 200 µL of 0.1% formic acid and centrifuged.

To elute the peptides, the collection plate was changed again. 100 µL 0.1% formic acid was added to 30% acetonitrile, mixed and centrifuged at 800rpm for 2 minutes. This process was

repeated for a second elution. Both elutions were combined and transferred to the labelled sample vials. All the samples were separated into peptide samples and pooled samples and were clearly labelled; pooled samples were used for quality control. Finally, the peptide samples were completely dried in the Heto vacuum centrifuge ready for liquid chromatography tandem mass spectrometry (LC MS/MS).

5.3.6 Liquid Chromatography and Mass Spectrometry (LC-MS/MS)

Liquid chromatography and mass spectrometry was undertaken by the Core MS Facility at the University of Manchester. The peptide samples were analysed using an UltiMate 3000 Rapid Separation LC System (Dionex Corporation) linked to an Orbitrap Elite (Thermo Fisher) mass spectrometer. Peptides were selected automatically by data dependent analysis for further fragmentation. Mass spectrometry data was analysed using Progenesis QI for proteomics (version 3.0, Nonlinear Dynamics) and results were imported into Progenesis LC-MS for evaluation of peptide peaks. The data was analysed with the support and guidance from Mr Julian Selley (proteomic experimental officer). The final analysis was carried out with Miss Rabia Gangrekar (Masters student) and some of the following data has been presented in her Masters thesis in 2020.

As a part of the quality control measure, total protein abundance in each sample was measured and compared to other samples to ensure similar protein abundance in samples before proceeding to further in-depth analysis. These results are shown in the box plot in figure 5.1. Protein samples from each group are colour coded, $PMCA1^{cko}$:TAC – orange, $PMCA1^{cko}$: sham – blue, $PMCA1^{F/F}$: TAC – red, $PMCA1^{F/F}$: sham – green. This data shows total abundance ratio to be comparable amongst various groups.

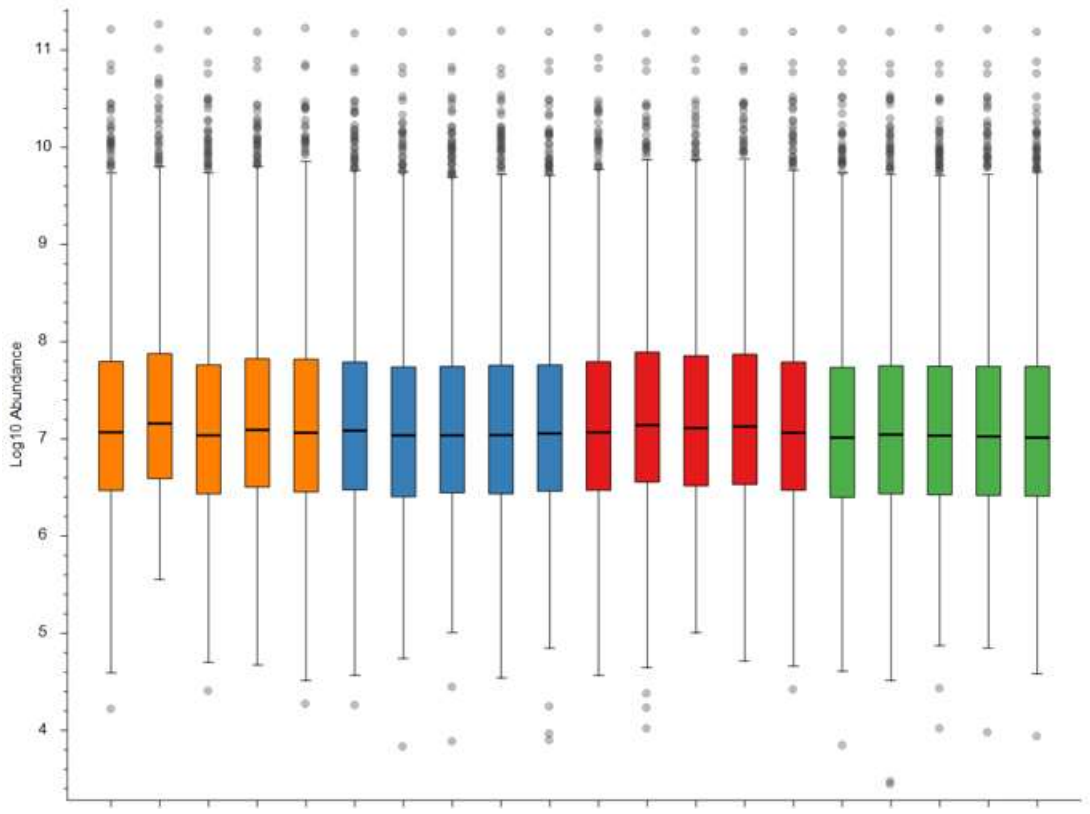

Figure 5.1: Sample abundances: box plot of the total protein abundance in each sample. Proteins are colour coded, PMCA1^{cko} :TAC – orange, PMCA1^{cko} : sham – blue, PMCA1$^{F/F}$: TAC – red, PMCA1$^{F/F}$: sham – green.

5.4 Results

The experiment described in the previous chapter shows that PMCA1^{cko} TAC mice develop heart failure with pulmonary oedema. To evaluate and analyse highly regulated proteins in order to understand the cellular and mechanistic pathways involved in the development of heart failure in PMCA1^{cko} mice after two weeks of TAC LC-MS was performed.

For LS-MS proteomic analysis, five samples were taken each from PMCA1$^{F/F}$: sham, PMCA1$^{F/F}$:TAC, PMCA1^{cko} :sham and PMCA1^{cko} :TAC groups. The LC-MS identified a total of 3634 proteins. The number of peptide sequences unique to a protein group is termed as unique peptide count (UPC). From these results the proteins with a UPC of 2 or below were filtered out in order to improve robustness of the data. Log2 fold change represents the log-ratio of a protein's expression in two different conditions and is routinely used to describe

the abundance ratio and is documented as + or – value denoting upregulation or downregulation of proteins between two different experimental groups, respectively. The results from these experimental groups were compared with each other to identify the significantly upregulated and downregulated proteins (p≤0.05). These results are shown in table 5.1.

	Regulated proteins		**Upregulated proteins**		**Downregulated proteins**	
Group	**Total**	**p≤0.05**	**Total**	**p≤0.05**	**Total**	**p≤0.05**
PMCA1^{cko} sham vs PMCA1$^{F/F}$ sham	2402	88	1695	51	726	35
PMCA1^{cko} TAC vs PMCA1$^{F/F}$ TAC	2424	94	822	41	1602	53
PMCA1$^{F/F}$ TAC vs PMCA1$^{F/F}$ sham	2430	82	1711	66	719	16

Table 5.1: A summary of regulated proteins that PMCA1^{cko} sham and PMCA1^{cko} TAC mice, compared to PMCA1$^{F/F}$ sham and PMCA1$^{F/F}$ TAC mice. One-way ANOVA used for statistical analysis of the results and p value of ≤0.05 was considered to be significant.

5.4.1 PMCA1^{cko} : sham vs PMCA1$^{F/F}$: sham

PMCA1^{cko} mice have a significantly reduced expression of PMCA1 protein in cardiomyocytes compared to their PMCA1$^{F/F}$ counterparts (add section number where this can be seen). The sham operation for TAC involves general anaesthesia, sternotomy and exploration of aorta, and whilst the surgical suture is passed around the ascending aorta, it is not tied, and no constriction is created. Hence, both PMCA1$^{F/F}$ and PMCA1 ^{cko} mice cohorts underwent the sham operation and were not subjected to pressure overload. A total of 3436 proteins were identified by the LC-MS of the left ventricular tissue obtained from these two mice cohorts of which 2438 proteins contained a unique peptide count of 2 or more. These were analysed further, and their abundance ratios converted to a log2 abundance ratio. As a result, 1695

proteins were found to be upregulated and 726 proteins were downregulated, Figure 5.2 (A) shows an enhanced volcano plot showing significantly up and down regulated proteins in $PMCA1^{cko}$: sham mice compared to $PMCA1^{F/F}$: sham mice.

$PMCA1^{cko}$: sham mice had 51 significantly upregulated and 35 significantly down regulated proteins when compared with $PMCA1^{F/F}$: sham group. The number of significantly up and down regulated proteins are represented in the bar chart in figure 5.2 (B).

A

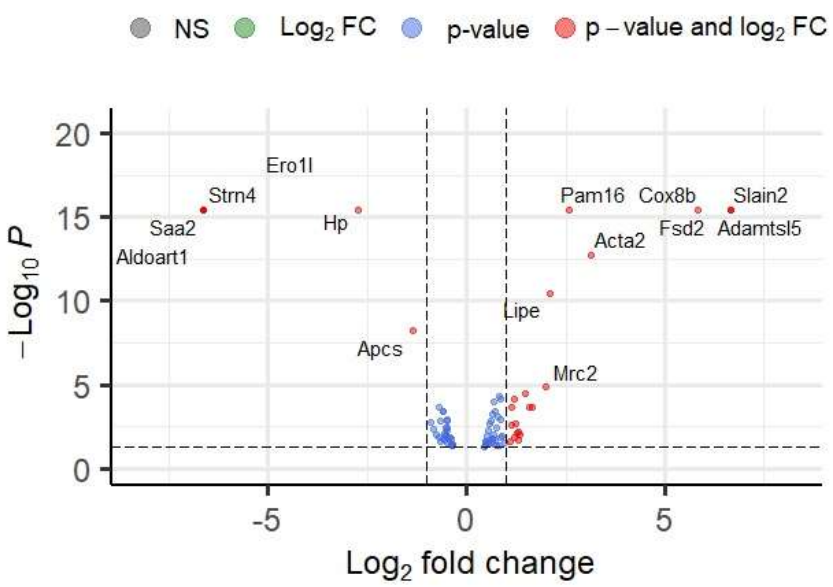

B

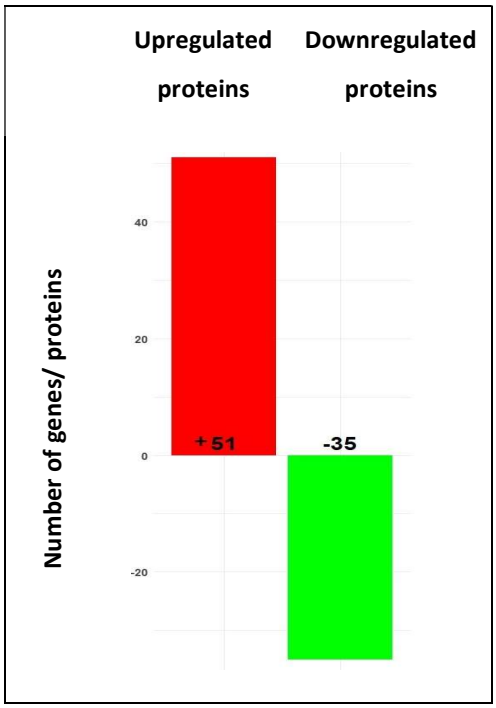

Figure 5.2: (A) An enhanced volcano plot showing proteins with significant log_2 fold change in PMCA1^{cko}: sham mice compared to PMCA1$^{F/F}$: sham mice. Each dot in the plot represents a specific protein and colour coding denotes whether the protein is regulated by log_2 fold change (green), whether it has a significant p-vale ≤ 0.05 (blue) or whether it is regulated by fold change as well as it has a significant p-vale ≤ 0.05 (red). **(B) Bar chart representing the number of significantly (p <0.05) upregulated and downregulated proteins in PMCA1^{cko}: sham mice compared to PMCA1$^{F/F}$: sham cohort.**

The significantly regulated proteins were organised into a heat map (figure 5.3). These results are further elaborated in tables 5.2 and 5.3, with the full name of proteins along with their abundance ratio, $\log_2$ abundance ratio and p values.

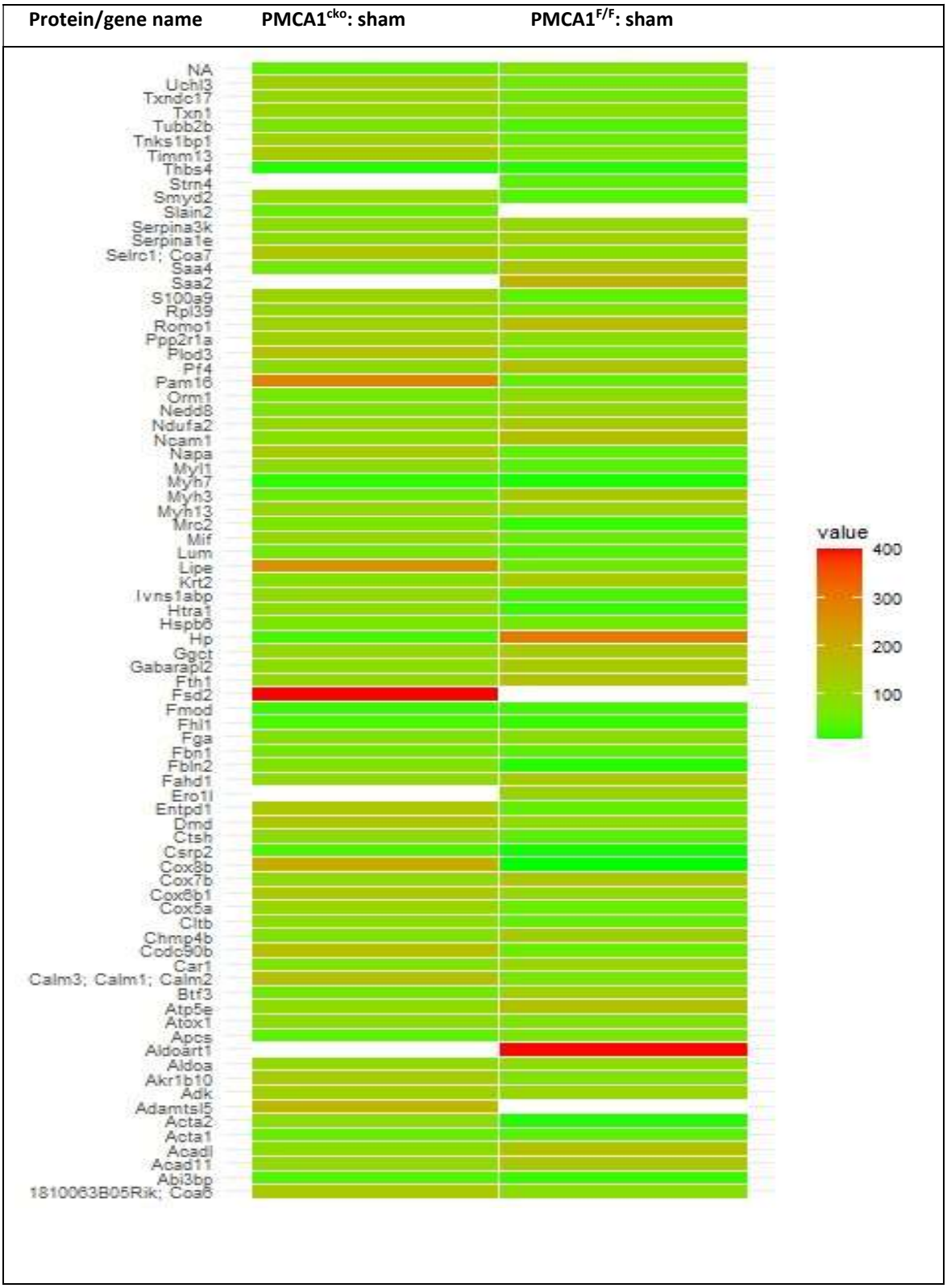

Figure 5.3: A heatmap of significantly regulated proteins in PMCA1^{cko}: sham mice compared to PMCA1$^{F/F}$: sham cohort. The red colour bars represent proteins that are significantly upregulated and green colour bars represent significantly downregulated proteins ($p<0.05$).

PMCA1^{cko} :sham vs PMCA1$^{F/F}$:sham				
Gene symbol	**Protein name**	**Abundance ratio**	**Log2 abundance ratio**	**p-value**
Abi3bp	Abi3bp protein	2.415	1.272023	0.0072
Acta1	Actin, alpha skeletal muscle	1.386	0.470927	0.0388
Acta2	Uncharacterized protein	8.743	3.128128	1.82E-13
Adamtsl5	ADAMTS-like 5	100	6.643856	3.58E-16
Adk	Adenosine kinase	1.374	0.458382	0.0498
Akr1b10	Aldo-keto reductase family 1, member B10 (Aldose reductase)	1.429	0.515006	0.0283
Atox1	Copper transport protein ATOX1	1.776	0.828632	4.97E-05
Calm3; Calm1; Calm2	Calmodulin	1.529	0.612588	0.0312
Ccdc90b	Coiled-coil domain-containing protein 90B, mitochondrial	2.184	1.126973	0.0026
Cltb	Clathrin light chain	1.932	0.950095	0.0280
Cox5a	Cytochrome c oxidase subunit 5A, mitochondrial	1.381	0.465713	0.0428
Cox6b1	Cytochrome c oxidase subunit 6B1	1.404	0.489543	0.0261
Cox8b	Cytochrome c oxidase subunit 8B, mitochondrial	57.461	5.844511	3.58E-16
Csrp2	Smooth muscle LIM protein	2.785	1.477677	3.26E-05
Ctsh	cathepsin H	2.445	1.289834	0.0063
Dmd	Dystrophin	1.407	0.492622	0.0245
Entpd1	Ectonucleoside triphosphate diphosphohydrolase 1	1.86	0.895303	0.0107
Fbln2	fibulin 2	2.304	1.204141	6.91E-05
Fbn1	Mutant fibrillin-1	1.524	0.607863	0.0015
Fhl1	four and a half LIM domains 1, isoform CRA_b	1.473	0.558757	0.0056
Fmod	Fibromodulin	2.522	1.334568	0.0100
Fsd2	Uncharacterized protein	100	6.643856	3.58E-16
Hspb6	Heat shock protein beta-6	1.512	0.596458	0.0020
Htra1	Serine protease HTRA1	3.162	1.660837	0.0002

Iah1	Isoamyl acetate-hydrolyzing esterase 1 homolog	1.774	0.827006	0.0388
Ivns1abp	Influenza virus NS1A-binding protein homolog	1.64	0.713696	0.0201
Lipe	hormone-sensitive lipase	4.318	2.110363	3.90E-11
Lum	Lumican	1.596	0.674461	0.0086
Mif	Macrophage Migration inhibitory factor	1.572	0.652601	0.0172
Mrc2	mannose receptor, C type 2	3.969	1.988776	1.35E-05
Myh7	Myosin-7	1.556	0.637842	0.0006
Myl1	Myosin light chain 1/3, skeletal muscle isoform	1.802	0.849599	0.0012
Napa	Uncharacterized protein	1.593	0.671746	0.0327
Pam16	Mitochondrial import inner membrane translocase subunit TIM16	5.936	2.569491	3.58E-16
Plod3	Procollagen-lysine,2-oxoglutarate 5-dioxygenase 3	2.464	1.301002	0.0191
Ppp2r1a	Uncharacterized protein	1.438	0.524064	0.0123
Rpl39	60S ribosomal protein L39	1.574	0.654436	0.0170
Rps12-ps3	40S ribosomal protein S12	1.489	0.574344	0.0211
S100a9	Protein S100-A9	2.209	1.143393	0.0002
Selrc1; Coa7	Cytochrome c oxidase assembly factor 7	1.806	0.852798	0.0125
Slain2	SLAIN motif-containing protein 2	100	6.643856	3.58E-16
Smyd2	N-lysine methyltransferase SMYD2	3.012	1.590722	0.0002
Thbs4	Thrombospondin-4	2.296	1.199123	0.0140
Timm13	mitochondrial import inner membrane translocase subunit TIM13	1.711	0.77484	0.0008
Tnks1bp1	182 kDa tankyrase-1-binding protein	2.164	1.1137	0.0263
Tubb2b	Tubulin beta-2B chain	2.355	1.235727	0.0021
Txn1	thioredoxin	1.628	0.703101	0.0004
Txn2	Thioredoxin, mitochondrial	1.608	0.685267	0.0001

Txndc17	Thioredoxin domain-containing protein 17	1.671	0.740712	0.0035
Uchl3	Ubiquitin carboxyl-terminal hydrolase isozyme L3	1.805	0.851999	6.83E-05

Table 5.2: A list of significantly upregulated proteins in PMCA1^{cko} :sham mice compared to PMCA1$^{F/F}$: sham cohort. One-way ANOVA test was used for statistical analysis and p-value <0.05 was considered to be significant.

PMCA1^{cko} : sham vs PMCA1$^{F/F}$: sham				
Gene symbol	**Protein name**	**Abundance ratio**	**Log2AR**	**Adjusted P-value**
Acad11	acyl-CoA dehydrogenase family member 11	0.766	-0.38458	0.0438
Acadl	Long-chain specific acyl-CoA dehydrogenase, mitochondrial	0.761	-0.39403	0.0162
Aldoart1	fructose-bisphosphate aldolase	0.01	-6.64386	3.58E-16
Ap2s1	AP-2 complex subunit sigma	0.689	-0.53742	0.0086
Apcs	Serum amyloid P-component	0.388	-1.36587	6.20E-09
Atp5e	ATP synthase subunit epsilon, mitochondrial	0.784	-0.35107	0.0413
Atpif1	ATPase inhibitor, mitochondrial	0.669	-0.57992	0.0004
Btf3	transcription factor BTF3	0.538	-0.89432	0.0016
Car1	carbonic anhydrase 1	0.718	-0.47794	0.0039
Chmp4b	Charged multivesicular body protein 4b	0.615	-0.70134	0.0002
Cox7b	Cytochrome c oxidase subunit 7B, mitochondrial	0.669	-0.57992	0.0158
Ero1l	ERO1-like protein alpha	0.01	-6.64386	3.58E-16
Fahd1	Acylpyruvase FAHD1, mitochondrial	0.72	-0.47393	0.0051
Fga	Fibrinogen alpha chain	0.707	-0.50022	0.0011
Fth1	Ferritin heavy chain	0.712	-0.49005	0.0015
Gabarapl2	Gamma-aminobutyric acid receptor-associated protein-like 2	0.588	-0.76611	0.0101
Ggct	gamma-glutamylcyclotransferase	0.708	-0.49818	0.0297
Hp	Haptoglobin	0.151	-2.72738	3.58E-16
Hsph1	Heat shock protein 105 kDa	0.677	-0.56277	0.0072
Krt2	Keratin, type II cytoskeletal 2 epidermal	0.61	-0.71312	0.0132
mt-Co3	Cytochrome c oxidase subunit 3	0.771	-0.3752	0.0346
Myh13	Myosin, heavy polypeptide 13, skeletal muscle	0.692	-0.53116	0.0035
Myh3	Myosin-3	0.664	-0.59074	0.0004
Ncam1	Neural cell adhesion molecule 1	0.632	-0.662	0.0245

Ndufa2	NADH dehydrogenase [ubiquinone] 1 alpha subcomplex subunit 2	0.778	-0.36216	0.0331
Nedd8	NEDD8	0.733	-0.44811	0.0159
Orm1	Alpha-1-acid glycoprotein 1	0.566	-0.82113	0.0047
Pf4	C-X-C motif chemokine	0.704	-0.50635	0.0106
Romo1	Reactive oxygen species modulator 1	0.676	-0.5649	0.0196
Saa2	Serum amyloid A protein	0.01	-6.64386	3.58E-16
Saa4	Serum amyloid A-4 protein	0.638	-0.64837	0.0015
Serpina1e	Alpha-1-antitrypsin 1-5	0.756	-0.40354	0.0131
Serpina3k	mCG1051009	0.783	-0.35292	0.0391
Strn4	Striatin-4	0.01	-6.64386	3.58E-16

Table 5.3: A list of significantly downregulated proteins in PMCA1^{cko} : sham mice compared to PMCA1$^{F/F}$: sham mice cohort. One-way ANOVA test was used for statistical analysis and p-value <0.05 was considered to be significant.

5.4.1.1 STRING analysis

The gene symbols of all significantly regulated proteins were added into the online STRING database tool to identify protein-protein interactions. This led to four specific clusters of protein- protein interactions with every protein interacting with a variable number of molecular partners (figure 5.4). The majority of proteins had few interaction partners whereas a small number of proteins had more than 10 interaction partners. Acta 2, Hp, myosin, calmodulin and striatin-4 were found to have higher number of interactions and are of key importance, in the context of their role in the development and progression of heart failure. These proteins are further described at the end of this section.

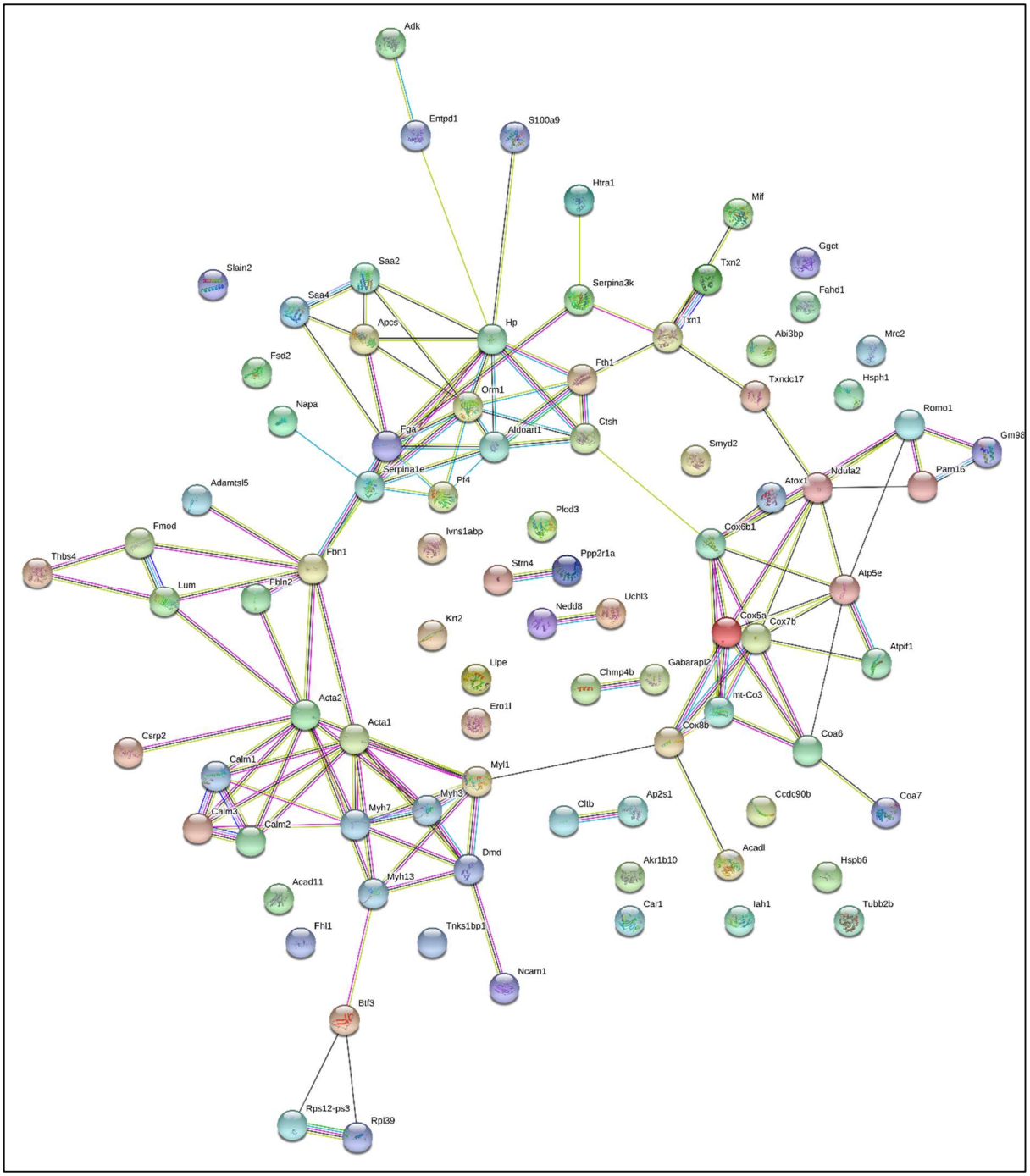

Figure 5.4: A schematic download from STRING database shows protein-protein interactions of significantly regulated proteins in PMCA1^{cko} : sham compared to PMCA1$^{F/F}$: sham mice. Each sphere represents a protein and the straight line represent protein-protein interaction.

5.4.1.2 Reactome analysis

Following the initial identification of protein-protein interactions by STRING database, the gene identifier names of all significantly regulated proteins were entered into the Reactome database. This highlighted the possible links between proteins with relevance to the cellular pathways. The probable pathways were then presented in a schematic diagram in figure 5.5 and labelled according to their associations with various physiological mechanisms. The centre of each pathway represents the top-tier pathway with subsequent branches showing the next level in the hierarchy. Some of the most significantly enhanced pathways identified from Reactome database were associated with striated muscle contraction, extracellular matrix organisation, nuclear envelope sealing and reassembly, gap junction and micro-tubule mediated trafficking. As these cellular pathways play a pivotal role in maintaining the normal structure and function of the heart, it is plausible that any impairment of these interactions could also lead to cardiac dysfunction. Striated muscle contraction pathways are of key importance in the context of PMCA1^{cko} mice and could possibly explain why these mice develop systolic dysfunction in heart failure following pressure overload.

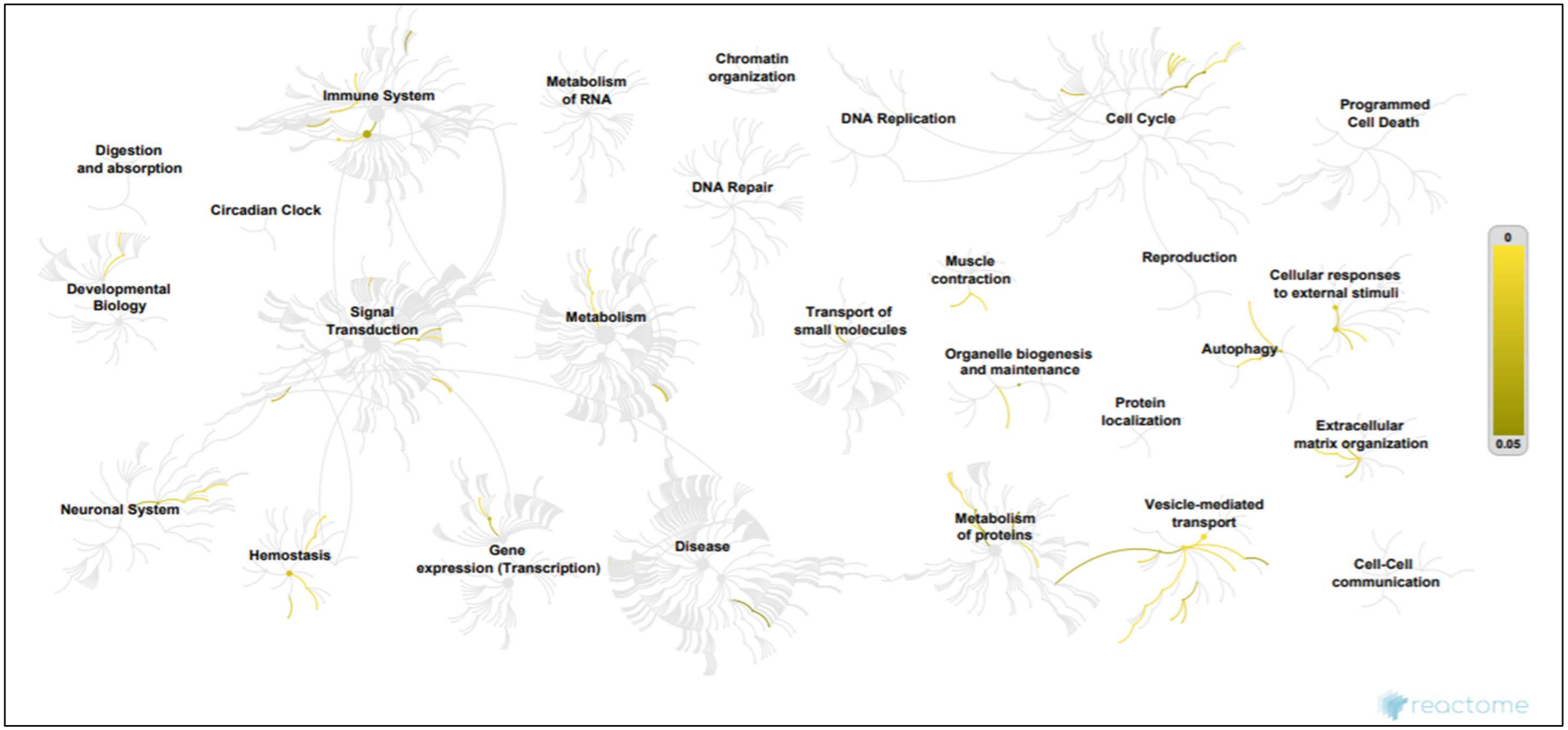

Figure 5.5: Reactome database schematic diagram of cellular pathways linking significantly regulated proteins in PMCA1^{cko} sham mice compared to PMCA1$^{F/F}$ sham cohort. These cellular pathways are organised as circular clusters in a hierarchy with the centre of each cluster representing the root of top-tier pathway. On moving away from the centre, each branch represents the next lower tier in the pathway hierarchy. For the significantly regulated proteins entered in the Reactome database, gold colour-coded pathways correspond to over-representation of that pathway and light grey colour-coded pathways are not significantly over-represented.

5.4.2 PMCA1$^{F/F}$: TAC vs PMCA1$^{F/F}$: sham

To determine the impact of pressure overload created by TAC on the protein expression, PMCA1$^{F/F}$:TAC mice were compared with PMCA1$^{F/F}$: sham mice. A total of 3436 proteins were identified in the LC/MS analysis of which 2438 had a total unique peptide count of 2 or more. Figure 5.6 (A) shows an enhanced volcano plot showing significantly up and down regulated proteins in PMCA1$^{F/F}$: TAC mice compared to PMCA1$^{F/F}$: sham mice. Of these, 82 proteins were significantly regulated ($p \leq 0.05$); 66 proteins were up-regulated and 16 were down-regulated, this is shown in the bar graph (figure 5.6 B).

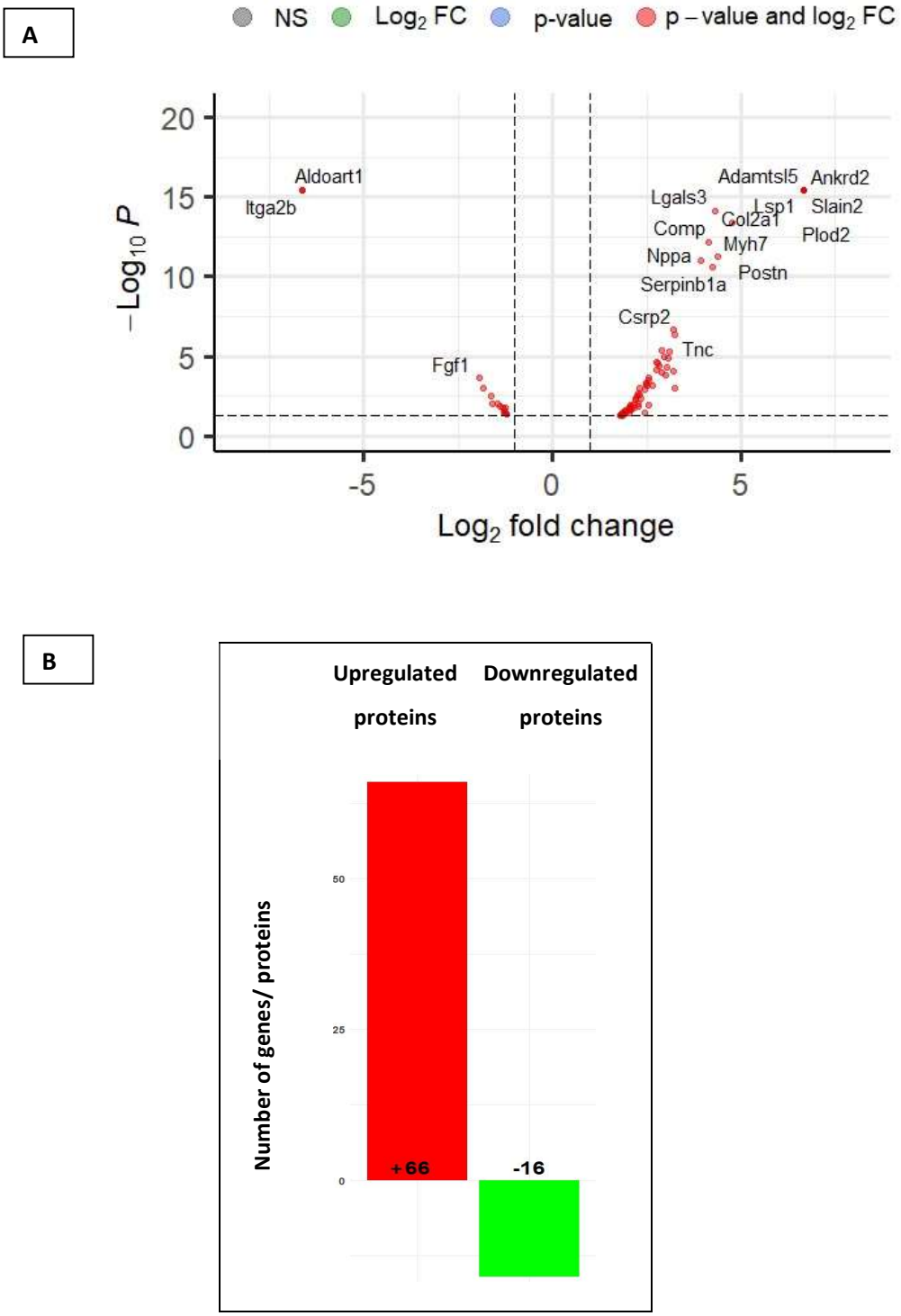

Figure 5.6: (A) An enhanced volcano plot showing proteins with significant log_2 fold change in PMCA1$^{F/F}$: TAC mice compared to PMCA1$^{F/F}$: sham mice. Each dot in the plot represents a specific protein and colour coding denotes whether the protein is regulated by log_2 fold change (green), whether it has a significant p-vale ≤ 0.05 (blue) or whether it is regulated by fold change as well as it has a significant p-vale ≤ 0.05 (red). **(B) Bar chart representing the number of significantly upregulated and down regulated proteins in PMCA1$^{F/F}$: TAC mice compared to PMCA1$^{F/F}$: sham cohort.**

The significantly regulated proteins are further demonstrated in the heat map in figure 5.7, and these results are further elaborated in tables 5.4 and 5.5.

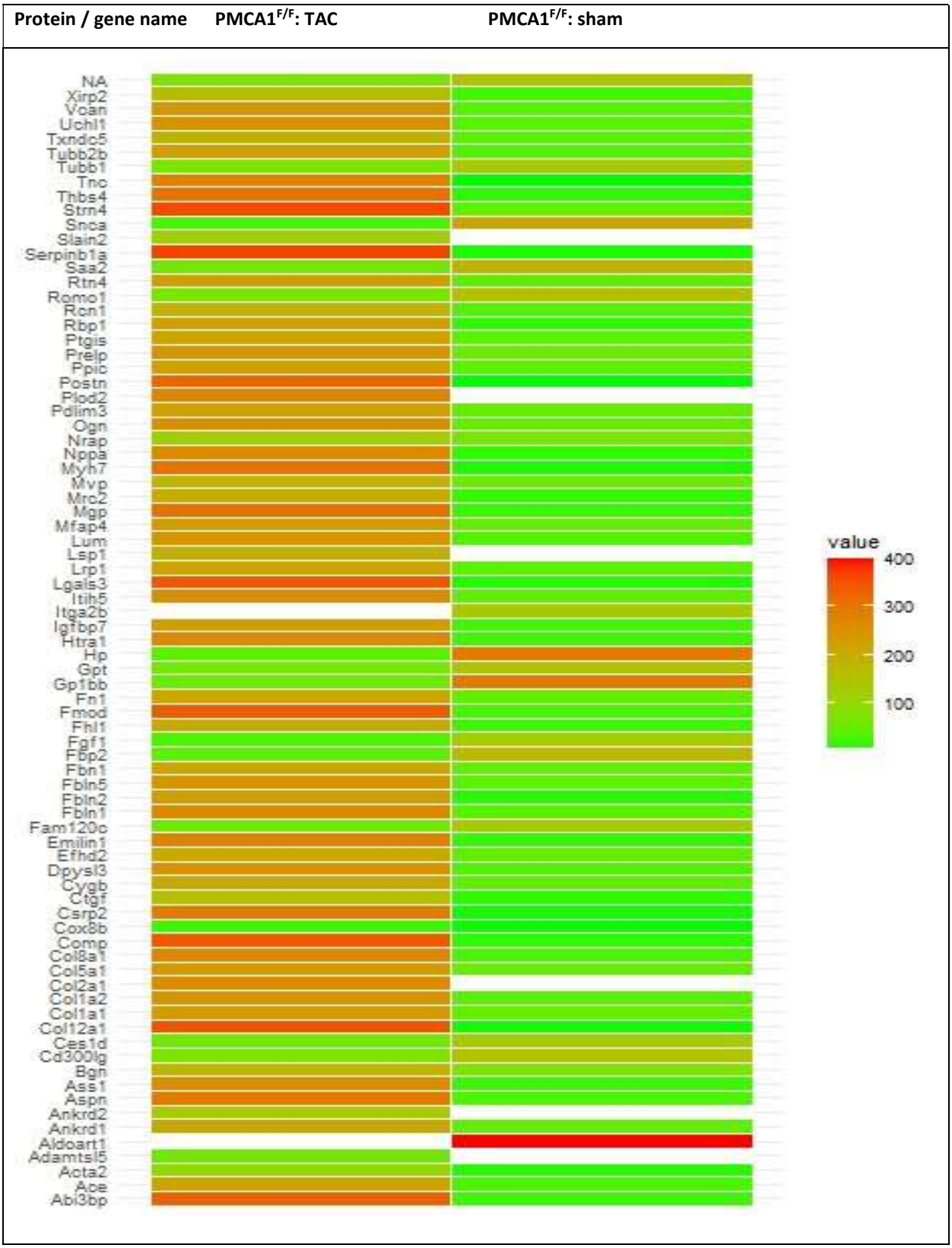

Figure 5.7: A heatmap of significantly upregulated proteins in PMCA1$^{F/F}$: TAC mice compared to PMCA1$^{F/F}$: sham cohort. The red colour bars represent proteins that are significantly upregulated and green colour bars represent significantly downregulated proteins ($p<0.05$).

PMCA1$^{F/F}$: TAC vs PMCA1$^{F/F}$: sham				
Gene symbol	**Protein name**	**Abundance ratio**	**Log2 abundance ratio**	**p-value**
Abi3bp	Abi3bp protein	7.156	2.839153	4.14E-05
Ace	Angiotensin-converting enzyme	4.662	2.220949	4.06E-03
Acta2	Uncharacterized protein	9.5	3.247928	9.63E-04
Adamtsl5	ADAMTS-like 5	100	6.643856	3.53E-16
Ankrd1	Ankyrin repeat domain-containing protein 1	4.283	2.098622	2.01E-02
Ankrd2	Ankyrin repeat domain-containing protein 2	100	6.643856	3.53E-16
Aspn	Asporin	8.359	3.06333	1.23E-05
Ass1	Argininosuccinate synthase	8.039	3.007016	1.53E-04
Bgn	biglycan	4.843	2.275901	8.56E-03
Col12a1	Collagen alpha-1(XII) chain	4.581	2.195663	5.85E-03
Col1a1	Collagen alpha-1(I) chain	4.171	2.060393	1.30E-02
Col1a2	Uncharacterized protein	4.22	2.077243	1.19E-02
Col2a1	Isoform 2 of Collagen alpha-1(II) chain	100	6.643856	3.53E-16
Col5a1	Collagen alpha-1(V) chain	3.597	1.846794	4.95E-02
Col8a1	collagen alpha-1(VIII) chain	7.511	2.909005	4.12E-06
Comp	Cartilage oligomeric matrix protein	17.795	4.1534	6.27E-13
Cox8b	Cytochrome c oxidase subunit 8B, mitochondrial	5.466	2.450485	3.67E-02
Csrp2	Smooth muscle LIM protein	9.251	3.209609	2.20E-07
Ctgf	Connective tissue growth factor	8.265	3.047015	4.98E-05
Cygb	Cytoglobin	3.683	1.880881	3.98E-02
Dpysl3	Dihydropyrimidinase-related protein 3	5.406	2.434562	1.23E-03
Efhd2	EF-hand domain-containing protein D2	3.582	1.840765	4.04E-02
Emilin1	EMILIN-1	5.921	2.565841	2.10E-04
Enah	Protein enabled homolog	3.81	1.929791	3.04E-02
Fbln1	Fibulin-1	6.286	2.652142	6.66E-04
Fbln2	fibulin 2	4.731	2.242145	2.93E-03

Fbln5	Fibulin-5	4.169	2.059701	2.62E-02
Fbn1	Mutant fibrillin-1	4.093	2.033159	1.52E-02
Fhl1	four and a half LIM domains 1, isoform CRA_b	8.678	3.117363	5.28E-06
Fmod	Fibromodulin	6.735	2.751678	6.72E-05
Fn1	fibronectin	3.489	1.802814	4.94E-02
Htra1	Serine protease HTRA1	7.373	2.882252	9.80E-05
Igfbp7	Insulin-like growth factor binding protein 7	6.792	2.763836	2.19E-05
Itih5	Inter-alpha-trypsin inhibitor heavy chain H5	4.826	2.270828	1.49E-02
Lgals3	Galectin	19.757	4.304292	7.77E-15
Lrp1	low density lipoprotein receptor-related protein 1	3.569	1.83552	4.93E-02
Lsp1	Lymphocyte-specific protein 1	100	6.643856	3.53E-16
Lum	Lumican	5.079	2.344544	4.33E-03
Mfap4	Microfibril-associated glycoprotein 4	3.557	1.830661	3.88E-02
Mgp	matrix Gla protein	7.775	2.958843	1.03E-05
Mrc2	mannose receptor, C type 2	9.257	3.210545	8.27E-05
Mvp	Uncharacterized protein	3.651	1.868292	3.60E-02
Myh7	Myosin-7	27.119	4.761232	3.87E-14
Nppa	Natriuretic peptides A	15.093	3.915808	1.04E-11
Nrap	Isoform 2 of Nebulin-related-anchoring protein	3.712	1.892197	3.29E-02
Ogn	Mimecan	5.592	2.483364	5.52E-04
Pdlim3	PDZ and LIM domain protein 3	4.045	2.01614	2.19E-02
Plod2	Uncharacterized protein	100	6.643856	3.53E-16
Postn	Periostin	20.761	4.375804	5.88E-12
Ppic	peptidyl-prolyl cis-trans isomerase C	4.798	2.262433	1.90E-03
Prelp	prolargin	3.813	1.930927	3.72E-02
Ptgis	prostacyclin synthase	5.821	2.541267	3.06E-04
Rbp1	Retinol-binding protein 1	6.963	2.799709	2.63E-05
Rcn1	Reticulocalbin-1	4.467	2.159306	1.75E-02
Rtn4	Reticulon-4	3.825	1.93546	2.63E-02
Serpinb1a	Leukocyte elastase inhibitor A	19.105	4.255878	2.64E-11

Slain2	SLAIN motif-containing protein 2	100	6.643856	3.53E-16
Sparc	Sparc	5.695	2.509696	6.30E-04
Strn4	Striatin-4	5.875	2.554589	1.11E-02
Thbs4	Thrombospondin-4	5.551	2.472748	5.08E-04
Tnc	Tenascin	9.473	3.243821	4.15E-07
Tubb2b	Tubulin beta-2B chain	4.396	2.136191	1.06E-02
Txndc5	Thioredoxin domain-containing protein 5	3.615	1.853996	3.26E-02
Uchl1	Ubiquitin carboxyl-terminal hydrolase isozyme L1	4.042	2.015069	3.38E-02
Vcan	Versican core protein	4.9	2.292782	1.03E-03
Xirp2	Isoform 2 of Xin actin-binding repeat-containing protein 2	5.003	2.322793	2.58E-03

Table 5.4: A list of significantly upregulated proteins PMCA1$^{F/F}$: TAC mice compared to PMCA1$^{F/F}$: sham. One-way ANOVA test was used for statistical analysis and p-value <0.05 was considered to be significant.

PMCA1$^{F/F}$: TAC vs PMCA1$^{F/F}$: sham				
Gene symbol	**Protein name**	**Abundance ratio**	**Log2 abundance ratio**	**p-value**
Aldoart1	fructose-bisphosphate aldolase	0.01	-6.64386	3.53E-16
Cd300lg	CMRF35-like molecule 9	0.419	-1.25498	3.38E-02
Ces1d	Carboxylesterase 1D	0.414	-1.2723	2.21E-02
Fam120c	constitutive coactivator of PPAR-gamma-like protein 2	0.364	-1.45799	9.65E-03
Fbp2	Uncharacterized protein	0.401	-1.31833	1.61E-02
Fgf1	Fibroblast growth factor 1	0.261	-1.93788	2.07E-04
Gp1bb	Platelet glycoprotein Ib beta chain	0.414	-1.2723	3.26E-02
Gpt	Alanine aminotransferase 1	0.422	-1.24469	1.76E-02
+Hp	Haptoglobin	0.328	-1.60823	9.45E-03
Itga2b	integrin alpha 2b	0.01	-6.64386	3.53E-16
Nav2	Neuron navigator 2	0.378	-1.40354	1.30E-02
Romo1	Reactive oxygen species modulator 1	0.324	-1.62593	2.88E-03
Saa2	Serum amyloid A protein	0.277	-1.85204	9.27E-04
Snca	Alpha-synuclein	0.43	-1.21759	4.16E-02
Tubb1	tubulin beta-1 chain	0.416	-1.26534	3.38E-02

Table 5.5: A list of significantly downregulated proteins in PMCA1$^{F/F}$: TAC mice compared to PMCA1$^{F/F}$: sham. One-way ANOVA test was used for statistical analysis and p-value <0.05 was considered to be significant.

5.4.2.1 STRING and Reactome analyses

In order to explore the protein-protein interactions, all of the significantly regulated proteins emerging from the direct comparison between PMCA1$^{F/F}$: TAC and PMCA1$^{F/F}$: Sham groups were inserted into the online STRING database. Out of the significantly regulated 82 proteins in this comparison, 34 were involved in ≤1 protein- protein interaction whereas 22 proteins were involved in ≥10 interactions. The proteins with ≥10 interactions are shown on the STRING analysis as the centre of interaction clusters (figure 5.8).

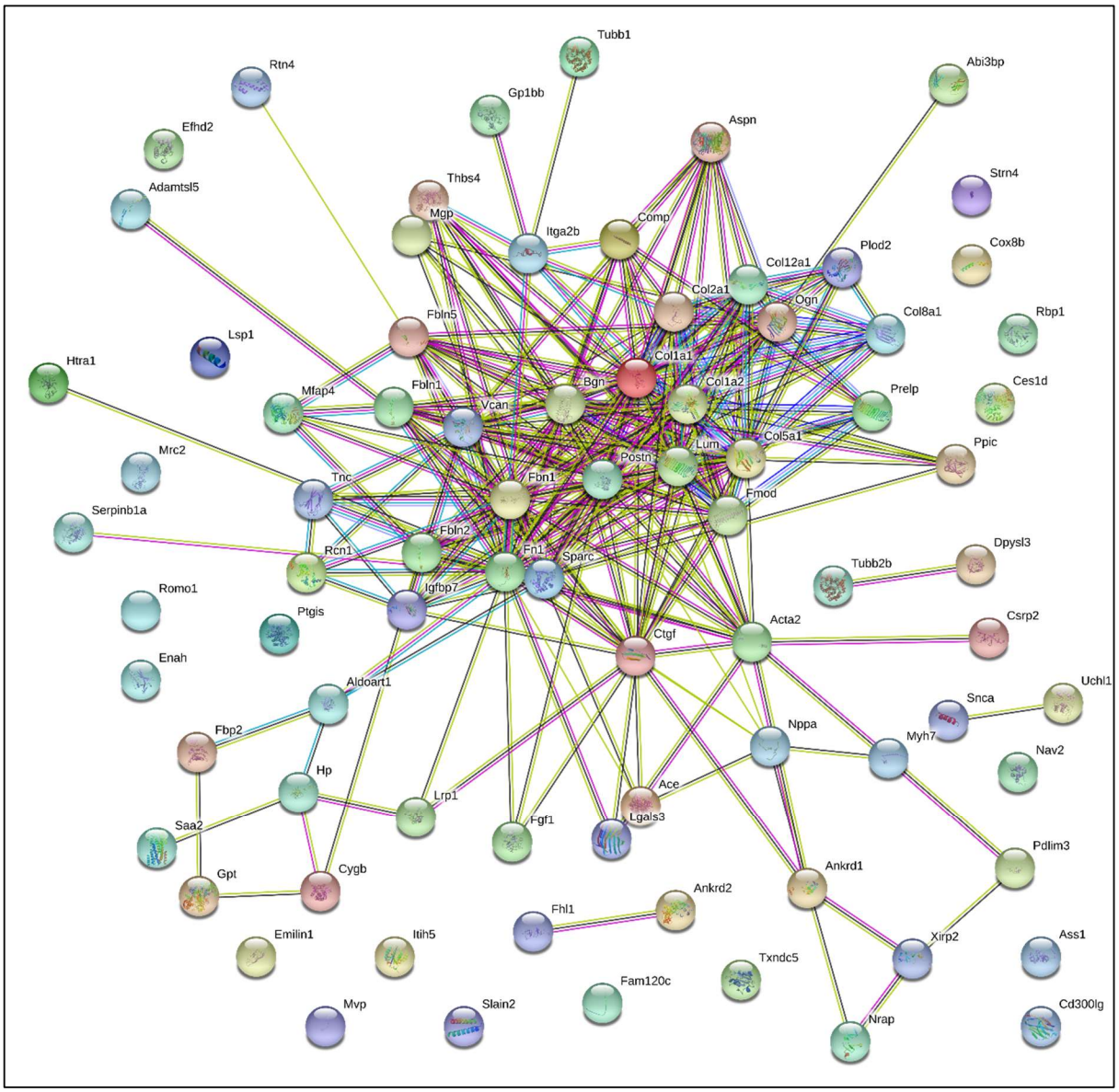

Figure 5.8: STRING schematic diagram showing protein-protein interactions of significantly regulated proteins in PMCA1$^{F/F}$: TAC compared to PMCA1$^{F/F}$: sham mice. Each sphere represents a protein and the straight line represent protein-protein interaction.

The gene names for the significantly regulated proteins were input into the online Reactome database. This presented visualisation of pathways enhanced in PMCA1$^{F/F}$ mice after undergoing pressure overload exerted by the TAC. The salient enhanced pathways in this comparison were linked with extra-cellular matrix organisation, ECM proteoglycans, integrin cell surface interactions, formation of elastic fibre formation, collagen chain trimerisation and degradation of extra cellular matrix (figure 5.9).

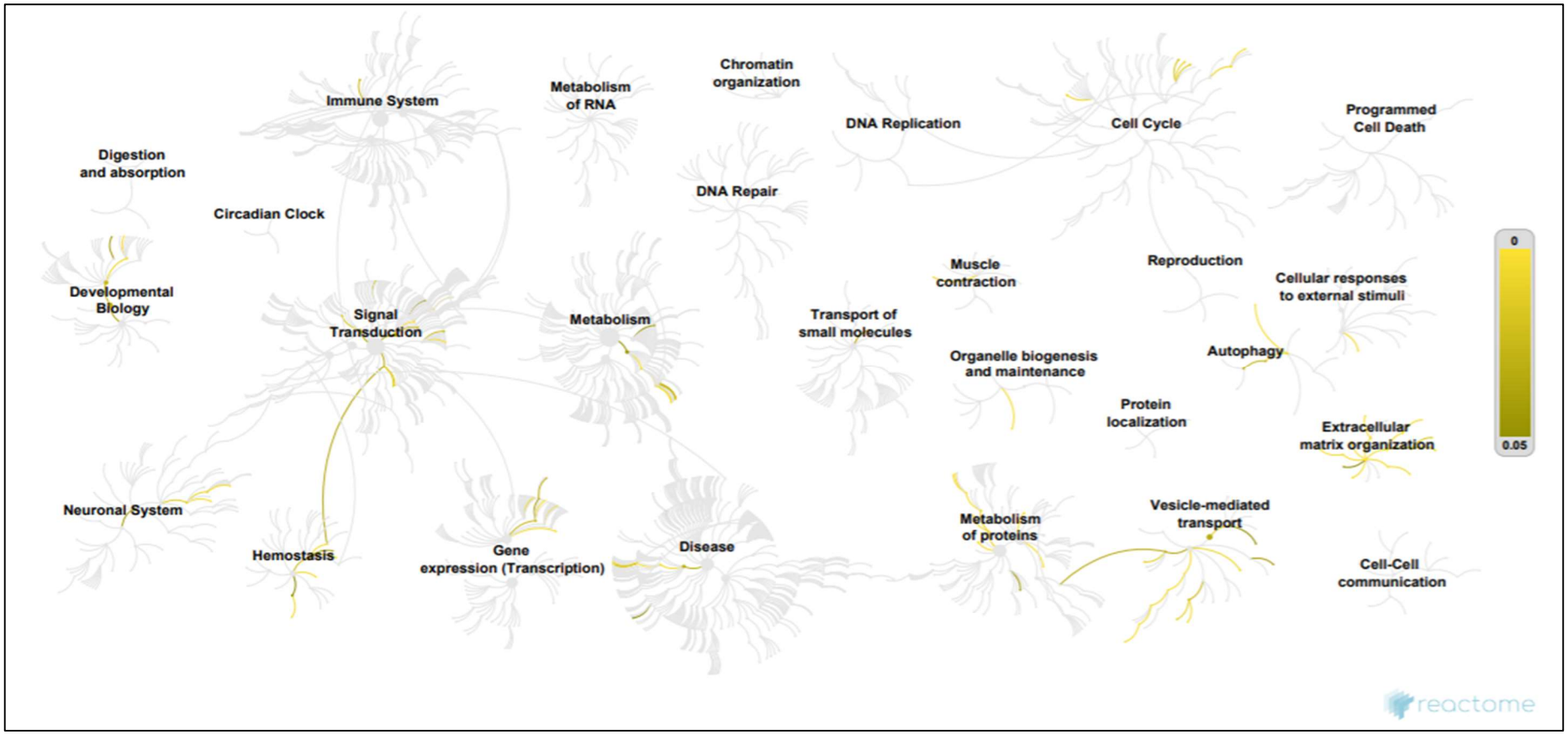

Figure 5.9: A diagram showing Reactome pathways involving significantly regulated proteins in PMCA1$^{F/F}$: TAC mice compared to PMCA1$^{F/F}$: sham mice. These cellular pathways are organised as circular clusters in a hierarchy with the centre of each cluster representing the root of top-tier pathway. On moving away from the centre, each branch represents the next lower tier in the pathway hierarchy. For the significantly regulated proteins entered in the Reactome database, gold colour-coded pathways correspond to over-representation of that pathway and light grey colour-coded pathways are not significantly over-represented.

5.4.3 PMCA1^{cko} TAC vs PMCA1$^{F/F}$ TAC

As presented in chapter 4, PMCA1^{cko} mice develop systolic dysfunction and pulmonary oedema following TAC whilst PMCA1$^{F/F}$ controls develop compensated concentric left ventricular hypertrophy after TAC. To explore the related protein expression changes and protein-protein interactions LC-MS/MS analysis was carried out on the samples of left ventricular tissue from PMCA1^{cko} and PMCA1$^{F/F}$ mice two weeks after TAC. Both mouse cohorts underwent the same TAC surgery leading to a similar pressure overload (see figure 4.2 for maximal left ventricular pressure exerted by TAC). LC-MS identified a total of 3436 proteins, with 2438 proteins having a total unique peptide count ≥ 2.

Figure 5.10 (A) shows an enhanced volcano plot showing significantly up and down regulated proteins in PMCA1^{cko}: TAC mice compared to PMCA1$^{F/F}$: TAC mice. There were 94 proteins significantly regulated proteins ; 41 were significantly upregulated and 53 were significantly downregulated ($P \leq 0.05$), as shown as bar graph in figure 5.10 (B).

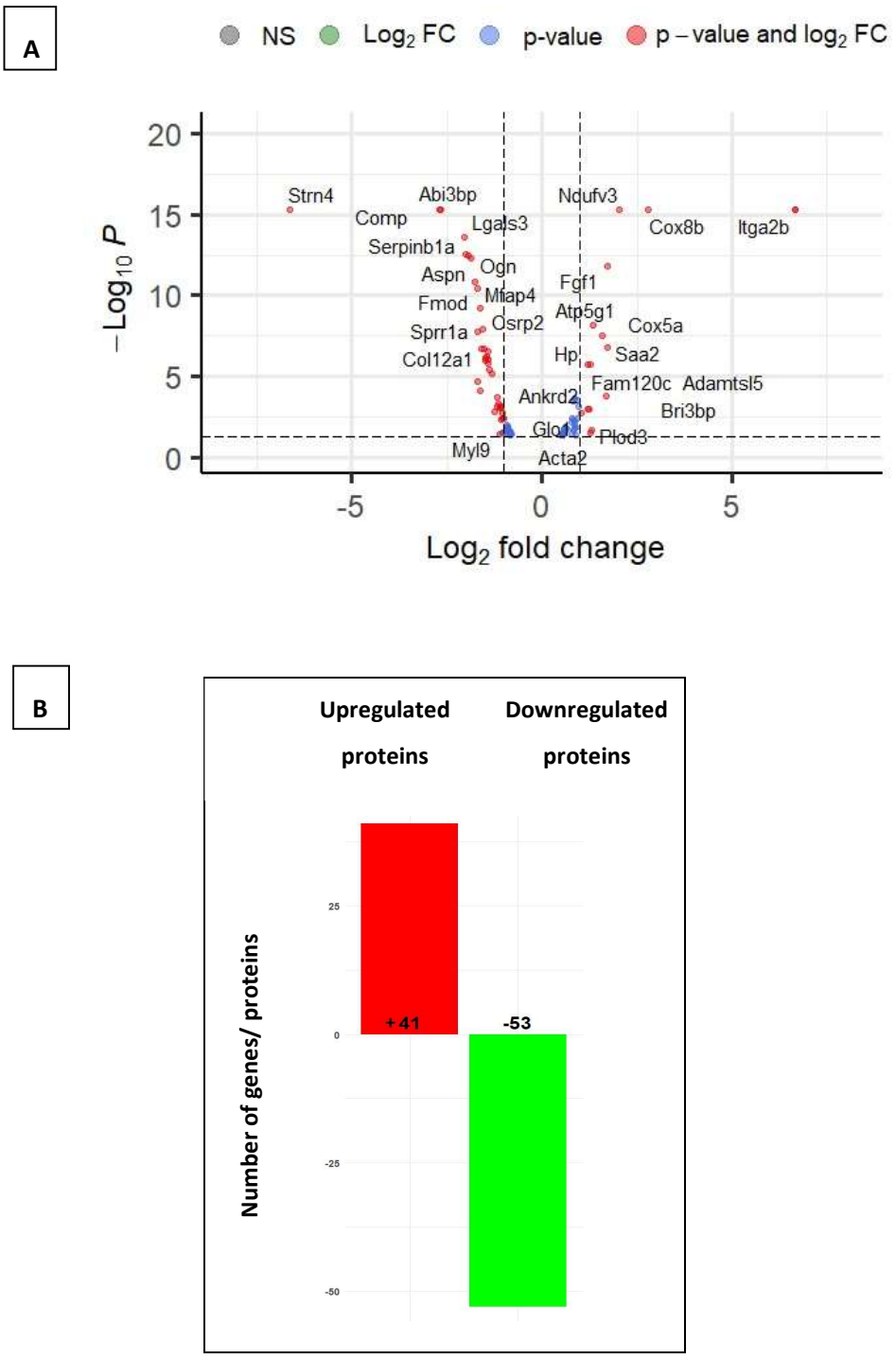

Figure 5.10: (A) An enhanced volcano plot showing proteins with significant log_2 fold change in PMCA1^{cko}: TAC mice compared to PMCA1$^{F/F}$: TAC mice. Each dot in the plot represents a specific protein and colour coding denotes whether the protein is regulated by log_2 fold change (green), whether it has a significant p-vale ≤ 0.05 (blue) or whether it is regulated by fold change as well as it has a significant p-vale ≤ 0.05 (red). **(B) Bar chart representing the number of significantly upregulated and down regulated proteins in PMCA1^{cko}: TAC mice compared to PMCA1$^{F/F}$: TAC cohort.**

The significantly regulated proteins are further illustrated as a heat map (figure 5.11) and in tables 5.6 and 5.7, which provide the full name of proteins along with their abundance ratio, $\log_2$ abundance ratio and p values.

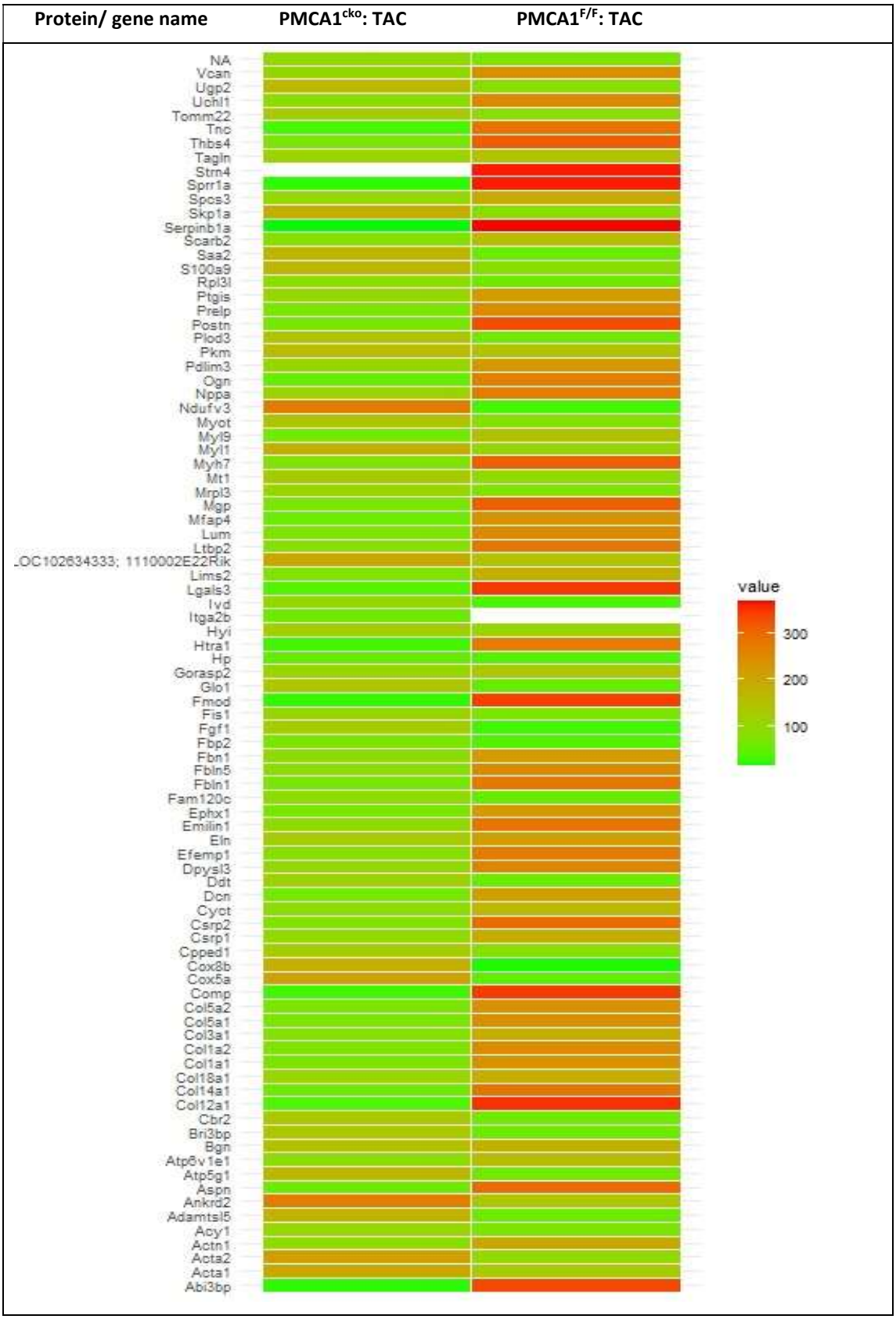

Figure 5.11: A heatmap of significantly upregulated proteins in PMCA1^{cko} : TAC mice compared to PMCA1$^{F/F}$: TAC cohort. The red colour bars represent proteins that are significantly upregulated and green colour bars represent significantly downregulated proteins ($p<0.05$).

PMCA1^{cko} :TAC vs PMCA1$^{F/F}$: TAC				
Gene symbol	**Protein name**	**Abundance ratio**	**Log2AR**	**p-value**
Acta1	Actin, alpha skeletal muscle	1.779	0.831067	2.11E-02
Acta2	Uncharacterized protein	2.412	1.27023	3.24E-02
Acy1	Aminoacylase-1	1.445	0.531069	4.60E-02
Adamtsl5	ADAMTS-like 5	3.2	1.678072	1.74E-04
Ankrd2	Ankyrin repeat domain-containing protein 2	2.291	1.195977	1.04E-03
Atp5g1	ATP synthase F(0) complex subunit C1, mitochondrial	2.558	1.355016	6.76E-09
Atpif1	ATPase inhibitor, mitochondrial	1.47	0.555816	3.43E-02
Bri3bp	BRI3-binding protein	2.345	1.229588	9.68E-04
Cbr2	Carbonyl reductase [NADPH] 2	1.581	0.660837	1.65E-02
Cox5a	Cytochrome c oxidase subunit 5A, mitochondrial	2.964	1.567545	3.24E-08
Cox8b	Cytochrome c oxidase subunit 8B, mitochondrial	6.925	2.791814	5.31E-16
Cpped1	Serine/threonine-protein phosphatase CPPED1	1.826	0.868687	2.43E-04
Ddt	D-dopachrome decarboxylase	1.946	0.960512	7.22E-04
Fam120c	constitutive coactivator of PPAR-gamma-like protein 2	2.392	1.258217	1.89E-06
Fbp2	Fructose bisphosphonate 2	1.882	0.912267	4.09E-03
Fgf1	Fibroblast growth factor 1	3.306	1.725087	1.58E-12
Fis1	mitochondrial fission 1 protein	1.424	0.509949	4.69E-02
Glo1	lactoylglutathione lyase	2.019	1.013641	1.74E-03
Gpcpd1	Glycerophosphocholine phosphodiesterase GPCPD1	1.87	0.903038	1.39E-02
Higd1a	HIG1 domain family member 1A, mitochondrial	1.506	0.590722	1.83E-02
Hp	Haptoglobin	2.301	1.202261	1.73E-06

Hyi	Putative hydroxypyruvate isomerase	1.815	0.85997	5.81E-03
Itga2b	integrin alpha 2b	100	6.643856	5.31E-16
Ivd	Isovaleryl-CoA dehydrogenase, mitochondrial	1.716	0.77905	3.80E-02
LOC102634333; 1110002E22Rik	RIKEN cDNA 1110002E22 gene	1.525	0.608809	1.49E-02
Mrpl3	39S ribosomal protein L3, mitochondrial	1.738	0.797428	6.41E-03
Mt1	Metallothionein-1	1.483	0.568519	2.87E-02
mt-Co3	Cytochrome c oxidase subunit 3 [OS=Mus musculus musculus]	1.468	0.553852	2.99E-02
Myl1	Myosin light chain 1/3, skeletal muscle isoform	1.776	0.828632	3.39E-04
Myot	Myotilin	1.881	0.9115	2.92E-04
Nav2	Neuron navigator 2	1.784	0.835116	4.65E-03
Ndufv3	NADH dehydrogenase [ubiquinone] flavoprotein 3, mitochondrial	4.058	2.020769	5.31E-16
Pkm	Pyruvate kinase PKM	1.812	0.857583	2.44E-04
Plod3	Procollagen-lysine,2-oxoglutarate 5-dioxygenase 3	2.462	1.299831	1.96E-02
Rpl3l	ribosomal protein L3-like	1.503	0.587845	1.66E-02
S100a9	Protein S100-A9	1.747	0.80488	3.58E-03
Saa2	Serum amyloid A protein	3.266	1.707525	1.71E-07
Skp1a	Uncharacterized protein	1.822	0.865523	1.04E-02
Tomm22	Mitochondrial import receptor subunit TOM22 homolog	1.848	0.885965	4.50E-02
Ugp2	UTP--glucose-1-phosphate uridylyltransferase	1.801	0.848798	1.71E-02

Table 5.6: A list of significantly upregulated proteins in PMCA1^{cko} :TAC mice compared to PMCA1$^{F/F}$: TAC cohort. One-way ANOVA test was used for statistical analysis and p-value <0.05 was considered to be significant.

PMCA1^{cko} :TAC vs PMCA1$^{F/F}$: TAC				
Gene symbol	**Protein name**	**Abundance ratio**	**Log2AR**	**p-value**
Abi3bp	Abi3bp protein	0.159	-2.6529	5.31E-16
Actn1	Alpha actinin 1a	0.566	-0.82113	3.27E-02
Aspn	Asporin	0.262	-1.93236	3.57E-13
Atp6v1e1	V-type proton ATPase subunit E 1	0.534	-0.90509	1.36E-02
Bgn	biglycan	0.439	-1.18771	7.22E-04
Col12a1	Collagen alpha-1(XII) chain	0.307	-1.70369	1.59E-08
Col14a1	Collagen alpha-1(XIV) chain	0.534	-0.90509	1.32E-02
Col18a1	Isoform 2 of Collagen alpha-1(XVIII) chain	0.542	-0.88364	2.00E-02
Col1a1	Collagen alpha-1(I) chain	0.35	-1.51457	2.14E-07
Col1a2	Uncharacterized protein	0.385	-1.37707	4.12E-06
Col3a1	collagen, type III, alpha 1	0.443	-1.17462	1.99E-04
Col5a1	Collagen alpha-1(V) chain	0.373	-1.42275	3.09E-07
Col5a2	Collagen alpha-2(V) chain	0.468	-1.09542	8.96E-04
Comp	Cartilage oligomeric matrix protein	0.153	-2.7084	5.31E-16
Csrp1	Cysteine and glycine-rich protein 1	0.551	-0.85988	3.43E-02
Csrp2	Smooth muscle LIM protein	0.341	-1.55216	1.20E-08
Cyct	Cytochrome c, testis-specific	0.485	-1.04394	2.86E-02
Dcn	decorin	0.335	-1.57777	2.06E-07
Dpysl3	Dihydropyrimidinase-related protein 3	0.571	-0.80844	3.74E-02
Efemp1	EGF-containing fibulin-like extracellular matrix protein 1	0.526	-0.92687	9.72E-03
Eln	ELN	0.515	-0.95736	2.59E-02
Emilin1	EMILIN-1	0.493	-1.02034	3.79E-03
Ephx1	epoxide hydrolase 1	0.479	-1.0619	4.74E-03
Fbln1	Fibulin-1	0.326	-1.61706	8.12E-05
Fbln5	Fibulin-5	0.448	-1.15843	4.83E-04

Fbn1	Mutant fibrillin-1	0.537	-0.89701	1.35E-02
Fmod	Fibromodulin	0.294	-1.76611	1.40E-11
Gorasp2	Golgi reassembly-stacking protein 2	0.563	-0.82879	3.55E-02
Htra1	Serine protease HTRA1	0.311	-1.68501	2.17E-05
Lgals3	Galectin	0.243	-2.04097	2.33E-14
Lims2	LIM and senescent cell antigen-like-containing domain protein 2	0.417	-1.26188	1.49E-03
Ltbp2	Latent-transforming growth factor beta-binding protein 2	0.405	-1.30401	7.31E-06
Lum	Lumican	0.352	-1.50635	1.03E-06
Mfap4	Microfibril-associated glycoprotein 4	0.305	-1.71312	3.39E-11
Mgp	matrix Gla protein	0.354	-1.49818	7.65E-07
Myh7	Myosin-7	0.371	-1.43051	1.40E-06
Myl9	Myosin regulatory light polypeptide 9	0.465	-1.1047	3.81E-02
Nppa	Natriuretic peptides A	0.472	-1.08314	7.72E-04
Ogn	Mimecan	0.273	-1.87303	4.67E-13
Pdlim3	PDZ and LIM domain protein 3	0.479	-1.0619	8.56E-04
Postn	Periostin	0.361	-1.46993	5.96E-07
Prelp	prolargin	0.372	-1.42663	9.18E-07
Ptgis	prostacyclin synthase	0.553	-0.85465	2.86E-02
Scarb2	Lysosome membrane protein 2	0.55	-0.8625	2.13E-02
Serpinb1a	Leukocyte elastase inhibitor A	0.246	-2.02327	3.14E-13
Spcs3	Signal peptidase complex subunit 3	0.5	-1	2.82E-02
Sprr1a	Cornifin-A	0.321	-1.63935	6.48E-10
Strn4	Striatin-4	0.01	-6.64386	5.31E-16
Tagln	transgelin	0.556	-0.84684	2.47E-02
Thbs4	Thrombospondin-4	0.489	-1.03209	1.84E-03
Tnc	Tenascin	0.562	-0.83136	4.50E-02

Uchl1	Ubiquitin carboxyl-terminal hydrolase isozyme L1	0.482	-1.05289	3.85E-03
Vcan	Versican core protein	0.536	-0.8997	1.27E-02

Table 5.7: A list of significantly downregulated proteins in PMCA1^{cko} :TAC mice compared to PMCA1$^{F/F}$: TAC cohort. One-way ANOVA test was used for statistical analysis and p-value <0.05 was considered to be significant.

5.4.3.1 STRING and Reactome analyses

The gene names of significantly regulated proteins were inserted into the STRING database to identify protein-protein interactions (figure 5.12). Of the significantly regulated proteins, 33 had ≤ 1 interaction partner and 10 proteins such as collagen isoforms and periostin, had interaction ≥20 partners. A dense cluster of interactions was identified amongst the genes involved in the regulation of extracellular matrix. This particularly includes several isoforms of collagen and fibulin. Relatively smaller cluster of interactions were identified centred around myosin heavy chain and active isoforms. These protein-protein interactions leading to changes in the extracellular matrix are the likely explanation for exaggerated fibrosis noted two weeks after being subjected to haemodynamic stress by TAC.

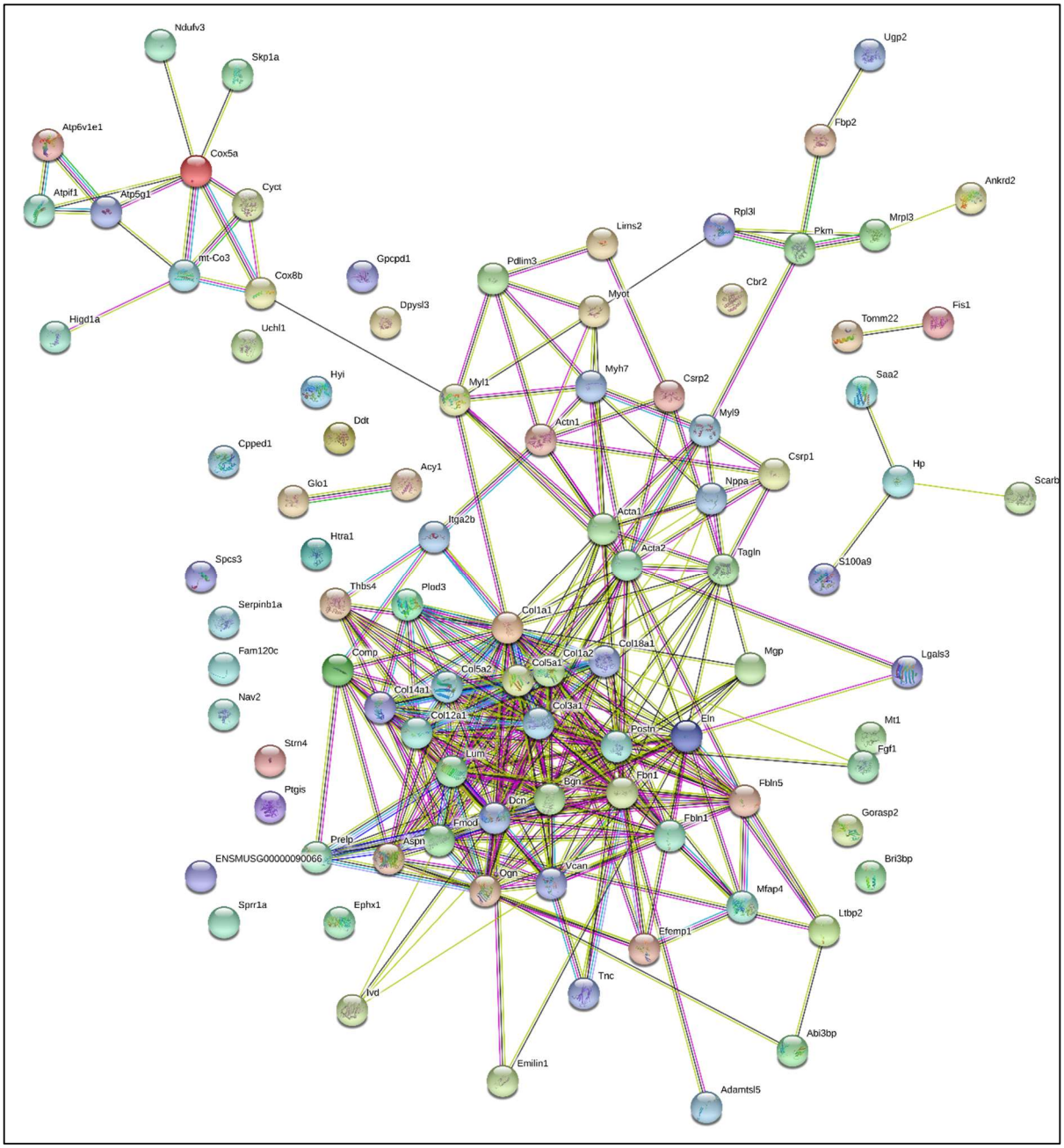

Figure 5.12: A schematic download from STRING database shows protein-protein interactions of significantly regulated proteins in PMCA1^{cko} : TAC compared to PMCA1$^{F/F}$: TAC mice. In this diagram, each sphere represents a protein and the straight line represent protein-protein interaction.

The gene names of significantly regulated proteins were then entered into the Reactome database in order to identify the cellular pathways involved in phenotype changes in PMCA1^{cko} TAC mice. Reactome identified these significantly related proteins to be involved

in over 400 pathways. Of these pathways, the most significantly enhanced pathways were related to the regulation of extracellular matrix and fibrosis. The Reactome pathways are shown in the figure 5.13; the centre of the cluster represents the top-tier pathway.

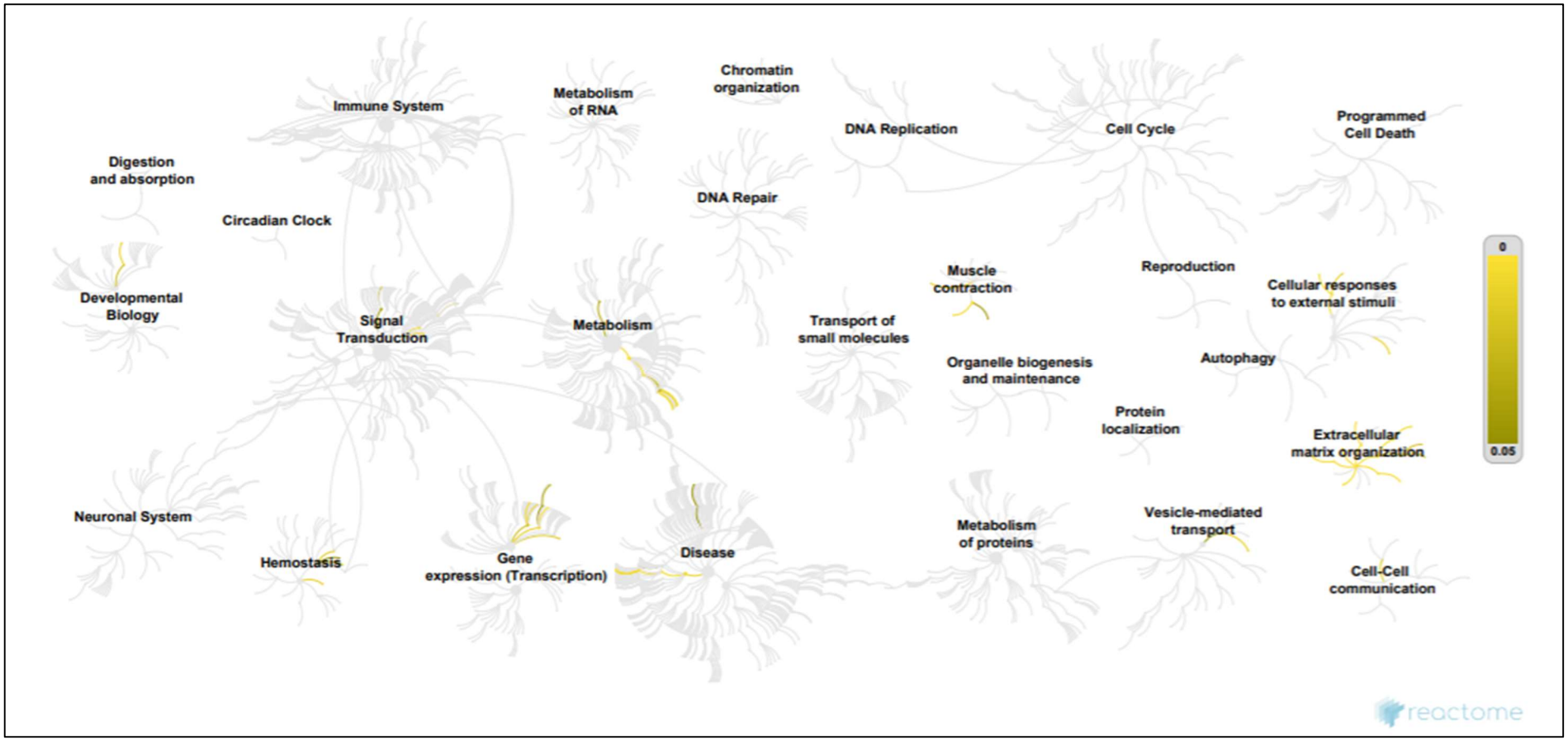

Figure 5.13: Reactome database schematic diagram of cellular pathways linking significantly regulated proteins in PMCA1^{cko} TAC mice compared to PMCA1$^{F/F}$: TAC cohort. These cellular pathways are organised as circular clusters in a hierarchy with the centre of each cluster representing the root of top-tier pathway. On moving away from the centre, each branch represents the next lower tier in the pathway hierarchy. For the significantly regulated proteins entered in the Reactome database, gold colour-coded pathways correspond to over-representation of that pathway and light grey colour-coded pathways are not significantly over-represented.

5.5 Discussion

Following the pressure overload exerted by TAC, both PMCA1^{cko} mice and PMCA1$^{F/F}$ mice developed myocardial hypertrophy, as described in the chapter 4. However, additionally, PMCA1^{cko} mice developed cardiac systolic dysfunction and signs of heart failure two weeks after the TAC procedure. As outlined earlier in this chapter, the main purpose of performing proteomic study was to explore and analyse significantly regulated proteins in the left ventricular tissue from PMCA1^{cko}: TAC mice and compare this to PMCA1^{cko}: sham mice, PMCA1$^{F/F}$: TAC and PMCA1$^{F/F}$: sham mice with a view to understand cellular mechanistic pathways that underpin this phenotype change. STRING and Reactome platforms were used to explore the protein-protein interactions and visualize significantly enhanced molecular pathways.

5.5.1 Cardiomyocyte specific deletion of PMCA1 (PMCA1^{cko}) results in upregulation of calmodulin and proteins involved in cardiac contraction

Firstly, LC/MS results from PMCA1^{cko} sham mice were compared with PMCA1$^{F/F}$ sham mice. Comparison between these two groups was carried out in order to understand whether a cardiomyocyte specific deletion of PMCA1 had any impact on the regulation of key proteins that play a part in the development and progression of heart failure. As described in chapter 4, no phenotype difference was noted between PMCA1^{cko}: sham and PMCA1$^{F/F}$: sham groups.

The proteomic results supported these finding and none of the proteins associated with cardiac hypertrophy and fibrosis such as natriuretic peptides and collagen isoforms were significantly regulated in PMCA1^{cko} mice compared to PMCA1$^{F/F}$ mice after the sham procedure. PMCA1 is abundant in cardiomyocytes and its deletion (as in PMCA1^{cko} mice) led to an upregulation of proteins associated with cardiac muscle contraction. These included Myh7, Acta1, Acta2 and Dmd. Proteomic results shows that calmodulin (CaM) isoforms (Calm1, Calm2, Calm3) were all significantly upregulated in PMCA1^{cko} sham group. Calmodulin is a principal Ca^{2+} sensor protein expressed in all eukaryotic cells and acts as a salient interaction partner for a number of proteins and ion channels including PMCA1 (Schuh, S, et al., 2003). Calmodulin can mediate the effect of Ca^{2+} on Ca^{2+} ion channels (Kasri et al., 2004). Upregulation of CaM in PMCA1^{cko} sham mice seems to be a compensatory mechanism secondary to the loss of PMCA1 protein in tis cohort. CaM also mediates the

functioning of other Ca^{2+} transport channels. It is possible that upregulation of CaM facilitates the Ca^{2+} exodus by NCX and SERCA to compensate the loss of PMCA1 under basal conditions.

In STRING analysis, calmodulin isoforms appeared to adopt a central position in the interaction clusters linking with various other proteins in the muscle contraction. Whilst, calmodulin's role in regulation of muscle contraction is well established (Walsh, 1994), its upregulation in $PMCA1^{cko}$ mice in the absence of pressure overload or any other physiological stress points towards the possibility of impairment of local calcium regulation following PMCA1 deletion in cardiomyocytes (Oceandy et al., 2011). It could also be hypothesized that upregulation of calmodulin and other proteins associated with muscle contraction in $PMCA1^{cko}$ mice may be compensatory mechanism aimed to minimize any possible detrimental effect of the deletion of PMCA1 on the cardiomyocytes.

As indicated above, myosin genes such as Myh1, 3 and 7, smooth muscle actin gene acta2, calmodulin and striatin 4 genes were identified through STRING analysis as the most active regulated proteins involved in protein-protein interactions. Myh7 was upregulated in in $PMCA1^{cko}$ sham mice. Myosin protein makes the contractile unit in myocytes along with actin and plays a very important role in muscle contraction. It should not come as surprise that mutations in Myh7 gene are linked with cardiac muscle disorders such as hypertrophic cardiomyopathy and dilated cardiomyopathy (Mattivi et al., 2020). Mutations in Myh7 gene are frequently seen in patients with hypertrophic cardiomyopathy (HCM) and are inherited in an autosomal dominant fashion (Velicki et al., 2020). HCM is associated with cardiac arrhythmias, syncope and sudden cardiac death (Maron, 2018). Dilated cardiomyopathy (DCM) is characterised by dilatation of the left ventricle (or both ventricles) along with systolic dysfunction in the absence of coronary artery disease or valvular heart disease and is an important cause of heart failure, particularly in the younger individuals (Pinto et al., 2016) . Mutations of Myh7 have also been reported in cases of familial DCM (de Frutos et al., 2022). Acta2 was also upregulated in $PMCA1^{cko}$ sham mice. Acta2 – smooth muscle actin helps to regulate blood vessels shape and elasticity. Mutations of actin genes have linked with cardiac dysfunction and heart failure (Velicki et al., 2020b). Calmodulin is coded by genes Calm1 – 3 and well known to be a key interaction partner and a major regulator of PMCA. $PMCA1^{cko}$:sham mice reveal a significantly upregulated expression of calmodulin when compared to the $PMCA1^{F/F}$: sham mice. It is conceivable that higher expression of calmodulin in $PMCA1^{cko}$: sham mice is a reflection of reduced clearance of cytosolic Ca^{2+}. Calmodulin, actin and myosin are known to be interaction partners and are closely linked to

Ca^{2+} signalling pathways and their mutations have been associated with the development of cardiomyopathy (Xu et al., 2018). Striatin is another important muscle protein that serves as an interaction partner with calmodulin. Interestingly, STRING analysis shows that in $PMCA1^{cko}$ sham mice, it fails to cross link with calmodulin, most likely due to an absence of PMCA1 which suggest that cardiac muscle function may be impaired due to the lack of PMCA1. This brief description of protein-protein interaction provides further evidence of PMCA1's involvement in salient cellular functions in cardiomyocytes and how the relative lack of PMCA1 (e.g in $PMCA1^{cko}$ sham mice) may adversely affect some of the key pathways leading to impairment of cardiac structure and function.

5.5.2 Two-week TAC induces upregulation of natriuretic peptides and collagen isoforms involved in myocardial hypertrophy and fibrosis in $PMCA1^{F/F}$ mice

As described in chapter 4, $PMCA1^{F/F}$ developed significant myocardial hypertrophy and fibrosis two weeks after TAC. The qPCR results also confirmed a significantly higher expression of ANP (nppa), BNP (nppb) and Collagen isoforms (col1α3 and col1α3) in $PMCA1^{F/F}$: TAC (please see figure 4.10 and 4.12). In line with these findings, the LC/ SM results also show a significant upregulation of natriuretic peptides (nppa) and collagen isoforms in $PMCA1^{F/F}$: TAC mice compared to the $PMCA1^{F/F}$: sham cohort. Additionally, there is also upregulation fibulin isoforms, fibronectin and matrix Gla protein in $PMCA1^{F/F}$ mice after two week TAC.

The pivotal role played by the extra cellular matrix (ECM) in cardiac homeostasis cannot be over emphasised. The ECM provides structural support, facilitates transmission of force, and offers a platform for signal transduction. Pressure overload induced by TAC is well known to stimulate cardiac hypertrophy both in animal models and human subjects, most of which is mediated by the expansion of extra cellular matrix (Frangogiannis, 2019). Enhancement of ECM organisation pathways in the $PMCA1^{F/F}$: TAC mice is in keeping with data emerging from other pressure overload studies where an increase in ECM was found in wild type mice (Russo et al., 2019).

Fibronectin (Fn1) is one of the significantly up-regulated protein in the comparison between $PMCA1^{F/F}$: TAC and $PMCA1^{F/F}$: sham groups. Subsequently, STRING analysis demonstrated this to be involved in a number of protein-protein interactions forming a cluster. Fibronectin is a glycoprotein in the ECM that is involved in interactions with cell surface integrins, collagen isoforms, fibrin, heparin, and actin. Enhanced expression of fibronectin has been

described in experimental models of ischemic heart disease and heart failure (Dawson et al., 2012). Fn1 is known to lead to cardiac hypertrophy which is mediated by NFTAT pathway (Konstandin et al., 2013). Fibulin 1 (Fbln 1) is another significantly upregulated protein when comparing PMCA1$^{F/F}$: TAC with PMCA1$^{F/F}$: sham mice.

Fbln1 is a calcium binding glycoprotein found in the extracellular matrix where it links with basement membranes and elastic fibres. Fibulin family of glycoproteins is known to be closely associated to the cardiovascular disease (Holmager et al., 2017). Fibulin 3 and 6 considered to play a key role in myocardial scar formation (Chowdhury et al., 2017) and Fibulin 1 is a known circulating biomarker of cardiac fibrosis (Holmager et al., 2017).

Upregulation of Fibulin1, fibronectin (fn1) and collagen isoforms in PMCA1$^{F/F}$: TAC mice on LC/MS supports the finding of increased levels of myocardial fibrosis in this cohort during histological examination and is in keeping with the evidence emerging from literature.

5.5.3 PMCA1^{cko} :TAC mice exhibit downregulation of proteins involved in cardiac fibrosis

Proteomic results from cardiac tissues from PMCA1^{cko}: TAC mice were compared with PMCA1$^{F/F}$: TAC mice. As described in chapter 4. whilst both these groups had undergone similar pressure overload exerted by the TAC procedure the PMCA1^{cko} mice exhibited an exacerbated response to the pressure overload and developed decompensated heart failure with dilated left ventricle, systolic dysfunction and pulmonary oedema. The histological analysis showed that tissue sections from PMCA1^{cko} TAC mice had exaggerated myocardial fibrosis compared to the PMCA1$^{F/F}$: TAC group. However, unexpectedly the LC/MS data revealed that various isoforms of collagen such as Col1, Col3, Col5 and Col8 were downregulated in PMCA1^{cko} mice following TAC when compared to the PMCA1$^{F/F}$: TAC mice. This implied a higher degree of fibrosis in the PMCA1$^{F/F}$:TAC group, in contradiction to the histological findings. In addition to this, Fibulin and Fibrillin isoforms were also upregulated in the PMCA1$^{F/F}$: TAC mice. Interestingly however, serum amyloid protein A, which is an independent predictor of cardiovascular disease in humans (Johnson et al., 2004) , was found to be significantly upregulated in PMCA1^{cko} mice after TAC. The finding of upregulation of proteins involved in cardiac fibrosis after TAC is well established in the literature (Ying et al., 2009) and this study also confirms this. However, significant upregulation of the mediators of cardiac fibrosis in PMCA1$^{F/F}$: TAC mice compared to the PMCA1^{cko} : sham mice was surprising considering the phenotype and histology findings and this should be further

explored. Myocardial fibrosis in heart failure tends to occur in a patchy distribution interspaced by areas of no fibrosis (Hinderer & Schenke-Layland, 2019b). For this study, tissue sections for histology were taken from the basal segments of the left ventricle whereas LV apical tissue was taken for LC/ MS analysis. It is plausible that cardiac fibrosis in PMCA1^{cko} :TAC mice is also patchy in distribution mainly affecting the basal segments of the LV with relative sparing of the apex, hence the discrepancy between histology and LC/MS data. Quantification of collagen isoforms (col1α1 and col1α3) by undertaking western blotting or LC/MS on cardiac homogenized cardiac tissue samples from PMCA1^{cko} after two weeks TAC may be a useful way forward to further investigate this.

The STRING database analysis showed that collagen isoform and other extracellular matrix proteins were highly regulated and were involved in the most protein-protein interactions. Several collagen isoforms have been identified; however, it is the isoform I and III, and proteoglycans that constitute the most of ECM and provide is with tensile strength and endurance, respectively. Many collagen isoforms such as collagens 1, 3, 5 and 8 were found to be significantly downregulated in PMCA1^{cko} mice two weeks after TAC, suggesting higher expression in WT TAC mice. This contradicts, the results from histological analysis described in the previous chapter where a higher degree of fibrosis was noted in sections from PMCA1^{cko} TAC group. Further work would be needed to revisit this subject and undertake further work to clarify this discrepancy. The other important proteins that contribute to the structure and function of ECM in cardiac tissues include elastin, laminin, fibrillin and fibronectin. Pathways involved in the organisation of ECM, degradation of ECM, elastic fibre formation and cell surface interaction were found to be significantly enhanced in the Reactome analysis in PMCA1^{cko} mice two weeks after TAC. Dysregulation of the proteins in maintenance of ECM may lead to cardiac fibrosis, which is a known risk factor for cardiac arrhythmias and heart failure (Liu et al., 2017). Other highly regulated proteins in PMCA1^{cko} TAC mice include Integrin and Syndecan. Integrin is known to have a number of protein-protein interactions within the ECM resulting involving signalling molecules which subsequently input into MAPK and JEK pathways (Yee , Weaver and Hammer , 2008) . On the other hand, Syndecan is considered to a marker of cardiac fibrosis, heart failure and cardiac death (Takahashi *et al.*, 2011). Lumican is another upregulated protein in PMCA1^{cko} mice after TAC. Increased expression of Lumican has been described in experimental and clinical heart failure (Frangogiannis, 2019). In PMCA1^{cko} TAC mice, enhancement of the pathways involved in ECM regulation and fibrosis offer further supportive evidence that lack

of PMCA1 predisposes mice to heart failure after pressure overload compared to $PMCA1^{F/F}$: TAC mice.

Previous work from our lab showed that deletion of PMCA4 in cardiac fibroblasts reduced the hypertrophic response to pressure overload which was mediated by a downregulation of Wnt signaling pathway (Mohamed et al., 2016). In line with this, it was hypothesized that the development heart failure secondary to pressure overload in $PMCA1^{cko}$ mice after TAC was mediated by the Wnt pathway. Wnt pathways is known to play a pivotal role in myocardial hypertrophy and remodeling (Bergmann, 2010). The Wnt pathway can be subdivided in Wnt/ β-catenin and Wnt/ Ca^{2+} signaling and its mediators include β-catenin, tyrosine-protein kinase like -7, Tyrosine-protein kinase receptor ROR2, Disheveled protein, Glycogen synthase kinase-3β and Rho-associated kinase (MacDonald et al., 2009). The proteomic analysis identified the presence of β-catenin and glycogen synthase kinase-3β in myocardial tissue samples; however, none of these components were significantly regulated in $PMCA1^{cko}$ TAC mice. This implies that the development of heart failure in this cohort is unlikely to be mediated by the Wnt pathway.

Work by our group in the past has also demonstrated that PMCA1 is required to maintain cellular Ca^{2+} homeostasis and electrical stability under basal as well as stress conditions. $PMCA1^{cko}$ hearts were found to be at a higher risk of atrial and ventricular arrhythmias compared to the WT mice (Wang et al., 2017; Wilson, 2017). There is a higher risk of cardiac arrhythmias in general and atrial arrhythmias in particular in patients with heart failure (Mulder et al., 2021). Conversely, uncontrolled cardiac arrhythmias can also lead to heart failure (Kotecha & Piccini, 2015). In the LC/MS data analysed in this study, none of cardinal proteins implicated in triggering and perpetuation of cardiac arrhythmias were significantly regulated in $PMCA1^{cko}$ TAC mice. However, it is important to appreciate that the majority of ion channels involved in cardiac arrhythmias are membrane bound and their close association with lipids makes it difficult to isolate and solubilize them in buffers and detergents before carrying out mass spectrometry. This is one of the key reasons which makes standard mass spectrometry less robust for analysing the expression of membrane bound ion channels (Mirza et al., 2007).

Whilst the current study identified a number of relevant protein-protein interactions in $PMCA1^{cko}$ mice following TAC which may be involved in the development of left ventricular hypertrophy and heart failure, the exact mechanism by which deletion of PMCA1 in cardiomyocytes puts them at a higher risk of developing heart failure still remains to be

determined. Understanding the mechanistic pathway in PMCA1^{cko} mice leading to heart failure is extremely important and may pave a way to find clinical interventions to halt the development and progression of heart failure.

5.6 Future work

As outlined above, the laboratory experiments and sample preparation for this study was carried out by the author, the LC/MS data analysis was carried out jointly with Miss Rabia Gangarekar (Masters student). For analysis of the data, MS excel, STRING and Reactome online databases were used. However, there are a number of other databases which are used for proteomic analysis such as Comet, EasyPROT and IPA (Ingenuity Pathway Analysis) which were not used due to strict time frame of the study. Future work should include a further exploration on this MS/LC data by using other gene databases such as Comet, EasyPROT and IPA (Ingenuity Pathway Analysis) to get new insights into molecular mechanism through which cardiomyocyte specific deletion of PMCA1 leads to the development of heart failure in pressure overload settings. Confirmation of significantly regulated proteins involved in the myocardial hypertrophy pathways with traditional laboratory methods like western blotting should also be considered.

Lastly, as highlighted above, whilst mass spectrometry is a robust tool for identification and analysis of cellular cytosolic proteins, it is less reliable in isolating and identifying membrane bound channel proteins which was a key interest in our study. Over the last decade, there have been some advancements in one our understanding of challenges in isolation, enrichment and identification of membrane bound proteins in large scale proteomics (Griffin & Schnitzer, 2011). Newer enrichment techniques employed in LC/MS involving ultracentrifugation followed by treatment with urea or alkaline solution have been claimed to quantify twice as many transmembrane proteins compared to the standard proteomics methods (Kongpracha et al., 2022) and should be considered in future work on PMCA1^{cko} TAC models.

The current study found higher level of fibrosis in PMCA1^{cko} mice after two weeks TAC. As the previous work from our group has shown that PMCA4 associated cardiac hypertrophy is mediated by fibroblast based cellular signalling (Mohamed et al., 2016); the future work to explore PMCA1's role in cardiac fibrosis would involve creation of a cardiac fibroblast specific PMCA1 knock out model to evaluate mechanistic pathways. Caloxin 1b3 is a selective PMCA1

inhibitor (Szewczyk et al., 2010) ; a TAC experiment using a caloxin 1b3 would offer further insights into PMCA1's role in cardiac fibrosis and heart failure.

Chapter 6 - General discussion

Cardiovascular diseases remain a leading cause of mortality and morbidity worldwide (Mensah et al., 2019), with hypertension remaining one of the major cardiovascular risk factors leading to pathological cardiac hypertrophy and eventually, heart failure (Kokubo & Iwashima, 2015). Heart failure continues to carry poor outcomes despite the introduction of guidelines directed pharmacological therapies (Taylor et al., 2019b). The current treatment strategies for heart failure mainly aim to tackle renin-angiotensin system and sympathetic overactivation and do not address myocardial hypertrophy that precedes the decompensated heart failure (Tham et al., 2015).

Calcium, as a second messenger, has a well-established role in cardiovascular health and disease. Calcium homeostasis is delicately maintained by a tight regulation of Ca^{2+} influx and exodus in cardiomyocytes and vascular cells (Siri-angkul et al., 2021). Voltage gated calcium influx channels have long been a target for pharmacological therapy for cardiovascular diseases such as hypertension, angina and cardiac arrhythmias (Godfraind, 2014). In a bid to identify and develop further pharmacological targets, substantial research is being carried out to study the role of Ca^{2+} exodus proteins in the cardiovascular system. Plasma membrane calcium ATPase (PMCA) is a calcium exodus protein that plays a major role in the Ca^{2+} extrusion from non- excitable cells (Schatzmann, 1966). Multiple large scale genome wide association studies have shown that the mutations in Atp2b1 – the gene coding for PMCA1 - are associated with hypertension (Cho et al., 2009; Fontana et al. 2009). At a functional level, previous work from our lab has shown that twelve month old mice with a reduced expression of PMCA1 develop high blood pressure compared to their age-matched controls (Little et al., 2017). Our group has also demonstrated that mice with reduced expression of PMCA1 develop electric abnormalities and are at a higher risk of developing cardiac arrhythmias (Wang et al., 2017; Wilson, 2017). In the light of this research, it was hypothesised that reduced levels of PMCA1 would have a detrimental impact on the cardiac remodelling in a pressure overload mouse model. To determine whether reduced levels of PMCA1 predispose mice to heart failure and to characterise cardiovascular remodelling as a result of pathophysiological stress two mutant mouse lines (heterozygous global deletion of PMCA1 - $PMCA1^{HT}$ and cardiomyocyte specific deletion of PMCA1- $PMCA1^{cko}$) were studied.

6.1 Cardiomyocyte specific deletion of PMCA1 leads to dilatation of the left ventricle with systolic dysfunction after 2 weeks TAC

Previous work by colleagues from our lab has shown that cardiomyocyte specific deletion of PMCA1 has no impact on cardiac structure and function under basal conditions, although these mice do have heart rhythm abnormalities related to ventricular repolarisation (Wilson, 2017). This PhD project has demonstrated that when these PMCA1^{cko} mice are subjected to increased pressure overload exerted by two week TAC that they develop dilated cardiomyopathy with systolic dysfunction and pulmonary oedema compared to the aged matched controls which remain in compensated hypertrophy.

During pressure overload experiments, it is most commonly reported that wild type mice remain in compensated myocardial hypertrophy until four weeks after TAC and it is only after four to six weeks when systolic dysfunction and decompensated heart failure develops (Chen et al., 2012). In fact, some reports have demonstrated preserved left ventricular function even after eight weeks TAC (Garcia-Menendez et al., 2013; Zi et al., 2019b). With this background data, the finding of poor left ventricular systolic function with dilatation of the left ventricle and thinning of the ventricular wall in PMCA1^{cko} mice suggests that PMCA1 is required to help cardiomyocytes deal with haemodynamic stress created by pressure overload. Hence, cardiomyocyte specific deletion of PMCA1 leads to poor tolerance of pressure overload with a resultant dilated cardiomyopathy, heart failure and pulmonary oedema. As previously mentioned, reduced PMCA1 levels are associated with hypertension and a higher risk of cardiac arrhythmia; the results of the current study further add to the body of evidence that suggests a protective role for PMCA1 in the cardiovascular system. It also further enhances the argument that PMCA1 may be a key player in the regulation of cardiac adaptations to stressful stimuli and may therefore have the potential to act as a therapeutic target in prevention of heart failure. However, the mice with simultaneous cardiomyocyte specific deletion of PMCA1 and 4 (PMCA1:4^{dcko}) displayed a preserved cardiac function after TAC (Stafford, 2013). PMCA4's role in cardiac hypertrophy was confirmed by our group by demonstrating that deletion of PMCA4 in cardiac fibroblasts led to an attenuation of Wnt signal pathway resulting in inhibition of hypertrophy in cardiac myocytes (Mohamed *et al.*, 2016).

6.2 Global heterozygous deletion of PMCA1 does not affect the development of myocardial hypertrophy due to pressure overload

This study showed that global heterozygous deletion of PMCA1 had no impact on the cardiac structure and function at basal levels. $PMCA1^{HT}$ mice developed concentric myocardial hypertrophy with significantly thicker interventricular septum and posterior wall, compared to their wild type control mice which developed eccentric myocardial hypertrophy after five weeks TAC. In addition, WT:TAC mice showed a significantly lower LV fractional shortening compared to the $PMCA1^{HT}$:TAC mice. As described in the previous chapters, heart failure leads to the sympathetic nervous system stimulation leading to tachycardia and subsequently hypo-perfusion of kidneys results in the activation of renin angiotensin aldosterone (Kemp & Conte, 2012). This goes on to demonstrate that multiple organs are involved and affected the development of the heart failure phenotype. Global heterozygous deletion of PMCA1 is characterised by reduction of PMCA1 levels not only in heart but also other organs including liver, kidneys, vascular smooth muscles and brain (Little et al., 2017). Whether the reduction of PMCA1 levels in $PMCA1^{HT}$ mice in the extra cardiac organs offers any protection to heart from the effects of pressure overload in the TAC model has not been explored before. Previous work by colleagues from our lab on the $PMCA1^{HT}$ mouse model did not note any gross abnormality in the structure of extra cardiac organs such as liver and kidneys. Whilst, previous work by our group has shown that $PMCA1^{HT}$ mice have a susceptibility to the development of hypertension with ageing (Little et al., 2017), in the present study no significant difference was found in the blood pressure of WT and $PMCA1^{HT}$, which were 8 weeks of age when the pressure overload was induced for a period of 5 weeks This study also showed that global heterozygous deletion of PMCA1 does not alter the expression of other Ca^{2+} exodus channels in the heart.

The difference in the cardiac phenotype in between $PMCA1^{cko}$ and $PMCA1^{HT}$ mice after TAC is interesting. As highlighted in chapter 4, cardiomyocyte specific knockout of PMCA1 ($PMCA1^{cko}$) leads to an approximately two thirds lower expression of PMCA1 in cardiomyocytes and PMCA1 expression in other cardiac cells such as fibroblasts is expected to remain unchanged. In the global heterozygous deletion of PMCA1 ($PMCA1^{HT}$ mouse model), PMCA1 expression is approximately halved in the cardiac tissue (includes all cardiac cells including cardiomyocytes and fibroblasts). An effective cross- talk between cardiomyocytes and cardiac fibroblasts is essential for coordinated electromechanical function of the heart (Rother et al., 2015). In fact, cardiomyocytes depend upon the

fibroblasts for their viability and calcium handling (Cartledge et al., 2015). Previous published work from our lab shows that cardiac fibroblasts lacking in PMCA4 inhibited the myocardial hypertrophic response by producing higher levels of secreted frizzled related protein 2 (sFRP-2) (Mohamed *et al.*, 2016). It is possible that the difference in cardiac phenotype seen between PMCA1^{cko} and PMCA1^{HT} mouse models in the current study is due to the key difference in PMCA1 expression in cardiac fibroblasts in these models.

6.3 Investigation into the mechanism of the development of dilated cardiomyopathy in PMCA1^{cko} mice

In order to explore and understand the mechanistic cellular pathways underpinning the development of heart failure phenotype in PMCA1^{cko} mice two weeks after, expression Ca^{2+} exodus genes was assessed by using real time quantitative PCR (qRT-PCR), as described in chapter 4. There was no significant difference in the expression of key Ca^{2+} handing genes involved in cardiac excitation-contraction coupling such as NCX, RyR and SERCA2. In particular, the data showed no compensatory increase in the expression of PMCA4 in PMCA1^{cko} mice after TAC or the sham procedures. The unchanged expression of these Ca^{2+} exodus genes goes on suggest that dilated cardiomyopathy in PMCA1^{cko} mice has developed due to a reduced expression of PMCA1.

For further investigation into the mechanism of development of dilated cardiomyopathy in PMCA1^{cko} mice, significantly regulated proteins in both experimental groups were explored by using liquid chromatography mass spectrometry (LC/MS) was performed. Proteomics results showed significant regulation of proteins involved in cardiac hypertrophy and fibrosis such as natriuretic peptides and collagen isoforms in PMCA1^{cko} mice compared to the controls. PMCA1 deletion also resulted in upregulation of proteins associated with cardiac muscle contraction. It also revealed calmodulin isoforms (Calm1, Calm2, Calm3) were all significantly upregulated in PMCA1^{cko} mice.

As previous work from our lab has shown that the deletion of PMCA4 in cardiac fibroblasts led to a reduced hypertrophic response to pressure overload mediated by a downregulation of Wnt signaling pathway (Mohamed et al., 2016). Wnt pathways has a well-established role in cardiac hypertrophy and remodeling (Bergmann, 2010). In fact, the proteomic analysis identified the presence of β-catenin and glycogen synthase kinase-3β in myocardial tissue

samples; but none of the Wnt pathway components were significantly regulated in PMCA1^{cko} TAC mice. This suggests that the Wnt pathway is unlikely to be involved in the development of dilated cardiomyopathy in mice after the deletion of PMCA1. Further work would be required to investigate cellular pathways involved in the development of heart failure in PMCA1^{cko} mice after pressure overload as this may help to shape future treatments to halt the development and progression of heart failure.

6.4 Impact of the research

The purpose of the project was to determine the role of PMCA1 in heart failure to determine whether it has the potential to be a target for therapeutic treatment of heart failure. The data generated from this piece of research suggests a new major role of the plasma membrane calcium pump (PMCA1) in the development of heart failure in a haemodynamic stress model. As a result, we have gained new insights into the development of heart failure in mice with reduced levels of PMCA1. Whilst PMCA1 mutant mice were known to be susceptible to developing high blood pressure with ageing (Little et al., 2017), it is the first time that the protective role of PMCA1 in the pressure overload model has emerged. This project has therefore provided an essential link between basic scientific research and future medical treatment. Despite recent therapeutic advancements, heart failure continues to be associated with considerable morbidity and mortality hence there is a pressing need to develop newer pharmacological targets to improve clinical outcomes. Being an ATPase and a membrane protein, PMCA1 offers a promising and attractive avenue to develop efficient and selective drugs to target the ion transport and cellular signalling pathways. With its protective role in the cardiovascular system emerging from this study, PMCA1 may harbour the potential to serve as a cornerstone for future pharmacological therapies in heart failure.

6.5 Future work

This research project shows for the first time that cardiomyocyte specific deletion of PMCA1 in mice increases their likelihood of development of heart failure after pressure overload. For now, the key cellular signalling pathways leading to this phenotype change remain unidentified. Although the LC/MS data analysis has shed some light on the significantly regulated proteins in PMCA1^{cko} mice, it is too early to offer a precise mechanistic explanation for the development of heart failure after cardiomyocyte specific deletion of PMCA1. Future

work utilising newer enrichment techniques and refined LC/MS which is claimed to be superior to the standard proteomics methods (Kongpracha et al., 2022), would help accurate identification and quantification PMCA1's cellular interaction partners accountable for the development of heart failure phenotype in this study.

It is well established that global deletion of PMCA1 is associated with embryonic lethality. In the current study decompensated heart failure along with exaggerated levels of myocardial fibrosis in $PMCA1^{cko}$ mice after two weeks TAC whereas $PMCA1^{HT}$ mice developed concentric left ventricular hypertrophy after five weeks TAC. It is now essential to see whether these changes in the cardiac phenotype are mediated by a particular cell type in the heart. Previous work from our group has shown that PMCA4 associated cardiac hypertrophy is mediated by fibroblast based cellular signalling (Mohamed et al., 2016). Future research to explore PMCA1's role in cardiac failure and fibrosis would involve the generation of a cardiac fibroblast specific PMCA1 knock out model and utilising it in a pressure overload setting to evaluate mechanistic pathways.

A selective inhibitor for PMCA1 named Caloxin 1b3 has been described in the literature (Szewczyk et al., 2010) ; designing TAC experiments using caloxin 1b3 would serve as a future platform to see if pharmacological inhibition of PMCA1 also produces decompensated in a pressure overload setting similar to the cardiomyocyte specific knockout in the current study. This will allow us to gain new insights into PMCA1's role in cardiac fibrosis and heart failure, and to further explore its potential as a therapeutic target in heart failure.

Obviously, the ultimate aim of this research project is to explore the development of newer treatment targets in order to improve the clinical care and outcome of the patients with heart failure. The transition from bench to the bedside also requires draggability of a potential therapeutic target. The data from this research project suggests that a cardiomyocyte specific knockout of PMCA1 is determinantal to the heart and as a result, $PMCA1^{cko}$ mice develop dilated cardiomyopathy with systolic dysfunction and pulmonary oedema in a pressure overload setting. From these results, we may be able to conclude if reduce PMCA1 levels in the heart increase the risk of heart failure; elevated PMCA1 levels may be beneficial. To date, there is no pharmacological PMCA1 activator, however a plausible avenue for the future research is to explore whether an overexpression of PMCA1 plays a protective role in a murine TAC model preventing decompensated heart failure. If successful, this may open avenues to develop PMCA1 overexpression as a therapeutic modality in the clinical management of heart failure.

References

Agah, R., Frenkel, P. A., French, B. A., Michael, L. H., Overbeek, P. A., & Schneider, M. D. (1997). Gene recombination in postmitotic cells: Targeted expression of Cre recombinase provokes cardiac-restricted, site-specific rearrangement in adult ventricular muscle in vivo. *Journal of Clinical Investigation*, *100*(1), 169–179. https://doi.org/10.1172/JCI119509

Akhtar, M., & Elliott, P. (2018). The genetics of hypertrophic cardiomyopathy. *Global Cardiology Science and Practice*, *2018*(3). https://doi.org/10.21542/gcsp.2018.36

Amgalan, D., & Kitsis, R. N. (2019). A mouse model for the most common form of heart failure. *Nature*, *568*(7752), 324–325. https://doi.org/10.1038/d41586-019-00983-4

Andino, L. M., Takeda, M., Kasahara, H., Jakymiw, A., Byrne, B. J., & Lewin, A. S. (2008). AAV-mediated knockdown of phospholamban leads to improved contractility and calcium handling in cardiomyocytes. *The Journal of Gene Medicine*, *10*(2), 132–142. https://doi.org/10.1002/jgm.1131

Armesilla, A. L., Williams, J. C., Buch, M. H., Pickard, A., Emerson, M., Cartwright, E. J., Oceandy, D., Vos, M. D., Gillies, S., Clark, G. J., & Neyses, L. (2004). Novel Functional Interaction between the Plasma Membrane Ca $^{2+}$ Pump 4b and the Proapoptotic Tumor Suppressor Ras-associated Factor 1 (RASSF1). *Journal of Biological Chemistry*, *279*(30), 31318–31328. https://doi.org/10.1074/jbc.M307557200

Barrick, C. J., Rojas, M., Schoonhoven, R., Smyth, S. S., & Threadgill, D. W. (2007). Cardiac response to pressure overload in 129S1/SvImJ and C57BL/6J mice: Temporal- and background-dependent development of concentric left ventricular hypertrophy. *American Journal of Physiology - Heart and Circulatory Physiology*, *292*(5). https://doi.org/10.1152/ajpheart.00816.2006

Bassani, J. W., Bassani, R. A., & Bers, D. M. (1994). Relaxation in rabbit and rat cardiac cells: species-dependent differences in cellular mechanisms. *The Journal of Physiology*, *476*(2), 279–293. https://doi.org/10.1113/jphysiol.1994.sp020130

Beard, N. A., Casarotto, M. G., Wei, L., Varsányi, M., Laver, D. R., & Dulhunty, A. F. (2005). Regulation of Ryanodine Receptors by Calsequestrin: Effect of High Luminal Ca2+ and Phosphorylation. *Biophysical Journal*, *88*(5), 3444. https://doi.org/10.1529/BIOPHYSJ.104.051441

Bedu-Addo, G., Meese, S., & Mockenhaupt, F. P. (2013). An ATP2B4 Polymorphism Protects Against Malaria in Pregnancy. *The Journal of Infectious Diseases*, *207*(10), 1600–1603. https://doi.org/10.1093/infdis/jit070

Bergmann, M. W. (2010). WNT Signaling in Adult Cardiac Hypertrophy and Remodeling. *Circulation Research*, *107*(10), 1198–1208. https://doi.org/10.1161/CIRCRESAHA.110.223768

Bers, D. M. (1997). Ca transport during contraction and relaxation in mammalian ventricular muscle. *Basic Research in Cardiology*, *92*(S1), 1–10. https://doi.org/10.1007/BF00794062

Bers, D. M. (2001). Excitation-Contraction Coupling. In *Excitation-Contraction Coupling and Cardiac Contractile Force*. https://doi.org/10.1007/978-94-010-0658-3_8

Bers, D. M. (2002). Cardiac excitation–contraction coupling. *Nature*, *415*(6868), 198–205.

https://doi.org/10.1038/415198a

Bers, D. M. (2006). Altered Cardiac Myocyte Ca Regulation In Heart Failure. *Physiology*, *21*(6), 380–387. https://doi.org/10.1152/physiol.00019.2006

Bers, D. M., Bassani, J. W., & Bassani, R. A. (1993). Competition and redistribution among calcium transport systems in rabbit cardiac myocytes. *Cardiovascular Research*, *27*(10), 1772–1777. http://www.ncbi.nlm.nih.gov/pubmed/8275522

Beuschlein, F., Boulkroun, S., Osswald, A., Wieland, T., Nielsen, H. N., Lichtenauer, U. D., Penton, D., Schack, V. R., Amar, L., Fischer, E., Walther, A., Tauber, P., Schwarzmayr, T., Diener, S., Graf, E., Allolio, B., Samson-Couterie, B., Benecke, A., Quinkler, M., … Reincke, M. (2013). Somatic mutations in ATP1A1 and ATP2B3 lead to aldosterone-producing adenomas and secondary hypertension. *Nature Genetics*, *45*(4), 440–444. https://doi.org/10.1038/ng.2550

Bluhm, W. F., Kranias, E. G., Dillmann, W. H., & Meyer, M. (2000). Phospholamban: a major determinant of the cardiac force-frequency relationship. *American Journal of Physiology-Heart and Circulatory Physiology*, *278*(1), H249–H255. https://doi.org/10.1152/ajpheart.2000.278.1.H249

Boczek, T., Lisek, M., Ferenc, B., & Zylinska, L. (2017). Cross talk among PMCA, calcineurin and NFAT transcription factors in control of calmodulin gene expression in differentiating PC12 cells. *Biochimica et Biophysica Acta - Gene Regulatory Mechanisms*, *1860*(4), 502–515. https://doi.org/10.1016/j.bbagrm.2017.01.012

Boczek, T., Radzik, T., Ferenc, B., & Zylinska, L. (2019). The Puzzling Role of Neuron-Specific PMCA Isoforms in the Aging Process. *International Journal of Molecular Sciences*, *20*(24). https://doi.org/10.3390/IJMS20246338

Boczek, T., Sobolczyk, M., Mackiewicz, J., Lisek, M., Ferenc, B., Guo, F., & Zylinska, L. (2021). Crosstalk among Calcium ATPases: PMCA, SERCA and SPCA in Mental Diseases. *International Journal of Molecular Sciences 2021, Vol. 22, Page 2785*, *22*(6), 2785. https://doi.org/10.3390/IJMS22062785

Bögeholz, N., Pauls, P., Bauer, B. K., Schulte, J. S., Dechering, D. G., Frommeyer, G., Kirchhefer, U., Goldhaber, J. I., Müller, F. U., Eckardt, L., & Pott, C. (2015). Suppression of Early and Late Afterdepolarizations by Heterozygous Knockout of the Na+/Ca2+ Exchanger in a Murine Model. *Circulation. Arrhythmia and Electrophysiology*, *8*(5), 1210–1218. https://doi.org/10.1161/CIRCEP.115.002927

Boluyt, M. O., O'Neill, L., Meredith, A. L., Bing, O. H., Brooks, W. W., Conrad, C. H., Crow, M. T., & Lakatta, E. G. (1994). Alterations in cardiac gene expression during the transition from stable hypertrophy to heart failure. Marked upregulation of genes encoding extracellular matrix components. *Circulation Research*, *75*(1), 23–32. http://www.ncbi.nlm.nih.gov/pubmed/8013079

Borlak, J., & Thum, T. (2003). Hallmarks of ion channel gene expression in end-stage heart failure. *The FASEB Journal*, *17*(12), 1592–1608. https://doi.org/10.1096/fj.02-0889com

Bosch, L., de Haan, J. J., Bastemeijer, M., van der Burg, J., van der Worp, E., Wesseling, M., Viola, M., Odille, C., el Azzouzi, H., Pasterkamp, G., Sluijter, J. P. G., Wever, K. E., & de Jager, S. C. A. (2021). The transverse aortic constriction heart failure animal model: a systematic review and meta-analysis. *Heart Failure Reviews*, *26*(6), 1515–1524. https://doi.org/10.1007/S10741-020-09960-W/FIGURES/7

Brancaccio, M., Fratta, L., Notte, A., Hirsch, E., Poulet, R., Guazzone, S., De Acetis, M., Vecchione, C., Marino, G., Altruda, F., Silengo, L., Tarone, G., & Lembo, G. (2003). Melusin, a muscle-specific integrin β1–interacting protein, is required to prevent cardiac failure in response to chronic pressure overload. *Nature Medicine*, *9*(1), 68–75. https://doi.org/10.1038/nm805

Breckenridge, R. (2010). Heart failure and mouse models. In *DMM Disease Models and Mechanisms* (Vol. 3, Issues 3–4, pp. 138–143). Dis Model Mech. https://doi.org/10.1242/dmm.005017

Brini, M., & Carafoli, E. (2009). Calcium Pumps in Health and Disease. *Physiological Reviews*, *89*(4), 1341–1378. https://doi.org/10.1152/physrev.00032.2008

Bruce, J. I. E. (2018). Metabolic regulation of the PMCA: Role in cell death and survival. *Cell Calcium*, *69*, 28–36. https://doi.org/10.1016/J.CECA.2017.06.001

Buford, T. W. (2016). Hypertension and aging. *Ageing Research Reviews*, *26*, 96–111. https://doi.org/10.1016/J.ARR.2016.01.007

Bui, A. L., Horwich, T. B., & Fonarow, G. C. (2011). Epidemiology and risk profile of heart failure. *Nature Reviews. Cardiology*, *8*(1), 30–41. https://doi.org/10.1038/nrcardio.2010.165

Calì, T., Lopreiato, R., Shimony, J., Vineyard, M., Frizzarin, M., Zanni, G., Zanotti, G., Brini, M., Shinawi, M., & Carafoli, E. (2015). A Novel Mutation in Isoform 3 of the Plasma Membrane Ca $^{2+}$ Pump Impairs Cellular Ca $^{2+}$ Homeostasis in a Patient with Cerebellar Ataxia and Laminin Subunit 1α Mutations. *Journal of Biological Chemistry*, *290*(26), 16132–16141. https://doi.org/10.1074/jbc.M115.656496

Camacho, P., Fan, H., Liu, Z., & He, J. Q. (2016). Small mammalian animal models of heart disease. In *American Journal of Cardiovascular Disease* (Vol. 6, Issue 3, pp. 70–80). E-Century Publishing Corporation. www.AJCD.us/

Campuzano, Ó., Sarquella-Brugada, G., Brugada, R., Brugada, P., & Brugada, J. (2009). The Genetic Basis of Malignant Arrhythmias and Cardiomyopathies. *Revista Española de Cardiología (English Edition)*, *62*(4), 422–436. https://doi.org/10.1016/S1885-5857(09)71669-X

Carayol, J., Sacco, R., Tores, F., Rousseau, F., Lewin, P., Hager, J., & Persico, A. M. (2011). Converging Evidence for an Association of ATP2B2 Allelic Variants with Autism in Male Subjects. *Biological Psychiatry*, *70*(9), 880–887. https://doi.org/10.1016/j.biopsych.2011.05.020

Carpinelli, M. R., Manning, M. G., Kile, B. T., Rachel, A. B., & Rachel, A. B. (2013). Two ENU-Induced Alleles of Atp2b2 Cause Deafness in Mice. *PLoS ONE*, *8*(6), e67479. https://doi.org/10.1371/journal.pone.0067479

Cartledge, J. E., Kane, C., Dias, P., Tesfom, M., Clarke, L., Mckee, B., Al Ayoubi, S., Chester, A., Yacoub, M. H., Camelliti, P., & Terracciano, C. M. (2015). Functional crosstalk between cardiac fibroblasts and adult cardiomyocytes by soluble mediators. *Cardiovascular Research*, *105*(3), 260–270. https://doi.org/10.1093/CVR/CVU264

Chaggar, P. S., Malkin, C. J., Shaw, S. M., Williams, S. G., & Channer, K. S. (2009). Neuroendocrine Effects on the Heart and Targets for Therapeutic Manipulation in Heart Failure. *Cardiovascular Therapeutics*, *27*(3), 187–193. https://doi.org/10.1111/j.1755-5922.2009.00094.x

Chatzinikolaou, A., Tzikas, S., & Lavdaniti, M. (2021). Assessment of Quality of Life in Patients With Cardiovascular Disease Using the SF-36, MacNew, and EQ-5D-5L Questionnaires. *Cureus*, *13*(9). https://doi.org/10.7759/CUREUS.17982

Chen, H., Valle, G., Furlan, S., Nani, A., Gyorke, S., Fill, M., & Volpe, P. (2013). Mechanism of calsequestrin regulation of single cardiac ryanodine receptor in normal and pathological conditions. *Journal of General Physiology*, *142*(2), 127–136. https://doi.org/10.1085/JGP.201311022

Chen, Y., Guo, H., Xu, D., Xu, X., Wang, H., Hu, X., Lu, Z., Kwak, D., Xu, Y., Gunther, R., Huo, Y., & Weir, E. K. (2012). Left ventricular failure produces profound lung remodeling and pulmonary hypertension in mice: Heart failure causes severe lung disease. *Hypertension*, *59*(6), 1170–1178. https://doi.org/10.1161/HYPERTENSIONAHA.111.186072

Cheng, J., Van Norstrand, D. W., Medeiros-Domingo, A., Valdivia, C., Tan, B. -h., Ye, B., Kroboth, S., Vatta, M., Tester, D. J., January, C. T., Makielski, J. C., & Ackerman, M. J. (2009). 1-Syntrophin Mutations Identified in Sudden Infant Death Syndrome Cause an Increase in Late Cardiac Sodium Current. *Circulation: Arrhythmia and Electrophysiology*, *2*(6), 667–676. https://doi.org/10.1161/CIRCEP.109.891440

Chengode, S. (2016). Left ventricular global systolic function assessment by echocardiography. In *Annals of Cardiac Anaesthesia* (Vol. 19, Issue 5, pp. S26–S34). Medknow Publications. https://doi.org/10.4103/0971-9784.192617

Cho, G. W., Altamirano, F., & Hill, J. A. (2016). Chronic heart failure: Ca2 +, catabolism, and catastrophic cell death. *Biochimica et Biophysica Acta (BBA) - Molecular Basis of Disease*, *1862*(4), 763–777. https://doi.org/10.1016/J.BBADIS.2016.01.011

Cho, Y. S., Go, M. J., Kim, Y. J., Heo, J. Y., Oh, J. H., Ban, H.-J., Yoon, D., Lee, M. H., Kim, D.-J., Park, M., Cha, S.-H., Kim, J.-W., Han, B.-G., Min, H., Ahn, Y., Park, M. S., Han, H. R., Jang, H.-Y., Cho, E. Y., … Kim, H.-L. (2009). A large-scale genome-wide association study of Asian populations uncovers genetic factors influencing eight quantitative traits. *Nature Genetics*, *41*(5), 527–534. https://doi.org/10.1038/ng.357

Chorvatova, A., Hart, G., & Hussain, M. (2004). Na+/Ca2+ exchange current (INa/Ca) and sarcoplasmic reticulum Ca2+ release in catecholamine-induced cardiac hypertrophy. *Cardiovascular Research*, *61*(2), 278–287. https://doi.org/10.1016/j.cardiores.2003.11.019

Chowdhury, A., Hasselbach, L., Echtermeyer, F., Jyotsana, N., Theilmeier, G., & Herzog, C. (2017). Fibulin-6 regulates pro-fibrotic TGF-β responses in neonatal mouse ventricular cardiac fibroblasts. *Scientific Reports 2017 7:1*, *7*(1), 1–13. https://doi.org/10.1038/srep42725

Chung, J. H., Biesiadecki, B. J., Ziolo, M. T., Davis, J. P., & Janssen, P. M. L. (2016). Myofilament Calcium Sensitivity: Role in Regulation of In vivo Cardiac Contraction and Relaxation. *Frontiers in Physiology*, *7*(DEC), 562. https://doi.org/10.3389/FPHYS.2016.00562

Cleland, J. G. F., Daubert, J.-C., Erdmann, E., Freemantle, N., Gras, D., Kappenberger, L., & Tavazzi, L. (2005). The Effect of Cardiac Resynchronization on Morbidity and Mortality in Heart Failure. *New England Journal of Medicine*, *352*(15), 1539–1549. https://doi.org/10.1056/NEJMoa050496

Cohn, J. N. (1995). Structural basis for heart failure. Ventricular remodeling and its

pharmacological inhibition. *Circulation*, *91*(10), 2504–2507. http://www.ncbi.nlm.nih.gov/pubmed/7743609

Conrad, C. H., Brooks, W. W., Robinson, K. G., & Bing, O. H. (1991). Impaired myocardial function in spontaneously hypertensive rats with heart failure. *American Journal of Physiology-Heart and Circulatory Physiology*, *260*(1), H136–H145. https://doi.org/10.1152/ajpheart.1991.260.1.H136

Contreras, L., Drago, I., Zampese, E., & Pozzan, T. (2010). Mitochondria: The calcium connection. *Biochimica et Biophysica Acta (BBA) - Bioenergetics*, *1797*(6–7), 607–618. https://doi.org/10.1016/J.BBABIO.2010.05.005

Cook, C., Cole, G., Asaria, P., Jabbour, R., & Francis, D. P. (2014). The annual global economic burden of heart failure. *International Journal of Cardiology*, *171*(3), 368–376. https://doi.org/10.1016/J.IJCARD.2013.12.028

Cowie, M. R. (2017). The heart failure epidemic: a UK perspective. *Echo Research and Practice*, *4*(1), R15–R20. https://doi.org/10.1530/ERP-16-0043

Das, U. S., Paul, A., & Banerjee, S. (2021). SGLT2 inhibitors in heart failure with reduced ejection fraction. *Egyptian Heart Journal*, *73*(1), 1–7. https://doi.org/10.1186/S43044-021-00218-W/FIGURES/1

Dash, R., Kadambi, V., Schmidt, A. G., Tepe, N. M., Biniakiewicz, D., Gerst, M. J., Canning, A. M., Abraham, W. T., Hoit, B. D., Liggett, S. B., Lorenz, J. N., Dorn, G. W., & Kranias, E. G. (2001). Interactions between phospholamban and beta-adrenergic drive may lead to cardiomyopathy and early mortality. *Circulation*, *103*(6), 889–896. http://www.ncbi.nlm.nih.gov/pubmed/11171800

Daugirdas, J. T., Arrieta, J., Ye, M., Flores, G., & Battle, D. C. (1995). Intracellular acidification associated with changes in free cytosolic calcium. Evidence for Ca2+/H+ exchange via a plasma membrane Ca(2+)-ATPase in vascular smooth muscle cells. *Journal of Clinical Investigation*, *95*(4), 1480–1489. https://doi.org/10.1172/JCI117819

Davlouros, P. A., Gkizas, V., Vogiatzi, C., Giannopoulos, G., Alexopoulos, D., & Deftereos, S. (2016). Calcium Homeostasis and Kinetics in Heart Failure. *Medicinal Chemistry (Shariqah (United Arab Emirates))*, *12*(2), 151–161. http://www.ncbi.nlm.nih.gov/pubmed/26411602

Dawson, K., Wu, C.-T., Qi, X. Y., & Nattel, S. (2012). Congestive Heart Failure Effects on Atrial Fibroblast Phenotype: Differences between Freshly-Isolated and Cultured Cells. *PLOS ONE*, *7*(12), e52032. https://doi.org/10.1371/JOURNAL.PONE.0052032

de Frutos, F., Ochoa, J. P., Navarro-Peñalver, M., Baas, A., Bjerre, J. V., Zorio, E., Méndez, I., Lorca, R., Verdonschot, J. A. J., García-Granja, P. E., Bilinska, Z., Fatkin, D., Fuentes-Cañamero, M. E., García-Pinilla, J. M., García-Álvarez, M. I., Girolami, F., Barriales-Villa, R., Díez-López, C., Lopes, L. R., … Díez, C. H. (2022). Natural History of MYH7-Related Dilated Cardiomyopathy. *Journal of the American College of Cardiology*, *80*(15), 1447–1461. https://doi.org/10.1016/J.JACC.2022.07.023/SUPPL_FILE/MMC1.DOCX

De Montgolfier, O., Pinçon, A., Pouliot, P., Gillis, M. A., Bishop, J., Sled, J. G., Villeneuve, L., Ferland, G., Lévy, B. I., Lesage, F., Thorin-Trescases, N., & Thorin, É. (2019). High Systolic Blood Pressure Induces Cerebral Microvascular Endothelial Dysfunction, Neurovascular Unit Damage, and Cognitive Decline in Mice. *Hypertension*, *73*(1), 217–228. https://doi.org/10.1161/HYPERTENSIONAHA.118.12048

deAlmeida, A. C., van Oort, R. J., & Wehrens, X. H. T. (2010). Transverse Aortic Constriction

in Mice. *Journal of Visualized Experiments : JoVE*, *38*, 38. https://doi.org/10.3791/1729

DeMarco, S. J., Chicka, M. C., & Strehler, E. E. (2002). Plasma Membrane Ca $^{2+}$ ATPase Isoform 2b Interacts Preferentially with Na $^{+}$ /H $^{+}$ Exchanger Regulatory Factor 2 in Apical Plasma Membranes. *Journal of Biological Chemistry*, *277*(12), 10506–10511. https://doi.org/10.1074/jbc.M111616200

DeMarco, S. J., & Strehler, E. E. (2001). Plasma Membrane Ca $^{2+}$ -ATPase Isoforms 2b and 4b Interact Promiscuously and Selectively with Members of the Membrane-associated Guanylate Kinase Family of PDZ (PSD95/Dlg/ZO-1) Domain-containing Proteins. *Journal of Biological Chemistry*, *276*(24), 21594–21600. https://doi.org/10.1074/jbc.M101448200

Despa, S., Brette, F., Orchard, C. H., & Bers, D. M. (2003). Na/Ca Exchange and Na/K-ATPase Function Are Equally Concentrated in Transverse Tubules of Rat Ventricular Myocytes. *Biophysical Journal*, *85*(5), 3388–3396. https://doi.org/10.1016/S0006-3495(03)74758-4

Di Leva, F., Domi, T., Fedrizzi, L., Lim, D., & Carafoli, E. (2008). The plasma membrane Ca2+ ATPase of animal cells: Structure, function and regulation. *Archives of Biochemistry and Biophysics*, *476*(1), 65–74. https://doi.org/10.1016/j.abb.2008.02.026

Dirkx, E., da Costa Martins, P. A., & De Windt, L. J. (2013). Regulation of fetal gene expression in heart failure. *Biochimica et Biophysica Acta (BBA) - Molecular Basis of Disease*, *1832*(12), 2414–2424. https://doi.org/10.1016/J.BBADIS.2013.07.023

Domi, T., Di Leva, F., Fedrizzi, L., Rimessi, A., & Brini, M. (2007). Functional specificity of PMCA isoforms? *Annals of the New York Academy of Sciences*, *1099*, 237–246. https://doi.org/10.1196/ANNALS.1387.043

Drago, I., De Stefani, D., Rizzuto, R., & Pozzan, T. (2012). Mitochondrial Ca2+ uptake contributes to buffering cytoplasmic Ca2+ peaks in cardiomyocytes. *Proceedings of the National Academy of Sciences*, *109*(32), 12986–12991. https://doi.org/10.1073/pnas.1210718109

Dridi, H., Kushnir, A., Zalk, R., Yuan, Q., Melville, Z., & Marks, A. R. (2020). Intracellular calcium leak: a unifying mechanism and therapeutic target for heart failure and atrial fibrillation. *Nature Reviews. Cardiology*, *17*(11), 732. https://doi.org/10.1038/S41569-020-0394-8

Durham, W. J., Wehrens, X. H. T., Sood, S., & Hamilton, S. L. (2007). Diseases associated with altered ryanodine receptor activity. *Sub-Cellular Biochemistry*, *45*, 273–321. http://www.ncbi.nlm.nih.gov/pubmed/18193641

Duygu, B., Poels, E. M., & Da Costa Martins, P. A. (2013). Genetics and epigenetics of arrhythmia and heart failure. *Frontiers in Genetics*, *0*, 219. https://doi.org/10.3389/FGENE.2013.00219

Edwards, A. G., Mørk, H., Stokke, M. K., Lipsett, D. B., Sjaastad, I., Richard, S., Sejersted, O. M., & Louch, W. E. (2021). Sarcoplasmic Reticulum Calcium Release Is Required for Arrhythmogenesis in the Mouse. *Frontiers in Physiology*, *12*, 1747. https://doi.org/10.3389/FPHYS.2021.744730/BIBTEX

Ehret, G. B., Munroe, P. B., Rice, K. M., Bochud, M., Johnson, A. D., Chasman, D. I., Smith, A. V., Tobin, M. D., Verwoert, G. C., Hwang, S. J., Pihur, V., Vollenweider, P., O'Reilly, P. F., Amin, N., Bragg-Gresham, J. L., Teumer, A., Glazer, N. L., Launer, L., Zhao, J. H., …

Johnson, T. (2011). Genetic variants in novel pathways influence blood pressure and cardiovascular disease risk. *Nature*, *478*(7367), 103–109. https://doi.org/10.1038/nature10405

Eisner, D., Caldwell, J., & Trafford, A. (2013). Sarcoplasmic reticulum Ca-ATPase and heart failure 20 years later. *Circulation Research*, *113*(8), 958–961. https://doi.org/10.1161/CIRCRESAHA.113.302187

Ellison, K. E., Stevenson, W. G., Sweeney, M. O., Epstein, L. M., & Maisel, W. H. (2003). Management of arrhythmias in heart failure. In *Congestive Heart Failure* (Vol. 9, Issue 2, pp. 91–99). Multidisciplinary Digital Publishing Institute (MDPI). https://doi.org/10.3390/jcdd4010003

Elwess, N. L., Filoteo, A. G., Enyedi, A., & Penniston, J. T. (1997). Plasma membrane Ca2+ pump isoforms 2a and 2b are unusually responsive to calmodulin and Ca2+. *The Journal of Biological Chemistry*, *272*(29), 17981–17986. https://doi.org/10.1074/JBC.272.29.17981

Ely, J. J., Bishop, M. A., Lammey, M. L., Sleeper, M. M., Steiner, J. M., & Lee, D. R. (2010). Use of biomarkers of collagen types I and III fibrosis metabolism to detect cardiovascular and renal disease in chimpanzees (Pan troglodytes). *Comparative Medicine*, *60*(2), 154–158. /pmc/articles/PMC2855044/

Enyedi, A., Flura, M., Sarkadi, B., Gardos, G., & Carafoli, E. (1987). The maximal velocity and the calcium affinity of the red cell calcium pump may be regulated independently. *The Journal of Biological Chemistry*, *262*(13), 6425–6430. http://www.ncbi.nlm.nih.gov/pubmed/3032968

Fagard, R. H. (1997). Impact of different sports and training on cardiac structure and function. *Cardiology Clinics*, *15*(3), 397–412. http://www.ncbi.nlm.nih.gov/pubmed/9276165

Faggioni, M., Kryshtal, D. O., & Knollmann, B. C. (2012). Calsequestrin Mutations and Catecholaminergic Polymorphic Ventricular Tachycardia. *Pediatric Cardiology*, *33*(6), 959. https://doi.org/10.1007/S00246-012-0256-1

Falchetto, R., Vorherr, T., & Carafoli, E. (1992). The calmodulin-binding site of the plasma membrane Ca $^{2+}$ pump interacts with the transduction domain of the enzyme. *Protein Science*, *1*(12), 1613–1621. https://doi.org/10.1002/pro.5560011209

Fearnley, C. J., Roderick, H. L., & Bootman, M. D. (2011). Calcium signaling in cardiac myocytes. *Cold Spring Harbor Perspectives in Biology*, *3*(11), a004242. https://doi.org/10.1101/cshperspect.a004242

Feldman, A. M., Kontos, C. D., McClung, J. M., Gerhard, G. S., Khalili, K., & Cheung, J. Y. (2017). Precision Medicine for Heart Failure: Lessons from Oncology. *Circulation: Heart Failure*, *10*(6), 1–5. https://doi.org/10.1161/CIRCHEARTFAILURE.117.004202

Ferguson, J. F., Matthews, G. J., Townsend, R. R., Raj, D. S., Kanetsky, P. A., Budoff, M., Fischer, M. J., Rosas, S. E., Kanthety, R., Rahman, M., Master, S. R., Qasim, A., Li, M., Mehta, N. N., Shen, H., Mitchell, B. D., O'Connell, J. R., Shuldiner, A. R., Ho, W. K., … CRIC Study Principal Investigators. (2013). Candidate Gene Association Study of Coronary Artery Calcification in Chronic Kidney Disease. *Journal of the American College of Cardiology*, *62*(9), 789–798. https://doi.org/10.1016/j.jacc.2013.01.103

Fontana, V., McDonough, C. W., Gong, Y., El Rouby, N. M., Sa, A. C. C., Taylor, K. D., Chen, Y.-D. I., Gums, J. G., Chapman, A. B., Turner, S. T., Pepine, C. J., Johnson, J. A., &

Cooper-DeHoff, R. M. (2014). Large-Scale Gene-Centric Analysis Identifies Polymorphisms for Resistant Hypertension. *Journal of the American Heart Association*, *3*(6), e001398–e001398. https://doi.org/10.1161/JAHA.114.001398

Fontana, V., McDonough, C. W., Gong, Y., El Rouby, N. M., Sá, A. C. C., Taylor, K. D., Ida Chen, Y. D., Gums, J. G., Chapman, A. B., Turner, S. T., Pepine, C. J., Johnson, J. A., & Cooper-DeHoff, R. M. (2014). Large-scale gene-centric analysis identifies polymorphisms for resistant hypertension. *Journal of the American Heart Association*, *3*(6), e001398–e001398. https://doi.org/10.1161/JAHA.114.001398

Fozzard, H. A. (1992). Afterdepolarizations and triggered activity. *Basic Research in Cardiology*, *87 Suppl 2*(SUPPL. 2), 105–113. https://doi.org/10.1007/978-3-642-72477-0_10

Frangogiannis, N. G. (2019a). The Extracellular Matrix in Ischemic and Nonischemic Heart Failure. *Circulation Research*, *125*(1), 117–146. https://doi.org/10.1161/CIRCRESAHA.119.311148

Frangogiannis, N. G. (2019b). The Extracellular Matrix in Ischemic and Nonischemic Heart Failure. *Circulation Research*, *125*(1), 117–146. https://doi.org/10.1161/CIRCRESAHA.119.311148

Furuta, H., Luo, L., Hepler, K., & Ryan, A. F. (1998). Evidence for differential regulation of calcium by outer versus inner hair cells: plasma membrane Ca-ATPase gene expression. *Hearing Research*, *123*(1–2), 10–26. http://www.ncbi.nlm.nih.gov/pubmed/9745951

Gad, S. C. (2014). Calcium Channel Blockers. *Encyclopedia of Toxicology: Third Edition*, 621–624. https://doi.org/10.1016/B978-0-12-386454-3.00824-1

Garcia-Menendez, L., Karamanlidis, G., Kolwicz, S., & Tian, R. (2013). Substrain specific response to cardiac pressure overload in C57BL/6 mice. *American Journal of Physiology - Heart and Circulatory Physiology*, *305*(3). https://doi.org/10.1152/ajpheart.00088.2013

Gardin, J. M. (2016). The Value of Left Ventricular Relative Wall Thickness in Predicting Ventricular Arrhythmia and Related Death∗. *Journal of the American College of Cardiology*, *67*(3), 313–315. https://doi.org/10.1016/J.JACC.2015.10.078

Giamouzis, G., Dimos, A., Xanthopoulos, A., Skoularigis, J., & Triposkiadis, F. (2021). Left ventricular hypertrophy and sudden cardiac death. *Heart Failure Reviews 2021 27:2*, *27*(2), 711–724. https://doi.org/10.1007/S10741-021-10134-5

Gibbs, R. A., Belmont, J. W., Hardenbol, P., Willis, T. D., Yu, F., Zhang, H., Zeng, C., Matsuda, I., Fukushima, Y., Macer, D. R., Suda, E., Stein, L. D., Cunningham, F., Kanani, A., Thorisson, G. A., Chakravarti, A., Chen, P. E., Cutler, D. J., Kashuk, C. S., … Tanaka, T. (2003). The International HapMap Project. *Nature*, *426*(6968), 789–796. https://doi.org/10.1038/nature02168

Godfraind, T. (2014). Calcium channel blockers in cardiovascular pharmacotherapy. *Journal of Cardiovascular Pharmacology and Therapeutics*, *19*(6), 501–515. https://doi.org/10.1177/1074248414530508

Godfraind, T. (2017). Discovery and development of calcium channel blockers. *Frontiers in Pharmacology*, *8*(MAY), 286. https://doi.org/10.3389/FPHAR.2017.00286/BIBTEX

Goellner, G. M., DeMarco, S. J., & Strehler, E. E. (2003). Characterization of PISP, a novel

single-PDZ protein that binds to all plasma membrane Ca2+-ATPase b-splice variants. *Annals of the New York Academy of Sciences*, *986*, 461–471. http://www.ncbi.nlm.nih.gov/pubmed/12763866

Gorski, P. A., Ceholski, D. K., & Hajjar, R. J. (2015). Altered Myocardial Calcium Cycling and Energetics in Heart Failure—A Rational Approach for Disease Treatment. *Cell Metabolism*, *21*(2), 183–194. https://doi.org/10.1016/J.CMET.2015.01.005

Griffin, N. M., & Schnitzer, J. E. (2011). Overcoming Key Technological Challenges in Using Mass Spectrometry for Mapping Cell Surfaces in Tissues. *Molecular & Cellular Proteomics : MCP*, *10*(2). https://doi.org/10.1074/MCP.R110.000935

Guerini, D. (1998). The significance of the isoforms of plasma membrane calcium ATPase. *Cell and Tissue Research*, *292*(2), 191–197. https://doi.org/10.1007/s004410051050

Guerini, D., Pan, B., & Carafoli, E. (2003). Expression, purification, and characterization of isoform 1 of the plasma membrane Ca2+ pump: focus on calpain sensitivity. *The Journal of Biological Chemistry*, *278*(40), 38141–38148. https://doi.org/10.1074/jbc.M302400200

Guerini, D., Zecca-Mazza, A., & Carafoli, E. (2000). Single amino acid mutations in transmembrane domain 5 confer to the plasma membrane Ca2+ pump properties typical of the Ca2+ pump of endo(sarco)plasmic reticulum. *The Journal of Biological Chemistry*, *275*(40), 31361–31368. https://doi.org/10.1074/jbc.M003474200

Guerrero-Hernandez, A., Dagnino-Acosta, A., & Verkhratsky, A. (2010). An intelligent sarco-endoplasmic reticulum Ca2+ store: release and leak channels have differential access to a concealed Ca2+ pool. *Cell Calcium*, *48*(2–3), 143–149. https://doi.org/10.1016/j.ceca.2010.08.001

Gürtl, B., Kratky, D., Guelly, C., Zhang, L., Gorkiewicz, G., Das, S. K., Tamilarasan, K. P., & Hoefler, G. (2009). Apoptosis and fibrosis are early features of heart failure in an animal model of metabolic cardiomyopathy. *International Journal of Experimental Pathology*, *90*(3), 338–346. https://doi.org/10.1111/j.1365-2613.2009.00647.x

Haddad, F., Doyle, R., Murphy, D. J., & Hunt, S. A. (2008). Right Ventricular Function in Cardiovascular Disease, Part II: Pathophysiology, Clinical Importance, and Management of Right Ventricular Failure. *Circulation*, *117*(13), 1717–1731. https://doi.org/10.1161/CIRCULATIONAHA.107.653584

Hammes, A., Oberdorf-Maass, S., Rother, T., Nething, K., Gollnick, F., Linz, K. W., Meyer, R., Hu, K., Han, H., Gaudron, P., Ertl, G., Hoffmann, S., Ganten, U., Vetter, R., Schuh, K., Benkwitz, C., Zimmer, H. G., & Neyses, L. (1998). Overexpression of the sarcolemmal calcium pump in the myocardium of transgenic rats. *Circulation Research*, *83*(9), 877–888. https://doi.org/10.1161/01.res.83.9.877

Harris, S. P., & de Tombe, P. P. (2019). Sarcomeric mutations in cardiac diseases. *Pflügers Archiv - European Journal of Physiology 2019 471:5*, *471*(5), 659–660. https://doi.org/10.1007/S00424-019-02275-2

Harvey, P. A., & Leinwand, L. A. (2011). The cell biology of disease: Cellular mechanisms of cardiomyopathy. *The Journal of Cell Biology*, *194*(3), 355. https://doi.org/10.1083/JCB.201101100

Heineke, J., & Molkentin, J. D. (2006). Regulation of cardiac hypertrophy by intracellular signalling pathways. *Nature Reviews Molecular Cell Biology*, *7*(8), 589–600. https://doi.org/10.1038/nrm1983

Heineke, J., Ruetten, H., Willenbockel, C., Gross, S. C., Naguib, M., Schaefer, A., Kempf, T., Hilfiker-Kleiner, D., Caroni, P., Kraft, T., Kaiser, R. A., Molkentin, J. D., Drexler, H., & Wollert, K. C. (2005). Attenuation of cardiac remodeling after myocardial infarction by muscle LIM protein-calcineurin signaling at the sarcomeric Z-disc. *Proceedings of the National Academy of Sciences of the United States of America*, *102*(5), 1655–1660. https://doi.org/10.1073/pnas.0405488102

Henderson, S. A., Goldhaber, J. I., So, J. M., Han, T., Motter, C., Ngo, A., Chantawansri, C., Ritter, M. R., Friedlander, M., Nicoll, D. A., Frank, J. S., Jordan, M. C., Roos, K. P., Ross, R. S., & Philipson, K. D. (2004a). Functional adult myocardium in the absence of Na+-Ca2+ exchange: cardiac-specific knockout of NCX1. *Circulation Research*, *95*(6), 604–611. https://doi.org/10.1161/01.RES.0000142316.08250.68

Henderson, S. A., Goldhaber, J. I., So, J. M., Han, T., Motter, C., Ngo, A., Chantawansri, C., Ritter, M. R., Friedlander, M., Nicoll, D. A., Frank, J. S., Jordan, M. C., Roos, K. P., Ross, R. S., & Philipson, K. D. (2004b). Functional Adult Myocardium in the Absence of Na^{+}-Ca^{2+} Exchange. *Circulation Research*, *95*(6), 604–611. https://doi.org/10.1161/01.RES.0000142316.08250.68

Hinderer, S., & Schenke-Layland, K. (2019a). Cardiac fibrosis – A short review of causes and therapeutic strategies. In *Advanced Drug Delivery Reviews* (Vol. 146, pp. 77–82). Elsevier B.V. https://doi.org/10.1016/j.addr.2019.05.011

Hinderer, S., & Schenke-Layland, K. (2019b). Cardiac fibrosis – A short review of causes and therapeutic strategies. *Advanced Drug Delivery Reviews*, *146*, 77–82. https://doi.org/10.1016/J.ADDR.2019.05.011

Ho, P. W.-L., Pang, S. Y.-Y., Li, M., Tse, Z. H.-M., Kung, M. H.-W., Sham, P.-C., & Ho, S.-L. (2015). PMCA4 (ATP2B4) mutation in familial spastic paraplegia causes delay in intracellular calcium extrusion. *Brain and Behavior*, *5*(4), n/a-n/a. https://doi.org/10.1002/brb3.321

Hofer, A. M., & Lefkimmiatis, K. (2007). Extracellular calcium and cAMP: Second messengers as “third messengers”? *Physiology*, *22*(5), 320–327. https://doi.org/10.1152/PHYSIOL.00019.2007/ASSET/IMAGES/LARGE/Y0019-07-04.JPEG

Holmager, P., Egstrup, M., Gustafsson, I., Schou, M., Dahl, J. S., Rasmussen, L. M., Møller, J. E., Tuxen, C., Faber, J., & Kistorp, C. (2017). Galectin-3 and fibulin-1 in systolic heart failure - relation to glucose metabolism and left ventricular contractile reserve. *BMC Cardiovascular Disorders*, *17*(1). https://doi.org/10.1186/S12872-016-0437-6

Holton, M. L., Wang, W., Emerson, M., Neyses, L., & Armesilla, A. L. (2010). Plasma membrane calcium ATPase proteins as novel regulators of signal transduction pathways. *World Journal of Biological Chemistry*, *1*(6), 201. https://doi.org/10.4331/WJBC.V1.I6.201

Holubarsch, C., Goulette, R. P., Litten, R. Z., Martin, B. J., Mulieri, L. A., & Alpert, N. R. (1985). The economy of isometric force development, myosin isoenzyme pattern and myofibrillar ATPase activity in normal and hypothyroid rat myocardium. *Circulation Research*, *56*(1), 78–86. https://doi.org/10.1161/01.RES.56.1.78

Hoshijima, M. (2005). Gene therapy targeted at calcium handling as an approach to the treatment of heart failure. *Pharmacology & Therapeutics*, *105*(3), 211–228. https://doi.org/10.1016/j.pharmthera.2004.10.006

Houser, S. R. (2000). When Does Spontaneous Sarcoplasmic Reticulum CA2+ Release Cause a Triggered Arrythmia? Cellular Versus Tissue Requirements. *Circulation Research*, *87*(9), 725–727. https://doi.org/10.1161/01.RES.87.9.725

Hove-Madsen, L., & Bers, D. M. (1993). *No Title*. *73*(5). https://doi.org/10.1161/01.RES.73.5.820

Hsu, C.-L., & Lee, W.-C. (2010). Detecting differentially expressed genes in heterogeneous diseases using half Student's t-test. *International Journal of Epidemiology*, *39*(6), 1597–1604. https://doi.org/10.1093/ije/dyq093

Hu, V. W., Nguyen, A., Kim, K. S., Steinberg, M. E., Sarachana, T., Scully, M. A., Soldin, S. J., Luu, T., & Lee, N. H. (2009). Gene Expression Profiling of Lymphoblasts from Autistic and Nonaffected Sib Pairs: Altered Pathways in Neuronal Development and Steroid Biosynthesis. *PLoS ONE*, *4*(6), e5775. https://doi.org/10.1371/journal.pone.0005775

Hu, Z., Wang, J. W., Yu, D., Soon, J. L., De Kleijn, D. P. V., Foo, R., Liao, P., Colecraft, H. M., & Soong, T. W. (2016). Aberrant Splicing Promotes Proteasomal Degradation of L-type CaV1.2 Calcium Channels by Competitive Binding for CaVβ Subunits in Cardiac Hypertrophy. *Scientific Reports 2016 6:1*, *6*(1), 1–12. https://doi.org/10.1038/srep35247

Hurtado, C., Ander, B. P., Maddaford, T. G., Lukas, A., Hryshko, L. V., & Pierce, G. N. (2005). Adenovirally delivered shRNA strongly inhibits Na+–Ca2+ exchanger expression but does not prevent contraction of neonatal cardiomyocytes. *Journal of Molecular and Cellular Cardiology*, *38*(4), 647–654. https://doi.org/10.1016/J.YJMCC.2005.02.007

James, A. D., Patel, W., Butt, Z., Adiamah, M., Dakhel, R., Latif, A., Uggenti, C., Swanton, E., Imamura, H., Siriwardena, A. K., & Bruce, J. I. E. (2015). The Plasma Membrane Calcium Pump in Pancreatic Cancer Cells Exhibiting the Warburg Effect Relies on Glycolytic ATP. *The Journal of Biological Chemistry*, *290*(41), 24760–24771. https://doi.org/10.1074/jbc.M115.668707

Johnson, B. D., Kip, K. E., Marroquin, O. C., Ridker, P. M., Kelsey, S. F., Shaw, L. J., Pepine, C. J., Sharaf, B., Merz, C. N. B., Sopko, G., Olson, M. B., & Reis, S. E. (2004). Serum Amyloid A as a Predictor of Coronary Artery Disease and Cardiovascular Outcome in Women. *Circulation*, *109*(6), 726–732. https://doi.org/10.1161/01.CIR.0000115516.54550.B1

Joiner, M. A., Koval, O. M., Li, J., He, B. J., Allamargot, C., Gao, Z., Luczak, E. D., Hall, D. D., Fink, B. D., Chen, B., Yang, J., Moore, S. A., Scholz, T. D., Strack, S., Mohler, P. J., Sivitz, W. I., Song, L.-S., & Anderson, M. E. (2012). CaMKII determines mitochondrial stress responses in heart. *Nature*, *491*(7423), 269–273. https://doi.org/10.1038/nature11444

Kaneko, M., Hashikami, K., Yamamoto, S., Matsumoto, H., & Nishimoto, T. (2016). Phospholamban Ablation Using CRISPR/Cas9 System Improves Mortality in a Murine Heart Failure Model. *PloS One*, *11*(12). https://doi.org/10.1371/JOURNAL.PONE.0168486

Karwi, Q. G., Uddin, G. M., Ho, K. L., & Lopaschuk, G. D. (2018). Loss of Metabolic Flexibility in the Failing Heart. *Frontiers in Cardiovascular Medicine*, *5*, 68. https://doi.org/10.3389/FCVM.2018.00068/BIBTEX

Kasri, N. N., Parys, J. B., Callewaert, G., Missiaen, L., & De Smedt, H. (2004). Calmodulin and calcium-release channels. *Biological Research*, *37*(4), 577–582.

https://doi.org/10.4067/S0716-97602004000400011

Keeton, T. P., Burk, S. E., & Shull, G. E. (1993). Alternative splicing of exons encoding the calmodulin-binding domains and C termini of plasma membrane Ca(2+)-ATPase isoforms 1, 2, 3, and 4. *The Journal of Biological Chemistry*, *268*(4), 2740–2748. http://www.ncbi.nlm.nih.gov/pubmed/8428948

Kehat, I., & Molkentin, J. D. (2010). Molecular Pathways Underlying Cardiac Remodeling During Pathophysiological Stimulation. *Circulation*, *122*(25), 2727–2735. https://doi.org/10.1161/CIRCULATIONAHA.110.942268

Kemp, C. D., & Conte, J. V. (2012). The pathophysiology of heart failure. *Cardiovascular Pathology*, *21*(5), 365–371. https://doi.org/10.1016/j.carpath.2011.11.007

Kim, H.-Y. (2015). Statistical notes for clinical researchers: post-hoc multiple comparisons. *Restorative Dentistry & Endodontics*, *40*(2), 172. https://doi.org/10.5395/RDE.2015.40.2.172

Kiriazis, H., & Kranias, E. G. (2000). Genetically Engineered Models with Alterations in Cardiac Membrane Calcium-Handling Proteins. *Annual Review of Physiology*, *62*(1), 321–351. https://doi.org/10.1146/annurev.physiol.62.1.321

KL, Y., VM Weaver, & DA, H. (2008). Integrin-mediated signalling through the MAP-kinase pathway. *IET Systems Biology*, *2*(1), 8–15. https://doi.org/10.1049/IET-SYB:20060058

Knöll, R., Hoshijima, M., Hoffman, H. M., Person, V., Lorenzen-Schmidt, I., Bang, M.-L., Hayashi, T., Shiga, N., Yasukawa, H., Schaper, W., McKenna, W., Yokoyama, M., Schork, N. J., Omens, J. H., McCulloch, A. D., Kimura, A., Gregorio, C. C., Poller, W., Schaper, J., … Chien, K. R. (2002). The cardiac mechanical stretch sensor machinery involves a Z disc complex that is defective in a subset of human dilated cardiomyopathy. *Cell*, *111*(7), 943–955. http://www.ncbi.nlm.nih.gov/pubmed/12507422

Kobayashi, T., Jin, L., & De Tombe, P. P. (2008). Cardiac thin filament regulation. In *Pflugers Archiv European Journal of Physiology* (Vol. 457, Issue 1, pp. 37–46). NIH Public Access. https://doi.org/10.1007/s00424-008-0511-8

Kobayashi, Y., Hirawa, N., Tabara, Y., Muraoka, H., Fujita, M., Miyazaki, N., Fujiwara, A., Ichikawa, Y., Yamamoto, Y., Ichihara, N., Saka, S., Wakui, H., Yoshida, S. -i., Yatsu, K., Toya, Y., Yasuda, G., Kohara, K., Kita, Y., Takei, K., … Umemura, S. (2012a). Mice Lacking Hypertension Candidate Gene ATP2B1 in Vascular Smooth Muscle Cells Show Significant Blood Pressure Elevation. *Hypertension*, *59*(4), 854–860. https://doi.org/10.1161/HYPERTENSIONAHA.110.165068

Kobayashi, Y., Hirawa, N., Tabara, Y., Muraoka, H., Fujita, M., Miyazaki, N., Fujiwara, A., Ichikawa, Y., Yamamoto, Y., Ichihara, N., Saka, S., Wakui, H., Yoshida, S. I., Yatsu, K., Toya, Y., Yasuda, G., Kohara, K., Kita, Y., Takei, K., … Umemura, S. (2012b). Mice lacking hypertension candidate gene ATP2B1 in vascular smooth muscle cells show significant blood pressure elevation. *Hypertension*, *59*(4), 854–860. https://doi.org/10.1161/HYPERTENSIONAHA.110.165068

Kokubo, Y., & Iwashima, Y. (2015). Higher Blood Pressure as a Risk Factor for Diseases Other Than Stroke and Ischemic Heart Disease. *Hypertension*, *66*(2), 254–259. https://doi.org/10.1161/HYPERTENSIONAHA.115.03480/-/DC1

Kongpracha, P., Wiriyasermkul, P., Isozumi, N., Moriyama, S., Kanai, Y., & Nagamori, S. (2022). Simple but Efficacious Enrichment of Integral Membrane Proteins and Their

Interactions for In-Depth Membrane Proteomics. *Molecular and Cellular Proteomics*, *21*(5), 100206. https://doi.org/10.1016/J.MCPRO.2022.100206/ATTACHMENT/0E8BFCF7-60E4-4B08-9F17-2857C5EF3B90/MMC8.XLSX

Kotecha, D., & Piccini, J. P. (2015). Atrial fibrillation in heart failure: what should we do? *European Heart Journal*, *36*(46), 3250–3257. https://doi.org/10.1093/EURHEARTJ/EHV513

Kranias, E. G., & Bers, D. M. (2007). Calcium Signalling and Disease. In *Sub-cellular biochemistry* (Vol. 45). https://doi.org/10.1007/978-1-4020-6191-2

Krey, J. F., & Dolmetsch, R. E. (2007). Molecular mechanisms of autism: a possible role for Ca2+ signaling. *Current Opinion in Neurobiology*, *17*(1), 112–119. https://doi.org/10.1016/j.conb.2007.01.010

Kuhn, M., Holtwick, R., Baba, H. A., Perriard, J. C., Schmitz, W., & Ehler, E. (2002). Progressive cardiac hypertrophy and dysfunction in atrial natriuretic peptide receptor (GC-A) deficient mice. *Heart*, *87*(4), 368–374. https://doi.org/10.1136/heart.87.4.368

Kuo, T. H., Tsang, W., Wang, K. K. W., & Carlock, L. (1992). Simultaneous reduction on the sarcolemmal and SR calcium ATPase activities and gene expression in cardiomyopathic hamster. *Biochimica et Biophysica Acta (BBA) - Molecular Basis of Disease*, *1138*(4), 343–349. https://doi.org/10.1016/0925-4439(92)90013-D

Kurabayashi, M., Tsuchimochi, H., Komuro, I., Takaku, F., & Yazaki, Y. (1988). Molecular cloning and characterization of human cardiac alpha- and beta-form myosin heavy chain complementary DNA clones. Regulation of expression during development and pressure overload in human atrium. *The Journal of Clinical Investigation*, *82*(2), 524–531. https://doi.org/10.1172/JCI113627

Kwong, J. Q., Lu, X., Correll, R. N., Schwanekamp, J. A., Vagnozzi, R. J., Sargent, M. A., York, A. J., Zhang, J., Bers, D. M., & Molkentin, J. D. (2015). The mitochondrial calcium uniporter selectively matches metabolic output to acute contractile stress in the heart. *Cell Reports*, *12*(1), 15. https://doi.org/10.1016/J.CELREP.2015.06.002

Lawes, C. M., Hoorn, S. Vander, Rodgers, A., & International Society of Hypertension. (2008). Global burden of blood-pressure-related disease, 2001. *The Lancet*, *371*(9623), 1513–1518. https://doi.org/10.1016/S0140-6736(08)60655-8

Lehnart, S. E., Maier, L. S., & Hasenfuss, G. (2009). Abnormalities of calcium metabolism and myocardial contractility depression in the failing heart. *Heart Failure Reviews*, *14*(4), 213–224. https://doi.org/10.1007/s10741-009-9146-x

Levy, D., Ehret, G. B., Rice, K., Verwoert, G. C., Launer, L. J., Dehghan, A., Glazer, N. L., Morrison, A. C., Johnson, A. D., Aspelund, T., Aulchenko, Y., Lumley, T., Köttgen, A., Vasan, R. S., Rivadeneira, F., Eiriksdottir, G., Guo, X., Arking, D. E., Mitchell, G. F., … van Duijn, C. M. (2009). Genome-wide association study of blood pressure and hypertension. *Nature Genetics*, *41*(6), 677–687. https://doi.org/10.1038/ng.384

Levy, D., Ehret, G. B., Rice, K., Verwoert, G. C., Launer, L. J., Dehghan, A., Glazer, N. L., Morrison, A. C., Johnson, A. D., Aspelund, T., Aulchenko, Y., Lumley, T., Köttgen, A., Vasan, R. S., Rivadeneira, F., Eiriksdottir, G., Guo, X., Arking, D. E., Mitchell, G. F., … Van Duijn, C. M. (2009). Genome-wide association study of blood pressure and hypertension. *Nature Genetics*, *41*(6), 677–687. https://doi.org/10.1038/ng.384

Levy, D., Garrison, R. J., Savage, D. D., Kannel, W. B., & Castelli, W. P. (1990). Prognostic

Implications of Echocardiographically Determined Left Ventricular Mass in the Framingham Heart Study. *New England Journal of Medicine*, *322*(22), 1561–1566. https://doi.org/10.1056/NEJM199005313222203

Li, J., Wu, N., Dai, W., Jiang, L., Li, Y., Li, S., & Wen, Z. (2016). Association of serum calcium and heart failure with preserved ejection fraction in patients with type 2 diabetes. *Cardiovascular Diabetology*, *15*(1), 1–9. https://doi.org/10.1186/S12933-016-0458-6/FIGURES/1

Li, L., Louch, W. E., Niederer, S. A., Aronsen, J. M., Christensen, G., Sejersted, O. M., & Smith, N. P. (2012). Sodium accumulation in SERCA knockout-induced heart failure. *Biophysical Journal*, *102*(9), 2039–2048. https://doi.org/10.1016/J.BPJ.2012.03.045/ATTACHMENT/2BCC959D-F705-4FFC-B0E7-A20086CC9BBB/MMC1.PDF

Liao, J., Li, H., Zeng, W., Sauer, D. B., Belmares, R., & Jiang, Y. (2012). Structural Insight into the Ion-Exchange Mechanism of the Sodium/Calcium Exchanger. *Science*, *335*(6069), 686–690. https://doi.org/10.1126/science.1215759

Lip, G. Y. H., Heinzel, F. R., Gaita, F., Juanatey, J. R. G., Le Heuzey, J. Y., Potpara, T., Svendsen, J. H., Vos, M. A., Anker, S. D., Coats, A. J., Haverkamp, W., Manolis, A. S., Chung, M. K., Sanders, P., Pieske, B., Gorenek, B., Lane, D., Boriani, G., Linde, C., … Savelieva, I. (2016). European Heart Rhythm Association/Heart Failure Association joint consensus document on arrhythmias in heart failure, endorsed by the Heart Rhythm Society and the Asia Pacific Heart Rhythm Society. *Europace*, *18*(1), 12–36. https://doi.org/10.1093/europace/euv191

Little, R., Zi, M., Hammad, S. K., Nguyen, L., Njegic, A., Kurusamy, S., Prehar, S., Armesilla, A. L., Neyses, L., Austin, C., & Cartwright, E. J. (2017). Reduced expression of PMCA1 is associated with increased blood pressure with age which is preceded by remodelling of resistance arteries. *Aging Cell*, *16*(5), 1104–1113. https://doi.org/10.1111/acel.12637

Liu, L., Ishida, Y., Okunade, G., Pyne-Geithman, G. J., Shull, G. E., & Paul, R. J. (2007). Distinct roles of PMCA isoforms in Ca^{2+} homeostasis of bladder smooth muscle: evidence from PMCA gene-ablated mice. *American Journal of Physiology-Cell Physiology*, *292*(1), C423–C431. https://doi.org/10.1152/ajpcell.00313.2006

Liu, T., Song, D., Dong, J., Zhu, P., Liu, J., Liu, W., Ma, X., Zhao, L., & Ling, S. (2017). Current Understanding of the Pathophysiology of Myocardial Fibrosis and Its Quantitative Assessment in Heart Failure. *Frontiers in Physiology*, *8*(APR), 238. https://doi.org/10.3389/FPHYS.2017.00238

Liu, Y., Beyer, A., & Aebersold, R. (2016). Leading Edge Review On the Dependency of Cellular Protein Levels on mRNA Abundance. *Cell*, *165*, 535–550. https://doi.org/10.1016/j.cell.2016.03.014

Lopreiato, R., Giacomello, M., & Carafoli, E. (2014). The plasma membrane calcium pump: new ways to look at an old enzyme. *The Journal of Biological Chemistry*, *289*(15), 10261–10268. https://doi.org/10.1074/jbc.O114.555565

Louch, W. E., Hougen, K., Mørk, H. K., Swift, F., Aronsen, J. M., Sjaastad, I., Reims, H. M., Roald, B., Andersson, K. B., Christensen, G., & Sejersted, O. M. (2010). Sodium accumulation promotes diastolic dysfunction in end-stage heart failure following *Serca2* knockout. *The Journal of Physiology*, *588*(3), 465–478.

https://doi.org/10.1113/jphysiol.2009.183517

Lu, Y.-M., Huang, J., Shioda, N., Fukunaga, K., Shirasaki, Y., Li, X., & Han, F. (2011). CaMKIIδB Mediates Aberrant NCX1 Expression and the Imbalance of NCX1/SERCA in Transverse Aortic Constriction-Induced Failing Heart. *PLoS ONE*, *6*(9), e24724. https://doi.org/10.1371/journal.pone.0024724

Lu, Y. M., Huang, J., Shioda, N., Fukunaga, K., Shirasaki, Y., Li, X. ming, & Han, F. (2011). Camkiiδb mediates aberrant NCX1 expression and the imbalance of NCX1/SERCA in transverse aortic Constriction-Induced failing heart. *PLoS ONE*, *6*(9). https://doi.org/10.1371/journal.pone.0024724

Luo, M., & Anderson, M. E. (2013). Mechanisms of Altered Ca2+ Handling in Heart Failure. *Circulation Research*, *113*(6), 690–708. https://doi.org/10.1161/CIRCRESAHA.113.301651

Luo, T., Chen, B., & Wang, X. (2015). 4-PBA prevents pressure overload-induced myocardial hypertrophy and interstitial fibrosis by attenuating endoplasmic reticulum stress. *Chemico-Biological Interactions*, *242*, 99–106. https://doi.org/10.1016/J.CBI.2015.09.025

Luongo, T. S., Lambert, J. P., Yuan, A., Zhang, X., Gross, P., Song, J., Shanmughapriya, S., Gao, E., Jain, M., Houser, S. R., Koch, W. J., Cheung, J. Y., Madesh, M., & Elrod, J. W. (2015). The Mitochondrial Calcium Uniporter Matches Energetic Supply with Cardiac Workload during Stress and Modulates Permeability Transition. *Cell Reports*, *12*(1), 23. https://doi.org/10.1016/J.CELREP.2015.06.017

Lüscher, T. F. (2015). Risk factors for and management of heart failure. *European Heart Journal*, *36*(34), 2267–2269. https://doi.org/10.1093/eurheartj/ehv348

Lyon, A. R., Babalis, D., Morley-Smith, A. C., Hedger, M., Suarez Barrientos, A., Foldes, G., Couch, L. S., Chowdhury, R. A., Tzortzis, K. N., Peters, N. S., Rog-Zielinska, E. A., Yang, H. Y., Welch, S., Bowles, C. T., Rahman Haley, S., Bell, A. R., Rice, A., Sasikaran, T., Johnson, N. A., … Harding, S. E. (2020). Investigation of the safety and feasibility of AAV1/SERCA2a gene transfer in patients with chronic heart failure supported with a left ventricular assist device – the SERCA-LVAD TRIAL. *Gene Therapy 2020 27:12*, *27*(12), 579–590. https://doi.org/10.1038/s41434-020-0171-7

MacDonald, B. T., Tamai, K., & He, X. (2009). Wnt/β-catenin signaling: components, mechanisms, and diseases. *Developmental Cell*, *17*(1), 9. https://doi.org/10.1016/J.DEVCEL.2009.06.016

MacLennan, D. H., Asahi, M., & Tupling, A. R. (2003). The regulation of SERCA-type pumps by phospholamban and sarcolipin. *Annals of the New York Academy of Sciences*, *986*, 472–480. http://www.ncbi.nlm.nih.gov/pubmed/12763867

Maillet, M., van Berlo, J. H., & Molkentin, J. D. (2013). Molecular basis of physiological heart growth: fundamental concepts and new players. *Nature Reviews Molecular Cell Biology*, *14*(1), 38–48. https://doi.org/10.1038/nrm3495

Marchi, S., & Pinton, P. (2014). The mitochondrial calcium uniporter complex: molecular components, structure and physiopathological implications. *The Journal of Physiology*, *592*(5), 829–839. https://doi.org/10.1113/jphysiol.2013.268235

Maron, B. J. (2018). Clinical Course and Management of Hypertrophic Cardiomyopathy. *New England Journal of Medicine*, *379*(7), 655–668. https://doi.org/10.1056/NEJMRA1710575/SUPPL_FILE/NEJMRA1710575_DISCLOSURE

S.PDF

Marx, S. O., Reiken, S., Hisamatsu, Y., Jayaraman, T., Burkhoff, D., Rosemblit, N., & Marks, A. R. (2000). PKA phosphorylation dissociates FKBP12.6 from the calcium release channel (ryanodine receptor): defective regulation in failing hearts. *Cell*, *101*(4), 365–376. https://doi.org/10.1016/S0092-8674(00)80847-8

Matsushita, N., Ishida, N., Ibi, M., Saito, M., Sanbe, A., Shimojo, H., Suzuki, S., Koepsell, H., Takeishi, Y., Morino, Y., Taira, E., Sawa, Y., & Hirose, M. (2018). Chronic pressure overload induces cardiac hypertrophy and fibrosis via increases in SGLT1 and IL-18 gene expression in mice. *International Heart Journal*, *59*(5), 1123–1133. https://doi.org/10.1536/ihj.17-565

Mattivi, C. L., Bos, J. M., Bagnall, R. D., Nowak, N., Giudicessi, J. R., Ommen, S. R., Semsarian, C., & Ackerman, M. J. (2020). Clinical utility of a phenotype-enhanced myh7- specific variant classification framework in hypertrophic cardiomyopathy genetic testing. *Circulation: Genomic and Precision Medicine*, *13*, 453–459. https://doi.org/10.1161/CIRCGEN.120.003039

Mayosi, B. M., Kardos, A., Davies, C. H., Gumedze, F., Hovnanian, A., Burge, S., & Watkins, H. (2006). Heterozygous disruption of SERCA2a is not associated with impairment of cardiac performance in humans: Implications for SERCA2a as a therapeutic target in heart failure. *Heart*, *92*(1), 105–109. https://doi.org/10.1136/hrt.2004.051037

McMurray, J. J. V., Packer, M., Desai, A. S., Gong, J., Lefkowitz, M. P., Rizkala, A. R., Rouleau, J. L., Shi, V. C., Solomon, S. D., Swedberg, K., & Zile, M. R. (2014). Angiotensin–Neprilysin Inhibition versus Enalapril in Heart Failure. *New England Journal of Medicine*, *371*(11), 993–1004. https://doi.org/10.1056/NEJMoa1409077

Mensah, G. A., Roth, G. A., & Fuster, V. (2019). The global burden of cardiovascular diseases and risk factors: 2020 and beyond. *J Am Coll Cardiol*, *74*(20), 2529–2532. https://doi.org/10.1016/j.jacc.2019.10.009

Mirza, S. P., Halligan, B. D., Greene, A. S., & Olivier, M. (2007). Improved method for the analysis of membrane proteins by mass spectrometry. *Physiological Genomics*, *30*(1), 89. https://doi.org/10.1152/PHYSIOLGENOMICS.00279.2006

Moens, A. L., Leyton-Mange, J. S., Niu, X., Yang, R., Cingolani, O., Arkenbout, E. K., Champion, H. C., Bedja, D., Gabrielson, K. L., Chen, J., Xia, Y., Hale, A. B., Channon, K. M., Halushka, M. K., Barker, N., Wuyts, F. L., Kaminski, P. M., Wolin, M. S., Kass, D. A., & Barouch, L. A. (2009). Adverse ventricular remodeling and exacerbated NOS uncoupling from pressure-overload in mice lacking the β3-adrenoreceptor. *Journal of Molecular and Cellular Cardiology*, *47*(5), 576–585. https://doi.org/10.1016/j.yjmcc.2009.06.005

Mohamed, T. M. A. A., Abou-Leisa, R., Stafford, N., Maqsood, A., Zi, M., Prehar, S., Baudoin-Stanley, F., Wang, X., Neyses, L., Cartwright, E. J., & Oceandy, D. (2016). The plasma membrane calcium ATPase 4 signalling in cardiac fibroblasts mediates cardiomyocyte hypertrophy. *Nature Communications*, *7*, 1–16. https://doi.org/10.1038/ncomms11074

Mohamed, T. M. A., Abou-Leisa, R., Baudoin, F., Stafford, N., Neyses, L., Cartwright, E. J., & Oceandy, D. (2013). Development and characterization of a novel fluorescent indicator protein PMCA4-GCaMP2 in cardiomyocytes. *Journal of Molecular and Cellular Cardiology*, *63*, 57–68. https://doi.org/10.1016/j.yjmcc.2013.07.007

Mohamed, T. M. A., Abou-Leisa, R., Stafford, N., Maqsood, A., Zi, M., Prehar, S., Baudoin-Stanley, F., Wang, X., Neyses, L., Cartwright, E. J., & Oceandy, D. (2016a). The plasma membrane calcium ATPase 4 signalling in cardiac fibroblasts mediates cardiomyocyte hypertrophy. *Nature Communications*, *7*, 11074. https://doi.org/10.1038/ncomms11074

Mohamed, T. M. A., Abou-Leisa, R., Stafford, N., Maqsood, A., Zi, M., Prehar, S., Baudoin-Stanley, F., Wang, X., Neyses, L., Cartwright, E. J., & Oceandy, D. (2016b). The plasma membrane calcium ATPase 4 signalling in cardiac fibroblasts mediates cardiomyocyte hypertrophy. *Nature Communications*, *7*. https://doi.org/10.1038/ncomms11074

Mohamed, T. M. A., Oceandy, D., Prehar, S., Alatwi, N., Hegab, Z., Baudoin, F. M., Pickard, A., Zaki, A. O., Nadif, R., Cartwright, E. J., & Neyses, L. (2009). Specific Role of Neuronal Nitric-oxide Synthase when Tethered to the Plasma Membrane Calcium Pump in Regulating the β-Adrenergic Signal in the Myocardium. *Journal of Biological Chemistry*, *284*(18), 12091–12098. https://doi.org/10.1074/jbc.M809112200

Molkentin, J. D. (2004). Calcineurin-NFAT signaling regulates the cardiac hypertrophic response in coordination with the MAPKs. In *Cardiovascular Research* (Vol. 63, Issue 3, pp. 467–475). Oxford Academic. https://doi.org/10.1016/j.cardiores.2004.01.021

Monteith, G. R., Wanigasekara, Y., & Roufogalis, B. D. (1998). The plasma membrane calcium pump, its role and regulation: new complexities and possibilities. *Journal of Pharmacological and Toxicological Methods*, *40*(4), 183–190. http://www.ncbi.nlm.nih.gov/pubmed/10465152

Moon, H. S., Choi, E., & Hyun, C. (2008). The Cardiac Sodium-Calcium Exchanger Gene (NCX-1) is a Potential Canine Cardiac Biomarker of Chronic Mitral Valvular Insufficiency. *Journal of Veterinary Internal Medicine*, *22*(6), 1360–1365. https://doi.org/10.1111/J.1939-1676.2008.0209.X

Mulder, B. A., Rienstra, M., Gelder, I. C. Van, & Blaauw, Y. (2021). Update on management of atrial fibrillation in heart failure: a focus on ablation. *Heart*, *0*, 1–7. https://doi.org/10.1136/HEARTJNL-2020-318081

Müller, A. L., & Dhalla, N. S. (2013). Differences in concentric cardiac hypertrophy and eccentric hypertrophy. *Cardiac Adaptations: Molecular Mechanisms*, *4*, 147–166. https://doi.org/10.1007/978-1-4614-5203-4_8/COVER/

Murphy, R. M., Mollica, J. P., Beard, N. A., Knollmann, B. C., & Lamb, G. D. (2011). Quantification of calsequestrin 2 (CSQ2) in sheep cardiac muscle and Ca2+-binding protein changes in CSQ2 knockout mice. *American Journal of Physiology. Heart and Circulatory Physiology*, *300*(2), H595-604. https://doi.org/10.1152/ajpheart.00902.2010

Nakamura, A., Rokosh, D. G., Paccanaro, M., Yee, R. R., Simpson, P. C., Grossman, W., & Foster, E. (2001). LV systolic performance improves with development of hypertrophy after transverse aortic constriction in mice. *American Journal of Physiology - Heart and Circulatory Physiology*, *281*(3 50-3). https://doi.org/10.1152/ajpheart.2001.281.3.h1104

Nauta, J. F., Hummel, Y. M., Tromp, J., Ouwerkerk, W., van der Meer, P., Jin, X., Lam, C. S. P., Bax, J. J., Metra, M., Samani, N. J., Ponikowski, P., Dickstein, K., Anker, S. D., Lang, C. C., Ng, L. L., Zannad, F., Filippatos, G. S., van Veldhuisen, D. J., van Melle, J. P., & Voors, A. A. (2020). Concentric vs. eccentric remodelling in heart failure with reduced

ejection fraction: clinical characteristics, pathophysiology and response to treatment. *European Journal of Heart Failure*, *22*(7), 1147–1155. https://doi.org/10.1002/EJHF.1632

Neef, S., & Maier, L. S. (2007). Remodeling of excitation-contraction coupling in the heart: Inhibition of sarcoplasmic reticulum Ca2+ leak as a novel therapeutic approach. In *Current Heart Failure Reports* (Vol. 4, Issue 1, pp. 11–17). https://doi.org/10.1007/s11897-007-0020-7

Negretti, N., O'Neill, S. C., & Eisner, D. A. (1993). The relative contributions of different intracellular and sarcolemmal systems to relaxation in rat ventricular myocytes. *Cardiovascular Research*, *27*(10), 1826–1830. http://www.ncbi.nlm.nih.gov/pubmed/8275530

Nicin, L., Abplanalp, W. T., Schänzer, A., Sprengel, A., John, D., Mellentin, H., Tombor, L., Keuper, M., Ullrich, E., Klingel, K., Dettmeyer, R. B., Hoffmann, J., Akintuerk, H., Jux, C., Schranz, D., Zeiher, A. M., Rupp, S., & Dimmeler, S. (2021). Single Nuclei Sequencing Reveals Novel Insights Into the Regulation of Cellular Signatures in Children With Dilated Cardiomyopathy. *Circulation*, *143*(17), 1704–1719. https://doi.org/10.1161/CIRCULATIONAHA.120.051391

Niggli, V., Adunyah, E. S., & Carafoli, E. (1981). Acidic phospholipids, unsaturated fatty acids, and limited proteolysis mimic the effect of calmodulin on the purified erythrocyte Ca2+ - ATPase. *The Journal of Biological Chemistry*, *256*(16), 8588–8592. http://www.ncbi.nlm.nih.gov/pubmed/6455424

Nishikimi, T., Maeda, N., & Matsuoka, H. (2006). The role of natriuretic peptides in cardioprotection. In *Cardiovascular Research* (Vol. 69, Issue 2, pp. 318–328). https://doi.org/10.1016/j.cardiores.2005.10.001

O'Neal, W. T., Singleton, M. J., Roberts, J. D., Tereshchenko, L. G., Sotoodehnia, N., Chen, L. Y., Marcus, G. M., & Soliman, E. Z. (2017). Association between QT-interval components and sudden cardiac death: The ARIC study (Atherosclerosis Risk in Communities). *Circulation: Arrhythmia and Electrophysiology*, *10*(10). https://doi.org/10.1161/CIRCEP.117.005485

Oceandy, D., Mohamed, T. M. A., Cartwright, E. J., & Neyses, L. (2011a). Local signals with global impacts and clinical implications: Lessons from the plasma membrane calcium pump (PMCA4). *Biochimica et Biophysica Acta (BBA) - Molecular Cell Research*, *1813*(5), 974–978. https://doi.org/10.1016/j.bbamcr.2010.12.007

Oceandy, D., Mohamed, T. M. A., Cartwright, E. J., & Neyses, L. (2011b). Local signals with global impacts and clinical implications: Lessons from the plasma membrane calcium pump (PMCA4). *Biochimica et Biophysica Acta (BBA) - Molecular Cell Research*, *1813*(5), 974–978. https://doi.org/10.1016/J.BBAMCR.2010.12.007

Oceandy, D., Pickard, A., Prehar, S., Zi, M., Mohamed, T. M. A., Stanley, P. J., Baudoin-Stanley, F., Nadif, R., Tommasi, S., Pfeifer, G. P., Armesilla, A. L., Cartwright, E. J., & Neyses, L. (2009a). Tumor Suppressor Ras-Association Domain Family 1 Isoform A Is a Novel Regulator of Cardiac Hypertrophy. *Circulation*, *120*(7), 607–616. https://doi.org/10.1161/CIRCULATIONAHA.109.868554

Oceandy, Pickard, A., Prehar, S., Zi, M., Mohamed, T. M. A., Stanley, P. J., Baudoin-Stanley, F., Nadif, R., Tommasi, S., Pfeifer, G. P., Armesilla, A. L., Cartwright, E. J., & Neyses, L. (2009b). Tumor suppressor Ras-association domain family 1 isoform A is a novel

regulator of cardiac hypertrophy. *Circulation*, *120*(7), 607–616. https://doi.org/10.1161/CIRCULATIONAHA.109.868554

Oh, G. C., & Cho, H.-J. (2020). Blood pressure and heart failure. *Clinical Hypertension 2020 26:1*, *26*(1), 1–8. https://doi.org/10.1186/S40885-019-0132-X

Okunade, G. W., Miller, M. L., Pyne, G. J., Sutliff, R. L., O'Connor, K. T., Neumann, J. C., Andringa, A., Miller, D. A., Prasad, V., Doetschman, T., Paul, R. J., & Shull, G. E. (2004). Targeted ablation of plasma membrane Ca2+-ATPase (PMCA) 1 and 4 indicates a major housekeeping function for PMCA1 and a critical role in hyperactivated sperm motility and male fertility for PMCA4. *Journal of Biological Chemistry*, *279*(32), 33742–33750. https://doi.org/10.1074/JBC.M404628200

Park, W. J., & Oh, J. G. (2013). SERCA2a: a prime target for modulation of cardiac contractility during heart failure. *BMB Reports*, *46*(5), 237. https://doi.org/10.5483/BMBREP.2013.46.5.077

Patterson, M., Sneyd, J., & Friel, D. D. (2007). Depolarization-induced Calcium Responses in Sympathetic Neurons: Relative Contributions from Ca^{2+} Entry, Extrusion, ER/Mitochondrial Ca^{2+} Uptake and Release, and Ca^{2+} Buffering. *The Journal of General Physiology*, *129*(1), 29–56. https://doi.org/10.1085/jgp.200609660

Pedersen, P. L., & Carafoli, E. (1987). Ion motive ATPases. I. Ubiquity, properties, and significance to cell function. *Trends in Biochemical Sciences*, *12*, 146–150. https://doi.org/10.1016/0968-0004(87)90071-5

Periasamy, M., & Kalyanasundaram, A. (2007). SERCA pump isoforms: Their role in calcium transport and disease. *Muscle Nerve*, *35*, 430–442. https://doi.org/10.1002/mus.20745

Periasamy, M., Reed, T. D., Liu, L. H., Ji, Y., Loukianov, E., Paul, R. J., Nieman, M. L., Riddle, T., Duffy, J. J., Doetschman, T., Lorenz, J. N., & Shull, G. E. (1999). Impaired cardiac performance in heterozygous mice with a null mutation in the sarco(endo)plasmic reticulum Ca2+-ATPase isoform 2 (SERCA2) gene. *Journal of Biological Chemistry*, *274*(4), 2556–2562. https://doi.org/10.1074/jbc.274.4.2556

Philippe, R., Antigny, F., Buscaglia, P., Norez, C., Becq, F., Frieden, M., & Mignen, O. (2015). SERCA and PMCA pumps contribute to the deregulation of Ca2+ homeostasis in human CF epithelial cells. *Biochimica et Biophysica Acta*, *1853*(5), 892–903. https://doi.org/10.1016/J.BBAMCR.2015.01.010

Phrommintikul, A., & Chattipakorn, N. (2006). Roles of cardiac ryanodine receptor in heart failure and sudden cardiac death. *International Journal of Cardiology*, *112*(2), 142–152. https://doi.org/10.1016/j.ijcard.2005.11.106

Piek, A., de Boer, R. A., & Silljé, H. H. W. (2016). The fibrosis-cell death axis in heart failure. *Heart Failure Reviews*, *21*(2), 199. https://doi.org/10.1007/S10741-016-9536-9

Pinto, Y. M., Elliott, P. M., Arbustini, E., Adler, Y., Anastasakis, A., Böhm, M., Duboc, D., Gimeno, J., De Groote, P., Imazio, M., Heymans, S., Klingel, K., Komajda, M., Limongelli, G., Linhart, A., Mogensen, J., Moon, J., Pieper, P. G., Seferovic, P. M., … Charron, P. (2016). Proposal for a revised definition of dilated cardiomyopathy, hypokinetic non-dilated cardiomyopathy, and its implications for clinical practice: a position statement of the ESC working group on myocardial and pericardial diseases. *European Heart Journal*, *37*(23), 1850–1858. https://doi.org/10.1093/EURHEARTJ/EHV727

Pitoulis, F. G., & Terracciano, C. M. (2020). Heart Plasticity in Response to Pressure- and Volume-Overload: A Review of Findings in Compensated and Decompensated Phenotypes. *Frontiers in Physiology*, *11*, 92. https://doi.org/10.3389/FPHYS.2020.00092/BIBTEX

Platt, M. J., Huber, J. S., Romanova, N., Brunt, K. R., & Simpson, J. A. (2018). Pathophysiological mapping of experimental heart failure: Left and right ventricular remodeling in transverse aortic constriction is temporally, kinetically and structurally distinct. *Frontiers in Physiology*, *9*(MAY), 472. https://doi.org/10.3389/fphys.2018.00472

Pocock, S. J., Ariti, C. A., McMurray, J. J. V., Maggioni, A., Køber, L., Squire, I. B., Swedberg, K., Dobson, J., Poppe, K. K., Whalley, G. A., & Doughty, R. N. (2013). Predicting survival in heart failure: a risk score based on 39 372 patients from 30 studies. *European Heart Journal*, *34*(19), 1404–1413. https://doi.org/10.1093/EURHEARTJ/EHS337

Pogwizd, S. M., Schlotthauer, K., Li, L., Yuan, W., & Bers, D. M. (2001). Arrhythmogenesis and Contractile Dysfunction in Heart Failure. *Circulation Research*, *88*, 1159–1167. https://doi.org/10.1161/hh1101.091193

Pott, C., Eckardt, L., & Goldhaber, J. I. (2011). Triple Threat: The Na+/Ca2+ Exchangerin the Pathophysiology of Cardiac Arrhythmia, Ischemia and Heart Failure. *Current Drug Targets*, *12*(5), 737. https://doi.org/10.2174/138945011795378559

Pott, C., Yip, M., Goldhaber, J. I., & Philipson, K. D. (2007). Regulation of Cardiac L-Type Ca2+ Current in Na+-Ca2+ Exchanger Knockout Mice: Functional Coupling of the Ca2+ Channel and the Na+-Ca2+ Exchanger. *Biophysical Journal*, *92*(4), 1431–1437. https://doi.org/10.1529/BIOPHYSJ.106.091538

Powers, S. K., Smuder, A. J., Kavazis, A. N., & Quindry, J. C. (2014). Mechanisms of Exercise-Induced Cardioprotection. *Physiology*, *29*(1), 27–38. https://doi.org/10.1152/physiol.00030.2013

Prandini, P., Pasquali, A., Malerba, G., Marostica, A., Zusi, C., Xumerle, L., Muglia, P., Da Ros, L., Ratti, E., Trabetti, E., Franco Pignatti, P., & Italian Autism Network (ITAN). (2012). The association of rs4307059 and rs35678 markers with autism spectrum disorders is replicated in Italian families. *Psychiatric Genetics*, *22*(4), 177–181. https://doi.org/10.1097/YPG.0b013e32835185c9

Prasad, V., Lorenz, J. N., Lasko, V. M., Nieman, M. L., Jiang, M., Gao, X., Rubinstein, J., Wieczorek, D. F., & Shull, G. E. (2014). Ablation of plasma membrane Ca2+-ATPase isoform 4 prevents development of hypertrophy in a model of hypertrophic cardiomyopathy. *Journal of Molecular and Cellular Cardiology*, *77*, 53–63. https://doi.org/10.1016/j.yjmcc.2014.09.025

Prasad, V., Okunade, G. W., Miller, M. L., & Shull, G. E. (2004). Phenotypes of SERCA and PMCA knockout mice. *Biochemical and Biophysical Research Communications*, *322*(4), 1192–1203. https://doi.org/10.1016/J.BBRC.2004.07.156

Pritchard, T. J., Bowman, P. S., Jefferson, A., Tosun, M., Lynch, R. M., & Paul, R. J. (2010). Corrigendum. *American Journal of Physiology-Gastrointestinal and Liver Physiology*, *299*(2), G548–G548. https://doi.org/10.1152/ajpgi.zh3-5666-corr.2010

Pugach, E. K., Richmond, P. A., Azofeifa, J. G., Dowell, R. D., & Leinwand, L. A. (2015). Prolonged Cre expression driven by the α-myosin heavy chain promoter can be cardiotoxic. *Journal of Molecular and Cellular Cardiology*, *86*, 54–61.

https://doi.org/10.1016/J.YJMCC.2015.06.019

R, T., K, N., A, W., M, A., F, N., Y, O., & M, K. (2011). Serum syndecan-4 is a novel biomarker for patients with chronic heart failure. *Journal of Cardiology*, *57*(3), 325–332. https://doi.org/10.1016/J.JJCC.2011.01.012

Razeghi, P., Young, M. E., Alcorn, J. L., Moravec, C. S., Frazier, O. H., & Taegtmeyer, H. (2001). Metabolic gene expression in fetal and failing human heart. *Circulation*, *104*(24), 2923–2931. http://www.ncbi.nlm.nih.gov/pubmed/11739307

Rea, M. E., & Dunlap, M. E. (2008). Renal hemodynamics in heart failure: implications for treatment. *Current Opinion in Nephrology and Hypertension*, *17*(1), 87–92. https://doi.org/10.1097/MNH.0b013e3282f357da

Reinhardt, T. A., & Horst, R. L. (1999). Ca^{2+} -ATPases and their expression in the mammary gland of pregnant and lactating rats. *American Journal of Physiology-Cell Physiology*, *276*(4), C796–C802. https://doi.org/10.1152/ajpcell.1999.276.4.C796

Reuter, H., Han, T., Motter, C., Philipson, K. D., & Goldhaber, J. I. (2004). Mice overexpressing the cardiac sodium-calcium exchanger: defects in excitation-contraction coupling. *The Journal of Physiology*, *554*(Pt 3), 779–789. https://doi.org/10.1113/jphysiol.2003.055046

Rimessi, A., Coletto, L., Pinton, P., Rizzuto, R., Brini, M., & Carafoli, E. (2005). Inhibitory Interaction of the 14-3-3ϵ Protein with Isoform 4 of the Plasma Membrane Ca^{2+} -ATPase Pump. *Journal of Biological Chemistry*, *280*(44), 37195–37203. https://doi.org/10.1074/jbc.M504921200

Rockman, H. A., Ross, R. S., Harris, A. N., Knowlton, K. U., Steinhelper, M. E., Field, L. J., Ross, J., & Chien, K. R. (1991). Segregation of atrial-specific and inducible expression of an atrial natriuretic factor transgene in an in vivo murine model of cardiac hypertrophy. *Proceedings of the National Academy of Sciences of the United States of America*, *88*(18), 8277–8281. https://doi.org/10.1073/pnas.88.18.8277

Røe, Å. T., Frisk, M., & Louch, W. E. (2015). Targeting Cardiomyocyte Ca 2+ Homeostasis in Heart Failure. *Current Pharmaceutical Design*, *21*(4), 431–448. https://doi.org/10.2174/1381612821041412041241 29

Roger, V. L. (2013). Epidemiology of heart failure. *Circulation Research*, *113*(6), 646–659. https://doi.org/10.1161/CIRCRESAHA.113.300268

Roger, V. L. (2021). Epidemiology of Heart Failure. *Circulation Research*, *128*(10), 1421–1434. https://doi.org/10.1161/CIRCRESAHA.121.318172

Ross, R. S., & Borg, T. K. (2001). Integrins and the myocardium. In *Circulation Research* (Vol. 88, Issue 11, pp. 1112–1119). https://doi.org/10.1161/hh1101.091862

Roston, T. M., Yuchi, Z., Kannankeril, P. J., Hathaway, J., Vinocur, J. M., Etheridge, S. P., Potts, J. E., Maginot, K. R., Salerno, J. C., Cohen, M. I., Hamilton, R. M., Pflaumer, A., Mohammed, S., Kimlicka, L., Kanter, R. J., Lapage, M. J., Collins, K. K., Gebauer, R. A., Temple, J. D., … Sanatani, S. (2018). The clinical and genetic spectrum of catecholaminergic polymorphic ventricular tachycardia: findings from an international multicentre registry. *EP Europace*, *20*(3), 541–547. https://doi.org/10.1093/EUROPACE/EUW389

Rother, J., Richter, C., Turco, L., Knoch, F., Mey, I., Luther, S., Janshoff, A., Bodenschatz, E., & Tarantola, M. (2015). Crosstalk of cardiomyocytes and fibroblasts in co-cultures.

Open Biology, *5*(6). https://doi.org/10.1098/RSOB.150038

Russo, I., Cavalera, M., S, H., Y, S., A, H., B, C., AV, S., SJ, C., J, G., & NG, F. (2019). Protective Effects of Activated Myofibroblasts in the Pressure-Overloaded Myocardium Are Mediated Through Smad-Dependent Activation of a Matrix-Preserving Program. *Circulation Research*, *124*(8), 1214–1227. https://doi.org/10.1161/CIRCRESAHA.118.314438

Ryan, Z. C., Craig, T. A., Filoteo, A. G., Westendorf, J. J., Cartwright, E. J., Neyses, L., Strehler, E. E., & Kumar, R. (2015). Deletion of the Intestinal Plasma Membrane Calcium Pump, Isoform 1, Atp2b1, in Mice is Associated with Decreased Bone Mineral Density and Impaired Responsiveness to 1, 25-Dihydroxyvitamin D3. *Biochemical and Biophysical Research Communications*, *467*(1), 152. https://doi.org/10.1016/J.BBRC.2015.09.087

Santangeli, P., Rame, J. E., Birati, E. Y., & Marchlinski, F. E. (2017). Management of Ventricular Arrhythmias in Patients With Advanced Heart Failure. In *Journal of the American College of Cardiology* (Vol. 69, Issue 14, pp. 1842–1860). Elsevier USA. https://doi.org/10.1016/j.jacc.2017.01.047

Savarese, G., & Lund, L. H. (2017). Global Public Health Burden of Heart Failure. *Cardiac Failure Review*, *3*(1), 7–11. https://doi.org/10.15420/cfr.2016:25:2

Schaible, T. F., & Scheuer, J. (1984). Comparison of heart function in male and female rats. *Basic Research in Cardiology*, *79*(4), 402–412. https://doi.org/10.1007/BF01908140

Schatzmann, H. J. (1966). ATP-dependent Ca++-extrusion from human red cells. *Experientia*, *22*(6), 364–365. http://www.ncbi.nlm.nih.gov/pubmed/5961668

Schuh, K., S, U., S, G., N, R., & L, N. (2003). Interaction of the plasma membrane Ca2+ pump 4b/CI with the Ca2+/calmodulin-dependent membrane-associated kinase CASK. *The Journal of Biological Chemistry*, *278*(11), 9778–9783. https://doi.org/10.1074/JBC.M212507200

Schuh, K., Uldrijan, S., Gambaryan, S., Roethlein, N., & Neyses, L. (2003). Interaction of the plasma membrane Ca2+ pump 4b/CI with the Ca2+/calmodulin-dependent membrane-associated kinase CASK. *The Journal of Biological Chemistry*, *278*(11), 9778–9783. https://doi.org/10.1074/jbc.M212507200

Schuh, K., Uldrijan, S., Telkamp, M., Röthlein, N., & Neyses, L. (2001). The plasmamembrane calmodulin–dependent calcium pump. *The Journal of Cell Biology*, *155*(2), 201–206. https://doi.org/10.1083/jcb.200104131

Schwinger, R. H. G. (2021). Pathophysiology of heart failure. *Cardiovascular Diagnosis and Therapy*, *11*(1), 263. https://doi.org/10.21037/CDT-20-302

Segura, A. M., Frazier, O. H., & Buja, L. M. (2014). Fibrosis and heart failure. *Heart Failure Reviews*, *19*(2), 173–185. https://doi.org/10.1007/S10741-012-9365-4

Sergeeva, I. A., & Christoffels, V. M. (2013). Regulation of expression of atrial and brain natriuretic peptide, biomarkers for heart development and disease. In *Biochimica et Biophysica Acta - Molecular Basis of Disease* (Vol. 1832, Issue 12, pp. 2403–2413). Elsevier. https://doi.org/10.1016/j.bbadis.2013.07.003

Shanks, J., Herring, N., Johnson, E., Liu, K., Li, D., & Paterson, D. J. (2017). Overexpression of Sarcoendoplasmic Reticulum Calcium ATPase 2a Promotes Cardiac Sympathetic Neurotransmission via Abnormal Endoplasmic Reticulum and Mitochondria Ca2+ Regulation. *Hypertension*, *69*(4), 625–632.

https://doi.org/10.1161/HYPERTENSIONAHA.116.08507/-/DC1

Shen, J., & He, X. (2014). Generalized *F* Test and Generalized Deviance Test in Two-Way ANOVA Models for Randomized Trials. *Journal of Biopharmaceutical Statistics*, *24*(3), 523–534. https://doi.org/10.1080/10543406.2014.888435

Siddiqui, J. K., Tikunova, S. B., Walton, S. D., Liu, B., Meyer, M., de Tombe, P. P., Neilson, N., Kekenes-Huskey, P. M., Salhi, H. E., Janssen, P. M. L., Biesiadecki, B. J., & Davis, J. P. (2016). Myofilament Calcium Sensitivity: Consequences of the Effective Concentration of Troponin I. *Frontiers in Physiology*, *7*(DEC), 632. https://doi.org/10.3389/FPHYS.2016.00632

Sikkel, M. B., Hayward, C., MacLeod, K. T., Harding, S. E., & Lyon, A. R. (2014). SERCA2a gene therapy in heart failure: an anti-arrhythmic positive inotrope. *British Journal of Pharmacology*, *171*(1), 38–54. https://doi.org/10.1111/BPH.12472

Sipido, K. R., Volders, P. G. A., Vos, M. A., & Verdonck, F. (2002). Altered Na/Ca exchange activity in cardiac hypertrophy and heart failure: a new target for therapy? *Cardiovascular Research*, *53*(4), 782–805. https://doi.org/10.1016/S0008-6363(01)00470-9

Siri-angkul, N., Dadfar, B., Jaleel, R., Naushad, J., Parambathazhath, J., Doye, A. A., Xie, L. H., & Gwathmey, J. K. (2021). Calcium and Heart Failure: How Did We Get Here and Where Are We Going? *International Journal of Molecular Sciences*, *22*(14). https://doi.org/10.3390/IJMS22147392

Solaro, R. J., & Rarick, H. M. (1998). Troponin and tropomyosin: proteins that switch on and tune in the activity of cardiac myofilaments. *Circulation Research*, *83*(5), 471–480. https://doi.org/10.1161/01.RES.83.5.471

Stafford, N., Neyses, L., & Oceandy, D. (2017). The Control of Sub-Plasma Membrane Calcium signalling by the membrane calcium ATPase pump PMCA4. In *Microdomains in the Cardiovascular system* (pp. 351–359). Springer International Publishing AG. https://doi.org/10.1007/978-3-319-54579-0

Stafford, N. P. (2013). *The independent roles of PMCA1 and PMCA4 in the development and progression of left ventricular hypertrophy and failure*. https://www.research.manchester.ac.uk/portal/files/54547654/FULL_TEXT.PDF

Stafford, N., Wilson, C., Oceandy, D., Neyses, L., & Cartwright, E. J. (2017). The Plasma Membrane Calcium ATP ases and Their Role as Major New Players in Human Disease. *Physiological Reviews*, *97*(3), 1089–1125. https://doi.org/10.1152/physrev.00028.2016

Stahl, W. L., Eakin, T. J., Owens, J. W., Breininger, J. F., Filuk, P. E., & Anderson, W. R. (1992). Plasma membrane Ca(2+)-ATPase isoforms: distribution of mRNAs in rat brain by in situ hybridization. *Brain Research. Molecular Brain Research*, *16*(3–4), 223–231. http://www.ncbi.nlm.nih.gov/pubmed/1337931

Stankovikj, V. (2017). *The role of PMCA1 in post-myocardial infarction remodelling*.

Stauffer, T. P., Hilfiker, H., Carafoli, E., & Strehler, E. E. (1993). Quantitative analysis of alternative splicing options of human plasma membrane calcium pump genes. *The Journal of Biological Chemistry*, *268*(34), 25993–26003. http://www.ncbi.nlm.nih.gov/pubmed/8245032

Stern, M. D. (1992). Theory of excitation-contraction coupling in cardiac muscle. *Biophysical*

Journal, *63*(2), 497–517. https://doi.org/10.1016/S0006-3495(92)81615-6

Street, V. A., McKee-Johnson, J. W., Fonseca, R. C., Tempel, B. L., & Noben-Trauth, K. (1998). Mutations in a plasma membrane Ca2+-ATPase gene cause deafness in deafwaddler mice. *Nature Genetics*, *19*(4), 390–394. https://doi.org/10.1038/1284

Strehler, E. E. (2013). Plasma Membrane Calcium ATPases as Novel Candidates for Therapeutic Agent Development. *Journal of Pharmacy & Pharmaceutical Sciences : A Publication of the Canadian Society for Pharmaceutical Sciences, Societe Canadienne Des Sciences Pharmaceutiques*, *16*(2), 190. https://doi.org/10.18433/J3Z011

Strehler, E. E., Filoteo, A. G., Penniston, J. T., & Caride, A. J. (2007). Plasma-membrane Ca $^{2+}$ pumps: structural diversity as the basis for functional versatility. *Biochemical Society Transactions*, *35*(5), 919–922. https://doi.org/10.1042/BST0350919

Strehler, E. E., & Treiman, M. (2004). Calcium pumps of plasma membrane and cell interior. *Current Molecular Medicine*, *4*(3), 323–335. http://www.ncbi.nlm.nih.gov/pubmed/15101689

Strehler, E. E., & Zacharias, D. A. (2001a). Role of Alternative Splicing in Generating Isoform Diversity Among Plasma Membrane Calcium Pumps. *Physiological Reviews*, *81*(1), 21–50. https://doi.org/10.1152/physrev.2001.81.1.21

Strehler, E. E., & Zacharias, D. A. (2001b). Role of Alternative Splicing in Generating Isoform Diversity Among Plasma Membrane Calcium Pumps. *Physiological Reviews*, *81*(1), 21–50. https://doi.org/10.1152/physrev.2001.81.1.21

Sun, Y. B., & Irving, M. (2010). The molecular basis of the steep force–calcium relation in heart muscle. *Journal of Molecular and Cellular Cardiology*, *48*(5), 859. https://doi.org/10.1016/J.YJMCC.2009.11.019

Sweeney, M., Corden, B., & Cook, S. A. (2020). Targeting cardiac fibrosis in heart failure with preserved ejection fraction: mirage or miracle? *EMBO Molecular Medicine*, *12*(10). https://doi.org/10.15252/emmm.201910865

Szewczyk, M. M., Pande, J., Akolkar, G., & Grover, A. K. (2010). Caloxin 1b3: a novel plasma membrane Ca(2+)-pump isoform 1 selective inhibitor that increases cytosolic Ca(2+) in endothelial cells. *Cell Calcium*, *48*(6), 352–357. https://doi.org/10.1016/J.CECA.2010.10.008

Tada, M., Inui, M., Yamada, M., Kadoma, M., Kuzuya, T., Abe, H., & Kakiuchi, S. (1983). Effects of phospholamban phosphorylation catalyzed by adenosine 3':5'-monophosphate- and calmodulin-dependent protein kinases on calcium transport ATPase of cardiac sarcoplasmic reticulum. *Journal of Molecular and Cellular Cardiology*, *15*(5), 335–346. http://www.ncbi.nlm.nih.gov/pubmed/6310131

Taegtmeyer, H., Sen, S., & Vela, D. (2010). Return to the fetal gene program: a suggested metabolic link to gene expression in the heart. *Annals of the New York Academy of Sciences*, *1188*, 191–198. https://doi.org/10.1111/j.1749-6632.2009.05100.x

Takeuchi, F., Isono, M., Yamamoto, K., Yokota, M., Akiyama, K., Katsuya, T., Kim, H.-S., Park, J. E., Jang, Y., Lee, J.-Y., Lee, J.-Y., Kato, N., & Kato, N. (2015). Heterogeneous Effects of Association Between Blood Pressure Loci and Coronary Artery Disease in East Asian Individuals. *Circulation Journal*, *79*(4), 830–838. https://doi.org/10.1253/circj.CJ-14-0841

Talarico, E. F., & Mangini, N. J. (2007). ALTERNATIVE SPLICE VARIANTS OF PLASMA

MEMBRANE CALCIUM-ATPases IN HUMAN CORNEAL EPITHELIUM. *Experimental Eye Research*, *85*(6), 869. https://doi.org/10.1016/J.EXER.2007.08.023

Taylor, C. J., Ordóñez-Mena, J. M., Roalfe, A. K., Lay-Flurrie, S., Jones, N. R., Marshall, T., & Hobbs, F. D. R. (2019a). Trends in survival after a diagnosis of heart failure in the United Kingdom 2000-2017: population based cohort study. *BMJ*, *364*, 223. https://doi.org/10.1136/BMJ.L223

Taylor, C. J., Ordóñez-Mena, J. M., Roalfe, A. K., Lay-Flurrie, S., Jones, N. R., Marshall, T., & Hobbs, F. D. R. (2019b). Trends in survival after a diagnosis of heart failure in the United Kingdom 2000-2017: population based cohort study. *BMJ*, *364*, 223. https://doi.org/10.1136/BMJ.L223

Tham, Y. K., Bernardo, B. C., Ooi, J. Y. Y., Weeks, K. L., & McMullen, J. R. (2015). Pathophysiology of cardiac hypertrophy and heart failure: signaling pathways and novel therapeutic targets. *Archives of Toxicology 2015 89:9*, *89*(9), 1401–1438. https://doi.org/10.1007/S00204-015-1477-X

Tiffert, T., & Lew, V. L. (2011). Elevated intracellular Ca $^{2+}$ reveals a functional membrane nucleotide pool in intact human red blood cells. *The Journal of General Physiology*, *138*(4), 381–391. https://doi.org/10.1085/jgp.201110660

Timmann, C., Thye, T., Vens, M., Evans, J., May, J., Ehmen, C., Sievertsen, J., Muntau, B., Ruge, G., Loag, W., Ansong, D., Antwi, S., Asafo-Adjei, E., Nguah, S. B., Kwakye, K. O., Akoto, A. O. Y., Sylverken, J., Brendel, M., Schuldt, K., … Horstmann, R. D. (2012). Genome-wide association study indicates two novel resistance loci for severe malaria. *Nature*, *489*(7416), 443–446. https://doi.org/10.1038/nature11334

Toischer, K., Rokita, A. G., Unsöld, B., Zhu, W., Kararigas, G., Sossalla, S., Reuter, S. P., Becker, A., Teucher, N., Seidler, T., Grebe, C., Preu, L., Gupta, S. N., Schmidt, K., Lehnart, S. E., Krüger, M., Linke, W. A., Backs, J., Regitz-Zagrosek, V., … Hasenfuss, G. (2010). Differential cardiac remodeling in preload versus afterload. *Circulation*, *122*(10), 993–1003. https://doi.org/10.1161/CIRCULATIONAHA.110.943431

Toischer, K., Teucher, N., Unsöld, B., Kuhn, M., Kögler, H., & Hasenfuss, G. (2010). BNP controls early load-dependent regulation of SERCA through calcineurin. *Basic Research in Cardiology*, *105*(6), 795–804. https://doi.org/10.1007/s00395-010-0115-2

Tomek, J., & Bub, G. (2017). Hypertension-induced remodelling: on the interactions of cardiac risk factors. *The Journal of Physiology*, *595*(12), 4027–4036. https://doi.org/10.1113/JP273043

Torrente, A. G., Zhang, R., Zaini, A., Giani, J. F., Kang, J., Lamp, S. T., Philipson, K. D., & Goldhaber, J. I. (2015). Burst pacemaker activity of the sinoatrial node in sodium-calcium exchanger knockout mice. *Proceedings of the National Academy of Sciences of the United States of America*, *112*(31), 9769–9774. https://doi.org/10.1073/PNAS.1505670112/SUPPL_FILE/PNAS.1505670112.SM04.AVI

Travers, J. G., Kamal, F. A., Robbins, J., Yutzey, K. E., & Blaxall, B. C. (2016). Cardiac fibrosis: The fibroblast awakens. In *Circulation Research* (Vol. 118, Issue 6, pp. 1021–1040). Lippincott Williams and Wilkins. https://doi.org/10.1161/CIRCRESAHA.115.306565

Vaduganathan, M., Docherty, K. F., Claggett, B. L., Jhund, P. S., de Boer, R. A., Hernandez, A. F., Inzucchi, S. E., Kosiborod, M. N., Lam, C. S. P., Martinez, F., Shah, S. J., Desai, A. S., McMurray, J. J. V., & Solomon, S. D. (2022). SGLT-2 inhibitors in patients with heart failure: a comprehensive meta-analysis of five randomised controlled trials. *The*

Lancet, *400*(10354), 757–767. https://doi.org/10.1016/S0140-6736(22)01429-5

van den Bosch, B. J. C., Lindsey, P. J., van den Burg, C. M. M., van der Vlies, S. A., Lips, D. J., van der Vusse, G. J., Ayoubi, T. A., Doevendans, P. A., & Smeets, H. J. M. (2006). Early and transient gene expression changes in pressure overload-induced cardiac hypertrophy in mice. *Genomics*, *88*(4), 480–488. https://doi.org/10.1016/j.ygeno.2006.04.012

van der Pol, A., Hoes, M. F., de Boer, R. A., & van der Meer, P. (2020). Cardiac foetal reprogramming: a tool to exploit novel treatment targets for the failing heart. *Journal of Internal Medicine*, *288*(5), 491–506. https://doi.org/10.1111/JOIM.13094

Velicki, L., Jakovljevic, D. G., Preveden, A., Golubovic, M., Bjelobrk, M., Ilic, A., Stojsic, S., Barlocco, F., Tafelmeier, M., Okwose, N., Tesic, M., Brennan, P., Popovic, D., Ristic, A., MacGowan, G. A., Filipovic, N., Maier, L. S., & Olivotto, I. (2020a). Genetic determinants of clinical phenotype in hypertrophic cardiomyopathy. *BMC Cardiovascular Disorders*, *20*(1), 1–10. https://doi.org/10.1186/S12872-020-01807-4/FIGURES/1

Velicki, L., Jakovljevic, D. G., Preveden, A., Golubovic, M., Bjelobrk, M., Ilic, A., Stojsic, S., Barlocco, F., Tafelmeier, M., Okwose, N., Tesic, M., Brennan, P., Popovic, D., Ristic, A., MacGowan, G. A., Filipovic, N., Maier, L. S., & Olivotto, I. (2020b). Genetic determinants of clinical phenotype in hypertrophic cardiomyopathy. *BMC Cardiovascular Disorders 2020 20:1*, *20*(1), 1–10. https://doi.org/10.1186/S12872-020-01807-4

Verdecchia, P., Schillaci, G., Borgioni, C., Ciucci, A., Battistelli, M., Bartoccini, C., Santucci, A., Santucci, C., Reboldi, G., & Porcellati, C. (1995). Adverse prognostic significance of concentric remodeling of the left ventricle in hypertensive patients with normal left ventricular mass. *Journal of the American College of Cardiology*, *25*(4), 871–878. https://doi.org/10.1016/0735-1097(94)00424-O

Walsh, M. (1994). Calmodulin and the regulation of smooth muscle contraction. *Molecular and Cellular Biochemistry*, *135*(1), 21–41. https://doi.org/10.1007/BF00925958

Wan, J.-P., Wang, H., Li, C.-Z., Zhao, H., You, L., Shi, D.-H., Sun, X.-H., Lv, H., Wang, F., Wen, Z.-Q., Wang, X.-T., & Chen, Z.-J. (2014). The Common Single-Nucleotide Polymorphism rs2681472 Is Associated With Early-Onset Preeclampsia in Northern Han Chinese Women. *Reproductive Sciences*, *21*(11), 1423–1427. https://doi.org/10.1177/1933719114527354

Wang, D., Oparil, S., An Feng, J., Li, P., Perry, G., Bo Chen, L., Dai, M., John, S. W., & Chen, Y.-F. (2003). *Effects of Pressure Overload on Extracellular Matrix Expression in the Heart of the Atrial Natriuretic Peptide-Null Mouse*. https://doi.org/10.1161/01.HYP.0000074905.22908.A6

Wang, S., Xue, H., Zou, Y., Sun, K., Fu, C., Wang, H., & Hui, R. (2014). Left ventricular hypertrophy, abnormal ventricular geometry and relative wall thickness are associated with increased risk of stroke in hypertensive patients among the Han Chinese. *Hypertension Research 2014 37:9*, *37*(9), 870–874. https://doi.org/10.1038/hr.2014.88

Wang, Y., Wilson, C., Cartwright, E. J., & Lei, M. (2017a). Plasma membrane Ca $^{2+}$ -ATPase 1 is required for maintaining atrial Ca $^{2+}$ homeostasis and electrophysiological stability in the mouse. *The Journal of Physiology*, *595*(24), 7383–7398.

https://doi.org/10.1113/JP274110

Wang, Y., Wilson, C., Cartwright, E. J., & Lei, M. (2017b). Plasma membrane Ca2+-ATPase 1 is required for maintaining atrial Ca2+ homeostasis and electrophysiological stability in the mouse. *Journal of Physiology*, *595*(24), 7383–7398. https://doi.org/10.1113/JP274110

Wang, Y., Wilson, C., Cartwright, E. J., & Lei, M. (2017c). Plasma membrane Ca2+-ATPase 1 is required for maintaining atrial Ca2+ homeostasis and electrophysiological stability in the mouse. *The Journal of Physiology*, *595*(24), 7383–7398. https://doi.org/10.1113/JP274110

Wang, Y., Wilson, C., Cartwright, E. J., & Lei, M. (2017d). Plasma membrane Ca2+-ATPase 1 is required for maintaining atrial Ca2+ homeostasis and electrophysiological stability in the mouse. *The Journal of Physiology*, *595*(24), 7383. https://doi.org/10.1113/JP274110

Weber, C. R., Piacentino, V., Houser, S. R., & Bers, D. M. (2003). Dynamic Regulation of Sodium/Calcium Exchange Function in Human Heart Failure. *Circulation*, *108*(18), 2224–2229. https://doi.org/10.1161/01.CIR.0000095274.72486.94

Weber, K. T., Sun, Y., & Campbell, S. E. (1995). Structural remodelling of the heart by fibrous tissue: role of circulating hormones and locally produced peptides. *European Heart Journal*, *16 Suppl N*, 12–18. https://doi.org/10.1093/eurheartj/16.suppl_N.12

Wehrens, X. H. T., Lehnart, S. E., & Marks, A. R. (2005). INTRACELLULAR CALCIUM RELEASE AND CARDIAC DISEASE. *Annual Review of Physiology*, *67*(1), 69–98. https://doi.org/10.1146/annurev.physiol.67.040403.114521

Weng, L., Taylor, K. D., Chen, Y.-D. I., Sopko, G., Kelsey, S. F., Bairey Merz, C. N., Pepine, C. J., Miller, V. M., Rotter, J. I., Gulati, M., Goodarzi, M. O., & Cooper-DeHoff, R. M. (2016). Genetic loci associated with nonobstructive coronary artery disease in Caucasian women. *Physiological Genomics*, *48*(1), 12–20. https://doi.org/10.1152/physiolgenomics.00067.2015

Williams, J. C., Armesilla, A. L., Mohamed, T. M. A., Hagarty, C. L., McIntyre, F. H., Schomburg, S., Zaki, A. O., Oceandy, D., Cartwright, E. J., Buch, M. H., Emerson, M., & Neyses, L. (2006a). The Sarcolemmal Calcium Pump, α-1 Syntrophin, and Neuronal Nitric-oxide Synthase Are Parts of a Macromolecular Protein Complex. *Journal of Biological Chemistry*, *281*(33), 23341–23348. https://doi.org/10.1074/jbc.M513341200

Williams, J. C., Armesilla, A. L., Mohamed, T. M. A., Hagarty, C. L., McIntyre, F. H., Schomburg, S., Zaki, A. O., Oceandy, D., Cartwright, E. J., Buch, M. H., Emerson, M., & Neyses, L. (2006b). The Sarcolemmal Calcium Pump, α-1 Syntrophin, and Neuronal Nitric-oxide Synthase Are Parts of a Macromolecular Protein Complex. *Journal of Biological Chemistry*, *281*(33), 23341–23348. https://doi.org/10.1074/jbc.M513341200

Wilson, C. (2017). Investigation of the role of PMCA1 in cardiac electrical function and heart rhythm stability. *PhD Thesis, University of Manchester*.

Wilson, C., Stafford, N., Zi, M., Chelu, A., Niort, B. C., Li, Y., Baudoin, F., Prehar, S., Trafford, A. W., & Cartwright, E. J. (2022). Cardiomyocyte-specific loss of plasma membrane calcium ATPase 1 impacts cardiac rhythm and is associated with ventricular repolarisation dysfunction. *Journal of Molecular and Cellular Cardiology*, *172*, 41–51.

https://doi.org/10.1016/J.YJMCC.2022.07.011

Wimalasundera, R. C., Wijetunge, S., Thom, S. M., Regan, L., & Hughes, A. D. (2010). Impaired recovery of intracellular calcium and force after activation in isolated myometrial and subcutaneous resistance arteries from women with preeclampsia. *Journal of Hypertension*, *28*(3), 568–574. https://doi.org/10.1097/HJH.0b013e328334f20b

Witte, J. S. (2010). Genome-wide association studies and beyond. *Annual Review of Public Health*, *31*, 9-20 4 p following 20. https://doi.org/10.1146/annurev.publhealth.012809.103723

Wu, J., Venkata Subbaiah, K. C., Xie, L. H., Jiang, F., Mickelsen, D., Myers, J. R., Tang, W. H. W., & Yao, P. (2019). EPRS regulates proline-rich pro-fibrotic protein synthesis during cardiac fibrosis. In *bioRxiv*. bioRxiv. https://doi.org/10.1101/777490

Wu, X., Chang, B., Blair, N. S., Sargent, M., York, A. J., Robbins, J., Shull, G. E., & Molkentin, J. D. (2009a). Plasma membrane Ca2+-ATPase isoform 4 antagonizes cardiac hypertrophy in association with calcineurin inhibition in rodents. *Journal of Clinical Investigation*, *119*(4), 976–985. https://doi.org/10.1172/JCI36693

Wu, X., Chang, B., Blair, N. S., Sargent, M., York, A. J., Robbins, J., Shull, G. E., & Molkentin, J. D. (2009b). Plasma membrane Ca2+-ATPase isoform 4 antagonizes cardiac hypertrophy in association with calcineurin inhibition in rodents. *Journal of Clinical Investigation*, *119*(4), 976–985. https://doi.org/10.1172/JCI36693

Xi, B., Shen, Y., Zhao, X., Chandak, G. R., Cheng, H., Hou, D., Li, Y., Ott, J., Zhang, Y., Wang, X., & Mi, J. (2014). Association of common variants in/near six genes (ATP2B1, CSK, MTHFR, CYP17A1, STK39 and FGF5) with blood pressure/hypertension risk in Chinese children. *Journal of Human Hypertension*, *28*(1), 32–36. https://doi.org/10.1038/jhh.2013.50

Xiao, D., Zhang, Y., Wang, R., Fu, Y., Zhou, T., Diao, H., Wang, Z., Lin, Y., Li, Z., Wen, L., Kang, X., Kopylov, P., Shchekochikhin, D., Zhang, Y., & Yang, B. (2019). Emodin alleviates cardiac fibrosis by suppressing activation of cardiac fibroblasts via upregulating metastasis associated protein 3. *Acta Pharmaceutica Sinica B*, *9*(4), 724–733. https://doi.org/10.1016/j.apsb.2019.04.003

Xiao, J., Li, J., Xu, T., Lv, D., Shen, B., Song, Y., & Xu, J. (2014). Pregnancy-induced physiological hypertrophy protects against cardiac ischemia-reperfusion injury. *International Journal of Clinical and Experimental Pathology*, *7*(1), 229. /pmc/articles/PMC3885477/

Xu, H., II, G. W. D., Shetty, A., Parihar, A., Dave, T., Robinson, S. W., Gottlieb, S. S., Donahue, M. P., Tomaselli, G. F., Kraus, W. E., Mitchell, B. D., & Liggett, S. B. (2018). A Genome-Wide Association Study of Idiopathic Dilated Cardiomyopathy in African Americans. *Journal of Personalized Medicine 2018, Vol. 8, Page 11*, *8*(1), 11. https://doi.org/10.3390/JPM8010011

Yamoah, E. N., Lumpkin, E. A., Dumont, R. A., Smith, P. J. S., Hudspeth, A. J., & Gillespie, P. G. (1998). Plasma Membrane Ca2+-ATPase Extrudes Ca2+from Hair Cell Stereocilia. *The Journal of Neuroscience*, *18*(2), 610. https://doi.org/10.1523/JNEUROSCI.18-02-00610.1998

Yano, M., Yamamoto, T., Ikemoto, N., & Matsuzaki, M. (2005). Abnormal ryanodine receptor function in heart failure. *Pharmacology & Therapeutics*, *107*(3), 377–391.

https://doi.org/10.1016/j.pharmthera.2005.04.003

Ying, X., Lee, K., Li, N., Corbett, D., Mendoza, L., & Frangogiannis, N. G. (2009). Characterization of the Inflammatory and Fibrotic Response in a Mouse Model of Cardiac Pressure Overload. *Histochemistry and Cell Biology*, *131*(4), 471. https://doi.org/10.1007/S00418-008-0541-5

Zacharias, D. A., & Kappen, C. (1999). Developmental expression of the four plasma membrane calcium ATPase (Pmca) genes in the mouse. *Biochimica et Biophysica Acta*, *1428*(2–3), 397–405. http://www.ncbi.nlm.nih.gov/pubmed/10434059

Zannad, F., McMurray, J. J. V., Krum, H., van Veldhuisen, D. J., Swedberg, K., Shi, H., Vincent, J., Pocock, S. J., Pitt, B., & EMPHASIS-HF Study Group. (2011). Eplerenone in Patients with Systolic Heart Failure and Mild Symptoms. *New England Journal of Medicine*, *364*(1), 11–21. https://doi.org/10.1056/NEJMoa1009492

Zanni, G., Calì, T., Kalscheuer, V. M., Ottolini, D., Barresi, S., Lebrun, N., Montecchi-Palazzi, L., Hu, H., Chelly, J., Bertini, E., Brini, M., & Carafoli, E. (2012). Mutation of plasma membrane Ca2+ ATPase isoform 3 in a family with X-linked congenital cerebellar ataxia impairs Ca2+ homeostasis. *Proceedings of the National Academy of Sciences of the United States of America*, *109*(36), 14514–14519. https://doi.org/10.1073/pnas.1207488109

Zhang, J., Xiao, P., & Zhang, X. (2009). Phosphatidylserine externalization in caveolae inhibits Ca2+ efflux through plasma membrane Ca2+-ATPase in ECV304. *Cell Calcium*, *45*(2), 177–184. https://doi.org/10.1016/J.CECA.2008.09.002

Zi, M., Maqsood, A., Prehar, S., Mohamed, T. M. A., Abou-Leisa, R., Robertson, A., Cartwright, E. J., Ray, S. G., Oh, S., Lim, D. S., Neyses, L., & Oceandy, D. (2014a). The mammalian Ste20-like kinase 2 (Mst2) modulates stress-induced cardiac hypertrophy. *Journal of Biological Chemistry*, *289*(35), 24275–24288. https://doi.org/10.1074/jbc.M114.562405

Zi, M., Stafford, N., Prehar, S., Baudoin, F., Oceandy, D., Wang, X., Bui, T., Shaheen, M., Neyses, L., & Cartwright, E. J. (2019a). Cardiac hypertrophy or failure? - A systematic evaluation of the transverse aortic constriction model in C57BL/6NTac and C57BL/6J substrains. *Current Research in Physiology*, *1*, 1–10. https://doi.org/10.1016/J.CRPHYS.2019.10.001

Zi, M., Stafford, N., Prehar, S., Baudoin, F., Oceandy, D., Wang, X., Bui, T., Shaheen, M., Neyses, L., & Cartwright, E. J. (2019b). Cardiac hypertrophy or failure? - A systematic evaluation of the transverse aortic constriction model in C57BL/6NTac and C57BL/6J substrains. *Current Research in Physiology*, *1*, 1–10. https://doi.org/10.1016/j.crphys.2019.10.001

Zi, Maqsood, A., Prehar, S., Mohamed, T. M. A., Abou-Leisa, R., Robertson, A., Cartwright, E. J., Ray, S. G., Oh, S., Lim, D. S., Neyses, L., & Oceandy, D. (2014b). The Mammalian Ste20-like Kinase 2 (Mst2) Modulates Stress-induced Cardiac Hypertrophy *. *Journal of Biological Chemistry*, *289*(35), 24275–24288. https://doi.org/10.1074/JBC.M114.562405